MANGANESE COMPLEXES AS CATALASE AND SUPEROXIDE DISMUTASE MIMICS; STRUCTURE AND REACTIVITY RELATIONSHIPS

BY

MUHAMMET KOSE

SUPERVISOR PROF. VICKIE MCKEE

A DOCTORAL THESIS SUBMITTED IN PARTIAL FULFILLMENT OF THE REQUIREMENTS FOR THE AWARD OF DOCTOR OF PHILOSOPHY OF LOUGHBOROUGH UNIVERSITY

Abstract

Macrocycle (H_2L1) was prepared by a Schiff base condensation reaction of 2,6-diformylpyridine and 1,3-diamino-2-propanol in the presence of Ba(II) as template ion. Seven-coordinate Mn(II) complexes were prepared by transmetallation reactions of the initial $[Ba(H_2L1)(\mu_{1,2}\text{-}ClO_4)]_2(ClO_4)_2$ complex. Two mononuclear, ring-contracted complexes were obtained when methanol or ethanol were used as solvents in transmetallation reactions. For both complexes, X-ray analysis showed that the H_2L1 macrocycle undergoes a ring-contraction *via* addition of methanol or ethanol across one imine bond, followed by a nucleophilic addition of the secondary amine across an adjacent imine bond resulting in a six-membered, hexahydropyrimidine ring sitting in a chair conformation. The ring-contraction process reduces the size of the cavity in the macrocycle to accommodate one Mn(II) ion in the macrocycle. The macrocyclic tetraimine ligand (H_2L1) gave access to the polynuclear, ring-expanded assemblies, $[Mn_4(H_2L^*)Cl_4][MnCl_4]$ and $[Mn_4(H_2L^*)(N_3)_4](ClO_4)_2$, when acetonitrile was used as a solvent. The macrocycle (H_2L1) undergoes rearrangement from a 20-membered to a 40-membered tetranuclear Mn(II) complex. Manganese complexes of acyclic ligands, derived from 2,6-diformylpyridine and several aminoalcohols and aminophenols, were prepared and structurally characterised by X-ray crystallography. Most of the complexes are seven-coordinate with approximate pentagonal bipyramidal geometry, however, some five, six and seven-coordinate complexes were identified.

Asymmetric and symmetric tripodal Schiff base ligands and their manganese complexes were also prepared and characterised. Additionally, N-alkylated benzimidazole 2,6-bis(1-butyl-1*H*-benzo[*d*]imidazol-2-yl)pyridine and its Mn(II) complexes were prepared and characterised. The potential application of the complexes has been tested in two main areas: (a) as new catalase mimics and (b) as new superoxide dismutase (SOD) mimics. The trinuclear, acyclic complex, $[Mn_3(L9)_2(OAc)_2(MeOH)_2]\cdot 2MeOH$, derived from 2,6-diformylpyridine and 2-aminophenol, was found to be the most efficient catalase mimic of the tested complexes with approximately 500 molecules of H_2O_2 broken down per second for each complex during the fastest rate of activity. Catalase testing showed that an increase of the arm size of the tripodal complexes produced an increase in activity

overall for the complexes. Most of the complexes tested for catalase activity showed an induction period prior to the activity being observed. This may be due to a rearrangement occurring before catalase activity is observed. The tripodal complex, $[Mn(L18)](ClO_4)_2$ is the only complex to show a catalase activity without added base, but with a long induction period. The results that are presented indicate that the axial ligands have an effect on both the rate of catalase activity and the observed induction period. The SOD results indicated that the complex, $[Mn(H_2L6)Cl(H_2O)]Cl{\cdot}H_2O$, derived from 2,6-diformylpyridine and 1-aminopropan-2-ol, shows the highest SOD activity amongst the complexes prepared, with a rate of $2.05x10^6$ $M^{-1}s^{-1}$ and the IC_{50} value of 0.78 μM. Most of the complexes showed SOD activity with a rate around 10^5-10^6 $M^{-1}s^{-1}$. The SOD results showed that the axial ligands have an effect on SOD activity; strongly bound ligands such as thiocyanate and azide generally result in lower SOD activity. Most of the complexes showed both SOD and catalase activity. Ring-contracted complexes, $[Mn(H_3L2)(NCS)_2]$ and $[Mn(H_3L3)(NCS)_2]$, show high rates of superoxide dismutase activity but possess limited catalase activity.

Acknowledgements

I would like to thank every person who has helped me to achieve my PhD at Loughborough University:

I would like to thank my supervisor, Prof. Vickie McKee for accepting me to her research group as a PhD student at Loughborough University and for guidance, support and enthusiasm during the study. I cannot thank you enough for all your support and encouragement throughout all the ups and downs of working in my PhD studies despite having your own work. I also thank Dr. Paul Lucas for allowing use of his UV instrument for biological testing and for helping calculations and equations. I would like to thank the Ministry of National Education of Turkey for funding this research.

Thank you to Mrs Pauline King who has provided support, advice and training during the study and for running the microanalysis for all of samples. I would like to thank EPSRC Swansea Laboratory for mass spectrometry. I wish also thank all other researches from the inorganic section, that is: Raf, Leanne, Anna, Chris, Simon, Tom, Rob, Endy, Jo, Rachel, Nuria, Rose, Neil, Dr. Kelly, Dr. Smith, Dr. Elsegood, Dr. Kirk, Dr. Dann (I hope I have not forgotten anyone). I would like to thank the technical service in the department, especially Dr. Mark Edgar, Sheena Grainger, Alistair Daley and Andy Kowalski. My special thanks go to Mr. Imdad Hussain for having joyful times in the lab.

I wish also thank to all my friends at Leicester University for very good moments, chats, laughs and gathering on Friday nights. I also thank to all chemistry lecturers at K.Maras Sutcuimam University for everything they taught me.

The biggest thanks go to my family who have always been a huge support thought my study and my personal life, I hope to repay somehow. I would also like to thank my fiancé and her family for their support.

Table of Contents

Title Page i

Abstract ii

Acknowledgements iv

Table of Contents v

Abbreviations x

Ligands referred to in the thesis xii

Chapter 1 Introduction 1

1.1 Introduction 2

1.2 Macrocyclic ligands 2

1.2.1 The chelate and macrocyclic effect 2

1.2.2 Coordination template effect 5

1.2.3 Hard/soft acid/base theory (HSAB) 6

1.2.4 Macrocyclic Schiff base compounds 7

1.3 Tripodal ligands 14

1.4 Superoxide and superoxide dismutase 18

1.4.1 Superoxide 18

1.4.2 SODs and their active metal centre structures 21

1.4.3 MnSOD model complexes 25

1.5 Catalase 30

1.6 Aims 36

Chapter 2 Mn(II) complexes containing pyridinediimine as a head unit; synthesis and characterisations 37

2.1 Introduction 38

2.2 Synthesis and characterisation 39

2.2.1 Oxidation of 2,6-pyridinedimethanol to 2,6-diformylpyridine (DFP) ... 39

2.2.2 Macrocyclic Ba(II) complex $[Ba(H_2L1)(ClO_4)]_2(ClO_4)_2$ (1) 41

2.2.3 Transmetallation reactions with Mn(II) 45

2.2.4 Ring-contracted mononuclear Mn(II) complexes $[Mn(H_3L2)(NCS)_2]$ (2) and $[Mn(H_3L3)(NCS)_2]$ (3) 46

2.2.5 The [4+4] ring-expanded polynuclear Mn(II) complexes; $[Mn_4(H_2L^*)Cl_4][MnCl_4]$ (4) and $[Mn_4(H_2L^*)(N_3)_4](ClO_4)_2$ (4a) 51

2.2.6 Comparison with macrocyclic Mn(II) complexes derived from 2,6-diacetylpyridine (DAP) analogues 60
2.2.7 The mononuclear [1+1] macrocyclic complex [Mn(L4)$(NCS)_2$] (5) 69
2.2.8 Mn(II) complexes of acyclic ligands 73
2.2.9 The ligand H_2L_4 (6) 74
2.2.10 [Mn(H_2L4)Cl_2] (7), [Mn_2(H_2L4)$_2$$(NCS)_4$] (8) and [Mn($H_2L_4$)$_2$$(N_3)_3$Cl] (9) 77
2.2.11 [Mn(L5)$(NCS)_2$] (10), [Mn(L5)$(N_3)_2$]·MeOH (11) and [Mn(L5)Cl_2] (12) 86
2.2.12 [Mn(H_2L6)$(N_3)_2$] (13), [Mn(H_2L6)Cl(H_2O)]Cl·(H_2O) (14) and [Mn_2(H_2L6)$(NCS)_2$] (15) 92
2.2.13 [Mn(H_2L7)$(NCS)_2$] (16) and [Mn(H_2L7)Cl_2(H_2O)]·H_2O (17) 95
2.2.14 [Mn(H_2L8)$(NCS)_2$] (18) 101
2.2.15 Ligands H_2L9 (19) and H_2L10 (20) 105
2.2.16 [Mn(H_2L9)Cl_2]·MeOH (19a) 109
2.2.17 [Mn_3(L9)$_2$$(OAc)_2$$(MeOH)_2$]·2MeOH (21) 112
2.2.18 [Mn_2Ca(L9)$_2$$(OAc)_2$$(MeOH)_2$]·2MeOH (22) 116
2.2.19 [Mn(H_2L10)$(NCS)_2$]·H_2O (23) and [Mn(H_2L10)$(N_3)_2$] (24) 120

Chapter 3 Manganese complexes of tripodal Schiff bases and N-alkylated benzimidazoles 122

3.1 Introduction 123
3.1.1 Organic synthesis 123
3.1.2 Characterisation of 2-bromoethylphthalimide (25) and 3-bromopropyl-phthalimide (26) 124
3.1.3 Characterisation of (27a) and (27b) 125
3.1.4 Characterisation of (28), (29) and (30) 126
3.1.5 Characterisation of BAEP·4HCl (31), ABAP·4HCl (32) and TRPN·4HCl (33) 126
3.1.6 Characterisation of Schiff base ligands with salicylaldehyde, H_3L13 (34), H_3L14 (35), H_3L12 (36) and H_3L11 (37) 127
3.1.7 Characterisation of Mn(III) complexes, [Mn(L11)] (38), [Mn(L12)] (39) and [Mn(L13)] (40) 129
3.1.8 Characterisation of Mn(II) complexes [Mn(L15)]$(ClO_4)_2$ (41), [Mn(L18)]$(ClO_4)_2$ (42), [Mn(L16)]$(ClO_4)_2$ (43) and [Mn(L17)]$(ClO_4)_2$ (44) derived from tripodal amines and 2-pyridinecarboxaldehyde 132

3.2 Characterisation of a pyridinebenzimidazole ligand and its Mn(II) complexes 136
3.2.1 The ligand L19 136
3.2.2 Mn(II) complexes of L19; $[Mn(L19)Cl_2]$ (47), $[Mn(L19)(NCS)_2]$ (48), $[Mn(L19)_2](ClO_4)_2$ (49), $[Mn(L19)(NO_3)_2]$ (50) and $[Mn(L19)_2](PF_6)_2$ (51) 139
3.2.3 Crystal structures of $[Mn(L19)Cl_2]$ (47) and $[Mn(L19)(NCS)_2]$ (48) 141
3.2.4 Crystal structure of $[Mn(L19)(NO_3)_2]$ (50) 145
3.2.5 Crystal structure of $[Mn(L19)_2](ClO_4)_2$ (49) 148

Chapter 4 Catalytic studies 151
4.1 Introduction 152
4.2 Catalase activity of complexes 152
4.2.1 Catalase activity of macrocyclic complexes 155
4.2.2 Catalase activity of acyclic Mn(II) complexes 160
4.2.3 Catalase activity of Mn(II) complexes of H_2L9 and H_2L10 163
4.2.4 Catalase activity of tripodal ligand complexes 166
4.2.5 Catalase activity of Mn(II) complexes of L19 170
4.2.6 Conclusions for catalase activity 173
4.3 SOD Activity 175
4.4 Measuring SOD activity 175
4.4.1 Direct analysis 175
4.4.2 Indirect analysis 177
4.5 SOD activity results&discussion 179
4.5.1 SOD activity of macrocyclic complexes 184
4.5.2 SOD activity of acyclic Mn(II) complexes 187
4.5.3 SOD activity of Mn(II) complexes of H_2L9 and H_2L10 189
4.5.4 SOD activity of tripodal ligand complexes 191
4.5.5 SOD activity of Mn(II) complexes of L19 192
4.5.6 Conclusions for SOD activity 193
Conclusions 194
Further Work 197

Chapter 5 Experimental 198
5.1 General conditions 199
5.1.1 Solvents and reagents 199
5.1.2 Physical measurements 199
5.1.3 Preparation of activated manganese dioxide 200
5.1.4 Preparation of 2,6-diformylpyridine (DFP) 200
5.1.5 Preparation of macrocyclic complexes 201
5.1.6 Preparation of $[Ba(H_2L1)(ClO_4)]_2(ClO_4)_2$ (1) 201
5.1.7 Preparation of $[Mn(H_3L2)(NCS)_2]$ (2) 202
5.1.8 Preparation of $[Mn(H_3L3)(NCS)_2]$ (3) 203
5.1.9 Preparation of $[Mn_4(H_2L^*)Cl_4][MnCl_4]$ (4) 204
5.1.10 Preparation of $[Mn(L4)(NCS)_2]$ (5) 205
5.1.11 Preparation of acyclic complexes 206
5.1.12 Preparation of (H_2L4) (6) 206
5.1.13 Preparation of $[Mn(H_2L4)Cl_2]$ (7) 207
5.1.14 Preparation of $[Mn_2(H_2L4)_2(NCS)_4]$ (8) 208
5.1.15 Preparation of $[Mn_2(H_2L4)_2(N_3)_3Cl]$ (9) 209
5.1.16 Preparation of $[Mn(L5)(NCS)_2]$ (10) 210
5.1.17 Preparation of $[Mn(L5)(N_3)_2]$ (11) 211
5.1.18 Preparation of $[Mn(L5)Cl_2]$ (12) 212
5.1.19 Preparation of $[Mn_2(H_2L6)_2(N_3)_4]$ (13) 213
5.1.20 Preparation of $[Mn(H_2L6)Cl(H_2O)]Cl\cdot H_2O$ (14) 214
5.1.21 Preparation of $[Mn(H_2L6)(NCS)_2]$ (15) 215
5.1.22 Preparation of $[Mn(H_2L7)(NCS)_2]$ (16) 216
5.1.23 Preparation of $[Mn(H_2L7)Cl_2(H_2O)]\cdot H_2O$ (17) 217
5.1.24 Preparation of $[Mn(H_2L8)(NCS)_2]$ (18) 218
5.1.25 Preparation of $[H_2L9]$ (19) 219
5.1.26 Preparation of $[H_2L10]$ (20) 220
5.1.27 Preparation of $[Mn_3(L9)_2(OAc)_2(MeOH)_2]\cdot 2MeOH$ (21) 221
5.1.28 Preparation of $[Mn_2Ca(L9)_2(OAc)_2(MeOH)_2]\cdot 2MeOH$ (22) 222
5.1.29 Preparation of $[Mn(H_2L10)(NCS)_2]$ (23) 223
5.1.30 Preparation of $[Mn(H_2L10)(N_3)_2]$ (24) 224
5.2 Preparation of tripodal ligands and their metal complexes 225
5.2.1 Organic synthesis 225

5.2.2 Preparation of compounds N-(2-bromoethyl)phthalimide (25) and N-(3-bromopropyl)phthalimide (26) 225
5.2.3 Preparation of compounds 2,2'-Diphthalimidoethylamine (27a) and 3,3'-Diphthalimidopropylamine (27b) 227
5.2.4 Preparation of compounds 2,2',3-triphthalimidoethylpropylamine (28) , 3,3',2-triphthalimidopropylethylamine (29) and 3,3',3-triphthalimidopropylamine (30) 229
5.2.5 Preparation of compounds BAEP.4HCl (31), ABAP.4HCl (32) and TRPN.4HCl (33) 231
5.2.6 Preparation of tripodal ligands H_3L12, H_3L13 and H_3L14 233
5.2.7 Preparation of H_3L12 (34) 233
5.2.8 Preparation of H_3L13 (35) and H_3L14 (36) 234
5.2.9 Preparation of compound H_3L11 (H_3Saltren)[188] (37) 235
5.2.10 Preparation of [Mn(L11)] (38) 236
5.2.11 Preparation of Mn(III) complexes (39)-(40) 236
5.2.12 Preparation of [Mn(L12)] (39) and [Mn(L13)] (40) 236
5.2.13 Preparation of L15 ligand 238
5.2.14 Preparation of $[Mn(L15)](ClO_4)_2$ (41) 238
5.2.15 Preparation of L16, L17, L18 and their Mn(II) complexes 239
5.2.16 Preparation of $[Mn(L18)](ClO_4)_2$ (42) 239
5.2.17 Preparation of $[Mn(L16](ClO_4)_2$ (43) and $[Mn(L17)] (ClO_4)_2$ (44) 240
5.3 Preparation of N-alkylated benzimidazole ligand (L19) 241
5.3.1 2,6-Bis(benzimidazol-2'-yl)pyridine (BBP) (45) 241
5.3.2 2,6-Bis(1-butyl-1H-benzo[d]imidazol-2'-yl)pyridine (L19) (46) 242
5.3.3 Preparation of metal complexes of L19 243
5.3.4 $[Mn(L19)Cl_2]$ (47) 243
5.3.5 $[Mn(L19)(NCS)_2]$ (48) 244
5.3.6 $[Mn(L19)](ClO_4)_2$ (49) 244
5.3.7 $[Mn(L19)(NO_3)_2]$ (50) 245
5.3.8 $[Mn(L19)_2](PF_6)_2$ (51) 245
References 246
Appendix 1 257
Appendix 2 259

Abbreviations

χ:	absolute electronegativity, Pearson scale
λ:	absolute hardness, Pearson scale
μ:	micro 10^{-6}
σ:	softness, Pearson scale
υ:	stretching frequency
δ:	chemical shift in ppm
°:	degrees
Å:	angstrom unit 10^{-10} meter
Abap:	2-aminoethylbis(3-aminopropyl)amine
Baep:	3-aminopropylbis(2-aminoethyl)amine
BBP:	2,6-Bis(benzimidazol-2'-yl)pyridine
benzimpn:	N,N,N`,N`-tetrakis(2-ethylenebenzamidazaly)-1,3-diamino-dipropan-2-ol
bpia:	bis-(picolyl)(N-methylimidazol-2-yl)amine
°C:	degrees centigrade
cm^{-1}:	wavenumber
CSD:	Cambridge structural database
Cyclam:	1,4,8,11-tetraazacyclopentadecane
d:	doublet
DAP:	2,6-diacetylpyridine
DFP:	2,6-diformylpyridine
dmf:	dimethyformamide
dmso:	dimethylsulfoxide
ESI-MS:	electrospray ionisation mass spectrometry
et al.	and others
EtOH:	ethanol
FAB:	fast atom bombardment
g:	gram(s)
hr:	hour
hrs:	hours
HSAB:	Hard Soft Acid Base
IC_{50}:	half maximal inhibitory concentration

IR:	infra-red
L:	litre
logK:	log of formation constant
M:	molar
m:	multiplet
MeOH:	methanol
ml:	millilitre
mmol:	millimole
Mol:	mole
m/z:	mass-to-charge ratio
N_A:	avagadro`s number
NBT:	tetra blue tetrazolium
NMR:	nuclear magnetic resonance
PDB:	Protein Data Base
ppm:	part per million
q	quintet
OEC:	oxygen evolving complex
RMM:	relative molecular mass
ROS:	reactive oxygen species
s:	singlet
Salen:	*N*,*N'*-ethylenebis(salicylideneiminate)
Salpn:	*N*,*N'*-bis(salicylidene)-1,3-diaminopropane
SOD:	superoxide dismutase
T:	temperature
TLC:	thin layer chromatography
THF:	tetrahydrofuran
Tren:	tris(2-aminoethyl)amine
Trpn:	tris(3-aminopropyl)amine
WST-1:	2-(4-iodophenyl)-5-(2,4-disulfophenyl)-2*H*-tetrazolium

Ligands referred to in the thesis

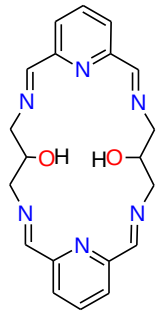

H_2L1

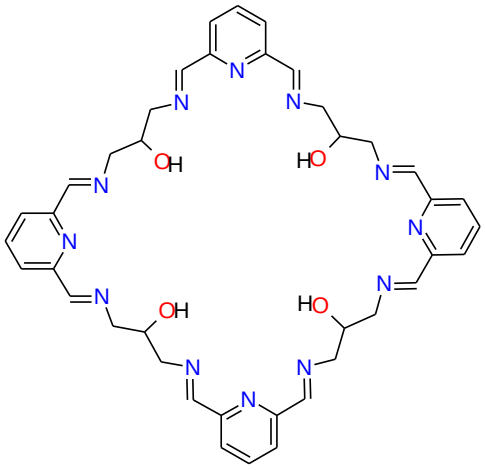

H_4L^*

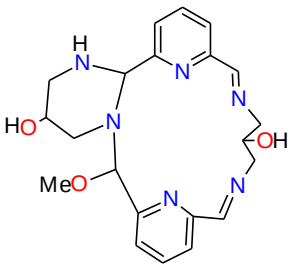

H_3L2

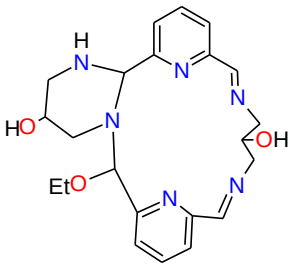

H_3L3

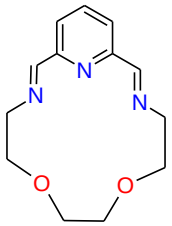

$L4$

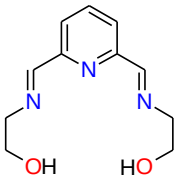

H_2L4

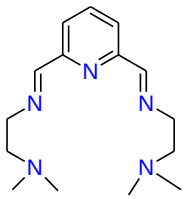

$L5$

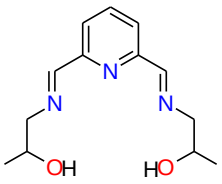

H_2L6

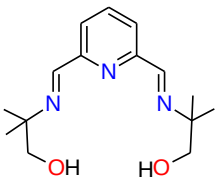

H_2L7

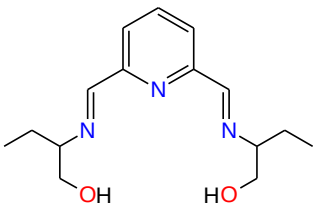

H_2L8

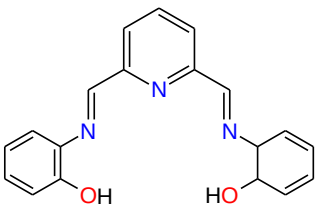

H_2L9

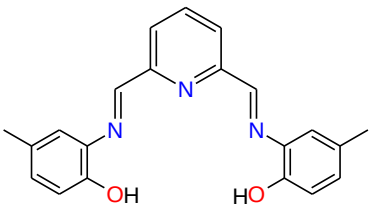

H_2L10

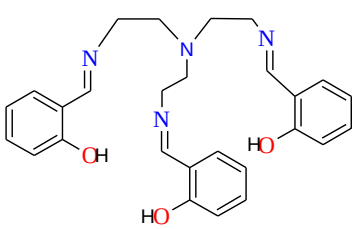

H_3L11

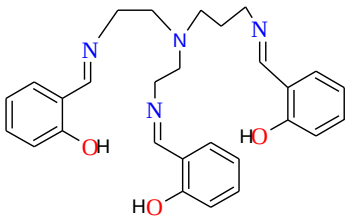

H_3L12

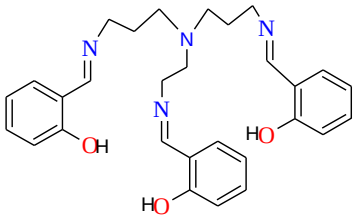

H_3L13

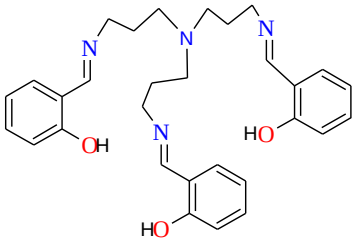

H_3L14

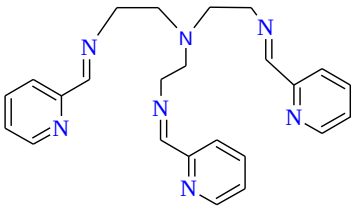

L15

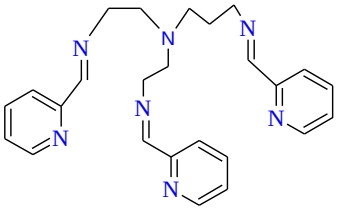

L16

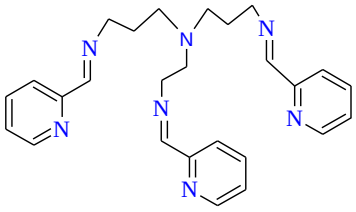

L17

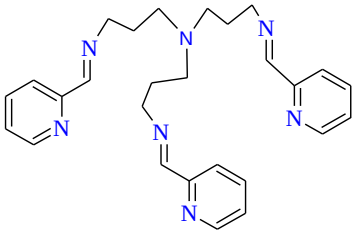

L18

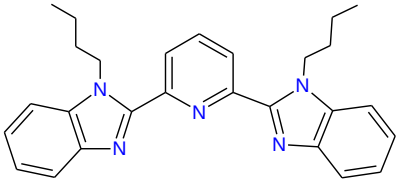

L19

Chapter 1

Introduction

1.1 Introduction

1.2 Macrocyclic ligands

Macrocyclic ligands have been of interest for many years due to their role in understanding molecular processes in biochemistry, materials science, catalysis, transport and so on.[1-3] A number of macrocyclic ligands have been prepared to mimic the catalytic activity of metalloenzymes and proteins. Macrocyclic ligands and complexes are widespread in biology and there is no doubt that life could not exist in the absence of such molecules. Macrocyclic ligands based upon the porphyrin ring system and close structural relations such as chlorophylls and corrins are ubiquitous, iron complexes of these ligands are involved in processes as divergent as electron transport, dioxygen storage and enzymic catalysis. Investigations of spectral, electrochemical, structural, kinetic and thermodynamic aspects of macrocyclic complex formation have all received considerable attention.[4,5]

Macrocyclic ligands are polydentate ligands which contain their donor atoms either incorporated in or, less commonly, attached to a cyclic backbone. As generally defined, they contain at least three donor atoms and the macrocyclic ring should consist of a minimum of nine atoms.[6] Macrocycles are versatile ligands that form well-defined complexes with a wide range of metal ions. The coordination behaviour of macrocycles is no different in principle from that of open-chain polydentate ligands, although in practice, the unusual and often unexpected properties of the systems justify their being given special treatment.

1.2.1 The chelate and macrocyclic effect

The term chelate, meaning the great claw or chela (chely- Greek) of the lobster or other crustaceans was first introduced by Morgan and Drew[7] in 1920 for the metal-organic or inorganic systems in which calliper groups bind the central metal to produce heterocyclic rings. The resulting complex has greater stability than an analogous complex with monodentate donors.[8,9] Macrocyclic complexes are thermodynamically and kinetically more stable than equivalent complexes with non-cyclic ligands.[10,11] The macrocyclic effect means the greater kinetic and thermodynamic stability of a complex with a cyclic polydentate ligand in comparison to the complex formed by a comparable noncyclic ligand. Cabbiness and Margerum[12,13] reported that the Cu(II) complex with cyclic compound

meso-5,7,7,12,14,14-hexamethyl-1,4,8-11-tetraazacyclotetradecane (tet a) has logK 4.1 higher than the complex with a non-cyclic ligand having a similar sequence of chelate rings (Figure 1-1). Thermodynamic stability of macrocyclic complexes has both enthalpic and entropic contributions.[14-18] The relative importance of these two contributions varies from case to case.

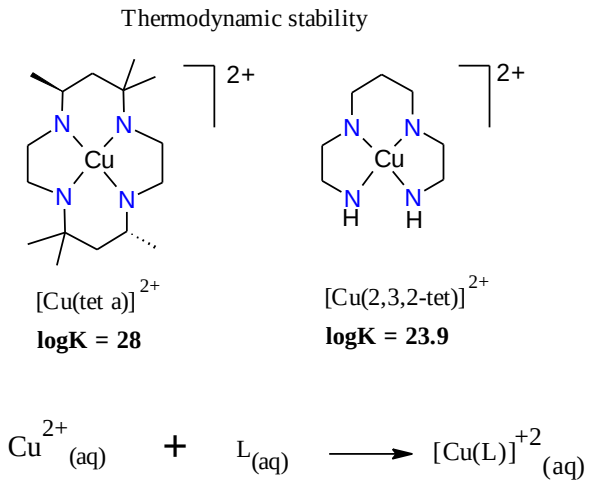

Figure 1-1 Thermodynamic stability of cyclic and nocyclic Cu(II) complexes.

The enthalpy term can be either favourable or unfavourable for the complexation of a macrocycle. The enthalpic contributions are related to a number of factors (e.g. solvation, geometry, strength of metal-ligand bond, sizes of the metal ion and macrocycle etc). The single most important factor seems to be the relative sizes of the metal ion and the macrocyclic cavity. The Cu(II) ion forms more stable complexes with macrocylic cyclam ligand than Ni(II) and Zn(II) ions as a result of better fit between the cation size and macrocycle hole (Figure 1-2).

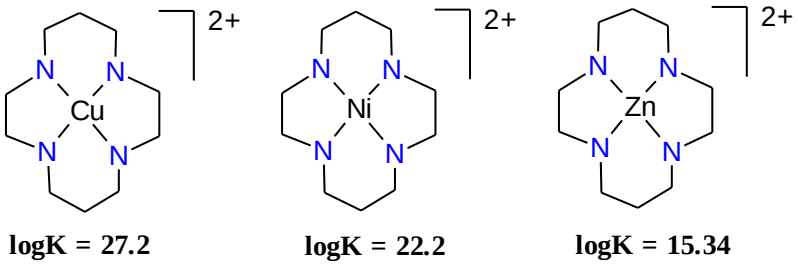

Figure 1-2 Stability of $[M(cyclam)]^{2+}$ complexes (where M=Cu, Ni, Zn).

The entropic contribution refers to less conformational flexibility of the macrocyclic ligand. Due to less flexibility, macrocyclic ligands lose fewer degrees of freedom when making a metal complex. The macrocyclic molecule is already pre-organised for complexation and requires less energy for conformational changes prior to binding to metal ions. Therefore the entropy contribution always favours formation of a macrocyclic complex over formation of an equivalent non-macrocyclic complex.

Macrocyclic complexes are also kinetically more stable than the open chain analogs. The dissociation rate of macrocyclic complexes is much slower than the open noncyclic complex. The acid dissociation rate of $[Cu(tet\ a)]^{2+}$ is found to be $3.6x10^{-7}$ s^{-1} whereas the open chain analog $[Cu(2,3,2\text{-tet})]^{2+}$ is 4.1 s^{-1} (Figure 1-3). The $[Cu(tet\ a)]^{2+}$ complex does not have any terminal donors to start dissociation, therefore the complex needs to fold before all bonds must break more or less together so the process has a higher activation energy than for the open chain ligand.

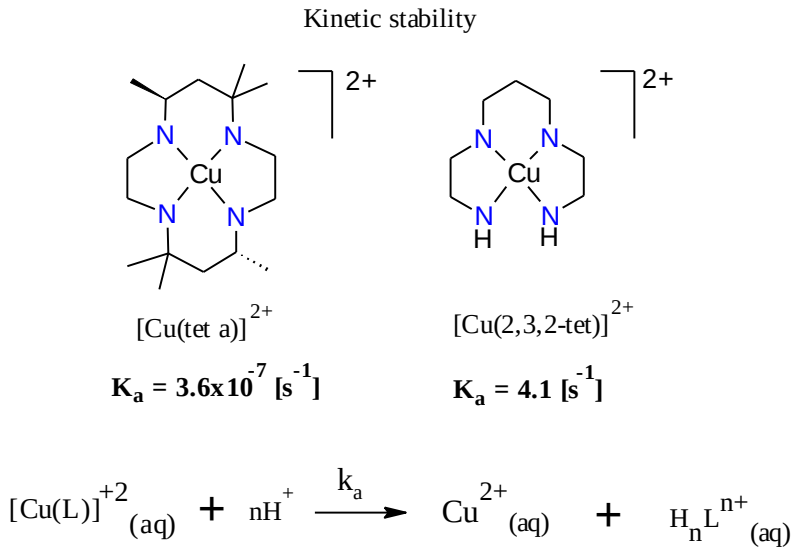

Figure 1-3 Kinetic stability of the macrocyclic and acyclic complex.

1.2.2 Coordination template effect

The coordination template effect is an effect in which a metal ion in a template reaction directs the cyclisation of a ligand. Metal ions bind to the donor atoms and organize the intermediates into the conformation that is required to access the desired cyclic product. Template reactions allow a greater control over the final conformation of the product due to the pre-organisation of the ligand around the metal centre (Figure 1-4).

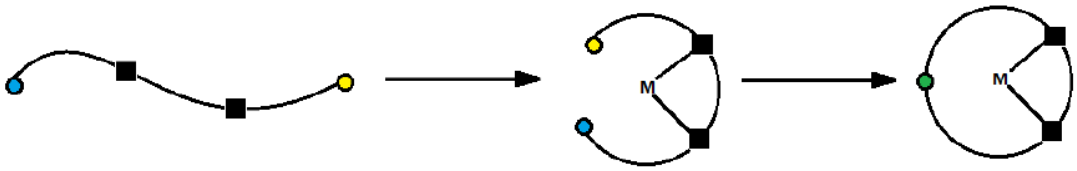

Figure 1-4 Pre-organisation during the cyclisation of a template reaction.

Thompson and Busch first reported this phenomenon in the 1960s.[19-24] They identified products obtained by the reaction of α-diketones with β-mercaptoethylamine in the presence and absence of a metal ion. An example of the template effect is shown in Figure 1-5. The reaction of biacetyl (MeCOCOMe) with $H_2NCH_2CH_2SH$ produces the cyclic product (a) as major product along with polymeric species in the absence of a metal template ion. However, when the biacetyl is reacted with the Ni(II) complex of $H_2NCH_2CH_2SH$, or Ni(II) salts are reacted with the cyclic product (a), the Ni(II) complex (b) is obtained.

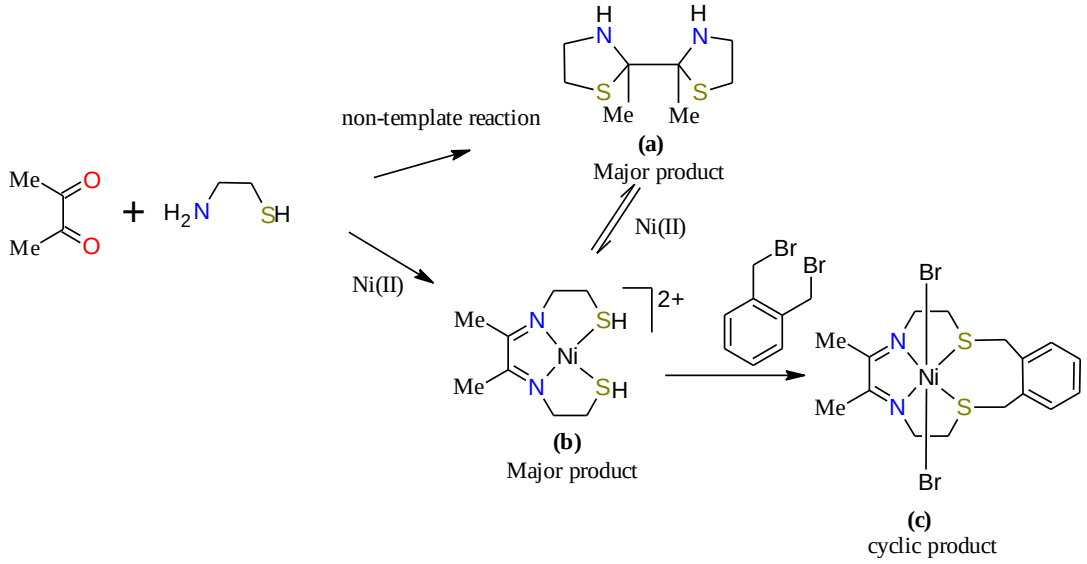

Figure 1-5 Synthesis of a Ni(II) macrocyclic complex via a template reaction.[22]

Thompson and Busch pointed out that the role of the template metal ion[21] was split into two parts, thermodynamic (or equilibrium) and kinetic template effect. The thermodynamic (or equilibrium) template effect is an effect where a metal ion coordinates to one component of a mixture, shifting the equilibrium in favour of production of a metal complex. The second class of template effect is the kinetic template effect. It involves coordination of reactive groups to a metal ion which promotes formation of cyclic product. The function of a metal ion is to arrange the reactants in a specific stereochemistry in which the cyclisation is favoured. In the kinetic effect, the cyclic product cannot be formed from the same reactants in the absence of a metal template ion. The reaction illustrated in Figure 1-5 is an example of kinetic template effect.[24] The Ni(II) ion stabilises the acyclic intermediate as a complex cation and prevents attack of the thiol group upon the imine carbon atoms to give cyclic product (a). When Ni(II) coordinates to the intermediate product, the nucleophilicity of the –SH groups are reduced as they are bonded to the electropositive metal centre and the thiolate groups are restrained so that they cannot access the imine bonds. The Ni(II) ion also arranges two thiolate groups in the correct orientation for reaction with 1,2-bis(bromoethy)benzene to give macrocyclic product (c).

1.2.3 Hard/soft acid/base theory (HSAB)

The hard/soft acid/base concept was introduced by Pearson and Songstad in the early 1960s as an extension to the Lewis acid-base theory.[24-27] Soft bases are of high polarizability or low electronegativity which can be oxidised easily and hard bases are of low polarizability, high electronegativity, hard to oxidise and have high energy empty orbitals. Soft acids have a low positive charge, large size with several easily excited outer electrons. The hard acids are of a large positive charge, small size and do not have easily excited outer electrons.[28]

According to HSAB theory, hard acids bind strongly to hard bases and soft acids bind strongly to soft bases. In 1983, Pearson converted qualitative definition of HSAB by using the idea of polarizability. The electronic properties of the atoms involved in a donor-acceptor interaction correlate to their hardness by equations[27]: $\chi = (I + A)/2$, $\eta = (I - A)/2$ and $\sigma = 1/\eta$ where I: ionisation potential, A: electron affinity, χ: absolute

electronegativity, η: absolute hardness and σ: softness. The classification of acids is shown in Table 1-1.

Table 1-1 Classification of hard acids and bases.

	Acids	Bases
Hard	H^+, Li^+, Na^+, K^+, Be^{2+}, Mg^{2+}, Ca^{2+}, Sr^{2+}, Sn^{2+}, Al^{3+}, Ga^{3+}, Se^{3+}, In^{3+}, Cr^{3+}, Co^{3+}, Fe^{3+}, Ir^{3+}, La^{3+}, Si^{4+}, Ti^{4+}, Zr^{4+}, Th^{4+}, VO^{2+}, UO_2^{2+}, $BeMe_2$, BF_3, BCl_3, $B(OR)_3$, $AlMe_3$, $InMe_3$, RPO_2^+, $ROPO_2^+$, RSO_2^+, $ROSO_2^+$, SO_3, R_3C^+, RCO^+, CO_2, NC^+	H_2O, OH^-, F^-, $CH_3CO_2^-$, PO_4^{3-}, SO_4^{2-}, CO_3^{2-}, NO_3^-, ClO_4^-, ROH, RO^-, R_2O, NH_3, RNH_2, N_2H_4
Soft	Cu^+, Ag^+, Au^+, Hg^+, Cs^+, Tl^+, Hg^{2+}, Pd^{2+}, Cd^{2+}, Pt^{2+}, Metal atoms in zero oxidation states	RSH, RS^-, R_2S, I^-, CN^-, SCN^-, $S_2O_3^{2-}$, Br^-, R_3P, R_3As $(RO)_3P$, RNC, CO, C_2H_4, C_6H_6, R^-, H^-
Borderline	Fe^{2+}, Co^{2+}, Ni^{2+}, Cu^{2+}, Zn^{2+}, Pb^{2+}, $B(CH_3)_3$, SO_2, NO^+, HX (hydrogen bonding molecules)	Aniline, pyridine, N_3^-, Cl^-, NO_2^-, SO_3^{2-}

HSAB theory is one of the cornerstones of coordination complex design and choosing appropriate metals and ligands that are likely to form stable complexes. It allows prediction of complexation preferences for ligands containing certain donor groups or design of macrocyclic or acyclic ligands for selective binding of metal ions.

1.2.4 Macrocyclic Schiff base compounds

Compounds containing imine (-C=N-) bond are called Schiff bases. They are named after Hugo Schiff who discovered them in 1854[29] and were first used as ligands by Pfeiffer in the 1930s.[30] Schiff bases can be obtained by nucleophilic addition of the primary amines to aldehydes or ketones (Figure 1-6).

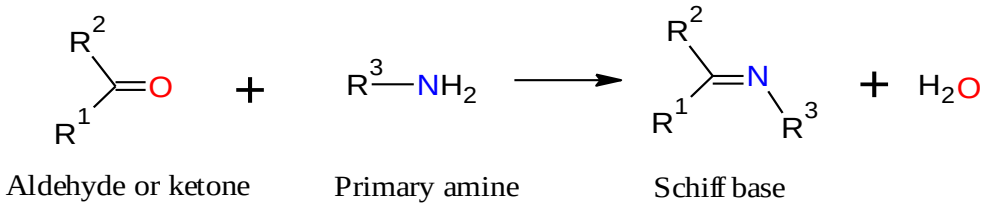

Figure 1-6 Formation of Schiff bases.[31]

Schiff bases are of great importance in the coordination chemistry of transition metals. Imines are medium-soft donors and they can form stable complexes with transition metals. Macrocyclic Schiff bases have a great interest because of their potential role in biochemistry, catalysis, encapsulation, activation, transport and separation.[32-36] Many Schiff base cyclic ligands have been studied intensively for different reasons such as: simplicity of their preparation, the fact that they can exist with additional donor groups (O, P, S). Schiff base acyclic and cyclic ligands and template synthesis of their complexes are well reviewed in the literature.[8,37-46]

In the 1960s, Neil Curtis reported the first macrocyclic Schiff base complex formed from the aldol condensation between $[Ni(en)_3]^{2+}$ and acetone.[47] Initially, Curtis proposed the yellow crystals obtained to be the square planar bis-(diimine) complex. A stability study showed that the compound is stable in boiling concentrated acids and alkalis. The structure of the macrocyclic compound was later elucidated and is shown in Figure 1-7. The macrocyclic compound contains two amines and two imines connected by two three-carbon bridges and two two-carbon bridges. The *trans* macrocycle, where two imines are diagonally opposite, was found to be the major product and the *cis* macrocycle was the minor product.[48-50]

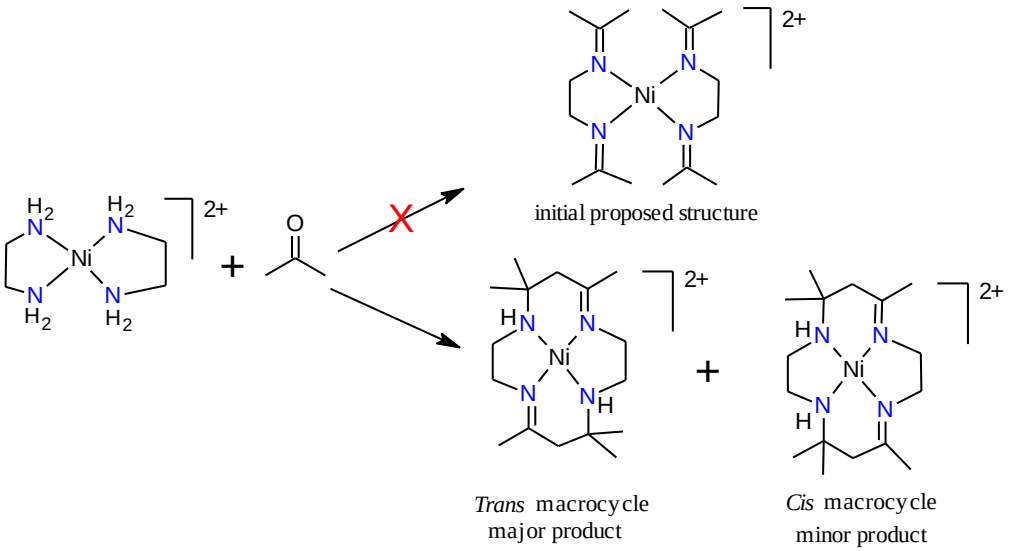

Figure 1-7 Synthesis of the first macrocyclic Schiff base ligand.[47]

Preparation of cyclic Schiff bases can be rather difficult; different condensation products (polymeric or oligomeric in nature) may result when di- or poly-functional precursors are used. This will require further steps to purify the desired macrocyclic

product and reduces the yield. To overcome this problem, high dilution conditions may be used; in which a large amount of solvent reduces the chances of cross reactions. An alternative way to avoid cross reactions is to use a metal ion in a template reaction.[37,38] High dilution is not always necessary for the preparation of Schiff base cyclic ligands. For example, a [2+3] macrobicycle can be prepared in good yield and purity by directly mixing three equivalents of 1,3-dibenzaldehyde and two equivalents of tren in refluxing methanol (Figure 1-8).[51]

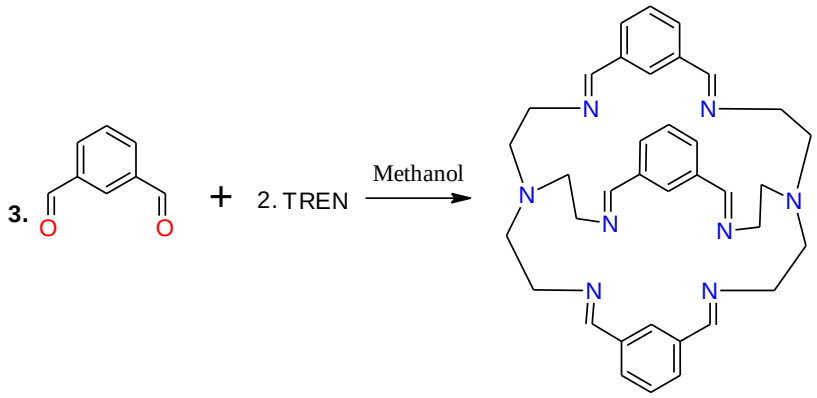

Figure 1-8 Synthesis of macro-bicyclic ligand.[51]

Schiff base condensation reactions with metal template ions are one of the most common methods to prepare macrocyclic systems. An example of a Schiff base template reaction is shown in Figure 1-9.[52-54]

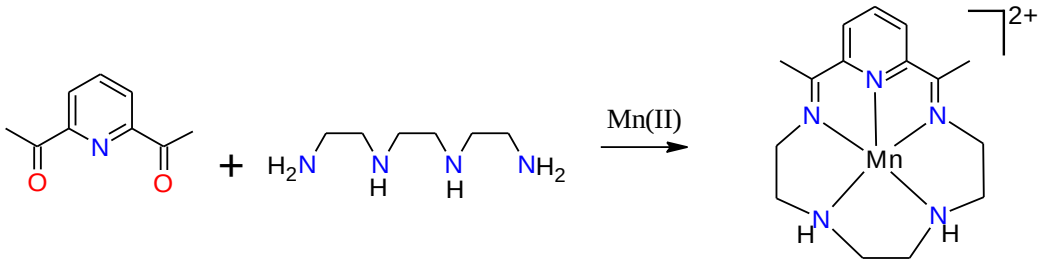

Figure 1-9 Template synthesis.[52-54]

Many metal complexes of macrocycles derived from dicarbonylpyridines and diprimary amines have been studied in detail.[55-67] Some interesting structures and behaviours of complexes and the mechanism of template synthesis of complexes of Schiff bases have been presented. Figure 1-10 shows some of the Schiff base condensation macrocyclic species formed from appropriate diamines and dicarbonyls.[44]

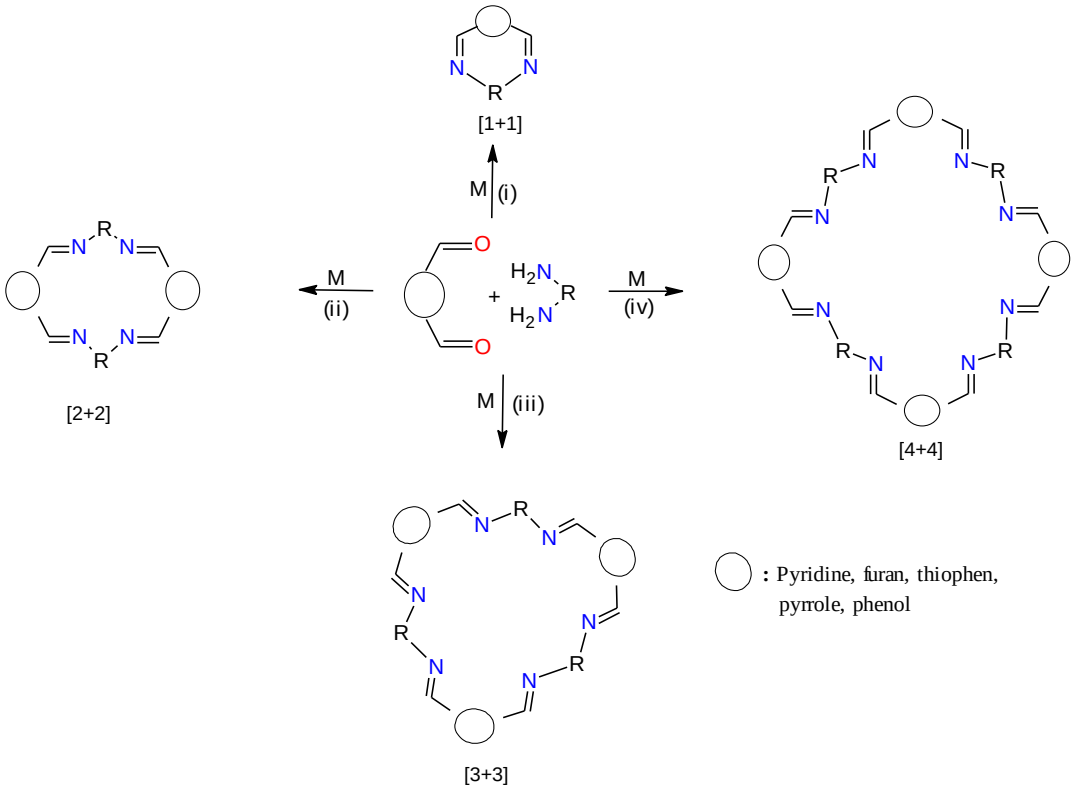

Figure 1-10 Macrocyclic species from diamine and dicarbonyl head units.[44]

In Figure 1-10, the [1+1] macrocycle is the condensation product of one molecule of dicarbonyl compound and one molecule of diamine. If two molecules of each component condense together the [2+2] macrocyle is formed and so on.

When designing the synthesis of a macrocyclic complex *via* template reactions, the size of the metal ion used as the template should be taken into account because not all metal ions will fit into a specific macrocyclic cavity.[68-70] The importance of the size of the cation in directing the synthetic pathway is shown with the following example. Schiff base condensation products of 2,6-diacetypyridine with respectively 1,8-diamino-3,6-dioxaoctane or 1,11-diamino-3,7,9-trioxadecane in the presence of alkaline earth metal cations are shown Figure 1-11. Only Mg(II) produces the [1+1] N_3O_2 macrocycle, yet, Mg(II) does not generate the [1+1] N_3O_3 macrocycle. The [1+1] N_3O_3 can be generated when larger cations are used as the template (calcium, strontium, barium and lead(II)). These larger cations also generate the [2+2] N_6O_4 macrocycle derivatives.[71,72]

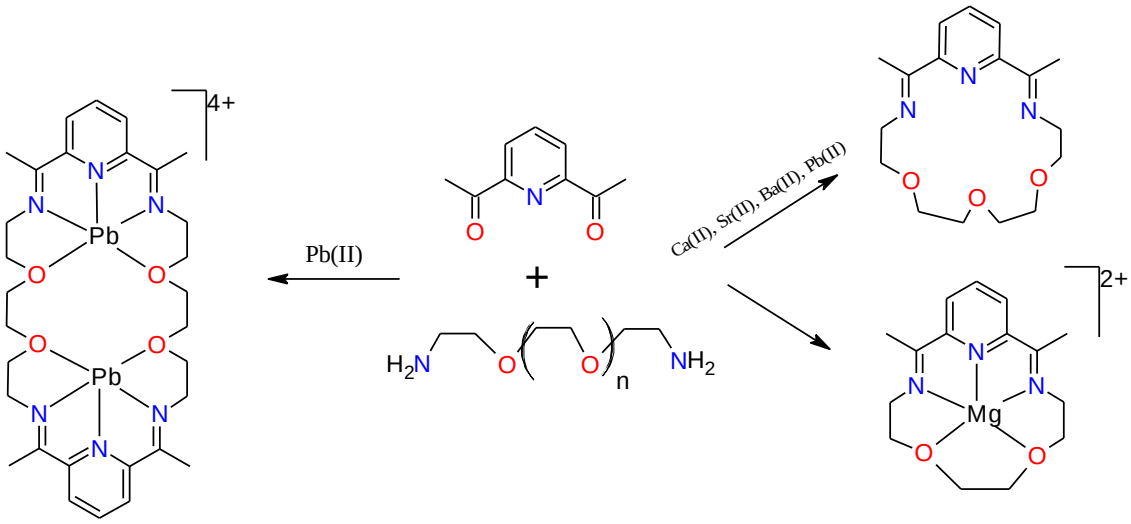

Figure 1-11 Formations of [1+1] and [2+2] macrocycles.

A mechanism for the formation of [1+1] and [2+2] macrocyles was proposed by Nelson and is shown in Figure 1-12**.** The initial product of the Schiff base condensation was proposed to be a mono-carbonyl mono-amine intermediate. This initial intermediate may undergo intramolecular condensation to give the [1+1] macrocycle (step ii) or an intermolecular condensation (steps iii, iv) and ring-closure to give the [2+2] ring (steps v, vi).

Nelson *et al.* also pointed out the formation of [1+1] and [2+2] macrocycles depends on a number of factors.[71]

- If the length of the diamine chain is insufficient to link two carbonyl groups, formation of the [1+1] macrocycle is not favoured.
- If the size of metal ion is large in relation to the size of the [1+1] macrocycle, the formation of the [2+2] macrocycle is favoured.

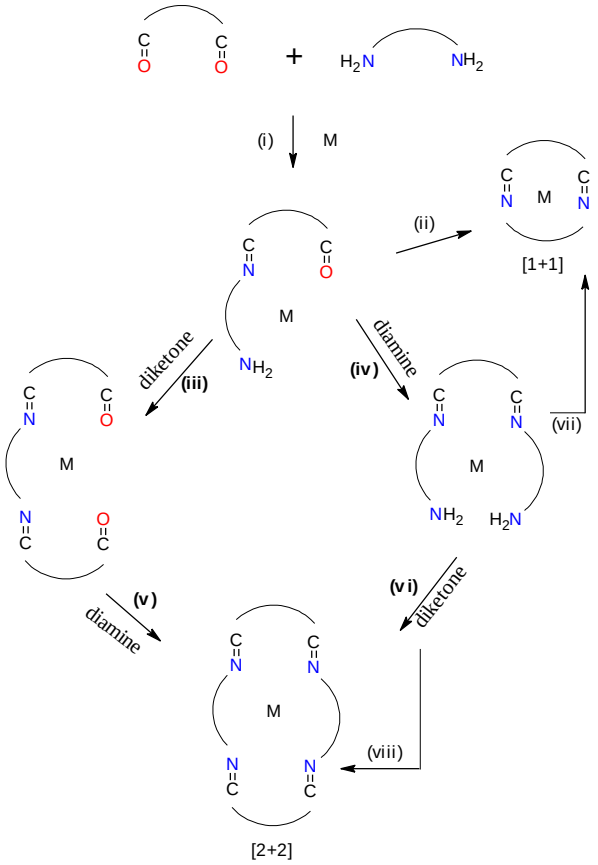

Figure 1-12 Mechanism for formation of the [2+2] and [1+1] macrocycles.[71]

Macrocyclic complexes prepared in the presence of a metal ion can undergo transmetallation reactions when treated with different metal salts; these methods allow the formation of the specific systems which are not accessible in any other methods. An example of transmetallation of barium(II) with copper(II) is shown in Figure 1-13.[73]

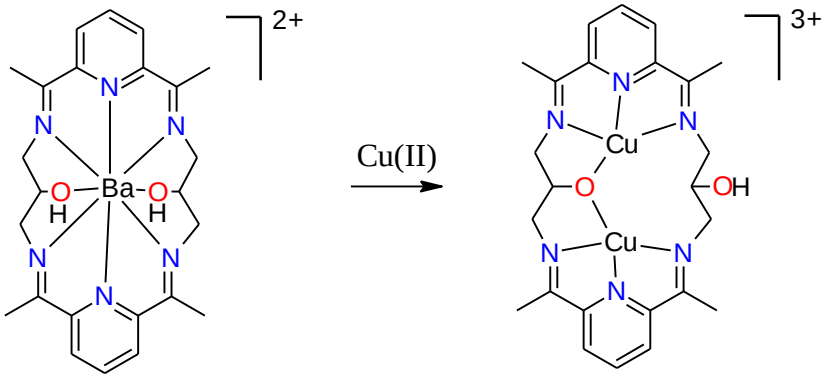

Figure 1-13 Transmetallation of barium(II) with copper(II) in a macrocyclic complex.[73]

During the template or transmetallation reactions, ring-contractions may occur when there is a functional group such as –OH or –NH available for addition to the imine bond and/or if there is a mismatch in size for the metal and macrocyclic cavity.[32] Several Schiff base macrocycles have been shown to undergo ring-contractions due to nucleophilic addition of a secondary amine across an adjacent imine bond.[74-78] One example of ring-contraction is shown in Figure 1-14.[79] The ring-contracted macrocycle (H_2D) illustrated in Figure 1-14 can be obtained by the reaction of 2,6-diacetylpyridine and diethylenetriamine in refluxing methanol solution in the presence of Ba(II), Sr(II) or Ca(II). When the ring-contracted Sr(II) complex $[Sr(H_2D)](ClO_4)_2$ is treated with two equivalents of $AgClO_4$, the dinuclear Ag(I) complex $[Ag_2(H_2E)](ClO_4)_2$ is obtained where a ring-expansion of the coordinated macrocycle has occured. Conversion of H_2D to H_2E macrocycle on exchange of the coordinated metal ions was found to be reversible; treatment of the complex $[Ag_2(H_2E)](ClO_4)_2$ with $BaCl_2$ in methanol resulted in the barium complex $[Ba(H_2D)](ClO_4)_2$, identical in properties to the complex prepared *via* the template method.[79]

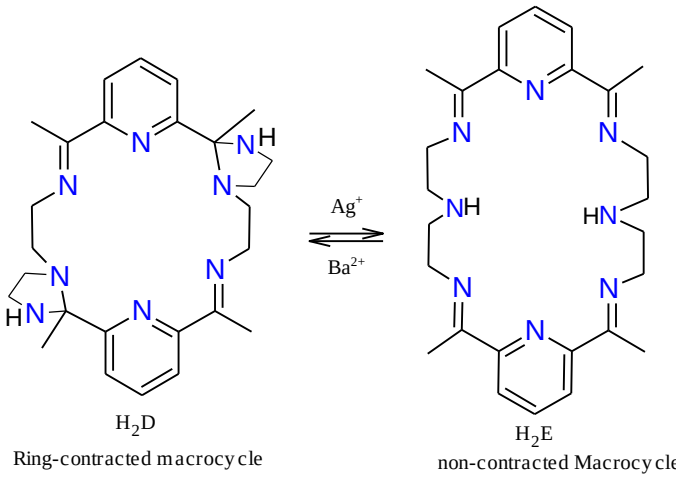

Figure 1-14 Reversible ring-contraction.[79]

1.3 Tripodal ligands

It is undeniable that polyamine ligands and their complexes have attracted much attention not only because they form very stable complexes with transition metals but also because of their ability to model active sites present in some metalloenzymes.[80]

Tripodal ligands have been widely used in both coordination and organometallic chemistry.[80] Tris(2-aminoethyl)amine (tren) was the first tripodal tetraamine ligand to be synthesised by Ristenpart as the trihydrochloride salt from the reaction of 2-bromoethylphtalimide with dry ammonia, and subsequent deprotection of the formed tris(2-phthalimidoethyl)amine using HCl, shown in Figure 1-15.[81] This method was slightly modified by Mann and Pope later.[83] There are many reports in the patent literature of the synthesis of tren by reduction of tris(cyanomethyl)amine. The base ligand is now commercially available.

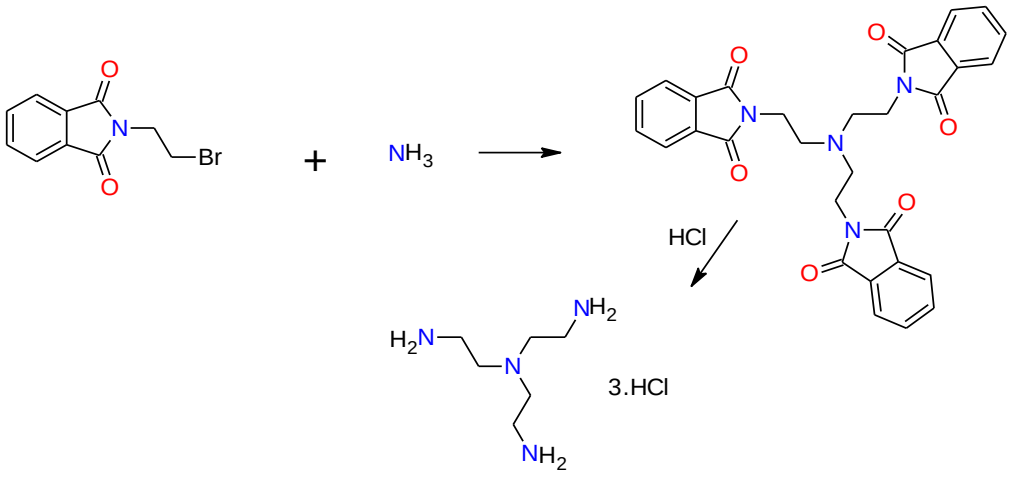

Figure 1-15 Synthetic scheme for formation of tren by Ristenpart.[82]

Tetradentate tripodal ligands show the general structure illustrated in Figure 1-16 and consist of a central donor atom X attached to three arms, each of which also contains at least one methylene group and a donor atom Y. The ligands can differ both in the lengths of the arms and in the nature of the donor atoms on each arm, and there are a number of such ligands known.

Tripodal tetraamines can be named in accordance with the number of carbon atoms in each arm which is illustrated in Figure 1-16 and given in the list of abbreviations.[80,81]

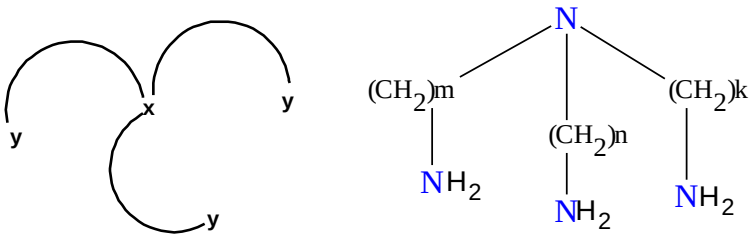

n=m=k=2 (tren) Tris(2-aminoethyl)amine
n=m=2, k=3 (baep)3-Aminopropylbis(2-aminoethyl)amine
n=m=3, k=2 (abap)2-Aminoethylbis(3-aminopropyl)amine
n=m=k=3 (trpn) Tris(3-aminopropyl)amine

Figure 1-16 Asymmetric and symmetric tripodal tetraamines.[80,81]

There are several methods for the synthesis of tripodal tetraamine ligands with the choice generally dictated by the nature of the donor atoms on the three arms. Bromo and chloroalkylphtalimides are useful for the synthesis of ligands having aliphatic donor atoms as they can alkylate both primary and secondary N atoms at fairly high temperature and deprotection using acid gives the amine directly. Tris(2-chloroethyl)amine hydrochloride is a powerful vesicant, while the free base form is a Chemical Weapons Convention chemical. Therefore, this method is not recommended for tren synthesis. Mannich reactions have also been used for the synthesis of several tripodal tetraamine ligands.[80]

A symmetrical tripodal tetraamine ligand has same length arms. These tend to have C_{3v} symmetry about the tertiary N atom. However, asymmetric tripodal amines tend to have a C_s symmetry or lower, and once the ligands are bonded to a transition metal, the symmetry tends to become lowered.[80]

A tripodal ligand such as tren can behave as a tetradentate ligand by using all four nitrogen atoms; however, there are some examples where the ligand coordinates to a metal using less than the total number of donor atoms available to it. One of these examples is shown in Figure 1-17.[81]

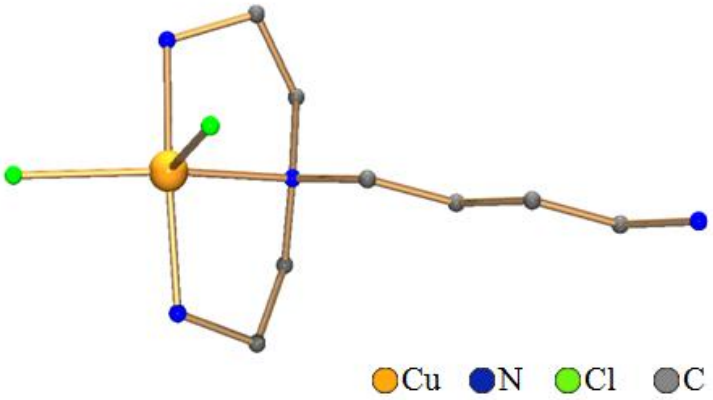

Figure 1-17 The Cu(II) complex of a tripodal ligand with one arm detached.[81]

The tripodal ligand coordinates to Cu(II) *via* three nitrogen donors leaving one nitrogen arm free. The reason why one nitrogen atom is left uncoordinated may be because of the stability of the complex produced. In this case, it may be explained by the chelate effect; chelate rings of six or more atoms are less favoured as the ring can become strained.[84]

A tripod having primary amine donors can undergo a Schiff base condensation reaction to form a Schiff base ligand that is available for complexation. H_3Saltren, for example, was prepared by the Schiff base condensation reaction of one equivalent of tren with three equivalents of salicylaldehyde (Figure 1-18). The coordination chemistry of the H_3Saltren ligand has also been examined in great detail.[85-89]

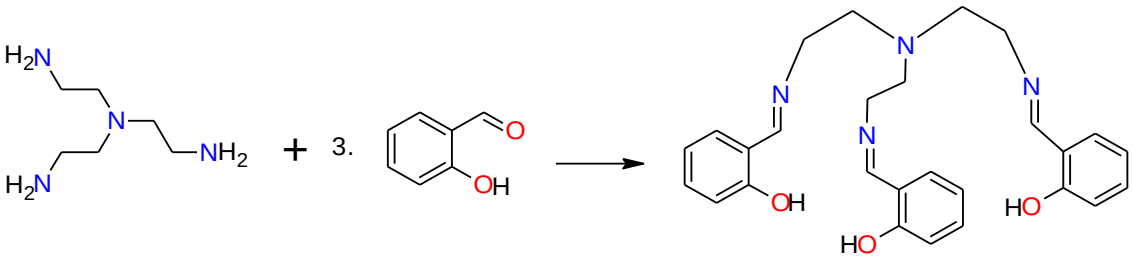

Figure 1-18 H_3Saltren.

McKee and co-workers prepared mononuclear and tetranuclear complexes derived fron H_3Saltren and manganese. A 1:1 molar ratio of manganese ion to H_3Saltren was used to prepare the mononuclear complex.[90] In this complex, the bridgehead nitrogen

atom remained uncoordinated. For the tetranuclear complex, a 2:1 ratio (Mn:Ligand) was used (Figure 1-19).[91]

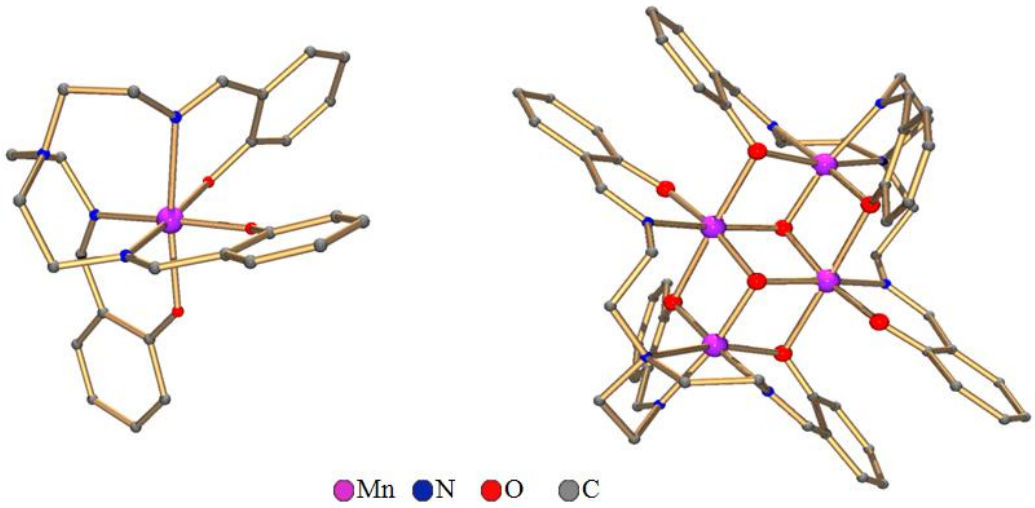

Figure 1-19 Mononuclear complex [Mn(saltren)] (left) and tetranuclear complex $[Mn_4(saltren)_2(O)_2]^{2+}$ *(right).*[90,91]

Tripodal tetraamine ligands with different arm combinations were synthesised and have attracted chemists to the chemistry of tripodal ligands and their metal complexes. Two examples of tripodal ligands reported in the literature are given in Figure 1-20. Tris(2-pyridylmethyl)amine was first synthesised by Anderegg and Wenk in 1967.[92] Various metal complexes such as Cu(II), Co(II), Fe(II) have been prepared and characterised. Tris(2-(2-pyridyl)ethyl)amine was prepared by Karlin and co-workers.[93]

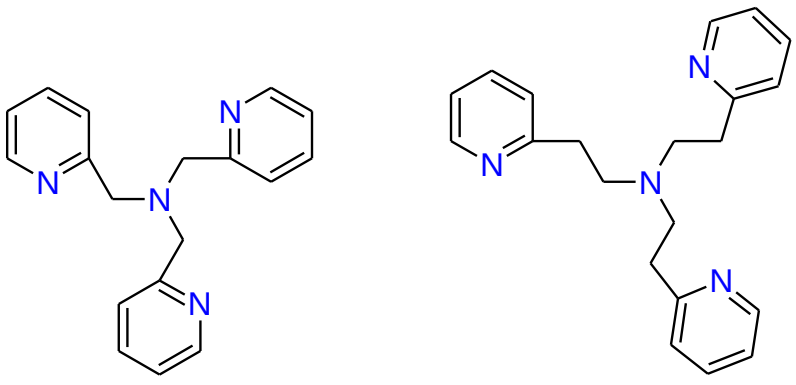

Figure 1-20 Tris(2-pyridylmethyl)amine and tris(2-(2-pyridyl)ethyl)amine.

1.4 Superoxide and superoxide dismutase

1.4.1 Superoxide

Aerobic non-photosynthetic organisms obtain energy *via* enzymatic reduction of the powerful dioxygen molecule to water. For respiring cells, dioxygen is crucial and must be supplied continuously. Diffusion of dioxygen by single celled and other small organisms may provide enough dioxygen to stay alive, however, for bigger multicellular organisms, diffusion of oxygen is not fast enough to supply each cell without help.[94] Haemoglobin and myoglobin are proteins that bind, store and release dioxygen to help in fast delivery of oxygen in vertebrates. Oxygen is the terminal acceptor in the respiratory electron transfer chain and is reduced by cytochrome *c* oxidase, four electrons are transferred to oxygen and water formed. However, these oxygen utilising processes are not 100 % efficient and a significant amount of dioxygen is lost as potentially damaging superoxide and peroxide species. Oxygen rarely reacts with other electron transport components.[94] Superoxide (O_2^-) is a free radical generated by one electron reduction of dioxygen.[95]

The molecular orbital diagram of molecular oxygen is shown in Figure 1-21. When oxygen undergoes a one electron reduction, the bond order is reduced from 2 to 1.5 as the extra electron is placed in an antibonding orbital. The superoxide ion then has a longer bond length because of the extra electron added to the molecule. Because of having the unpaired electron, superoxide can behave as a very reactive free radical.[96,97]

Superoxide is both a reducing (**Equation 1**) and an oxidising agent (**Equation 2**).[98]

$$O_2^- \longrightarrow O_2 + e^- \qquad E^o = -0.16\ V \quad (\textbf{Equation 1})$$

$$O_2^- + e^- + H^+ \longrightarrow HO_2^- \qquad E^o = 0.89\ V \quad (\textbf{Equation 2})$$

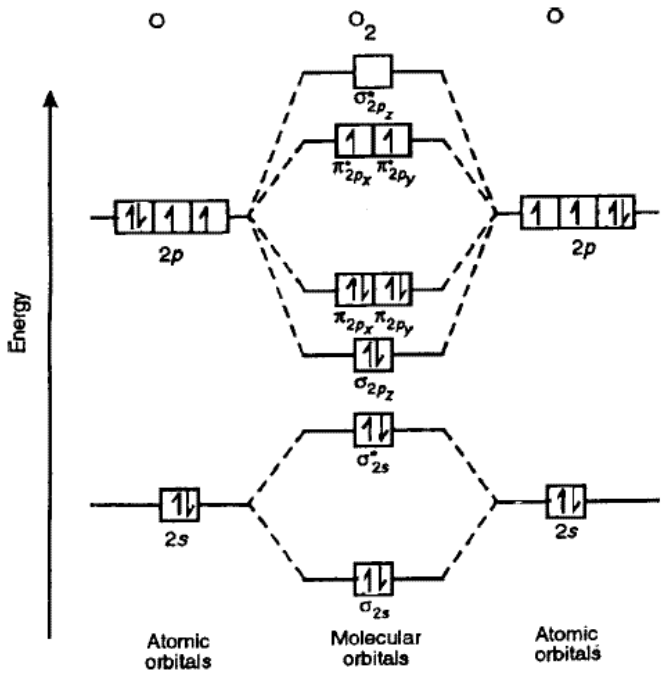

Figure 1-21 Molecular orbital diagram of dioxygen.

The oxidant and reductant properties of superoxide give rise to other dangerous reactive species (Figure 1-22) including hydrogen peroxide, hydroxyl radicals, hypochloride ions and peroxynitriles.[99-101]

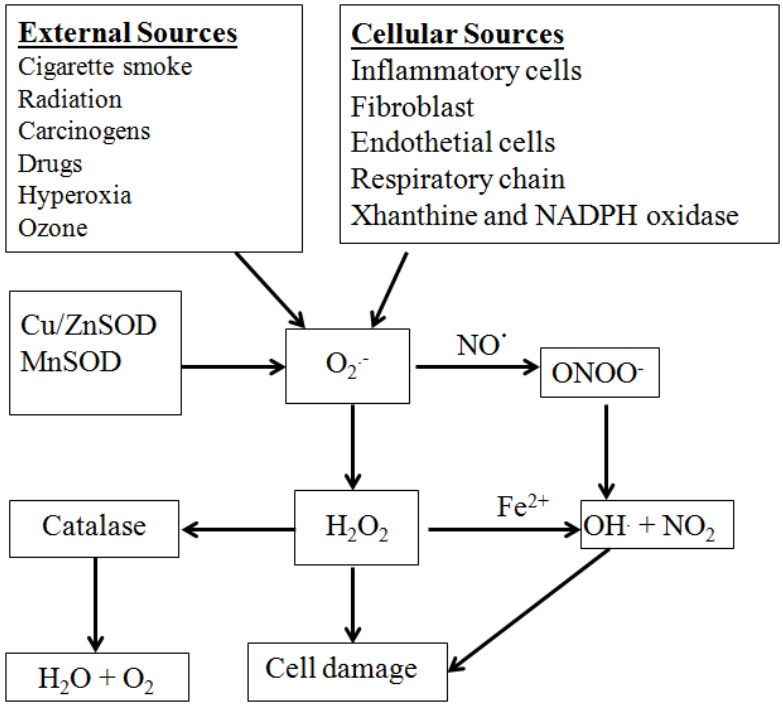

Figure 1-22 Production of radical oxygen species and dismutation by SODs.

Superoxide can inactivate iron-sulphur cluster-containing enzymes, releasing free iron ions into the cell. Free iron ions react with hydrogen peroxide to generate the very reactive hydroxyl radical, known one of the most reactive oxygen species (ROS), by the Fenton reaction shown in **Equation 3**.[102]

$$Fe^{2+} + H_2O_2 \rightarrow Fe^{3+} + OH\cdot + OH^-$$

$$\underline{Fe^{3+} + H_2O_2 \rightarrow Fe^{2+} + OOH\cdot + H^+}$$

$$\text{Net: } 2H_2O_2 \rightarrow OH\cdot + OOH\cdot + OH^- + H^+ \text{ (\textbf{Equation 3})}$$

In the formation of hydroxyl radicals, metal oxo or metal hydroxyl intermediates such as $(Fe^{IV}=O)^{2+}$ and $(Cu^{III}=OH)^{2+}$ are produced. Hydroxyl radicals and high-valent hydroxyl and oxo species initiate autoxidation of lipids and damage carbohydrates, proteins, nucleic acids and other organic molecules. The hydroxyl and hydroperoxide radicals can attack polyunsaturated fatty acids causing crosslinking polymerizations.[103] Highly cytotoxic $ONOO^-$ species can form when superoxide reacts with nitric oxide (NO).[104]

Superoxide is considered to be a contributing cause of many neurological disorders such as Parkinson`s[105,106] and Alzheimer`s diseases.[107,108] Moreover, some types of cancer are thought to be associated with superoxide.[109,110] Oxidative stress is mainly due to the overproduction of these reactive oxygen species. For the reasons given above, a biochemical defence system is required to control the level of superoxide and reactive oxygen species under physiological conditions.

1.4.2 SODs and their active metal centre structures

Healthy cells are capable of defending themselves against ROS damage through the use of superoxide dismutases enzymes (SODs) which control the level of superoxide at low levels. SODs are metalloenzymes that catalyze the dismutation of the superoxide anion (O_2^-) to hydrogen peroxide and dioxygen (**Equation 4)**.[94]

$$M^{n+1}\text{-SOD} + O_2^{-}\bullet \rightarrow M^{n+}\text{-SOD} + O_2$$

$$M^{n+}\text{-SOD} + O_2^{-}\bullet + 2H^{+} \rightarrow M^{n+1}\text{-SOD} + H_2O_2$$

Equation 4*- Dismutation of superoxide into oxygen and hydrogen peroxide; where M = Cu (n=1); Mn (n=2); Fe (n=2); Ni (n=2).*

Where M^n represents metalloenzyme in the reduced state and M^{n+1} represents metalloenzyme in the oxidised state. The disproportion of superoxide has been proposed to proceed by a ping-pong mechanism in which the metal oscillates between two oxidation states.[111-112] There are three types of superoxide dismutase enzyme existing in mammals. The first one is SOD1 or Cu/ZnSOD which is found in the cytoplasm and contains zinc and copper in the active site. SOD2 or MnSOD is restricted to mitochondria and contains a manganese core; SOD3 or Cu/ZnSOD is an extracellular enzyme containing copper and zinc in the active catalytic centre. Anaerobic prokaryotes contain FeSOD exclusively, if they have SOD activity.[113,114] Recently, a Ni containing SOD has been purified from *Streptomyces coelicolor*.[115]

These enzymes have very high efficiency. Mammalian Cu/ZnSOD has been found to possess catalytic rates of $2x10^9$ M^{-1} s^{-1},[116] while MnSOD and FeSOD are somewhat slower.[117]

Cu/ZnSOD has a copper and a zinc ion in its active site (Figure 1-23).[118] The metal ions are bridged by the imidazolate ring of residue His61. Three histidine residues (44, 46 and 118) and a water molecule coordinate to Cu(II) to form a distorted square pyramidal geometry. Zn is further coordinated to His69, His78 and Asp81 and has a distorted tetrahedral geometry. There is structural evidence from crystallography and EXAFS that the Cu–His61–Zn bridge in SOD1 is broken upon reduction to Cu(I), leaving an approximate trigonal planar Cu coordination.[119,120]

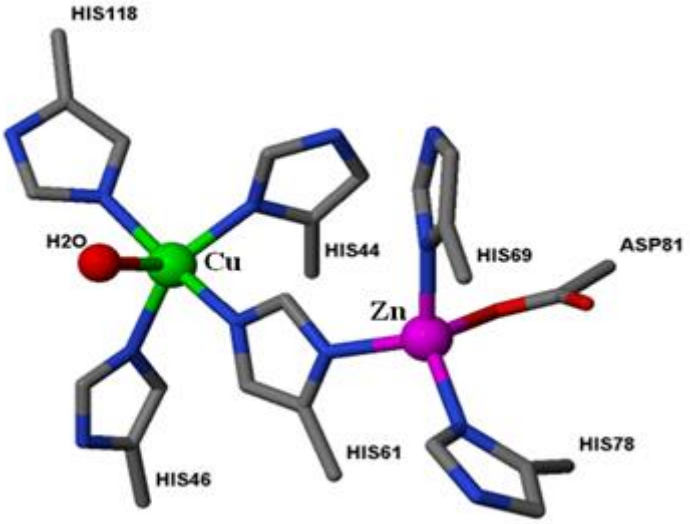

Figure 1-23 Active site of human Cu/ZnSOD (oxidised (Cu^{2+} form) (PDB code: 1HL5).[118]

The possible role of the Zn(II) ion may be to increase the stability of the enzyme. The enzyme is remarkably stable to heat and when the metal ions are removed from the enzyme, the stability reduces dramatically. The Zn(II) ion may also help to produce the electric field that attracts superoxide for catalytic reaction.[121,122]

A proposed catalytic mechanism for dismutation of superoxide is depicted in Figure 1-24.[121] In the first step, superoxide ion coordinates to the Cu(II) centre, releasing a water molecule. The second step is an inner sphere electron transfer between the coordinated superoxide and the Cu(II) centre. The Cu(II) is reduced to Cu(I) and molecular oxygen is released. In this step, the copper–imidazolate bond is also broken on protonation. In the third step, another superoxide ion coordinates to the reduced Cu(I) centre and hydrogen bonding occurs between protonated imidazolate and superoxide. In the final step, an electron is transferred from the Cu(I) centre to superoxide and a proton is transferred from the imidazolate ring reforming the copper–imidazolate bond and releasing hydrogen peroxide.[121,122]

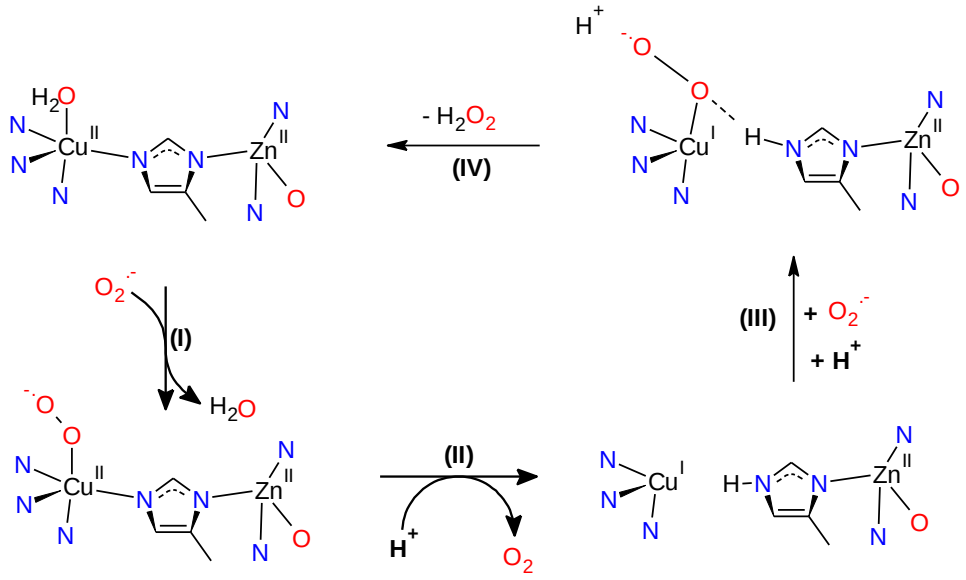

Figure 1-24 Proposed mechanism for dismutation of superoxide by Cu/ZnSOD.[121]

MnSOD and FeSODs have similiar structures to each other.[123] MnSODs contain five-coordinate Mn^{3+} ions at the active site as shown in Figure 1-25.[124] The donors are three nitrogen atoms from histidine residues (26, 81 and 171), one oxygen atom from Asp228 and an oxygen atom of an OH^- group (or water molecule) giving trigonal bipyrimidal geometry. His90 and O (OH^- or water) occupy the axial positions and His232, Asp228 and His145 are in the equatorial positions. At 1.55 Å resolution a low temperature structure from *E. coli* manganese superoxide dismutase has been determined to have a sixth hydroxyl ligand in the active site.[125] The sixth coordination site might be considered to close–off the active site. The metal active centre is stabilised by hydrogen bonding involving Tyr and Glu.

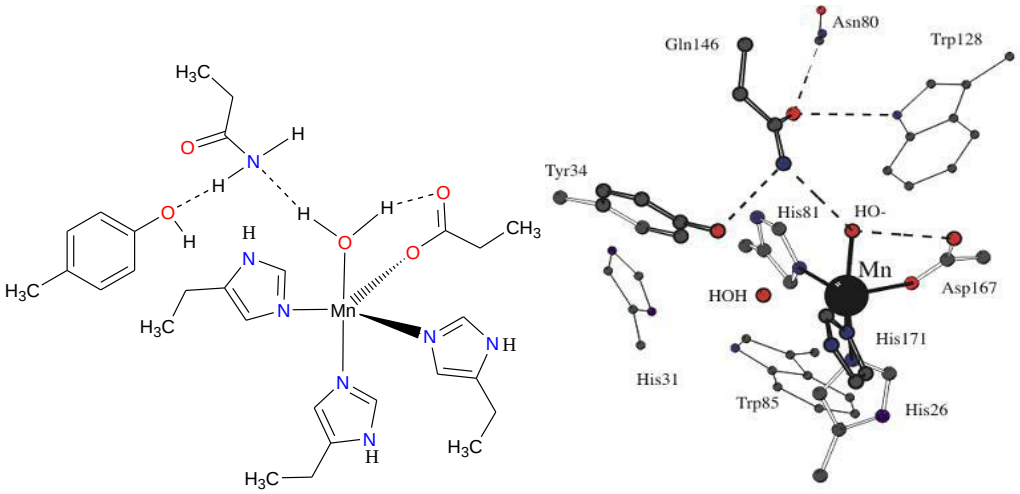

Figure 1-25 Crystal structure of MnSOD from E. coli (PDB code: 1VEW).[124]

The reduction of Mn(III)SOD by superoxide and the release of O_2 is fast (10^9 $M^{-1}s^{-1}$). Anion binding studies led to the proposal that the superoxide radical approaches the metal centre and coordinates to the Mn(III) ion to start electron transfer and that the reduction step follows an inner-sphere mechanism.

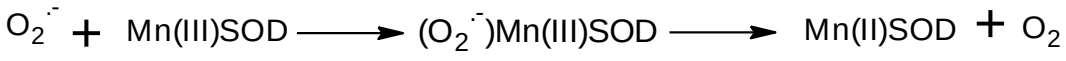

Oxidation of Mn(II)SOD also follows an inner-sphere mechanism. In the first place superoxide binds to the Mn(II) centre followed by proton-coupled electron transfer to produce the free hydroperoxide anion and releasing hydrogen peroxide.[94,127-129]

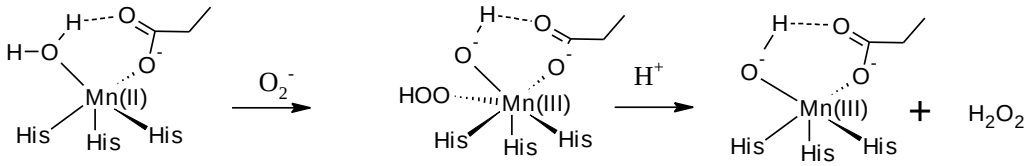

Figure 1-26 Inner-sphere oxidation of Mn(II)SOD by superoxide.

Fe in FeSOD is also five-coordinate and possesses distorted bipyrimidal geometry and the active site (Figure 1-27), His43 and O (water or OH) are in axial positions, His95, Asp171, and His199 are in equatorial plane (Figure 1-27). Reduction of Fe^{3+} to Fe^{2+} does not change ligand-metal geometry.[123,126]

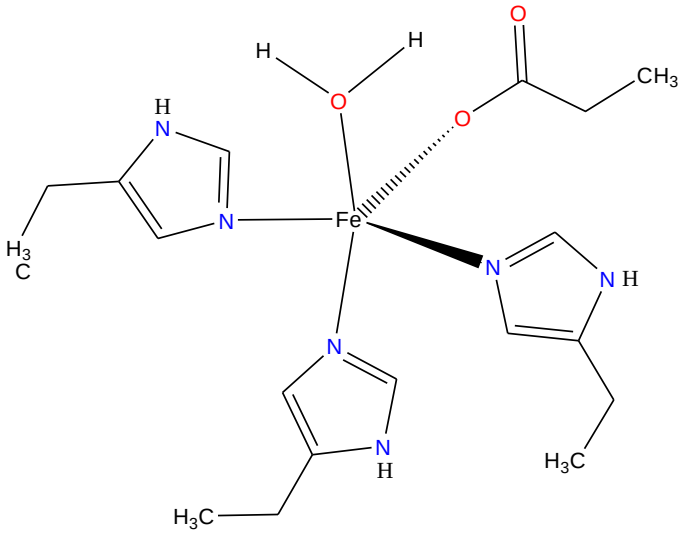

Figure 1-27 FeSOD active centre.[123]

1.4.3 MnSOD model complexes

Natural SOD enzymes have shown promising therapeutic properties yet suffer as drug candidates due to some drawbacks listed below:[114,130-134]

- Immunological problems
- Short half-lives in vivo
- Cost of production
- Large size prevents the molecules passing through cell wall membranes

Considerable efforts have been made to obtain stable, non-toxic, and inexpensive low molecular weight biomimetic molecules which are capable of catalyzing superoxide dismutation and therefore to provide important therapeutic applications.[114] Many systems have been isolated, displaying a superoxide scavenger activity and have been proposed as SOD models. Metal complexes of Cu, Mn, Fe and Ni are known to disproportionate the superoxide to molecular oxygen and hydrogen peroxide. During the 1970s and 1980s, most papers relating to SOD models were based on copper complexes;[135] Sorensen published a comprehensive review of this area.[136] There are some reports of iron- and manganese-containing molecules presented as FeSOD or MnSOD models. The SOD-like activity of these systems is still controversial due to possible uncertainties in using indirect methods to quantify their activity. In most cases, the catalytic mechanism is not clearly established because identification of transient species has been difficult.

The Cu(II) ion itself is a very good catalyst for the dismutation of superoxide, and is close to the activity of Cu/Zn enzymes.[137] This creates an issue; is the activity measured for a model complex really due to the dissociation of complex or free Cu(II) impurity.[114] In designing potential metal based drugs for therapeutic purpose, toxicity considerations are important. Nowadays, most SOD mimic metal complexes are based on manganese rather than copper or iron. Both copper and iron ions are very toxic in vivo and manganese ions are less toxic to mammalian systems. Moreover, manganese as free aquated metal ion does not involve Fenton chemistry to generate hydroxyl radicals by reacting with hydrogen peroxide.

Synthetic MnSOD mimic complexes should meet the following criteria to be used as metallodrugs:[114, 138]

- They should be non-toxic
- Non-immunogenic
- They should have a high metabolic half-life
- Be able to penentrate into the cell as well as having a high stability constant.
- Inexpensive

Mn(III)Salen complexes, prepared initially for chiral epoxidations by Jacobson,[139] have shown SOD and catalase activity.[140] SOD-like activity of Mn(III) salen type complexes on the basis of indirect analysis, showed that added EDTA reduced the activity in some cases.[141] Electrochemistry work by Taylor *et al.* showed that these complexes show quasireversible reduction in dmso solvent and the complexes behave as 1:1 electrolytes. The reduction of Mn(III) to Mn(II) forms the basis of the catalytic cycle.[142] Biological studies for two Mn(III)Salen complexes have been published (Figure 1-28).[143,144]

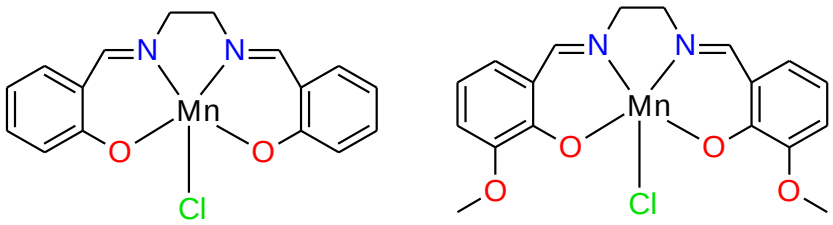

Figure 1-28 Mn(III)-Salen complexes.

The complexes EUK-8 and EUK-134 have been tested in a number of disease models related to oxidative stress. In clinical trials it was found that EUK series were effective to protect cells from oxidative damage in several animal models including Alzheimer's disease, Parkinson's disease, stroke, motor neuron disease and neural injury.[114,143] Riley *et al.* investigated the catalytic properties of these complexes *via* stopped flow analysis of superoxide decay. EUK-8 was found to have the catalytic rate (8.0×10^5 M^{-1} S^{-1}, pH=8).[114]

Mn(III)porphyrinato complexes also have been found to possess SOD-like activity based on indirect analysis; one example is shown in Figure 1-29.[144]

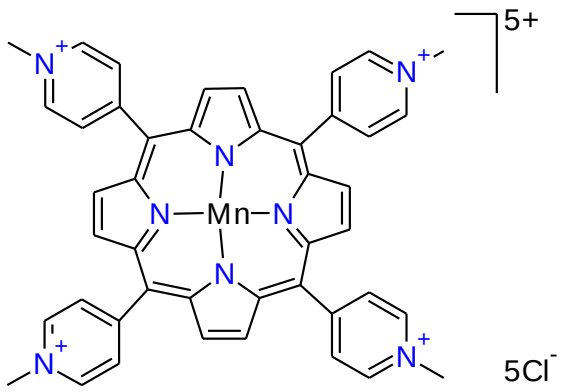

Figure 1-29 Mn(III) porphyrinato complex [Mn(III)(TMPyP)]5Cl.

The complex in Figure 1-30 has catalytic rates of 4 x 10^6 M^{-1} s^{-1} based on the cytochrome c assay.[145,146] Riley *et al.* later tested this complex *via* a direct method (stopped flow) and the catalytic rate of the complex was found to be 1x10^7 M^{-1} s^{-1}.[114] For further information, the catalytic rate of this complex decreases as the concentration of the complex increases. It was suggested that in the strong oxidising media oxo- or hydroxo-bridged species formed and dimers do not possess SOD catalytic activity.[146]

Riley and his co-workers prepared very active seven-coordinate Mn(II) complexes with C-substitued pentaazacyclopentadecane as SOD mimics. These series of complexes contain seven-coordinate, high spin d^5 Mn(II) ions. The generic structure is shown in Figure 1-30.[138,147-149]

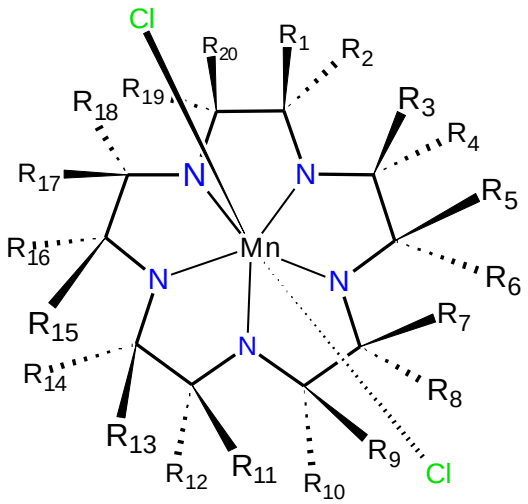

Figure 1-30 Generic structures of C-substituted pentaazacyclopentadecane Mn(II) chloride complex.

Changing the number of substituents, their placement and their stereochemistry tunes the stability of the complexes and their SOD-like activity, therefore reducing potential dosage and exposure to the metal. As the number of carbon substituents increases, the stability of the complexes increases non-linearly. The stereochemistry of methyl groups also had an effect on SOD activity; however this was a small effect on the stability of the complex as the number of methyl groups remains constant.[148]

Riley *et al.* prepared a similar seven-coordinate Mn(II) complex containing a pyridine head unit with the aid of computer modelling (Figure 1-31). The complex *S*,*S*-dimethyl-M40403 (K_{cat} 1.6x10^{9} M^{-1}s^{-1}) was found to exceed the catalytic rate of the native human MnSOD enzyme (K_{cat} 5.5x10^{8} M^{-1}s^{-1}) yet it has an advantage of being a much smaller molecule.[150,151] The complex M40403 showed therapeutic activity in a variety of animal models of inflammation and ischemia reperfusion injury.[98,152]

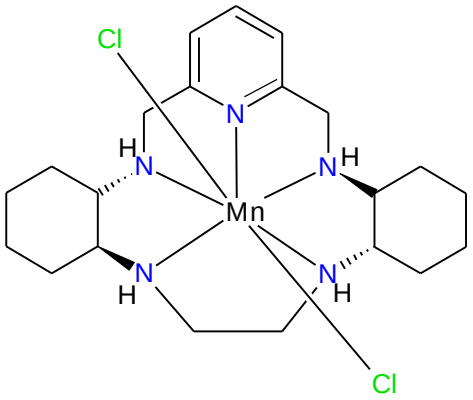

Figure 1-31 Mn(II) complex M40403.

Riley *et al.* proposed the catalytic cycle for the synthetic SOD mimic complexes shown in Figure 1-32.[147,149] There are two reaction pathways; a pH-independent inner sphere pathway and a pH-dependent outer-sphere pathway. Riley claimed that in the inner-sphere pathway, a superoxide radical anion coordinates to the vacant site of the manganese centre and the rate of formation of the vacant site is the rate determining step of the reaction. For the outer-sphere pathway, Riley concluded that the proton coupled electron transfer step was rate limiting.[149]

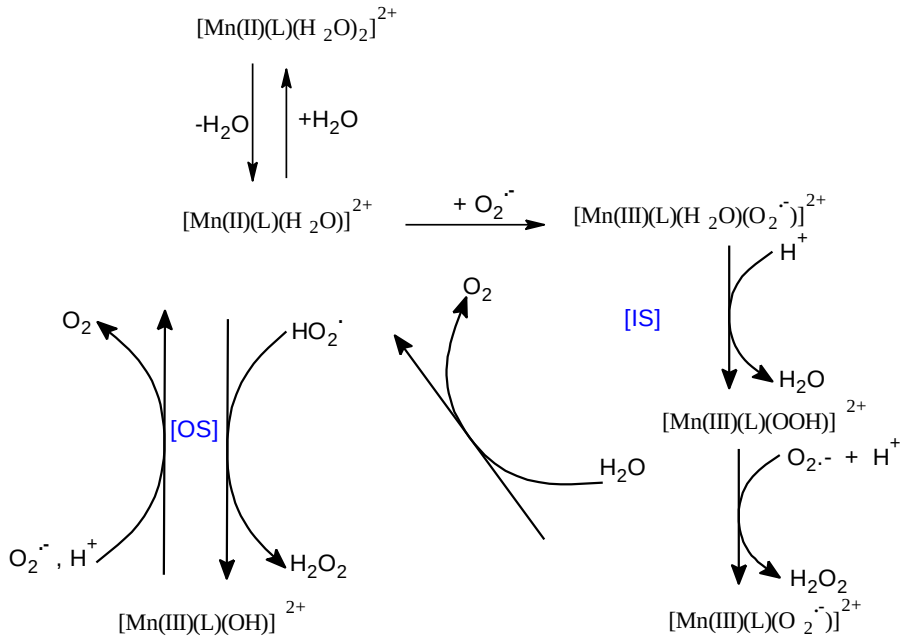

OS: Outer sphere and IS: inner sphere

Figure 1-32 Proposed catalytic cycle for synthetic SOD mimics.

Burmazovic *et al.* argued that the release of H_2O cannot be the rate limiting step as the second order rate was found to be higher than the values for the water exchange rate.[153] Burmazovic *et al.* suggested that for the inner sphere pathway the water exchange mechanism is an interchange dissociative mechanism and incoming superoxide radical also plays a role in the substitution process.[153]

Riley *et al.* also claimed that only ligands with conformational flexibility could have SOD like activity.[149] However, Burmazovic *et al.* prepared seven-coordinate iron(III) and Mn(II) complexes with the acyclic and rigid H_2dapsox ligand (Figure 1-33) which showed similar catalytic activity to macrocyclic pentadentate ligands. This clearly shows that water release and conformational rearrangement of the ligand are not the rate limiting steps in the overall inner sphere pathway.[154]

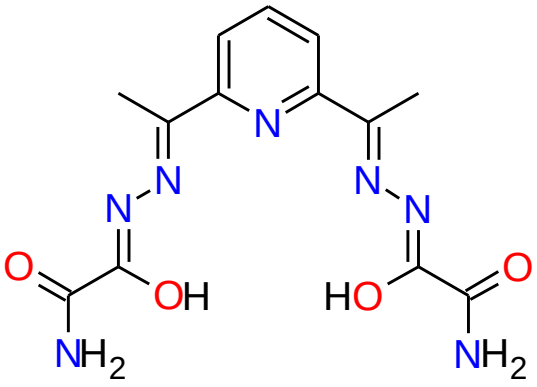

Figure 1-33 H_2dapsox.

1.5 Catalase

Catalases are hydroperoxidases, a class of antioxidant enzymes that catalyse the conversion of hydrogen peroxide to water and molecular oxygen, protecting cells from its toxic effects. Hydrogen peroxide is produced as a consequence of oxidative cellular metabolism and by SOD. Hydrogen peroxide can be converted to the highly reactive hydroxyl radical *via* transition metals such as Fe^{2+} or Cu^{2+} by Fenton reaction, this radical being able to damage a wide variety of molecules within a cell, leading to oxidative stress and cell death.[102] Because of the toxicity of H_2O_2, organisms have developed methods to help in its fast decomposition, which requires two electron catalysis.[155-158]

H_2O_2 is removed according to **Equation 5** shown below:

$$2H_2O_2 \xrightarrow{\text{Catalase}} 2H_2O + O_2$$

***Equation 5** - Removal of H_2O_2 via catalase activity.*[155-158]

Disproportionation of hydrogen peroxide is an exothermic reaction releasing 52 kcal mol^{-1}. Catalases are produced by all aerobic organisms ranging from bacteria to humans. Most catalases are mono-functional, heme-containing enzymes, although there are also bifunctional heme-containing peroxidase/catalases that are closely related to plant peroxidases, and non-heme, manganese-containing catalase possessing dimanganese in the active site are found in bacteria.[159,160]

Phylogenetic analyses have showed the existence of two distinct classes and subgroupings of small subunit enzymes and one class of large subunit enzymes among the monofunctional catalases. Bifunctional and heme-containing catalase-peroxidases have similar structure and sequence to plant peroxidises. Additionally, all heme-containing enzymes, such as chloroperoxidase, plant peroxidases and myoglobin, possess very low catalase activity.

Dimanganese-containing catalase from *Thermus thermophilus*[161] and *Lactobacillus plantarum*[162] organisms were characterized by X-ray crystallography in 1983 and the active site of MnCat is shown in Figure 1-34. Since then a number of manganese catalases have been isolated from other organisms.[160]

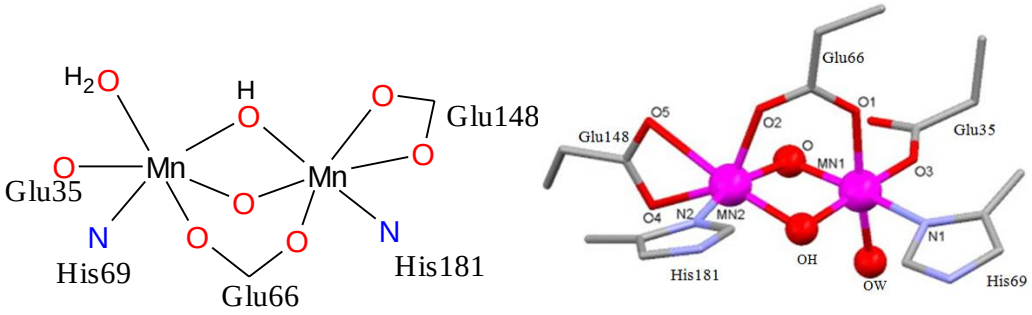

Figure 1-34 Active site of MnCat from Lactobacillus plantarum (PDB code: 1JKU).[162]

The active site contains two manganese(III) centres linked by a carboxylate and two oxygen bridges and are separated by 3.6 Å. Carboxylate bridges and their binding mode can alter the observed activity. In the vicinity of the active site of dinuclear manganese catalase from *Lactobacillus plantarum*, there are several histidines. These bases are believed to play an important role in the catalytic activity. The introduction of base during the testing of catalase mimics has often been shown to increase catalytic activity. Pecoraro *et al.* suggested that base was needed to deprotonate the hydrogen peroxide to initiate the reaction for binding to manganese ions.[160]

A proposed mechanism for dismutation of hydrogen peroxide by manganese containing catalase is illustrated in Figure 1-35. Mn(III) ions in the active site, cycle their oxidation states between (Mn^{II}, Mn^{II}) and (Mn^{III}, Mn^{III}).[163]

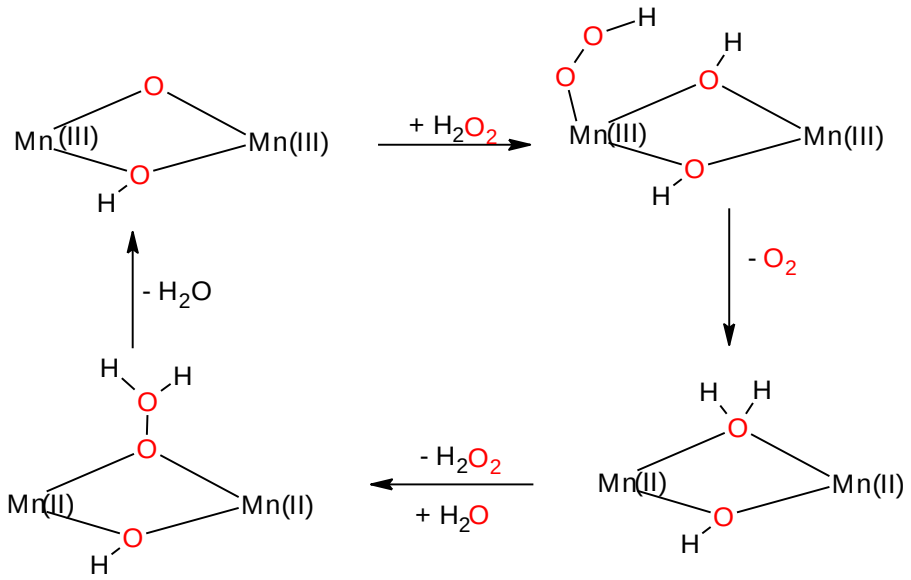

Figure 1-35 Mechanism of disproportionation of hydrogen peroxide by MnCat.[163]

During the catalase reaction, one H_2O_2 molecule replaces the water ligand from one of the Mn(III) centres and protonates the μ-oxo bridge. Two electrons are transferred from coordinated peroxide to Mn(III) centres releasing molecular oxygen. Another H_2O_2 molecule binds to reduced Mn(II) centres as a bridging hydroperoxo ligand. Two electrons are tranfered from Mn(II) centres to the hyroperoxo ligand followed by O-O bond cleavage releasing a water molecule.[163,164]

After the structures of the binuclear manganese catalases were characterised, numerous studies on catalase activity in Mn complexes were made. When preparing manganese catalase mimics, it is important to explore how changes in geometry of the metal centre can affect reaction rates and provide suggestions for increasing catalase activity. This will lead to a more detailed understanding of the mechanisms in the catalytic cycle. Porphyrin based dimeric manganese complexes are early examples of manganese catalase mimics. It was found that dimeric units dissociate during catalysis reaction. Some rigid linkers were introduced to stabilise the complex, however, the rate of catalase activity was less than natural enzymes. Since then several porphyrin derivatives have been prepared as catalase mimics.[160,164,165]

In 1994, Dismukes *et al.* prepared a family of dinuclear complexes with different co-ordination environments and oxidation states as MnCat model complexes. An example of this family is shown in Figure 1-36. The dinuclear Mn complex of

N,N,N`,N`-tetrakis(2-ethylenebenzamidazaly)-1,3-diamino-dipropan-2-ol (benzimpn) was found to show catalase activity with k_{obs}=0.23 $M^{-l}s^{-1}$.[166,167]

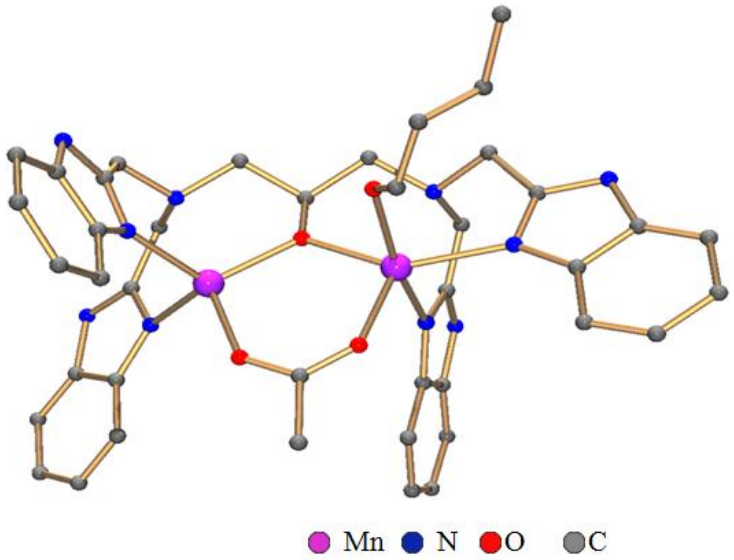

Figure 1-36 Mn(II) complex of benzimpn.

Dismukes proposed a mechanism for catalytic activity for a hydroxide derivative of the complex shown in Figure 1-37.[168] In step a→b, hydrogen peroxide displaces a water ligand and protonates the hydroxide bridge. In step b→c the terminal HO_2^- anion migrates to the bridging position to form a hydroperoxide bridge by exchange with a water bridge. In the next step c→d, bond cleavage of the hydroperoxide occurs by coupling protonation of the terminal hydroperoxide with Mn_2(II,II) oxidation to give the (μ-O)-Mn_2(III,III) species and releasing a free water molecule. The resulting Mn_2(III,III) species in d was shown to be accessible by air oxidation. The next step d→e involves binding and deprotonation of the second hydrogen peroxide molecule by the bound hydroxide to give a terminally bound hydroperoxide anion species and release of a water molecule. In this step, Dismukes *et al.* claimed that intermediate species might be stabilised by intramolecular H-bonding between the terminal hydroperoxide and the terminal acetate group. The final step e→a involves two-electron oxidation of the hydroperoxide to re-form the starting species and release the product O_2 molecule, completing the catalytic cycle.[168]

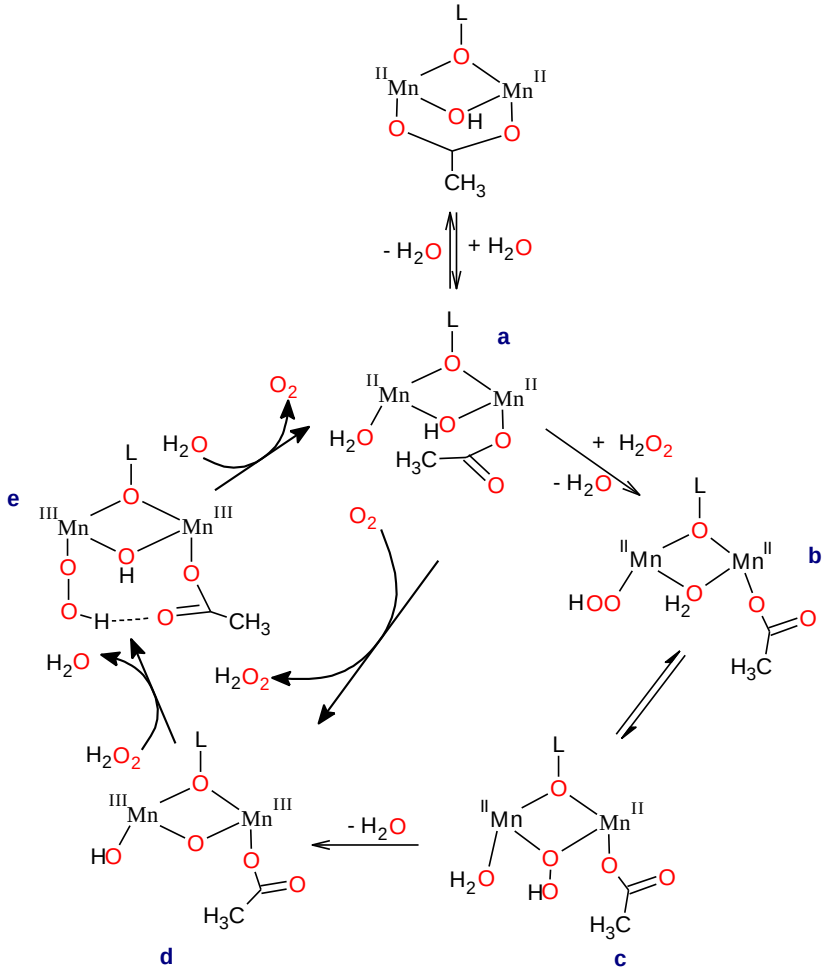

Figure 1-37 Proposed mechanism for catalase activity for a dinuclear complex.[168]

MnSalen complexes have also been tested for catalase activity and shown promising catalase activity.[157] These complexes possess superoxide dismutase activity as well as catalase activity, varying significantly with ligand substituents.

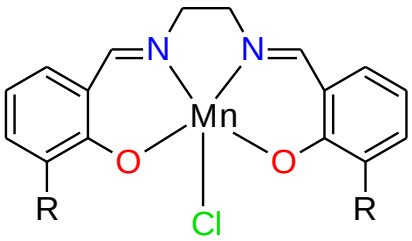

Figure 1-38 MnSalen complexes as catalase mimics.

A catalytic mechanism for MnSalen complexes was proposed by Abashkin and Burt[92] (Figure 1-39). In the first step; the H_2O_2 molecule coordinates to the Mn(III) centre and is oxidised, releasing a water molecule. In the second step, another peroxide

molecule approaches the oxo Mn(V) intermediate, transforming the oxygen back to peroxide, releasing molecular oxygen and a water molecule.[157]

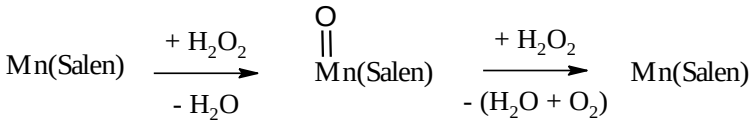

Figure 1-39 Proposed catalytic mechanism for disproportion of hydrogen peroxide.[157]

In 2002, Pecoraro *et al.* reported a series of di and mono-nuclear Mn complexes as catalase mimics with bis-(picolyl)(N-methylimidazol-2-yl)amine (bpia) (Figure 1-40). It was reported that $[Mn(bpia)(\mu\text{-}OAc)]_2(ClO_4)_2$ (Figure 1-40) is the most efficient catalase mimic with $k_{cat}/k_M = 3.4 \times 10^4\ M^{-1}s^{-1}$.[169]

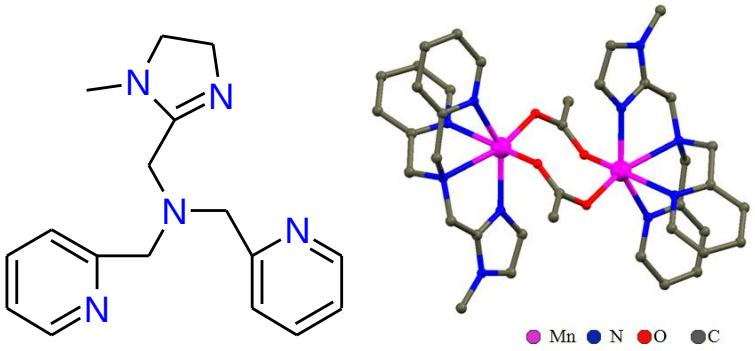

Figure 1-40 Bis-(picolyl)(N-methylimidazol-2-yl)amine (bpia) (left) and crystal structure of $[Mn(bpia)(\mu\text{-}OAc)]_2^{2+}$ (right).

1.6 Aims

Development of Mn-based SOD mimics as metallodrugs for treatment of oxidative stress is an important therapeutic target. Considerable advances have been made in this area using seven-coordinate complexes but the significance of the coordination geometry and mechanism of reactions are unclear. Arguments regarding flexibility/rigidity of the complexes, or need for cyclic ligands are unconvincing.

The aims of this project were:

1. To extend the range of mono and poly seven-coordinate Mn(II) complexes previously synthesised by the group.
2. To investigate new routes to related seven-coordinate complexes.
3. To investigate structure-function relationships relating to SOD and catalase activity of the complexes.
4. To investigate the underlying significance of seven-coordination in this area of chemistry.

Chapter 2

Mn(II) complexes containing pyridinediimine as a head unit; synthesis and characterisations

2.1 Introduction

In this chapter, the synthesis and characterisation of Mn(II) complexes containing pyridinediimine head units will be discussed in detail. Firstly, macrocyclic Mn(II) complexes derived 2,6-diformylpyridine (DFP) will be examined and then comparisons will be made with Mn(II) complexes derived from the 2,6-diacetylpyridine (DAP) analogue. Several Mn(II) complexes prepared using related acyclic ligands will also be described.

Most of the complexes in this chapter have been characterised by single X-ray crystallography and structural details of the complexes will be discussed. Graph set analysis proposed by Etter *et al.*[169] was sometimes used to describe the hydrogen bonding motifs of the structures. Graph set analysis was especially used for acyclic compounds which show several hydrogen bonds in their structure. Graph sets assigned to the hydrogen bond patterns take the form:

$$\mathbf{G^{a}_{d}(r)}$$

Where: G: Pattern designator, r: size of the pattern, a: the number of hydrogen bond acceptors and d: the number of hydrogen bond donors

The pattern designator (G) can take values C (chains), D (dimers), R (rings) and S (self, intramolecular). For example, the $R^2_2(8)$ graph set notation denotes an eight-membered ring with two hydrogen bond donors and two hydrogen bond acceptors. A carboxylic acid dimer is an example of the $R^2_2(8)$ graph set notation:

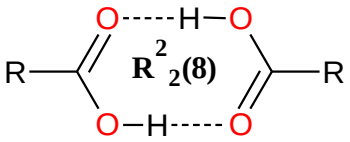

2.2 Synthesis and characterisation

2.2.1 Oxidation of 2,6-pyridinedimethanol to 2,6-diformylpyridine (DFP)

Activated manganese(IV) oxide is a widely used oxidant for the transformation of allylic and benzylic alcohols into aldehydes and ketones.[170] Ball *et al.* first reported the use of MnO_2 for the oxidation of vitamin A to the corresponding aldehyde.[171] MnO_2 is a selective oxidant that can be used in various solvents such as chloroform, dichloromethane, acetone, hexane etc. The solvent choice is important because water and alcohols compete with substrates in the absorption process occurring on the surface of MnO_2 causing its deactivation and alcohols can also be oxidised. MnO_2 can be prepared by reaction of permanganate ion with Mn(II) in a neutral or basic aqueous solution as is shown in the equation and activated by simply heating in an oven at 100-150 ºC.[170]

$$2KMnO_4 + 3MnSO_4 + 2H_2O \longrightarrow 5MnO_2 + K_2SO_4 + 2H_2SO_4$$

A mechanism for MnO_2 oxidation was suggested by Goldman (Figure 2-1).[172] The oxidation process is thought to involve an absorption stage, a coordination stage and an intermediate radical formation stage. Finally, one electron is transferred from the free radical to the Mn(III) centre releasing the free carbonyl compound.

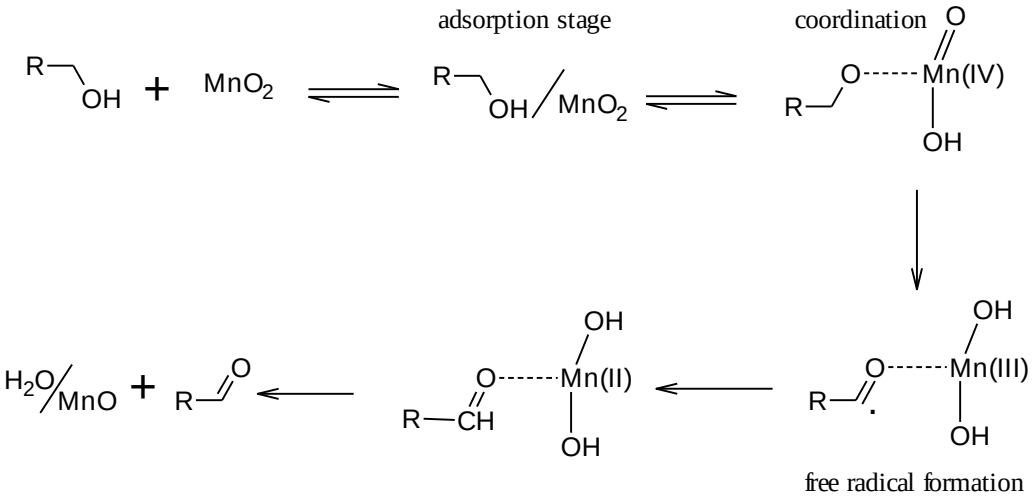

Figure 2-1 MnO_2 oxidation mechanism.[172]

Oxidation of 2,6-pyridinedimethanol to 2,6-diformylpyridine (DFP) was carried out with freshly prepared activated MnO_2 in a refluxing chloroform solution.[173] The

oxidation process was followed by TLC and, when the reaction had completed, the remaining MnO_2 was filtered off and washed with chloroform and diethylether. The combined filtrates were evaporated under vacuum to give cream coloured dialdehyde with over 60% yield and high purity.

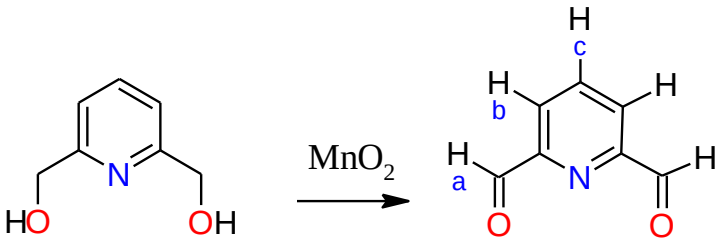

DFP

The purity of the dialdehyde (DFP) obtained was determined by ^{1}H NMR, IR, mass spectrometry and CHN analysis. The ^{1}H NMR spectrum of the compound is presented in Figure 2-2. The lack of a signal around 4-5 ppm belonging to (–CH_2–O) and occurrence of a new peak at 10.11 ppm assigned to (–CH=O) confirmed that oxidation was complete. In the IR spectrum, a peak at 1720 cm^{-1} can be assigned to the $\upsilon_{(C=O)}$ stretch. The FAB mass spectrum of the compound was also recorded: the peak at m/z 136 (100%) was assigned to $(DFP)H^+$.

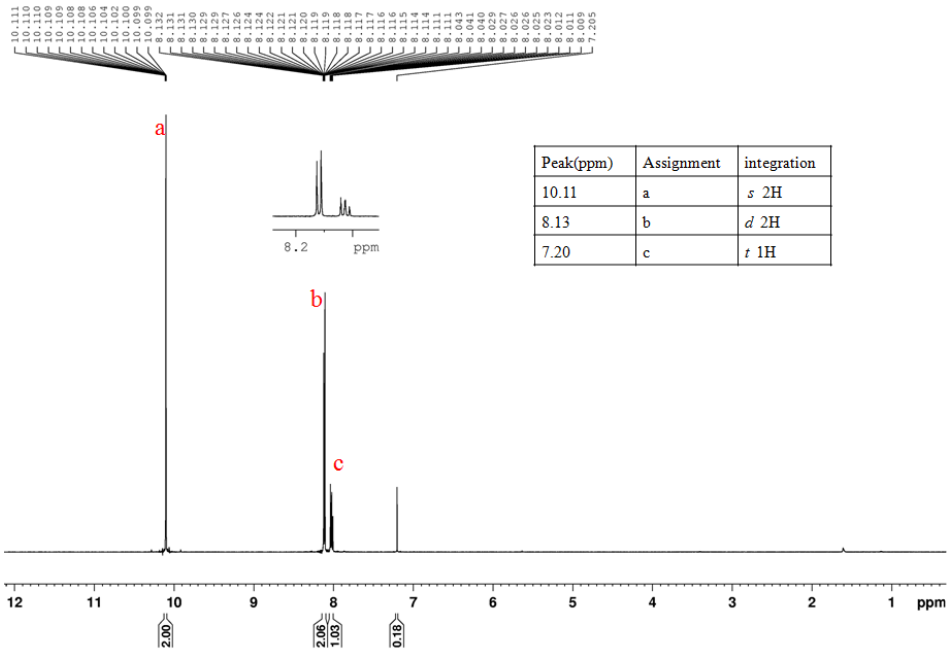

Peak(ppm)	Assignment	integration
10.11	a	*s* 2H
8.13	b	*d* 2H
7.20	c	*t* 1H

Figure 2-2 ^{1}H NMR spectrum of DFP in $CDCl_3$.

2.2.2 Macrocyclic Ba(II) complex $[Ba(H_2L1)(ClO_4)]_2(ClO_4)_2$ (1)

The complex $[Ba(H_2L1)(ClO_4)]_2(ClO_4)_2$ (1) was synthesised by a template reaction of 2,6-diformylpyridine and 1,3-diaminopropan-2-ol in the presence of $Ba(ClO_4)_2 \cdot 3H_2O$ in methanol (Figure 2-3) with high yield and purity. In the IR spectrum of the compound, there was no indication of primary amines or unreacted carbonyls and the formation of imine bonds was indicated by the appearance of a strong (C=N) absorption at 1654 cm^{-1}. The strong asymmetric ν_3 stretch of the perchlorate ions at 1100 cm^{-1} is split, suggesting at least some of these ions may be coordinated.

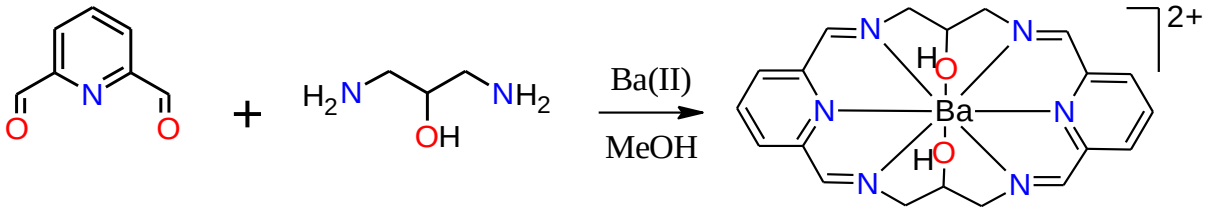

Figure 2-3 Formation of $[Ba(H_2L1)(ClO_4)]_2(ClO_4)_2$ (1).

The ESI mass spectrum of complex (1) is shown in Figure 2-4; the $[Ba(H_2L)](ClO_4)^+$ cation was seen as a main peak at m/z 615 (100%). There are also lower abundance clusters at m/z 515 (5%) and 258 (70%) assigned to $[Ba(HL)]^+$ and $[Ba(H_2L)]^{2+}$ respectively.

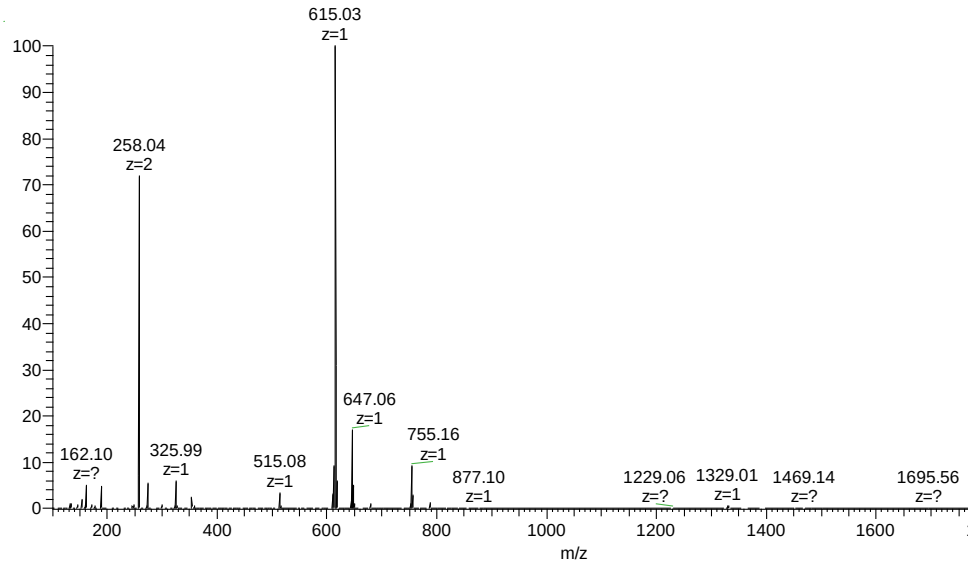

Figure 2-4 ESI mass spectrum of the $[Ba(H_2L1)(ClO_4)]_2(ClO_4)_2$ (1).

The ^{1}H NMR of the complex was recorded in CD_3CN. It confirms that the integrity of macrocyclic ligand H_2L1 in solution and assignments of the chemical shifts are presented in Figure 2-5. The ^{1}H-NMR spectrum of the complex displays two multiplet peaks at δ 7.91(*triplet*) and 7.46(*doublet*) ppm corresponding to the pyridine protons, a singlet at δ 8.32 ppm is assigned to azomethine protons (–N=CH-).

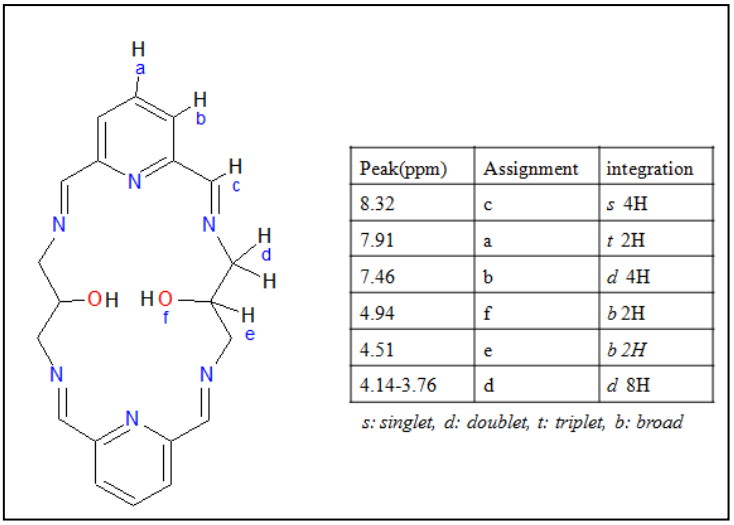

Peak(ppm)	Assignment	integration
8.32	c	*s* 4H
7.91	a	*t* 2H
7.46	b	*d* 4H
4.94	f	*b* 2H
4.51	e	*b 2H*
4.14-3.76	d	*d* 8H

s: singlet, d: doublet, t: triplet, b: broad

Figure 2-5 ^{1}H NMR data of complex (1) in CD_3CN.

Single crystals of complex (1) were grown by vapour diffusion of diethylether into an acetonitrile solution of the complex and the structure of the complex was determined by X-ray crystallography. The complex was found to crystallise in the triclinic space group $P\bar{1}$, details of the crystal structure and refinement can be found in Table A1 in Appendix 2.

The structural data show that the crystals contain centrosymmetric dimeric $[Ba(H_2L_1)(ClO_4)]_2^{2+}$ cations and uncoordinated perchlorate anions. A perspective view of the cation is shown in Figure 2-6. Each barium ion is 11-coordinate, bonded to all eight donors (N_6O_2) from one macrocycle and to two perchlorate ions, one acting as a monodentate donor while the other is bidentate. The coordinated perchlorate anions link the two halves of the dimer. The macrocycle is folded quite sharply (pyN2-Ba1-pyN5 69.83(9)°).

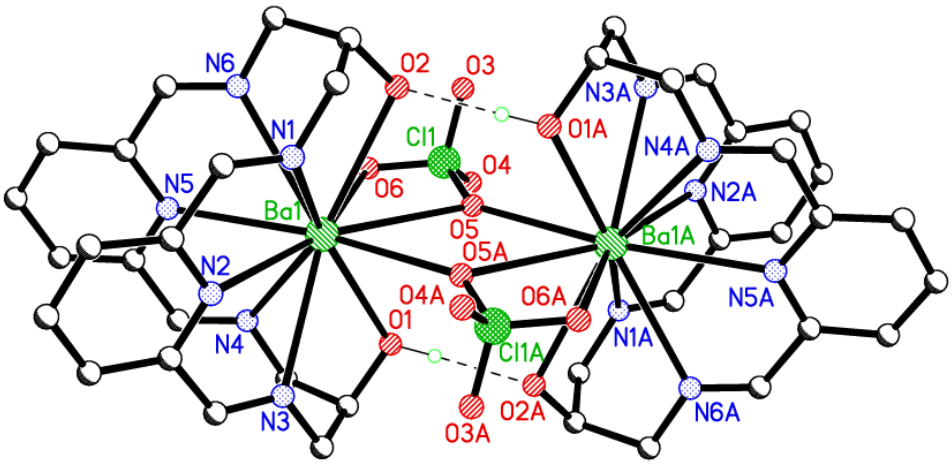

Figure 2-6 Perspective view of the dimeric cation $[Ba(H_2L)(ClO_4)]_2^{2+}$ dashed lines indicate hydrogen bonds. The non-coordinated perchlorate anions and the hydrogen atoms have been omitted for clarity.

Ba1-donor distances range between 2.786(4) and 3.090(4) Å. The two halves of the dimer are linked by two unsymmetric, single-atom bridges formed by coordinated perchlorate ions (Ba1-O5-Ba1A 119.63(15)°); the shorter bond is to the bidentate perchlorate. These bridges are supported by hydrogen bonding linking the alcohol groups on adjacent macrocycles (O1-H1…O2A 2.794(6) Å). The cations are linked into chains by hydrogen bonding, from one of the pendant alcohol groups (O2) to O3 of a bridging perchlorate in the same cation and to O3B of a bridging perchlorate in a neighbouring cation (under symmetry operation -x+2, -y+1, -z+1); this interaction is shown in Figure 2-7 and hydrogen bond parameters are given in Table 2-1.

Table 2-1 Hydrogen bonds for (1) [Å and °].

D—H···*A*	*D*—H	H···*A*	*D*···*A*	*D*—H···*A*
O1—H1A···O2A	0.85	1.95	2.794 (6)	173.4
O2—H2A···O3B	0.85	2.15	2.915 (6)	149.9
O2—H2A···O3	0.85	2.42	3.100 (7)	136.9

Symmetry codes: (A) -*x*+1, -*y*+1, -*z*+1; (B) -*x*+2, -*y*+1, -*z*+1.

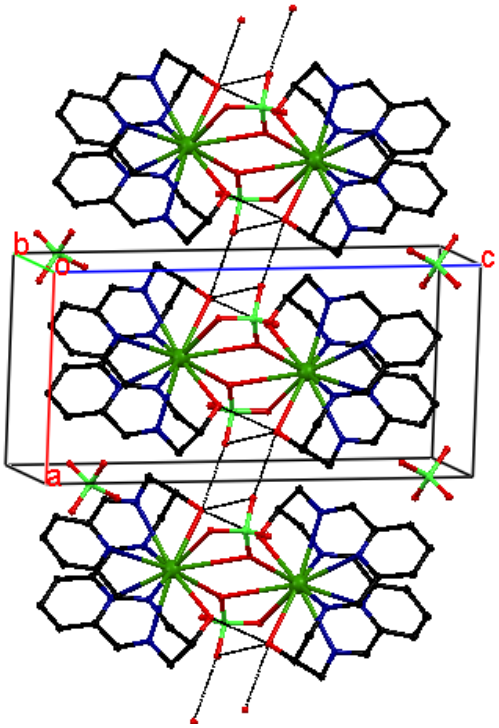

Figure 2-7 Packing diagram of (1) showing hydrogen bonding. Hydrogen atoms are omitted for clarity.

It is informative to compare the structure of this complex with the analogous complexes of the related ligands H_2A, formed by condensation of 2,6-diacetylpyridine with 1,3-diaminopropan-2-ol[174] and B derived from 2,6-diformylpyridine and 1,3-diaminopropane (Figure 2-8).[175,176]

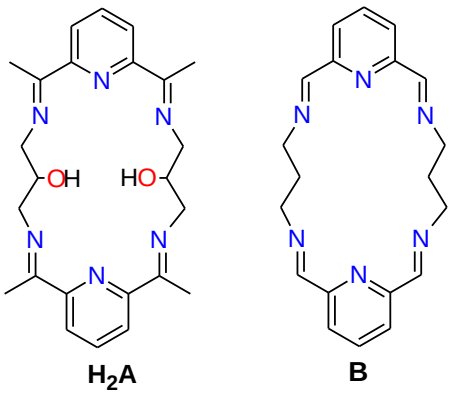

H_2A **B**

Figure 2-8 Macrocyclic ligands H_2A and B.

The published structure of $[Ba(H_2A)(H_2O)_2]_2(ClO_4)_4$ is very similar to the structure of complex (1). In both cases, the barium is 11-coordinate, both are dimeric and the Ba···Ba distances are almost identical (5.138 and 5.133 Å for complex (1) and H_2A

respectively). In the H_2A complex the non-macrocyclic ligands are water rather than perchlorate anions. The most striking difference between the two complexes including the propan-2-ol chains is the presence of a much sharper fold in the macrocycle (pyN-Ba-pyN angles are 69.8 and 83.2° for complex (1) and H_2A complexes, respectively.[174]

In $[Ba(B)(ClO_4)_2H_2O)]$ the macrocycle is only slightly bowl-shaped (pyN-Ba-Npy angle 130.7˚) and all six donors are coordinated (Figure 2-9). Two perchlorate anions and a water molecule are also bound and again the barium ions are 11-coordinate.[175,176]

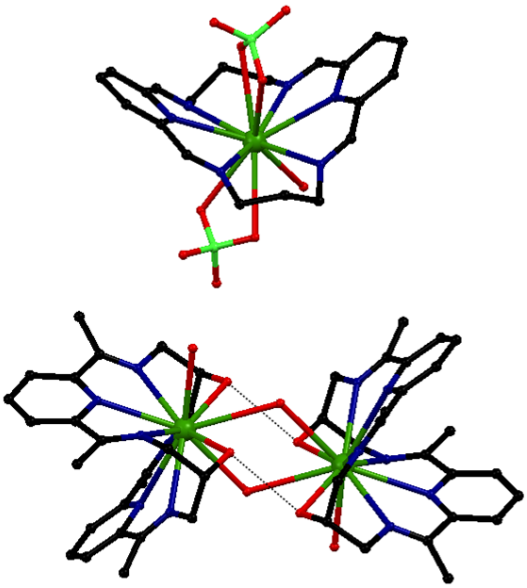

Figure 2-9 The structures of $[Ba(B)(ClO_4)_2(H_2O)]$(top) and the cation $[Ba(H_2A)(H_2O)_2]_2^{4+}$(bottom).

2.2.3 Transmetallation reactions with Mn(II)

Ba(II) was used as template for the formation of the macrocycle (H_2L1) as it produces the [2+2] macrocycle in good yield and purity. Once the barium complex is formed, it can be transmetallated by Mn(II) ions forming a complex which is more stable than the barium complex. Imine and pyridine nitrogen atoms are medium soft donors, however the barium ion is hard and so easily displaced by softer manganese(II) ions. In transmetallation reactions with Mn(II), formation of two different macrocyclic species was observed, depending on the solvent used. In methanol or ethanol ring-contracted mononuclear Mn(II) complexes were obtained, but when acetonitrile was used, ring-expanded polynuclear complexes formed (Figure 2-10).

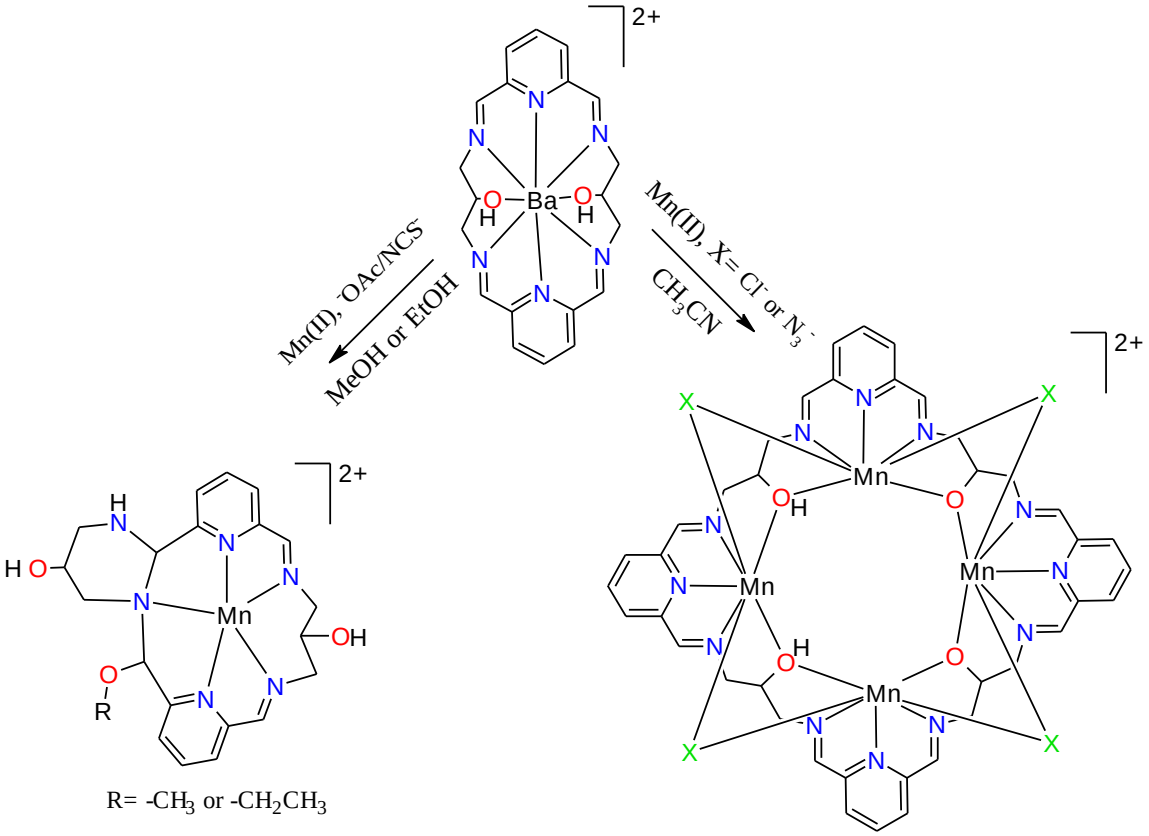

Figure 2-10 Transmetallation products derived from H_2L1.

2.2.4 Ring-contracted mononuclear Mn(II) complexes $[Mn(H_3L2)(NCS)_2]$ (2) and $[Mn(H_3L3)(NCS)_2]$ (3)

When the barium complex (1) reacted with $Mn(OAc)_2.4H_2O$ in a 1:1 ratio in ethanol or methanol, clear yellow solutions were obtained. Upon reduction of solvent to small volumes, yellow oils were obtained. These were redissolved in methanol or ethanol and excess NaNCS was added, yellow-orange products were collected and analysed. In the IR spectra of the complexes, imine bond vibrations $\upsilon_{(C=N)}$ were observed at 1642 and 1648 cm^{-1} for complex (2) and (3) respectively. Peaks at around 2920 cm^{-1} can be attributed to N-H stretches consistent with the formation of hexahydropyrimidine rings. Additionally, $\upsilon_{(C\equiv N)}$ for the NCS^- ions were observed at around 2060 cm^{-1}. ESI mass spectra of the complexes were also studied in methanol solution. Molecular cations were observed at (m/z) 523 (100%) and 537 (100%) corresponding to complex cations $[Mn(H_3L2)(NCS)]^+$ and $[Mn(H_3L3)(NCS)]^+$, respectively.

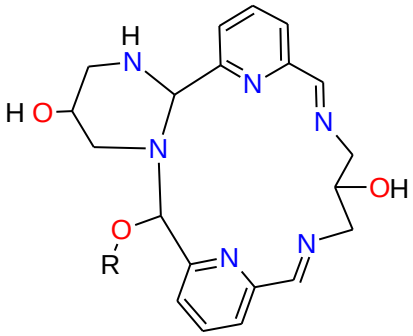

R= -CH_3 **H_3L2**

R= -CH_2CH_3 **H_3L3**

Good quality crystals of complex (3)·½EtOH were obtained from the reaction solution by slow evaporation and crystals of (2)·½dmf were obtained by slow diffusion of diethylether into a dmf solution of the complex. The complex (2)·½dmf was previously prepared by an Erasmus student (Soraya Sanchez Ballester) and the structure was determined by single X-ray crystallography. The unit cell parameters for the complex (2)·½dmf were same as before, therefore the data collection was not repeated and Soraya Sanchez Ballester`s data are used in the following discussion.

The details of the crystal structure and refinement can be found in Tables A2 and A3 of Appendix 2 for complexes (2)·½dmf and (3)·½EtOH respectively.

The molecules, each contain one seven-coordinate Mn(II) ion bound to five nitrogen atoms from the ring-contracted macrocycle forming a pentagonal bipyramidal geometry, with two N-bound thiocyanates at the axial positions (Figure 2-11). The asymmetric unit of complex (2) contains two independent complex molecules and a dmf molecule while the asymmetric unit of complex (3) contains a partial occupancy uncoordinated ethanol molecule.

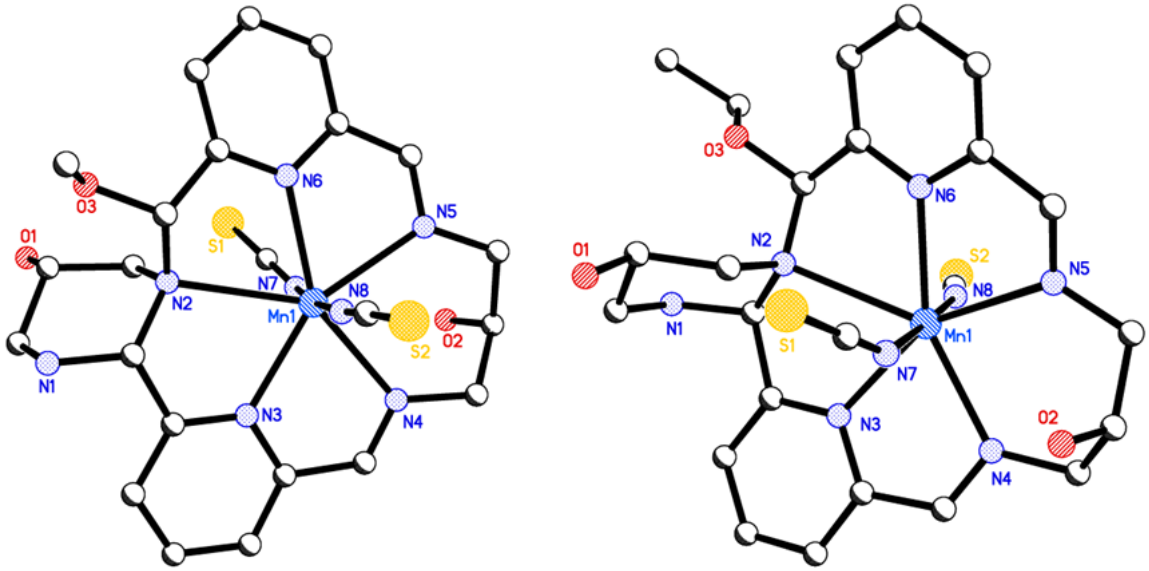

Figure 2-11 Crystal structures of complexes (2) and (3), hydrogen atoms and solvate molecules are omitted for clarity.

The pyridinediimine units exhibit bite angles of 72.01(11) and 70.39(11)° for complex (2) and 72.14(9) and 71.20(9)° for complex (3) and these angles are close to the ideal value of 72° for a pentagonal bipyramidal geometry. The Mn1-N2 bond distance (where N2 is a tertiary amine that has formed part of the six-membered hexahydropyrimidine ring but stays coordinated to the Mn(II) centre) is longer than all other Mn-N bond lengths (2.570(6) Å for (2) and 2.623(6) Å for (3)). Selected bond lengths are given in Table 2-2.

Table 2-2 Selected bond lengths (Å) for (2)·½dmf and (3)·½EtOH.

Complex (2)		Complex (3)	
Mn1—N2	2.585 (3)	Mn1—N2	2.623 (3)
Mn1—N3	2.274 (3)	Mn1—N3	2.272 (2)
Mn1—N4	2.343 (3)	Mn1—N4	2.340 (2)
Mn1—N5	2.426 (3)	Mn1—N5	2.378 (3)
Mn1—N6	2.263 (3)	Mn1—N6	2.256 (2)
Mn1—N7	2.237 (3)	Mn1—N7	2.245 (3)
Mn1—N8	2.179 (3)	Mn1—N8	2.192 (3)

In both complexes, the H_2L1 macrocycle undergoes a ring-contraction *via* addition of methanol (2) or ethanol (3) across one imine bond, followed by a nucleophilic addition of the secondary amine across an adjacent imine bond. Nucleophilic addition reaction results in a six-membered hexahydropyrimidine ring sitting in a chair

conformation. The ring-contraction process reduces the size of the cavity in the macrocycle to accommodate one Mn(II) ion. A proposed ring-contraction mechanism is shown in Figure 2-12.

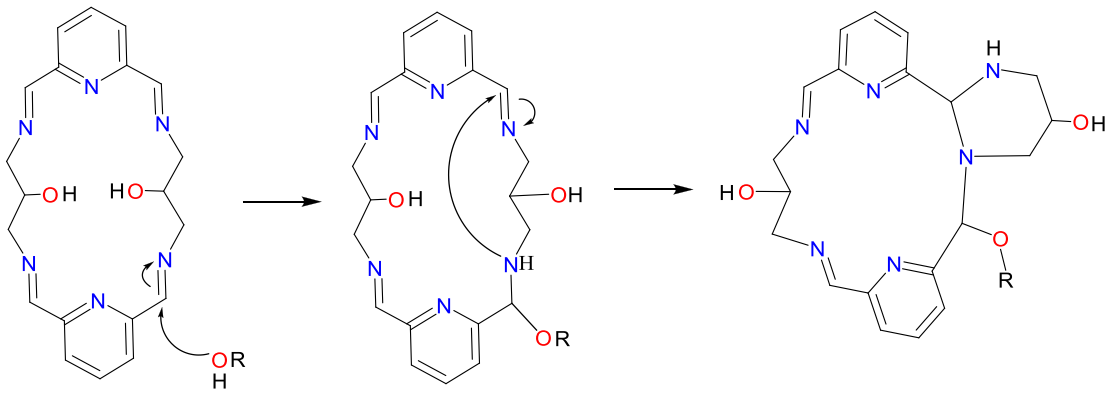

Figure 2-12 Ring-contraction mechanism (where R=OMe or OEt).

Changing the ratio of precursors to 1:2 (Ba:Mn) did not change the structure of the complexes formed. The same ring-contracted complexes were obtained and this was confirmed by X-ray crystallography.

It is informative to compare ring-contracted complexes prepared here with related ring-contracted complexes in the literature (Figure 2-12). Fenton and co-workers observed a metal induced ring-contraction of H_2A to form complex H_2C by the reaction of DAP and 1,3-diamine-2-propanol in the presence of Pb(II) as a template in methanol. In the presence of Ba(II), the same reaction produced macrocyle H_2A with no contraction.[76,174] Conversion of the 20-membered macrocycle (H_2A) to the 18-membered macrocycle (H_2C) was attributed to a mismatch of the cavity size of H_2A and the smaller Pb(II) ion; the two endogenous alcohol groups attacked across adjacent imine bonds resulting two oxazolidine rings (Figure 2-13).[76]

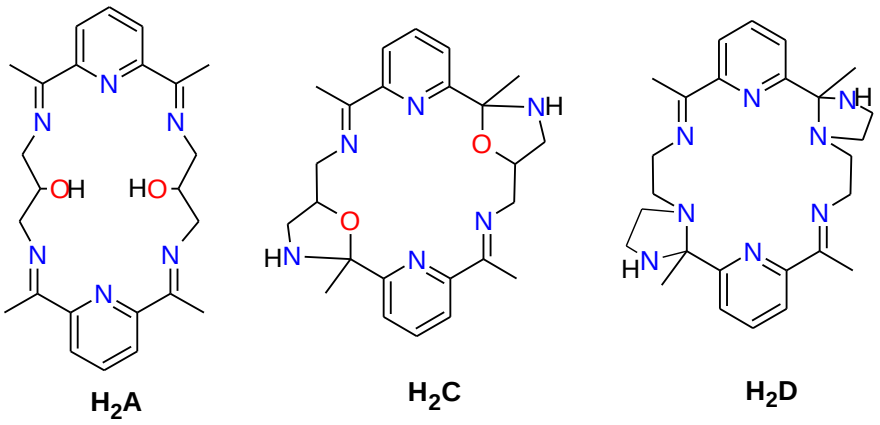

Figure 2-13 Related ring-contracted macrocycles.

Similarly, the ring-contracted macrocycle (H_2D) was prepared from DAP and diethylenetriamine in the presence of Ba(II) as a template to give an 18-membered ring-contracted macrocycle.[72] The secondary amine groups have added across neighbouring imine bonds *via* nucleophilic addition forming two five-membered imidazoline rings. However, treating the ring-contracted Ba(II) complex of H_2D with Cu(II) results in a ring-expansion from 18-membered to 24-membered (H_2E) to accommodate two Cu(II) ions within the cavity (Figure 2-14).

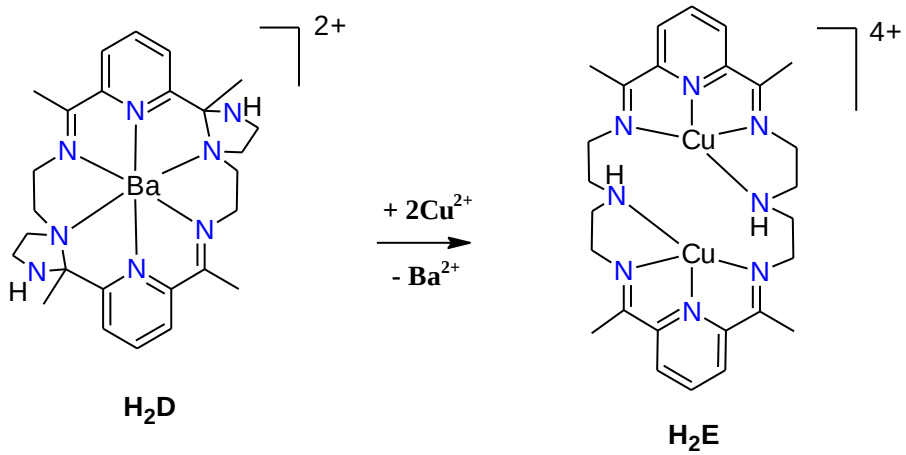

Figure 2-14 Formation of H_2E macrocycle from H_2D.[72]

2.2.5 The [4+4] ring-expanded polynuclear Mn(II) complexes; $[Mn_4(H_2L^*)Cl_4][MnCl_4]$ (4) and $[Mn_4(H_2L^*)(N_3)_4](ClO_4)_2$ (4a)

Since ring-contracted mononuclear complexes were obtained when methanol or ethanol were used as solvents, the transmetallation reaction was repeated in acetonitrile. Acetonitrile is an aprotic solvent and cannot undergo a nucleophilic addition reaction.

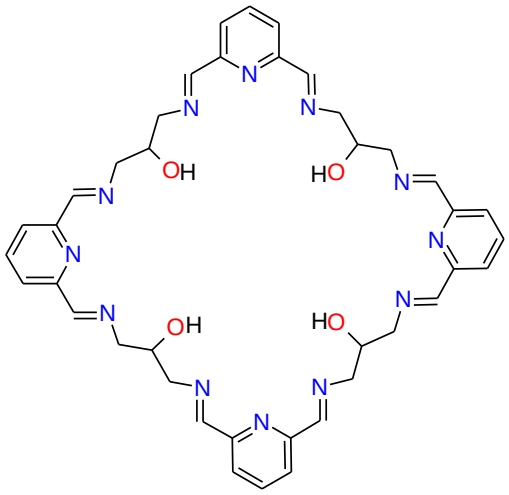

H_4L^*

When the barium complex (1) was refluxed in acetonitrile with $MnCl_2 \cdot 4H_2O$ (1:2 Ba:Mn ratio) for 4-6 hrs, a cloudy yellow solution was observed. White solid ($BaCl_2$) was removed from the reaction mixture *via* filtration while hot, resulting in a clear yellow solution. Large yellow crystals suitable for X-ray diffraction study grew in the solution after several hrs. The crystals had a cubic unit cell with a very large cell volume (68081(10) $Å^3$). The structure was solved but the refinement was poor, due to weak diffraction and severe disorder of the anions. These problems were overcome by changing Ba:Mn ratio from 1:2 to 1:2.5 in the reaction mixture. Similarly, large crystals were obtained and analysed by single X-ray diffraction study.

In this case, the complex $[Mn_4(H_2L^*)Cl_4][MnCl_4] \cdot 4.5CH_3CN$ crystallised in the orthorhombic space group $Pna2_1$. The details of the crystal structure and refinement can be found in Table A4 in Appendix 2. A perspective view of the complex cation is shown in Figure 2-15. The asymmetric unit consists of the H_2L^* ring-expanded tetranuclear complex cation, a tetrachloromanganate(II) anion and acetonitrile molecules.

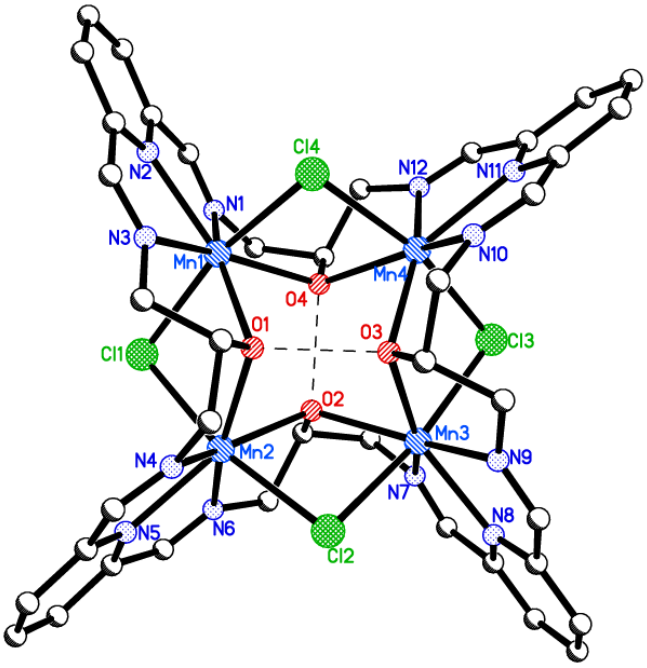

Figure 2-15 Perspective view of complex cation of $[Mn_4(H_2L^*)Cl_4]^{2+}$, hydrogen atoms are omitted for clarity.

The H_2L^* macrocycle contains four Mn(II) ions each of which sits in a pyridinediimine cavity and the pyridinediimine units provide bite angles ranging from 133.74(10) to 134.75(10)°. The Mn(II) ions are all seven-coordinate, bonded to three nitrogen atoms of a pyridinediimine unit and two alcohol oxygen atoms in a pentagonal plane with two chloride ions at the axial positions giving approximate pentagonal bipyramidal geometry. The four Mn-Cl-Mn bridge angles range from 89.48(3) to 93.53(3)° which are considerably smaller than tetrahedral angles. However, the Mn-O-Mn angles are bigger than those Mn-Cl-Mn angles ranging from 102.02(9) to 104.95(9)°. The Cl-Mn-Cl axial angles are between 163.73(3) and 167.96(3)° which are considerably bent away from the ideal linear angle of 180°.

Two of the four alcohol groups in the macrocycle are deprotonated and these are involved in hydrogen bonding to the non-deprotonated alcohols strengthening the H_2L^* structure (O1-O3 and O2-O4 2.463(3) and 2.455(3) Å respectively). Each H_2L^* tetranuclear Mn(II) complex cation has, therefore, a +2 charge, which is balanced by an approximately tetrahedral $[MnCl_4]^{2-}$ complex anion.

The principal interaction between adjacent complex cations is π-π stacking between pyridinediimine head units as illustrated in Figure 2-16. The head unit containing N5

of one complex cation is stacked with the head unit containing N8 of an adjacent cation under symmetry operation 1-x, 2-y, -½+z; the pyridine centroid-centroid distance is 3.495 Å. The π-π stacking can be seen in the packing diagram as viewed down the *a* axis shown in Figure 2-17. Neither the tetrahedral $[MnCl_4]^{2-}$ counter ion nor the acetonitrile solvate molecules interacts strongly with the complex cation.

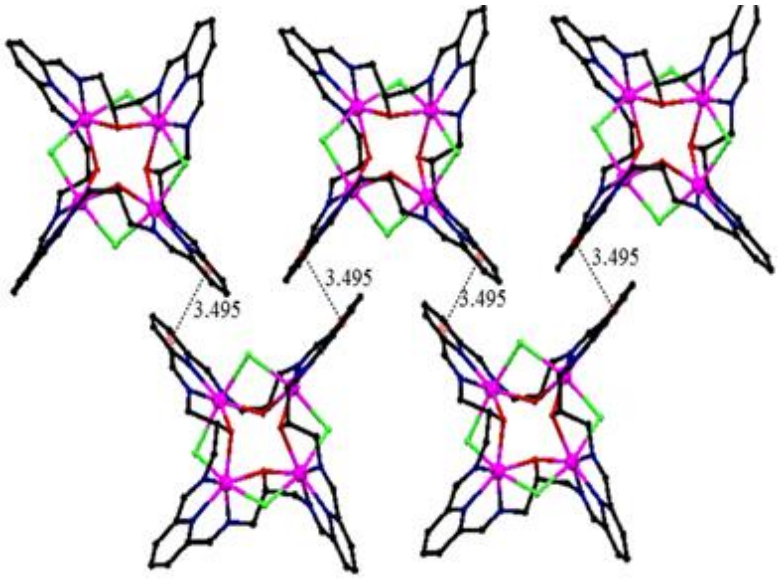

Figure 2-16 π-π stacking interactions in $[Mn_4(H_2L^*)Cl_4][MnCl_4]\cdot 4.5CH_3CN$.

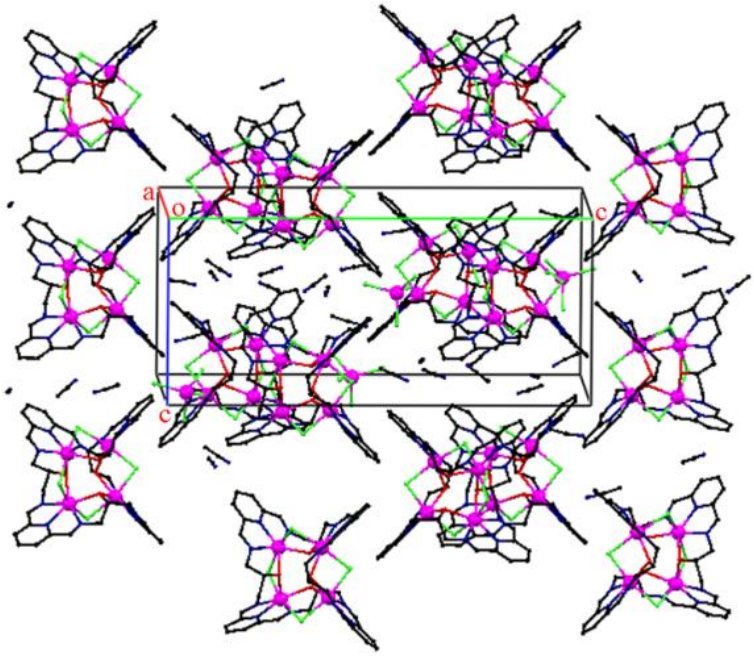

Figure 2-17 Packing diagram of $[Mn_4(H_2L^*)Cl_4][MnCl_4]\cdot 4.5CH_3CN$.

Table 2-3 Selected bond lengths [Å] and angles [°] for $[Mn_4(H_2L^*)Cl_4][MnCl_4]\cdot 4.5CH_3CN$.

Mn1—N1	2.308 (3)	Mn3—N7	2.286 (3)
Mn1—N2	2.307 (3)	Mn3—N8	2.299 (3)
Mn1—N3	2.278 (3)	Mn3—N9	2.281 (3)
Mn1—O1	2.389 (2)	Mn3—O2	2.326 (2)
Mn1—O4	2.315 (2)	Mn3—O3	2.345 (2)
Mn1—Cl1	2.5302 (9)	Mn3—Cl2	2.6121 (9)
Mn1—Cl4	2.5581 (9)	Mn3—Cl3	2.5586 (10)
Mn2—N4	2.302 (3)	Mn4—N10	2.311 (3)
Mn2—N5	2.319 (3)	Mn4—N11	2.318 (3)
Mn2—N6	2.268 (3)	Mn4—N12	2.267 (3)
Mn2—O1	2.301 (2)	Mn4—O3	2.296 (2)
Mn2—O2	2.346 (2)	Mn4—O4	2.399 (2)
Mn2—Cl1	2.5813 (9)	Mn4—Cl3	2.5638 (9)
Mn2—Cl2	2.5787 (9)	Mn4—Cl4	2.5521 (9)
N2—Mn1—N1	67.72 (10)	O2—Mn2—Cl1	88.28 (6)
N3—Mn1—N1	134.08 (10)	Cl2—Mn2—Cl1	166.44 (3)
N3—Mn1—N2	68.28 (11)	N9—Mn3—N7	134.75 (10)
N3—Mn1—O4	153.28 (9)	N9—Mn3—N8	68.00 (10)
N2—Mn1—O4	130.77 (9)	N7—Mn3—N8	68.41 (10)
N1—Mn1—O4	71.22 (9)	N9—Mn3—O2	153.42 (9)
N3—Mn1—O1	72.34 (9)	N7—Mn3—O2	70.83 (9)
N2—Mn1—O1	140.27 (9)	N8—Mn3—O2	132.47 (9)
N1—Mn1—O1	151.69 (9)	N9—Mn3—O3	72.94 (9)
O4—Mn1—O1	85.19 (7)	N7—Mn3—O3	149.39 (9)
N3—Mn1—Cl1	91.52 (8)	N8—Mn3—O3	140.93 (9)
N2—Mn1—Cl1	106.70 (8)	O2—Mn3—O3	84.73 (7)
N1—Mn1—Cl1	88.91 (8)	N9—Mn3—Cl3	91.31 (8)
O4—Mn1—Cl1	98.35 (6)	N7—Mn3—Cl3	85.55 (7)
O1—Mn1—Cl1	79.02 (6)	N8—Mn3—Cl3	101.08 (7)
N3—Mn1—Cl4	84.72 (7)	O2—Mn3—Cl3	99.08 (6)
N2—Mn1—Cl4	86.63 (8)	O3—Mn3—Cl3	80.26 (6)
N1—Mn1—Cl4	105.08 (8)	N9—Mn3—Cl2	86.51 (8)
O4—Mn1—Cl4	78.87 (6)	N7—Mn3—Cl2	104.36 (7)
O1—Mn1—Cl4	84.75 (6)	N8—Mn3—Cl2	89.09 (7)
Cl1—Mn1—Cl4	163.73 (3)	O2—Mn3—Cl2	78.24 (6)
N6—Mn2—O1	154.28 (9)	O3—Mn3—Cl2	87.78 (6)
N6—Mn2—N4	134.14 (10)	Cl3—Mn3—Cl2	167.96 (3)

O1—Mn2—N4	71.34 (9)	O3—Mn4—N10	71.71 (9)
N6—Mn2—N5	68.22 (11)	N12—Mn4—N11	68.40 (11)
O1—Mn2—N5	134.13 (9)	O3—Mn4—N11	133.56 (10)
N4—Mn2—N5	67.68 (11)	N10—Mn4—N11	67.56 (12)
N6—Mn2—O2	72.91 (9)	N12—Mn4—O4	72.08 (9)
O1—Mn2—O2	84.04 (7)	O3—Mn4—O4	85.00 (7)
N4—Mn2—O2	148.99 (9)	N10—Mn4—O4	149.57 (10)
N5—Mn2—O2	141.11 (10)	N11—Mn4—O4	140.49 (10)
N6—Mn2—Cl2	90.87 (7)	N12—Mn4—Cl4	93.17 (7)
O1—Mn2—Cl2	95.68 (6)	O3—Mn4—Cl4	92.97 (6)
N4—Mn2—Cl2	85.26 (8)	N10—Mn4—Cl4	84.28 (8)
N5—Mn2—Cl2	100.55 (7)	N11—Mn4—Cl4	104.05 (8)
O2—Mn2—Cl2	78.56 (6)	O4—Mn4—Cl4	77.49 (6)
N6—Mn2—Cl1	88.32 (7)	N12—Mn4—Cl3	87.06 (7)
O1—Mn2—Cl1	79.57 (6)	O3—Mn4—Cl3	81.08 (6)
N4—Mn2—Cl1	104.92 (8)	Mn1—Cl1—Mn2	91.38 (3)
N5—Mn2—Cl1	91.71 (7)	Mn2—Cl2—Mn3	91.14 (3)
N10—Mn4—Cl3	105.70 (8)	Mn3—Cl3—Mn4	89.48 (3)
N11—Mn4—Cl3	89.17 (8)	Mn4—Cl4—Mn1	93.53 (3)
O4—Mn4—Cl3	89.19 (6)	Mn2—O1—Mn1	102.48 (8)
Cl4—Mn4—Cl3	165.89 (3)	Mn3—O2—Mn2	105.02 (8)
N12—Mn4—O3	154.33 (9)	Mn4—O3—Mn3	101.95 (8)
N12—Mn4—N10	133.74 (11)	Mn1—O4—Mn4	104.30 (8)

Figure 2-18 shows the ESI mass spectrum of the complex obtained in acetonitrile. Signals assigned to complexes of H_4L^* and H_2L1 were indicated by star and rectangular shapes respectively. The peak assignments are listed in Table 2-4. The molecular complex cation, as a doubly charged peak, was observed at m/z 557 (100%). Several multi-charged signals arising from loss of some of the bridging chloride ions in the complex were seen (Table 2-3). From the mass spectrum analysis, the H_4L^* macrocycle is intact in acetonitrile solution. However, one doubly charged peak at m/z 216 and one single charged peak at m/z 432 assigned to $\{[Mn(H_2L1)]\}^{2+}$ and $\{[Mn(HL1)]\}^{+}$ respectively, were detected in the spectrum. These $[H_2L1]$ species may come from the original sample H_2L1 as a minor product or incomplete reorganisation.

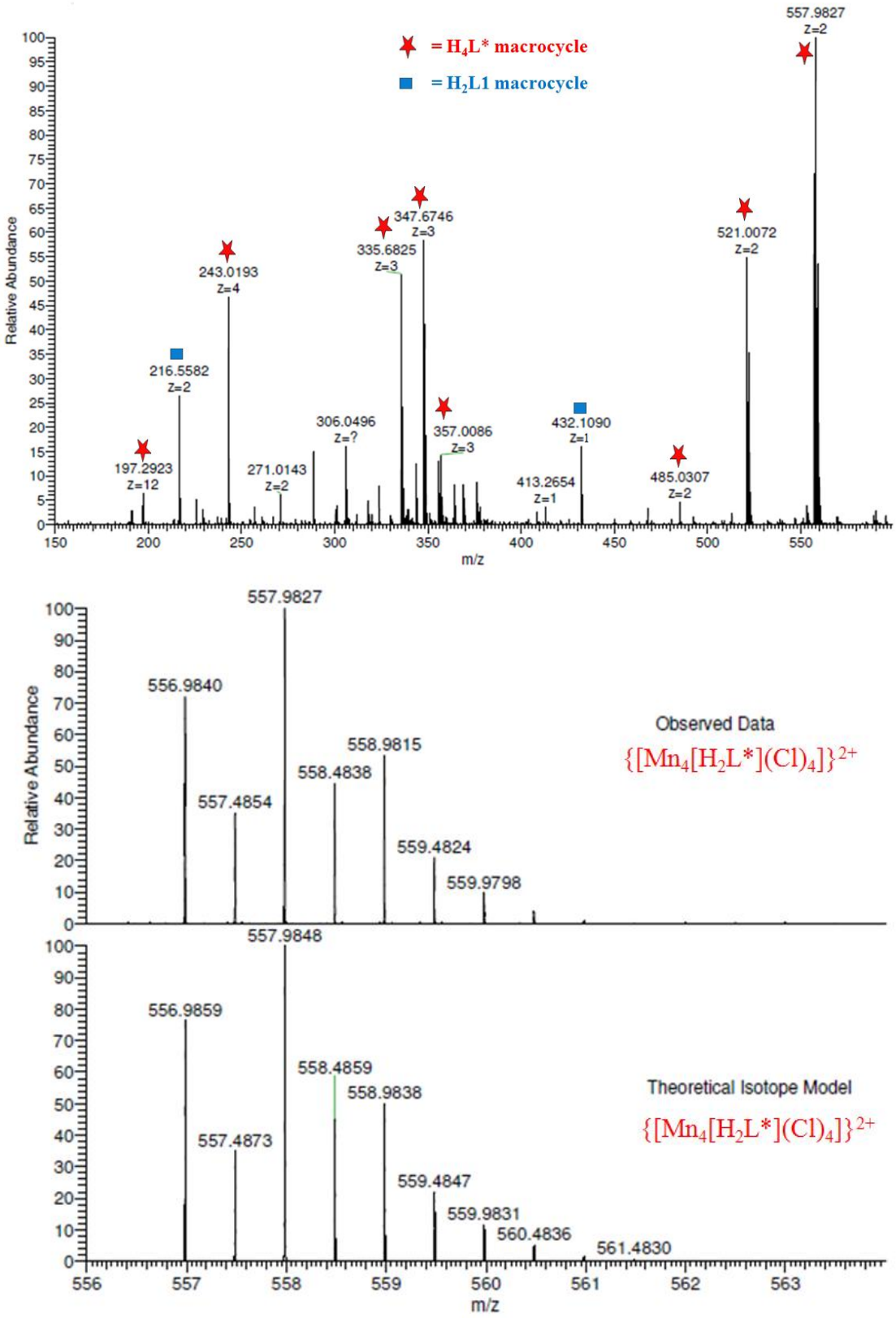

Figure 2-18 ESI mass spectrum of complex (4) in acetonitrile (top), experimental and theoretical isotope distribution of the complex cation (bottom).

The ESI mass spectrum of the sample was also recorded in methanol. To do this, the complex was dissolved in methanol and left for 4 hrs at room temperature. The aim was then to detect whether complex (4) converted to the ring-contracted complex when methanol was used as solvent. The ESI mass spectrum of the complex in methanol is shown in Figure 2-19. The spectrum is slightly different from that in acetonitrile, however, the H_2L^* molecular complex cation was observed at m/z 557 with lower abundance. A new singly charged peak appeared at m/z 532 (100%) and this peak was assigned to the ring-contracted complex $\{[Mn(H_3L2)Cl](CH_3OH)\}^+$. The main peak in the spectrum was seen at 468(100%) assigned to the complex cation $[Mn(H_2L1)Cl]^+$. Appearance of these two new peaks strongly suggests that, in methanol solution, there is equilibrium between H_4L^*, H_2L1 and H_3L2 complexes or slow conversion of H_4L^* to H_2L1 and H_3L2. The speed of conversion may be increased by stirring or heating.

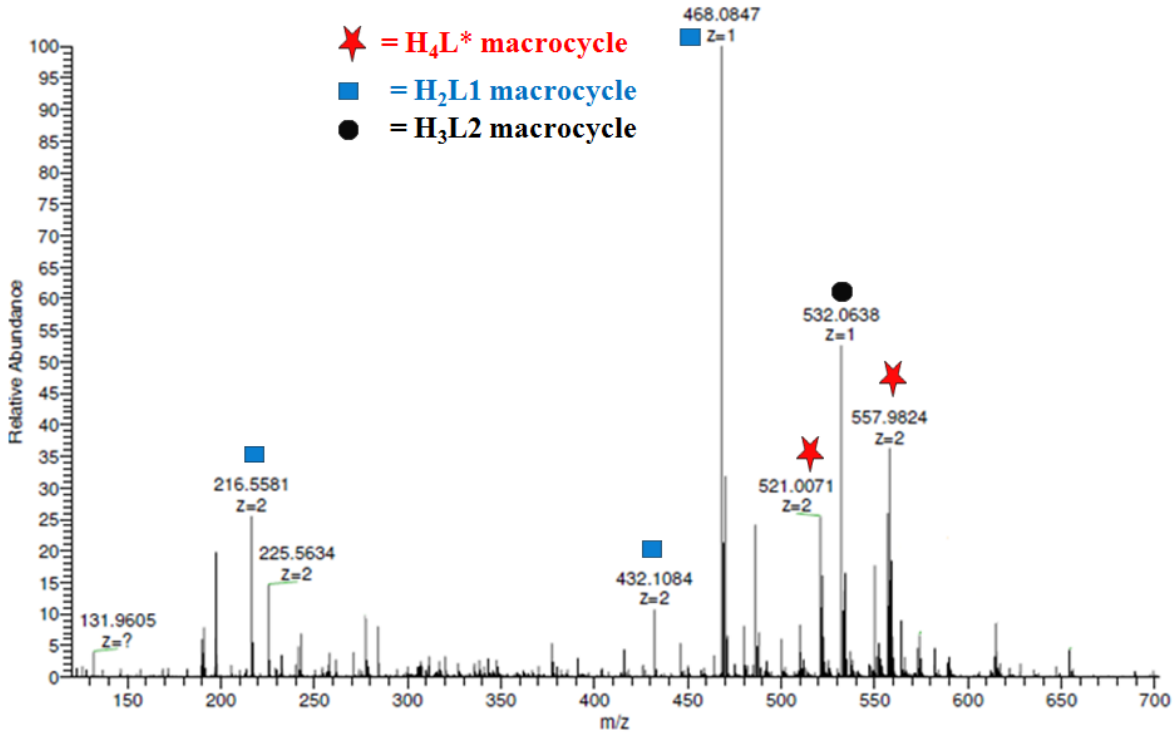

Figure 2-19 ESI mass spectrum of complex (4) in methanol.

Table 2-4 ESI mass spect. peaks assignment.

ESI in acetonitrile			
Found (M/z)	**Rel. Abundance (%)**	**Assignment**	**Calc. Mass**
557.98	100	$\{[Mn_4(H_2L^*)(Cl_4)]\}^{2+}$	557.98
521.00	50	$\{[Mn_4(H_2L^*)Cl_2]\}^{2+}$	521.00
485.03	5	$\{[Mn_4(H_2L^*)]\}^{2+}$	485.03
432.10	15	$\{[Mn_2(H_2L^*)]\}^{+}$	432.10
357.00	15	$\{[Mn_4(H_2L^*)Cl_3]\}^{3+}$	357.00
347.67	60	$\{[Mn_4(H_2L^*)Cl_2]\}^{3+}$	347.67
335.68	50	$\{[Mn_4(H_2L^*)Cl]\}^{3+}$	335.68
243.01	48	$\{[Mn_4(H_2L^*)]\}^{4+}$	243.01
216.55	25	$\{[Mn(H_2L^*)]\}^{2+}$	216.55
ESI in methanol			
557.98	40	$\{[Mn_4(H_2L^*)(Cl_4)]\}^{2+}$	557.98
532.06	50	$\{[Mn(H_3L2)Cl](CH_3OH\}^{+}$	532.06
521.00	30	$\{[Mn_4(H_2L^*)Cl_2]\}^{2+}$	521.00
468.08	100	$\{[Mn(H_2L1)Cl)]\}^{+}$	485.03
432.10	10	$\{[Mn_2(H_2L1)]\}^{+}$	432.10
216.55	25	$\{[Mn(H_2L1)]\}^{2+}$	216.55

An azide analog of (4) was also prepared. One equivalent of the complex $[Ba(H_2L1)(ClO_4)]_2(ClO_4)_2$ (1) was treated with two equivalents of manganese perchlorate in refluxing acetonitrile. On addition of four equivalents of sodium azide to the reaction mixture, a yellow-brown precipitate formed with a dark orange-brown solution. After refluxing for several hrs, the yellow-brown precipitate was filtered and the filtrate was left to evaporate in air. The bulky yellow-brown precipitate was analysed by CHN analysis and IR spectroscopy. In the IR spectrum, the imine bond stretch (C=N) was observed at 1610 cm^{-1} and peaks at 2053 and 1072 cm^{-1} could be assigned to azide and perchlorate stretches, respectively. However, CHN analysis showed than carbon and hydrogen content are very far

away from the calculated values for the H_2L^* Mn(II) azide complex. This suggested that the bulk precipitate contains a large amount of inorganic impurity. Attempts to remove impurities were unsuccessful due to the insolubility of the product in most organic solvents including dmso and dmf. However, from the filtrate a few dark orange-brown crystals formed over a few days. The structure of the crystals was determined by single X-ray diffraction study, but there was not enough material to do other analyses.

The complex $\{[Mn_4(H_2L^*)(N_3)_4](ClO_4)_2 \cdot 3CH_3CN$ was found to crystallise in the tetragonal space group *I*4/*m*. The details of the crystal structure and refinement can be found in Table A5 in Appendix 2 and a perspective view of the complex cation is shown in Figure 2-20. The asymmetric unit contains one quarter of the complex.

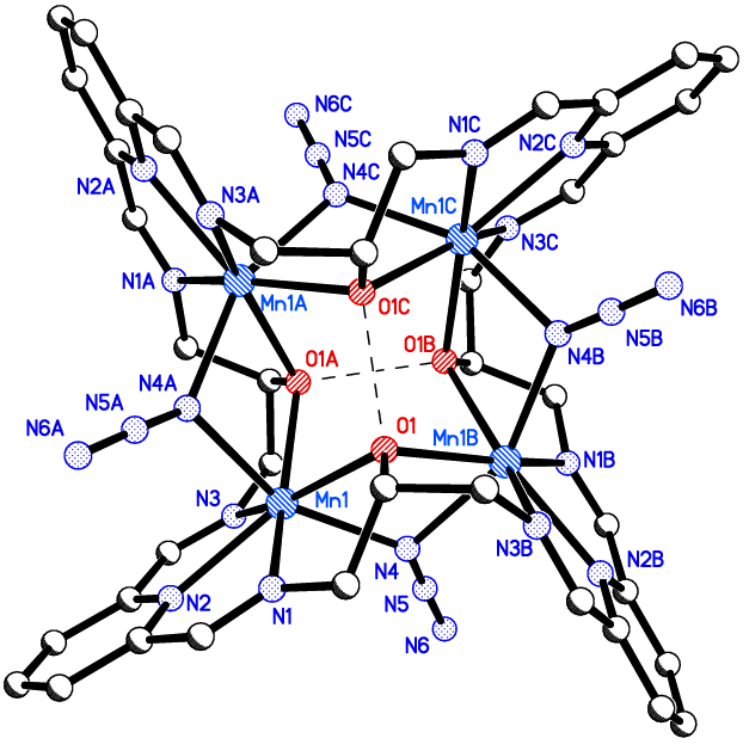

Figure 2-20 The structure of the complex cation $[Mn_4(H_2L^*)(N_3)_4]^{2+}$ *of the azide complex, hydrogen atoms are removed for clarity.*

The structure of the azide complex is similar to the chloride complex (4) with four azide ions each bridging two Mn(II) centres. Again π-π stacking interactions between pyridinediimine head units were observed in the azide complex but, in this case, symmetry requires all pyridinediimine head units are involved with a centroid-centroid distance of 3.874 Å. The π-π stacking can be seen in the packing diagram viewed down the *a* axis shown in Figure 2-21.

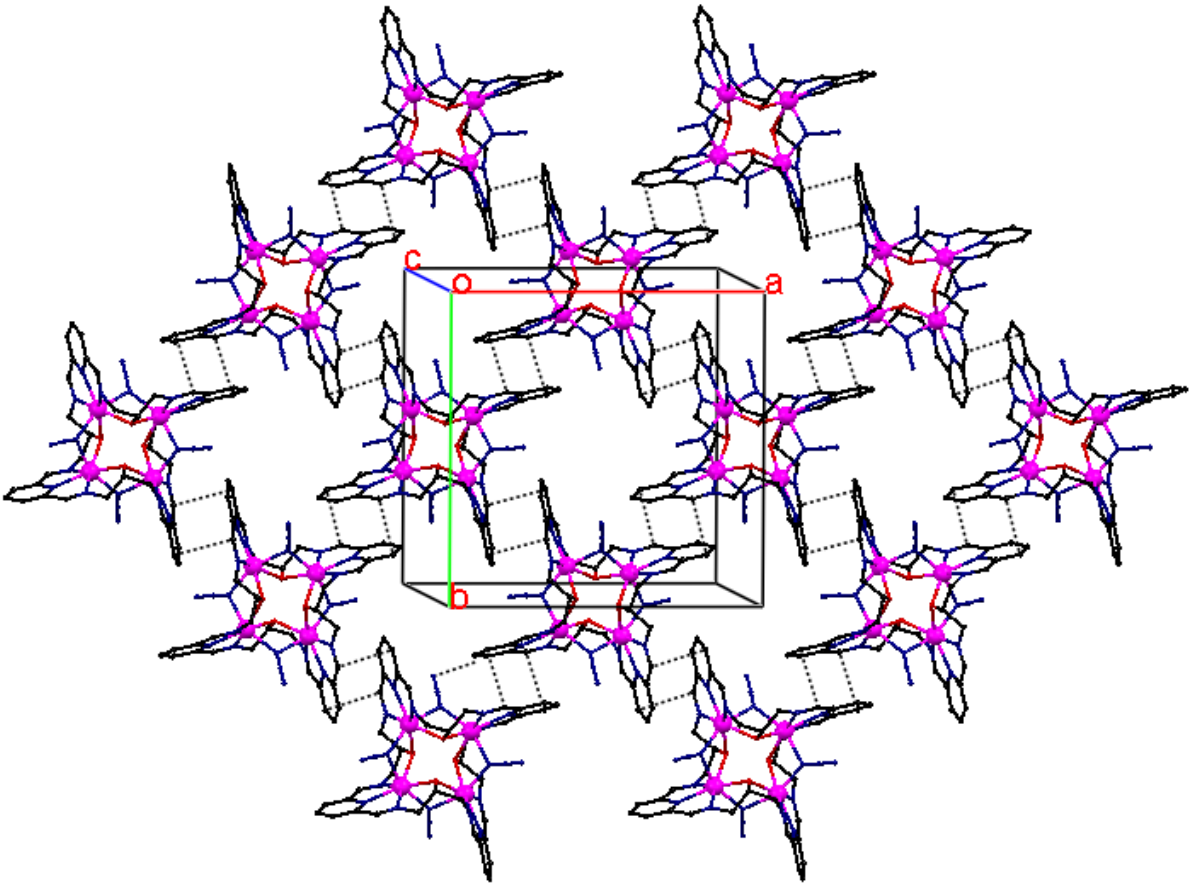

Figure 2-21 Packing diagram of the azide complex showing π-π stacking interactions. Perchlorate anions and acetonitrile molecules are omitted for clarity.

The transmetallation reaction of the complex $[Ba(H_2L1)(ClO_4)]_2(ClO_4)_2$ (1) with manganese perchlorate or acetate were also tried in refluxing acetonitrile. The reaction solutions were refluxed 12 hrs resulting in clear yellow solutions. Yellow-brown oils were obtained after air evaporation. Attempts to get solid products by redisolving the oil in acetonitrile failed.

2.2.6 Comparison with macrocyclic Mn(II) complexes derived from 2,6-diacetylpyridine (DAP) analogues

Transmetallation reactions of $[Ba(H_2L)(ClO_4)]_2(ClO_4)_2$ (1) with Mn(II) resulted in either ring-contracted or ring-expanded Mn(II) complexes, depending on the solvent used. When methanol or ethanol was used in the reaction, ring-contracted Mn(II) complexes were always obtained. However, if the transmetallation reaction was performed in acetonitrile ring-expanded Mn(II) complexes were produced.

It is informative to compare the behaviour of these Mn(II) complexes derived from 2,6-diacetylpyridine (DAP) rather than DFP (Figure 2-22). McKee *et al*. prepared a number

of macrocyclic Mn(II) complexes *via* transmetallation of the barium complex $[Ba(H_2A)(H_2O)_2]_2(ClO_4)_4$. During the transmetallation reactions in the presence of Cl^-, N_3^-, or OAc^-, the (H_2A) macrocycle did not undergo ring-contraction or ring-expansion reactions although poynuclear complexes formed.[177,178] On the other hand, when transmetallation was performed in the presence of manganese perchlorate, a ring-expanded [4+4] Mn(II) complex was obtained.[179] Now, we will look into structural detail and experimental conditions of those Mn(II) complexes prepared by McKee *et al*.

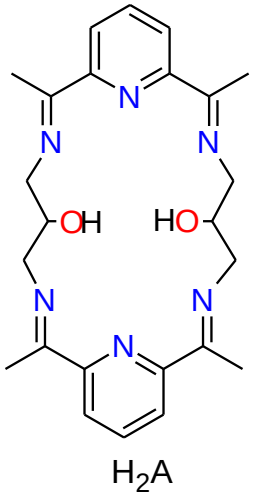

Figure 2-22 The [2+2] macrocycle H_2A.

The reaction of $[Ba(H_2A)(H_2O)_2]_2(ClO_4)_4$ and manganese chloride in methanol produces the tetranuclear dimeric Mn(II) complex $[Mn_2(HA)(C1)_2]_2(ClO_4)_2$. The azide complex $[Mn_2(HA)(N_3)_2]_2(ClO_4)_2$ can be prepared by the reaction of $[Ba(H_2A)(H_2O)_2]_2(ClO_4)_4$ and manganese perchlorate in the presence of sodium azide in methanol. The structures of the complexes are similar (Figure 2-23). During the synthesis of $\{[Mn_2(HA)Cl_2]_2\}^{2+}$ and $\{[Mn_2(HA)(N_3)_2]_2\}^{2+}$, two of the four pendant alcohol groups are deprotonated and these groups are involved in hydrogen bonding with alkoxy groups of the neighbouring macrocycle, strengthening the structures. Each macrocycle accommodates two Mn(II) ions resulting in tetranuclear complexes and each Mn(II) ion is seven-coordinate with approximate pentagonal bipyramidal geometry. The pentagonal planes contain three nitrogen atoms from a pyridinediimine unit and two oxygen atoms from the macrocycle and the axial positions are occupied by either Cl^- or N_3^- ligands. Two of the axial ligands bridge Mn(II) ions in different macrocycles linking two macrocycles together. The other two axial ligands bridge two Mn(II) ions within the same macrocycle.[177]

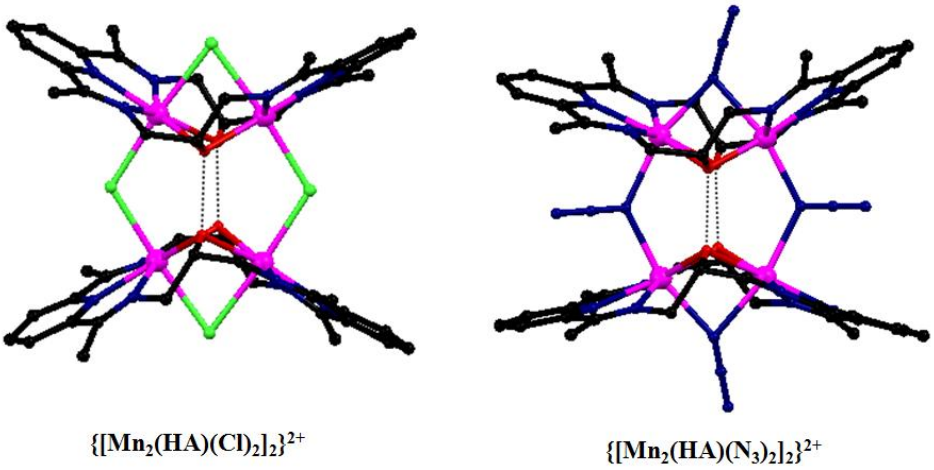

Figure 2-23 Structures of $\{[Mn_2(HA)Cl_2]_2\}^{2+}$ and $\{[Mn_2(HA)(N_3)_2]_2\}^{2+}$ redrawn from literature, H-bonds are shown as dotted lines.[177]

In the light of the ring-expansion discovered for H_2L1, the reactions were repeated in acetonitrile. Single crystals for both chloride and azide complex were obtained by the literature method (dmf-diethylether diffusion) and X-ray data were collected to determine the unit cells for both complexes. Both complexes were found to have the same unit cell parameters as previously prepared complexes from methanol. This confirmed that shifting solvent from methanol to acetonitrile did not cause either ring-contraction or ring-expansion. The only difference between the macrocycle H_2L1 and H_2A is the methyl group attached to the imine carbon atom. The methyl groups likely give some extra stability preventing re-arrangement in the structure.

Although the structures of Mn(II) complexes with chloride and azide with H_2A are different from Mn(II) complexes with H_2L^*, there are some structural similarities. Both sets of complexes are tetranuclear, each Mn(II) ion is seven-coordinate and the axial ligands each bridge two Mn(II) ions (Figure 2-24).[177]

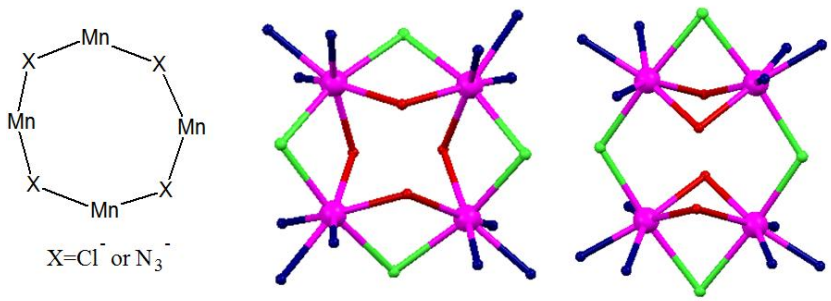

Figure 2-24 Coordination spheres of $[Mn_4(H_2L^*)Cl_4]^{2+}$ (middle) and $[Mn_2(HA)Cl_2]_2^{2+}$ (right).

The transmetallation of $[Ba(H_2A)(H_2O)_2]_2(ClO_4)_4$ with manganese acetate in methanol can yield either a pentamanganese $[Mn_5(A)_2(OAc)_2(ClO_4)_2](ClO_4)_2{\cdot}2H_2O$ or a tetramanganese complex $[Mn_2(A)_2(OAc)]_2(ClO_4)_2{\cdot}5H_2O$ depending on the Ba:Mn ratio used (Figure 2-25). When one equivalent of barium complex reacts with two equivalents of $Mn(OAc)_2{\cdot}4H_2O$, a tetranuclear Mn(II) complex formed; when 1:3 Ba:Mn was used, both tetranuclear and pentanuclear complexes were isolated and for Ba:Mn ratios greater than 1:3 only the pentanuclear complex is generated.[178]

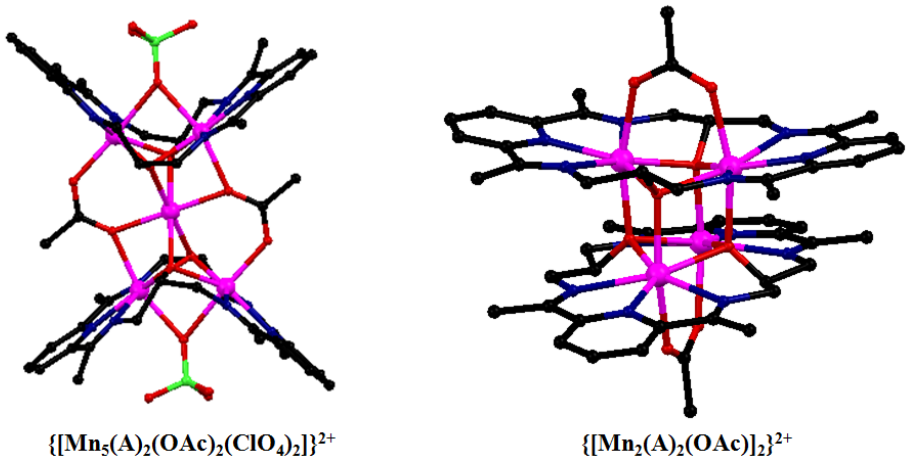

Figure 2-25 Molecular structures of $\{[Mn_5(A)_2(OAc)_2(ClO_4)_2]\}^{2+}$ and $\{[Mn_2(A)_2(OAc)]_2\}^{2+}$ redrawn from literature.[178]

The pentanuclear complex $\{[Mn_5(A)_2(OAc)_2(ClO_4)_2]\}^{2+}$ consists of two folded dinuclear macrocyclic units bridged by an six-coordinate Mn(II) ion and two acetate groups. The acetate ions each bridge three manganese ions. The Mn(II) ions in macrocyclic units are seven-coordinate with approximate pentagonal bipyramidal geometry but the bridging Mn(II) ion is six-coordinate. In tetranuclear complex $\{[Mn_2(A)_2(OAc)]_2\}^{2+}$ the complex is dimeric and each half contains a binuclear macrocycle and an acetate group. The dimers are held together by four manganese alkoxide bonds, resulting in formation of Mn_4O_4 cubane core. A similar tetranuclear complex was prepared by using $Mn(OOCH)_2$.[178]

McKee *et al.* also reported the ring-expanded tetranuclear Mn(II) complex $[Mn_4(A^*)(ClO_4)_4]$ prepared by the reaction of $[Ba(H_2A)(H_2O)_2]_2(ClO_4)_4$ with two equivalents of manganese perchlorate in methanol. The crystal structure of $[Mn_4(A^*)(ClO_4)_4]$ is shown in Figure 2-26. The alcohol groups are all deprotonated and each bridges three manganese centres, resulting a central cubane type structure Mn_4O_4; each Mn(II) in the cluster is seven-coordinate. This complex can also be prepared directly by a template reaction of 2,6-diacetylpyridine and 1,3-diamino-2-propanol in the presence of $Mn(ClO_4)_2.6H_2O$ in methanol.[179]

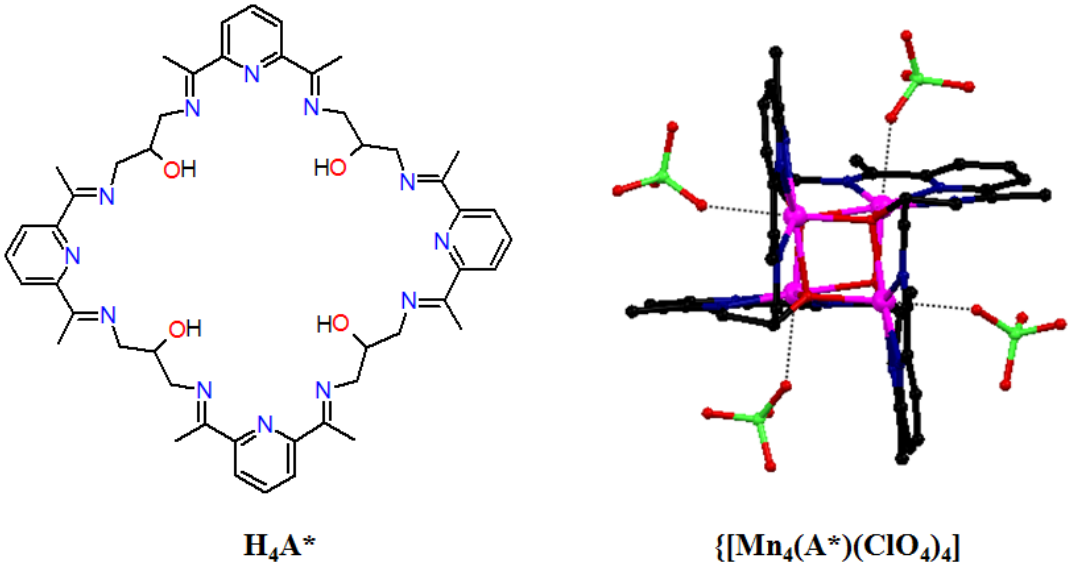

H_4A^* **$\{[Mn_4(A^*)(ClO_4)_4]$**

Figure 2-26 Structures of the ligand H_4A^* and its Mn(II) complex $[Mn_4(A^*)(ClO_4)]$.[179]

McKee *et al.* proposed a mechanism for the formation of the [4+4] macrocycle (A*) from the [2+2] (H_2A) macrocycle (Figure 2-27).[179]

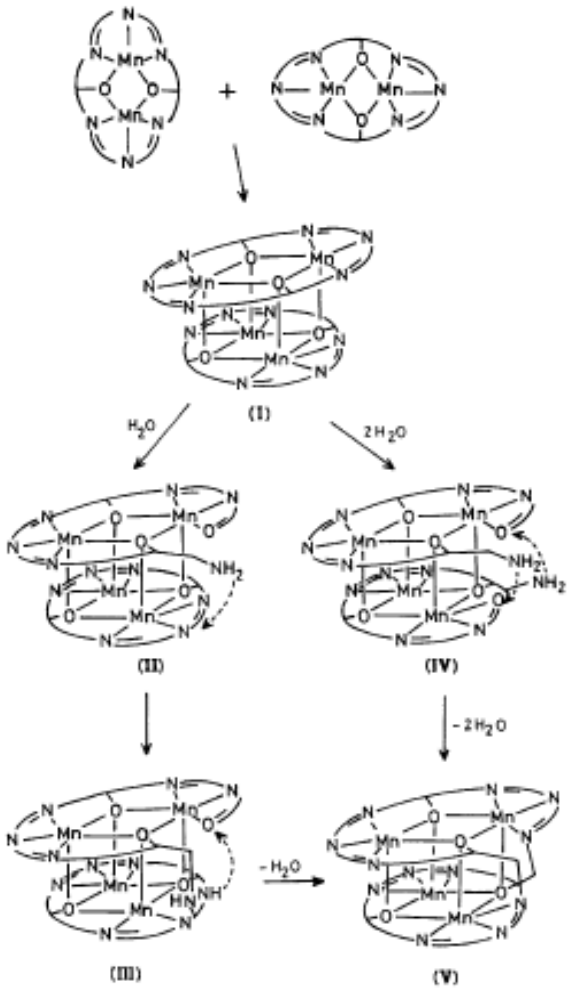

Figure 2-27 Suggested mechanism for formation the [4+4] macrocycle, taken from the reference.[179]

The initial step is formation of a sandwich analogous to the dimeric acetate structure (see Figure 2-24). Mn-O(alkoxide) bridging bonds form between two binuclear [2+2] macrocyclic units which are in a cofacial orientation (**I**), forming a cubane core. In the presence of strongly binding acetate ligand, the structure is stabilised (Figure 2-24). However, in the presence of weakly binding perchlorate, the structure undergoes further arrangement to stabilise the structure. In the next step, one of the imine bonds hydrolyses to give a free amine group (**II**). The amine then can attack one of the imine bonds on the second macrocycle at the carbon atom (**III**). One of the C-N single bonds then breaks, either forming (**II**) or leaving a new intermolecular imine link and releasing another free amine which can form another intermolecular imine bond to give the final product (**V**). Alternatively, two imine bonds, one in each macrocycle may hydrolyse to give free amines (**IV**). Each free amine then attacks the carbonyl of the neighbouring ligand to give the product (**V**).[179]

Comparison of the structures of the [2+2] complex cation $[Mn_2(HA)Cl_2]^{2+}$ derived from DAP and the [4+4] complex cation $[Mn_4(H_2L^*)Cl_4]^{2+}$ derived from DFP suggests a possible mechanism for the formation of the [4+4] macrocyclic complex (Figure 2-28). In $[Mn_2(HA)Cl_2]^{2+}$, two bimetallic [2+2] macrocyclic units are held together by two chloride ions and two intermolecular hydrogen bonds between alkoxy and alcohol oxygen atoms (-O⋯HO-) which bridge Mn(II) ions in two different macrocycles. The DAP-derived macrocyclic unit contains methyl groups attached the imine bonds; this makes the imine bond less susceptible to hydrolysis and stabilises the structure in this stage. However, in the case of the DFP complex, there are no methyl groups, therefore imine bonds are more susceptible to hydrolysis. The [2+2] structure is a possible intermediate species for the formation of the the [4+4] complex (**I**).

The next step is hydrolysis of an imine bond from one [2+2] macrocycle to form (**II**), the oxygen bridge between Mn(II) ions is also broken in this stage. The terminal amine group is then free to rotate and can attack an imine group on the second macrocycle at the carbon atom (**III**). One of the C-N bonds then breaks leaving an intermolecular imine link and releasing another amine group (**IV**). The free amine undergoes another condensation reaction with a free carbonyl group, releasing a water molecule to form the [4+4] product (**VI**). During the formation of the ring-expanded [4+4] (H_4L^*) macrocycle, the presence of chloride ions, which bridge Mn(II) ions, is vital as the two macrocyclic unit are held together by these bridges. Intermolecular hydrogen bonding between alkoxy and alcohol groups (O⋯HO) also supports the chloride bridges in holding the two macrocyclic units together.

An alternative route is the hydrolysis of two imine groups, one in each macrocycle (**V**). Each free amine then involves an intermolecular condensation with carbonyl group of the neighbouring ligand to give final product (**VI**). The second route seems less likely because it involves simultaneous hydrolysis of two imine bonds and intermolecular condensations in the correct spacial arrangement.

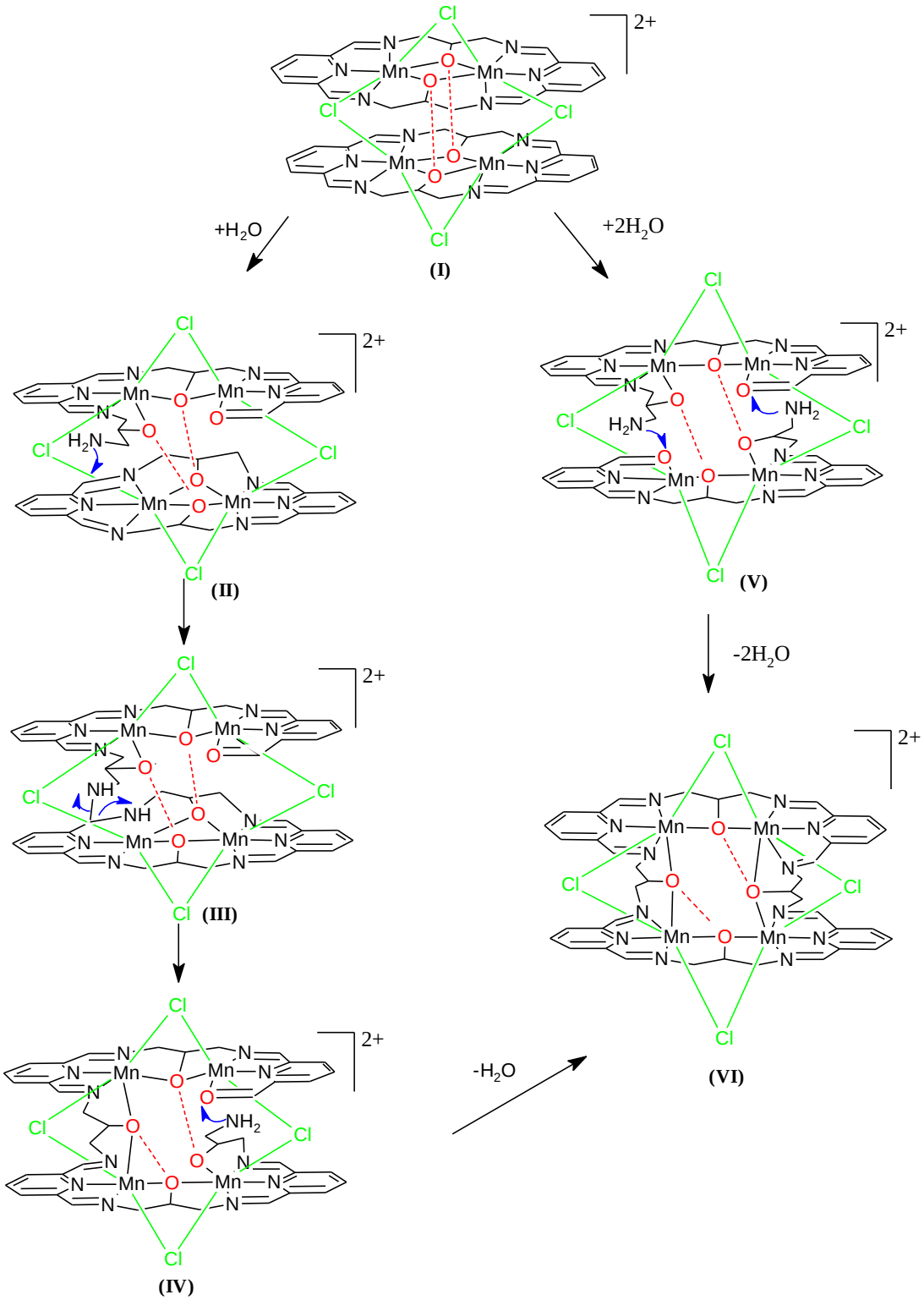

Figure 2-28 Proposed mechanism for the formation of the [4+4] macrocycle, hydrogen bond between alkoxy and alcohol groups are shown as red dotted lines.

In summary, transmetallation of the DAP-derived barium complex $[Ba(H_2A)(H_2O)_2]_2(ClO_4)_4$ with Mn(II) in methanol in the presence of Cl^-, N_3^- and OAc^- produced similar complexes. The H_2A ligand did not undergo either ring-contraction or ring-expansion. Changing the solvent from methanol to acetonitrile yielded the same chloride and azide complexes. On the other hand, in the presence of perchlorate, transmetallation resulted in rearrangement of the [2+2] to the [4+4] complex. Transmetallation of the analogous [2+2] barium complex of DFP with Mn(II) resulted in either ring-contracted complexes in methanol or ethanol, or ring-expanded Mn(II) complexes in acetonitrile (Figure 2-29).

Macrocyclic manganese complexes derived from DAP and DFP are all seven-coordinate with approximate pentagonal bipyramidal geometry. In each complex, the pyridinediimine unit provides a small bite angle and three nitrogen atoms constrained within an arc of 130-150° leaving ample space for two more donors in the same plane.[177-179]

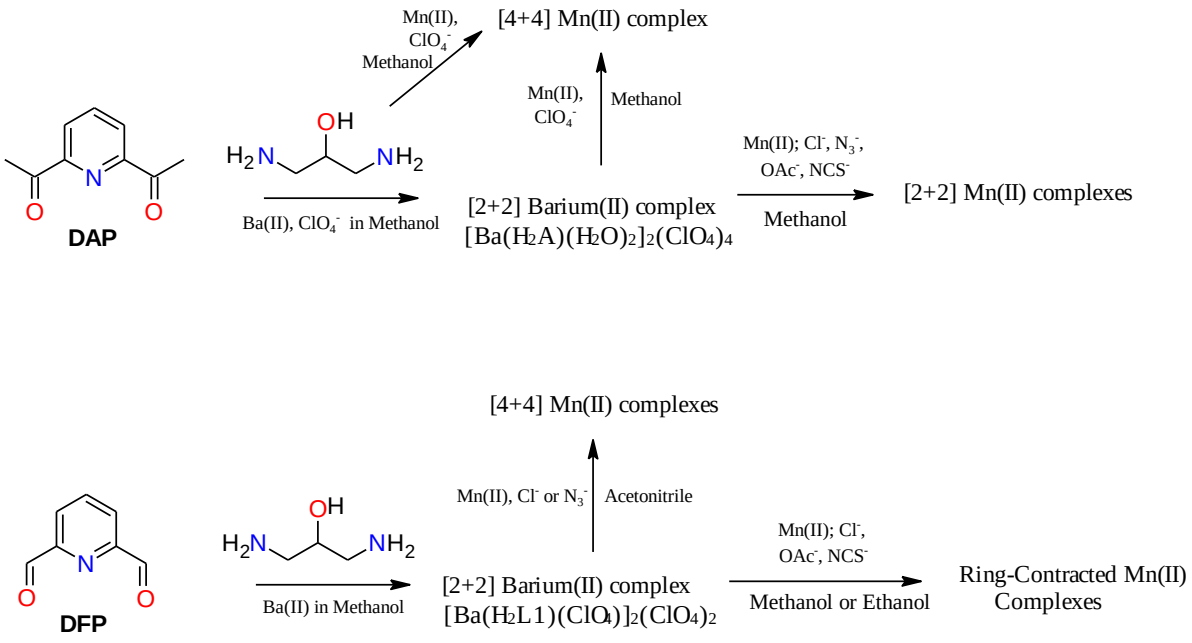

Figure 2-29 Mn(II) complexes derived from DAP and DFP head units.

2.2.7 The mononuclear [1+1] macrocyclic complex [Mn(L4)(NCS)$_2$] (5)

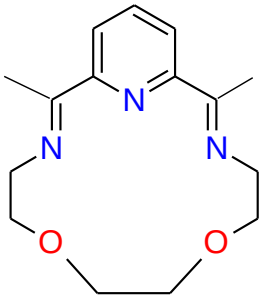

F

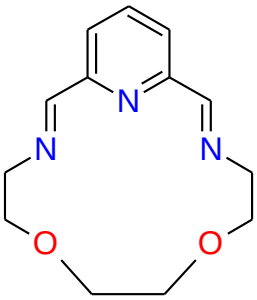

L4

A Schiff base condensation reaction of 2,6-diacetylpyridine (DAP) and 2,2'-[ethane-1,2-diylbis(oxy)]diethanamine in the presence of Mn(II) as template produces mononuclear complex of the [1+1] macrocycle (F).[180] The macrocyclic (F) complexes of Mn(II) are seven-coordinate with approximate pentagonal bipyramidal geometry and an N_3O_2 donor set with two axial ligands. The same reaction was repeated using 2,6-diformylpyridine (DFP) instead of DAP and an orange product was obtained in high yield (78%) and purity.

Orange crystals of complex suitable for X-ray diffraction studies were grown from dmf-diethylether diffusion. The complex was found to crystallise in the triclinic space group $P\bar{1}$. The details of the crystal structure and refinement can be found in Table A6 in Appendix 2.

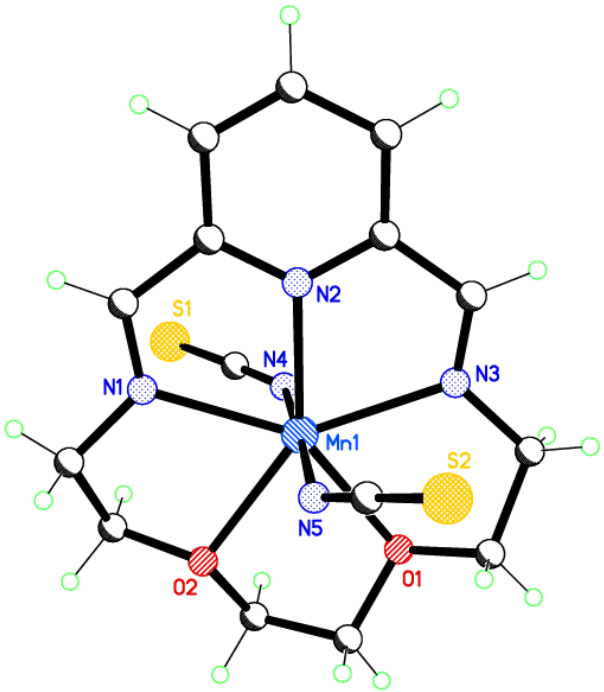

Figure 2-30 Crystal structure of the complex [Mn(L4)(NCS)$_2$] (5).

From the X-ray data the imine bond distances are found to be 1.263(9) and 1.267(9) Å which confirmed the double bond chracter of these bonds. The crystal structure is shown in Figure 2-30 and selected bond lengths and angles are given in Table 2-5. The structure contains a single seven-coordinate manganese(II) ion that is coordinated to the N_3O_2 donor set of the macrocylic ligand which forms a pentagonal plane, two thiocyanate ions are bound *via* the nitrogen donor in the axial positions. The Mn(II) ion has an approximate pentagonal bipyramidal geometry where the donors of the pentagonal plane are three pyridinediimine nitrogens and two oxygen atoms. Pyridinediimine donors provide angles of 71.3(2)° (N2-Mn1-N3) and 71.1(2)° (N1-Mn1-N2) which are slightly distorted from an ideal value of 72° for a pentagonal plane; these values are close to those in the Mn(II) complex of DAP which is analogous.[180]

Table 2-5 Selected bond lengths [Å] and angles [°] for [Mn(L4)(NCS)$_2$] and [Mn(F)(NCS)$_2$].

[Mn(L4)(NCS)$_2$]		*[Mn(F)(NCS)$_2$]*	
Mn1—N1	2.259 (5)	Mn1—N1	2.244(9)
Mn1—N2	2.207 (5)	Mn1—N2	2.214 (8)
Mn1—N3	2.253 (5)	Mn1—N3	2.254 (10)
Mn1—N4	2.190 (5)	Mn1—N4	2.254 (13)
Mn1—N5	2.180 (5)	Mn1—N5	2.277 (13)
Mn1—O1	2.288 (4)	Mn1—O1	2.296 (8)
Mn1—O2	2.293 (4)	Mn1—O2	2.270 (7)
N1—Mn1—N2	71.1 (2)	N1—Mn1—N2	71.5 (3)
N1—Mn1—N3	142.4 (2)	N1—Mn1—N3	141.7 (3)
N1—Mn1—N4	87.6 (2)	N1—Mn1—N4	87.9 (4)
N1—Mn1—N5	92.2 (2)	N1—Mn1—N5	90.6 (4)
N1—Mn1—O1	145.7 (2)	N1—Mn1—O1	145.9 (3)
N1—Mn1—O2	71.7 (2)	N1—Mn1—O2	73.2 (3)
N2—Mn1—N3	71.3 (2)	N2—Mn1—N3	70.2 (3)
N2—Mn1—N4	93.4 (2)	N2—Mn1—N4	93.4 (4)
N2—Mn1—N5	89.6 (2)	N2—Mn1—N5	93.2 (4)
N2—Mn1—O1	143.1 (2)	N2—Mn1—O1	144.6 (3)
N2—Mn1—O2	142.7 (2)	N2—Mn1—O2	142.2 (3)
N3—Mn1—N4	95.96 (19)	N3—Mn1—N4	90.4 (4)
N3—Mn1—N5	86.1 (2)	N3—Mn1—N5	95.4 (4)
N3—Mn1—O1	71.92 (19)	N3—Mn1—O1	72.11 (3)
N3—Mn1—O2	145.7 (2)	N3—Mn1—O2	145.1 (3)

N4—Mn1—N5	176.8 (2)	N4—Mn1—N5	172.3 (4)
N4—Mn1—O1	87.07 (18)	N4—Mn1—O1	83.5 (3)
N4—Mn1—O2	87.74 (18)	N4—Mn1—O2	93.7 (4)
N5—Mn1—O1	91.30 (19)	N5—Mn1—O1	88.9 (4)
N5—Mn1—O2	89.18 (18)	N5—Mn1—O2	83.4 (4)
O1—Mn1—O2	74.27 (17)	O1—Mn1—O2	73.2 (3)

The complex molecules interact with each other *via* π-π pyridine-pyridine stacking interactions shown in Figure 2-31; the edge of pyridine unit is stacked with the same section of a neighbouring molecule under symmetry operation -1-x, 2-y, 2-z; C4 and C6 are separated by a distance of 3.644 Å.

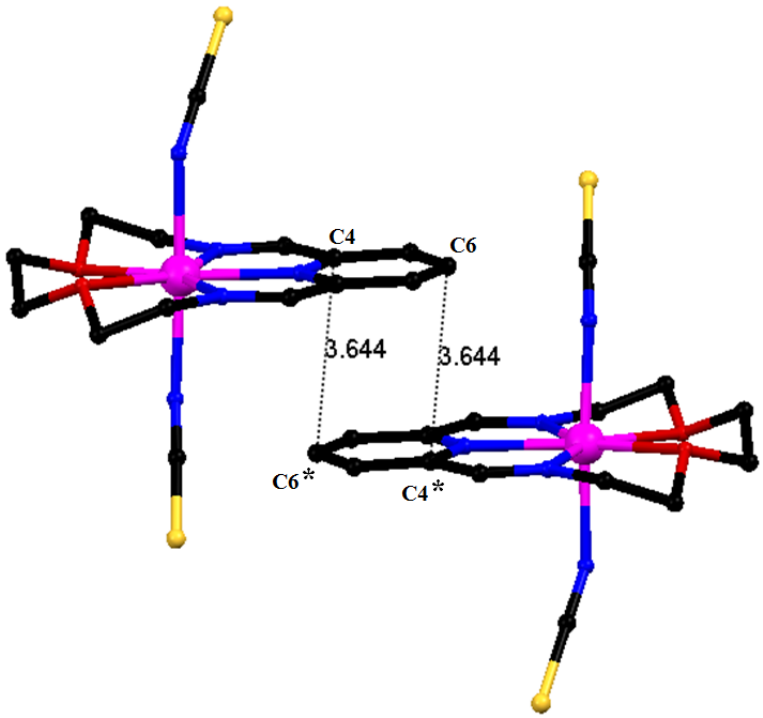

*Figure 2-31 π-π stacking interactions in (5). Symmetry operation: * -1-x, 2-y, 2-z.*

The π-π pyridine-pyridine stacking interactions shown in Figure 2-31 were supported by weak hydrogen bonds CH···S and CH···N interactions[180] (Figure 2-32 and Table 2-6).

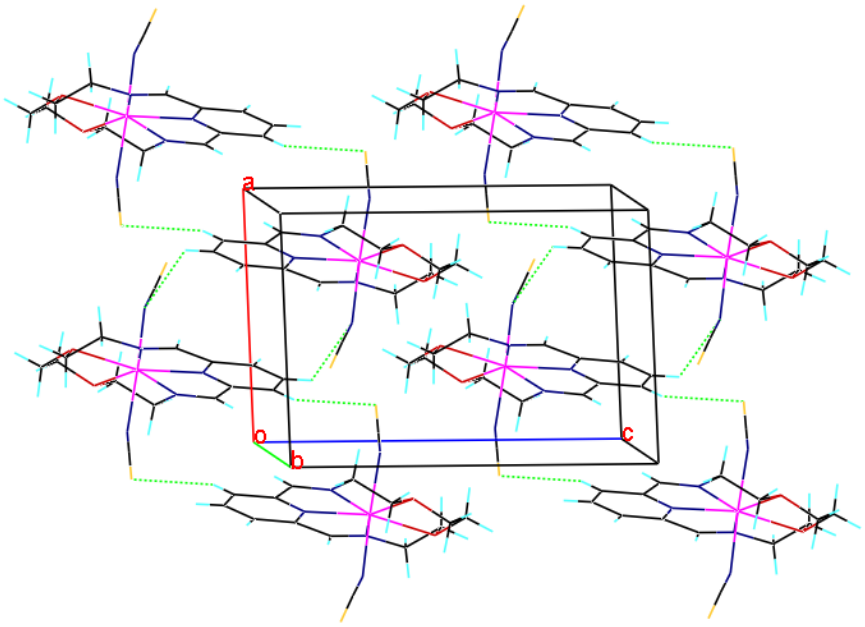

Figure 2-32 Packing diagram of complex (5).

Table 2-6 Hydrogen-bond geometry (Å, º) for (5).

D—H···*A*	*D*—H	H···*A*	*D*···*A*	*D*—H···*A*
C7—H7···S1^{i}	0.95	2.94	3.846 (7)	159.0
C4—H4···N4^{ii}	0.95	2.83	3.471 (11)	125.6
C3—H3···S2^{iii}	0.95	2.78	3.645 (9)	152.2

Symmetry codes: (i) *x*, *y*-1, *z*; (ii) -*x*-1, -*y*+2, -*z*+2; (iii) -*x*, -*y*+2, -*z*+2.

The DAP analogue of this complex [Mn(F)(NCS)$_2$] (Figure 2-33) was prepared by Nelson *et al. via* a template reaction.[180] The published structure of [Mn(F)(NCS)$_2$] is very similar to the structure of complex [Mn(L4)(NCS)$_2$] (5). In both cases, the manganese is seven-coordinate with the same coordination environment.

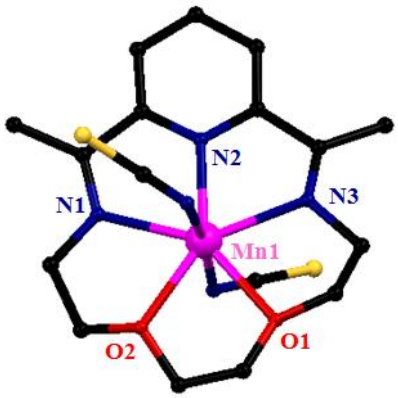

Figure 2-33 The structure of [Mn(F)(NCS)$_2$] (right).[180]

2.2.8 Mn(II) complexes of acyclic ligands

The macrocyclic Mn(II) complexes presented above are seven-coordinate with approximate pentagonal bipyramidal geometry and an N_3O_2 donor set with two axial ligands. Acyclic ligands having the same N_3O_2 donor set can also be prepared *via* Schiff base condensation reactions by using 2,6-diformylpyridine and primary amines containing additional donor groups (Figure 2-34). The aim was then to investigate whether seven-coordination would be maintained in the acyclic and flexible systems. In the macrocyclic tetranuclear manganese complexes (see section 2.2.5 Figure 2.15 and 2.20), the alcohol groups deprotonate and bridge two manganese atoms. Similar deprotonation and bridging of alcohol groups was also observed for the macrocyclic manganese complexes of DAP analogues.[177-179] These complexes have an advantage of ease of preparation and cost compared to macrocyclic complexes.

The free acyclic ligands can be prepared by a non-template Schiff base condensation of one equivalent of 2,6-diformylpyridine (DFP) with two equivalents of monoamine compounds in methanol or ethanol. Solid products were obtained by Schiff base condensation reaction of 2,6-diformylpyridine with ethanolamine or aminophenols. However, other acyclic ligands formed oils even under reduced pressure; therefore, those ligands were used directly in complexation reactions. Freshly prepared ligands were used readily in the preparation of the complexes to avoid hydrolysis of imine bond in free ligands. Several complexes were synthesised by using variety of negatively charged ligands in axial positions.

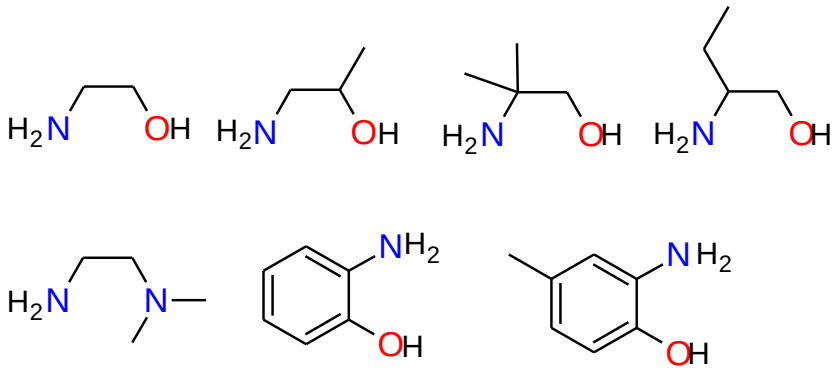

Figure 2-34 Amine precursors used to prepare acyclic complexes.

All complexes and solid Schiff bases were initially characterised by IR analysis. Appearance of an imine bond stretch (-C=N-) at ~ 1600-1660 cm^{-1} and disappearance of the carbonyl stretch at ~ 1700 cm^{-1} confirmed the formation of ligands and complexes. Mass spectra of the

acyclic complexes were obtained using ESI mass spectrometry and usually showed peaks corresponding to $[Mn(Ligand)X]^+$ (X= negatively charged ligands such as Cl^- and SCN^-) and $[Mn(Ligand)]^{2+}$ charged species.

2.2.9 The ligand H_2L_4 (6)

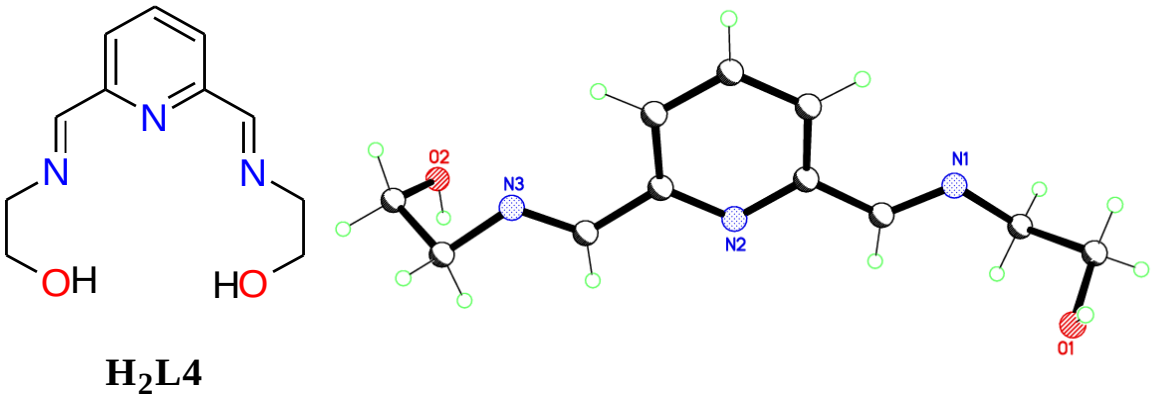

H_2L4

Figure 2-35 Perspective view of H_2L4.

H_2L_4 was prepared by a Schiff base condensation reaction of 2,6-diformylpyridine and ethanolamine in methanol at room temperature. The IR spectrum of the compound a showed C=N stretch at 1645 cm^{-1}. The ESI mass spectrum of the compound showed two major peaks at m/z 222 and 244 corresponding to $\{[H_2L_4]H\}^+$ and $\{[H_2L_4]Na\}^+$ respectively. The ligand was recrystallised from acetonitrile to give nice colourless crystals suitable for X-ray diffraction study. The ligand was found to crystallise in the monoclinic space group $P2_1/c$, details of the crystal structure and refinement can be found in Table A7 in Appendix 2. A perspective view of the structure is shown in Figure 2-35.

The molecule has two imine (-C=N-) and two OH groups, one each side of the pyridine unit. The crystal structure shows that there are two different, strong intermolecular hydrogen bonds in the structure (Figure 2-36, Table 2-7). O2 is linked by an intermolecular hydrogen bond with N2 of a neighbouring molecule with a distance of 2.939(3) Aº (under symmetry operation -x-1, -y, -z) forming a $R^2_2(16)$ ring motif. The other strong intermolecular hydrogen bond is between O1 of one molecule and N1 (imine) of the adjacent molecule with a distance of 2.924(3) (under symmetry operation -x, y-½, -z+½) resulting in a 2D hydrogen bond network.

Table 2-7 Hydrogen-bond geometry for H_2L4 (Å, °).

D–H····A	d(D–H)	d(H····A)	d(D····A)	<(DHA)
O(1)–H(1)····N(1A)**	0.84	2.10	2.924(3)	168.2
O(2)–H(2)····N(2B)*	0.84	2.10	2.939(3)	175.2

Symmetry codes: ** –x,y–½,–z+½ * –x–1,–y,–z

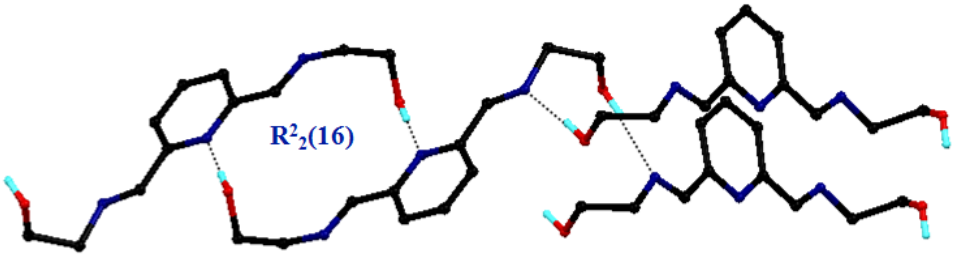

Figure 2-36 Strong intermolecular hydrogen bonds in H_2L4, hydrogen atoms bonded to carbon atoms are removed for clarity.

There is an evidence of π-π stacking interactions within the structure. The edge of the pyridine ring is stacked with one pyridine-imine arm of a neighbouring molecule under symmetry operation x, -1+y, z; C7 and N3* are separated by a distance 3.391 Å (Figure 2-37).

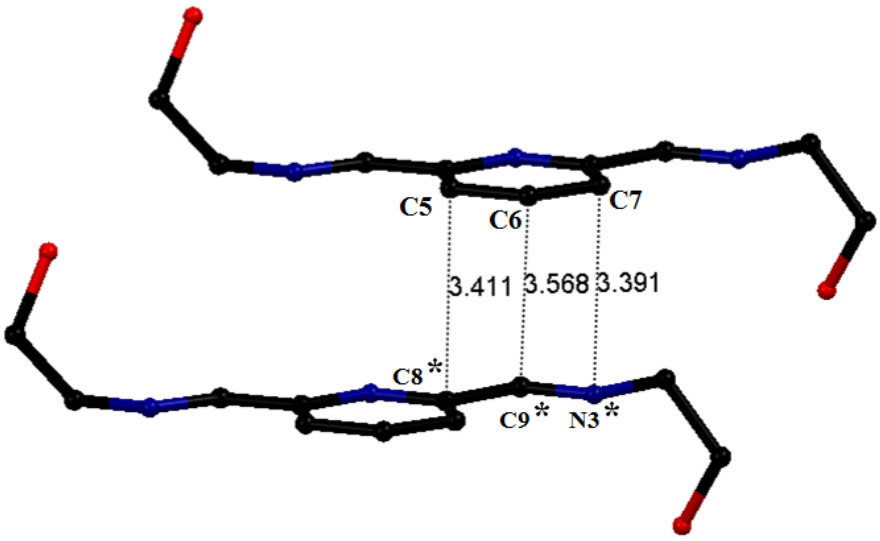

*Figure 2-37 π-π stacking interactions in H_2L4. Symmetry operation: * x, -1+y, z.*

Molecules are linked *via* an intermolecular hydrogen bonding network within the structure and this was supported by π-π stacking interactions (Figure 2-38).

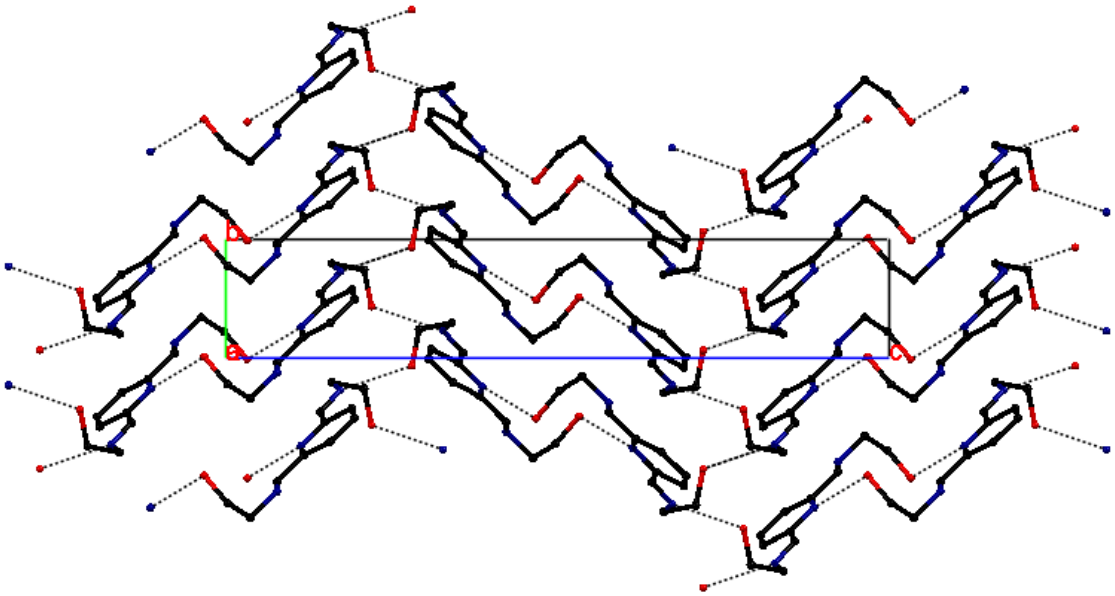

Figure 2-38 Packing plot of H_2L4 viewing down the a axis. Hydrogen bonding is shown as dotted lines and hydrogen atoms are omitted for clarity.

2.2.10 $[Mn(H_2L4)Cl_2]$ (7), $[Mn_2(H_2L4)_2(NCS)_4]$ (8) and $[Mn(H_2L_4)_2(N_3)_3Cl]$ (9)

Complexes (7), (8) and (9) were prepared by simply mixing the corresponding Mn(II) salt with (6), H_2L_4 in alcohol. IR spectra showed strong -C=N- stretches at 1659, 1656 and 1648 cm^{-1} for complexes (7)-(9), respectively. A strong thiocyanate peak υ(CN) for (8) was observed at 2078 cm^{-1} with no splitting. The IR spectrum of complex (8) showed two asymmetric azide $\upsilon_{asym}(N_3)$ peaks at 2078 and 2055 cm^{-1}. This suggests that there may be two types of azide coordination in the structure. This was later confirmed by X-ray crystallography. In the ESI mass spectra of all three complexes, molecular cations were observed.

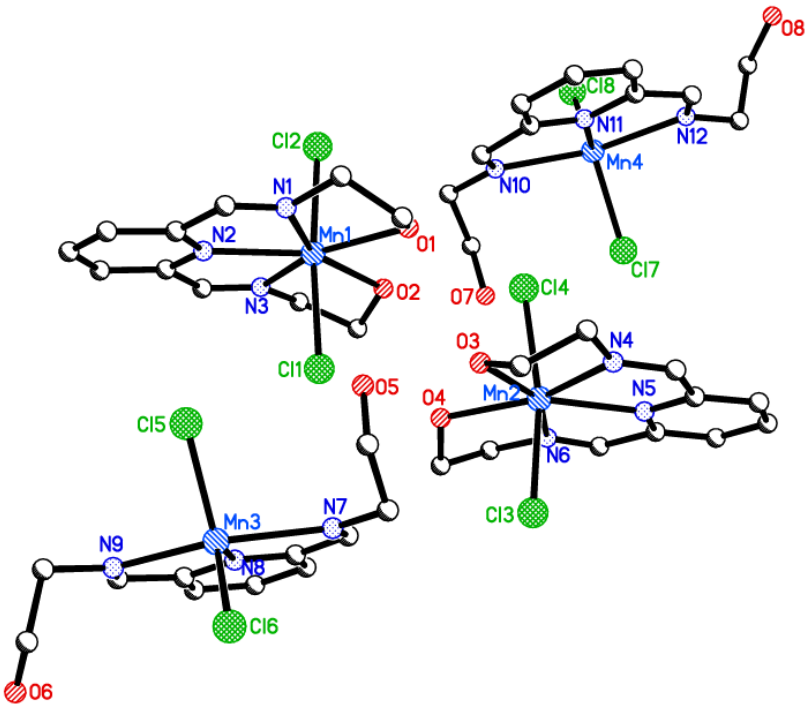

Figure 2-39 Asymmetric unit of (7) $[Mn(H_2L4)Cl_2]$ showing four independent molecules.

Single crystals of (7), (8) and (9) suitable for X-ray diffraction study were obtained by slow diffusion of diethylether into dmf solutions of the complexes. The details of the crystal structure and refinement for (7), (8) and (9) can be found in Tables A8, A9 and A10 respectively, in Appendix 2. A perspective view of (7) is shown in Figure 2-39. The crystal contains four mononuclear complexes in the asymmetric unit; two are seven- coordinate and the other two are five-coordinate and they also differ from each other by hydrogen bonding. The seven-coordinate Mn(II) centres have the expected pentagonal bipyramidal geometry bonded to two imines, one pyridine and two alcohol oxygen atoms located in a pentagonal plane with two chloride ions at the axial positions. Selected bond lengths and angles are given

in Table 2-8. All Mn-donor distances and bond angles for seven-coordinate molecules are similar to Mn-donor distances observed in the macrocyclic complex $[Mn_4(H_2L^*)Cl_4][MnCl_4]\cdot 4.5CH_3CN$ (see section 2.2.5 Table 2.3). Mn-Cl axial distances in the five-coordinate units are shorter than the Mn-Cl axial distances in the seven-coordinate units in the structure.

Table 2-8 Selected bond lengths and angles for (7) (Å, º).

7-coordinate molecule		7-coordinate molecule		5-coordinate molecule		5-coordinate molecule	
Mn1—N1	2.299 (2)	Mn2—N4	2.320 (2)	Mn3— N7	2.309 (2)	Mn4—N10	2.307 (2)
Mn1— N2	2.294 (2)	Mn2—N5	2.306 (2)	Mn3— N8	2.184 (2)	Mn4—N11	2.181 (2)
Mn1— N3	2.310 (2)	Mn2— N6	2.336 (2)	Mn3— N9	2.287 (2)	Mn4—N12	2.286 (2)
Mn1— O1	2.331 (2)	Mn2—O3	2.387 (2)	Mn3—Cl5	2.3689 (9)	Mn4—Cl7	2.3697 (8)
Mn1— O2	2.325 (2)	Mn2— O4	2.288 (2)	Mn3—Cl6	2.3592 (9)	Mn4—Cl8	2.3570 (8)
Mn1—Cl1	2.5707 (9)	Mn2—Cl3	2.5137 (9)				
Mn1—Cl2	2.4951 (9)	Mn2—Cl4	2.5122 (8)				
N1—Mn1—N2	68.69 (8)	N4—Mn2—N5	68.22 (8)	N7—Mn3—N8	71.26 (8)	N10—Mn4—N11	71.64 (9)
N2—Mn1—N3	68.38 (8)	N5—Mn2—N6	68.10 (8)	N8—Mn3—N9	72.00 (8)	N11—Mn4—N12	72.19 (9)
N1—Mn1—N3	136.86 (8)	N4—Mn2—N6	136.25 (8)	N9—Mn3—N7	143.25 (8)	N10—Mn4—N12	143.76 (9)
N1—Mn1—O2	152.70 (8)	N4—Mn2—O3	68.83 (8)	N7—Mn3—Cl5	100.19 (6)	N10—Mn4—Cl7	98.71 (6)
N2—Mn1—O2	138.52 (8)	N5—Mn2—O3	136.94 (8)	N8—Mn3—Cl5	115.15 (6)	N11—Mn4—Cl7	115.85 (6)
N3—Mn1—O2	70.43 (8)	N6—Mn2—O3	154.92 (8)	N9—Mn3—Cl5	95.39 (6)	N12—Mn4—Cl7	94.89 (6)
N1—Mn1—O1	70.09 (8)	N4—Mn2—O4	154.37 (8)	N7—Mn3—Cl6	95.63 (6)	N10—Mn4—Cl8	98.54 (6)
N2—Mn1—O1	138.73 (8)	N5—Mn2—O4	137.41 (8)	N8—Mn3—Cl6	126.21 (6)	N11—Mn4—Cl8	122.74 (6)
N3—Mn1—O1	152.87 (8)	N6—Mn2—O4	69.35 (8)	N9—Mn3—Cl6	105.79 (6)	N12—Mn4—Cl8	102.65 (7)
O1—Mn1—O2	82.62 (8)	O3—Mn2—O4	85.57 (8)	Cl6—Mn3—Cl5	118.51 (3)	Cl8—Mn4—Cl7	121.41 (3)
N1—Mn1—Cl1	91.70 (6)	N4—Mn2—Cl3	92.42 (6)				
N2—Mn1—Cl2	94.27 (6)	N5—Mn2—Cl3	93.22 (6)				
N3—Mn1—Cl1	92.92 (6)	N6—Mn2—Cl3	92.43 (6)				
O1—Mn1—Cl1	88.41 (6)	O3—Mn2—Cl3	85.50 (6)				
O2—Mn1—Cl1	86.44 (6)	O4—Mn2—Cl3	86.63 (6)				
N1—Mn1—Cl2	90.27 (6)	Cl3—Mn2—Cl4	169.39 (3)				
N2—Mn1—Cl1	90.84 (6)	N4—Mn2—Cl4	91.97 (6)				
N3—Mn1—Cl2	88.86 (6)	N5—Mn2—Cl4	97.38 (6)				
O1—Mn1—Cl2	87.83 (6)	N6—Mn2—Cl4	91.07 (6)				
O2—Mn1—Cl2	89.65 (6)	O3—Mn2—Cl4	87.10 (6)				
Cl1—Mn1—Cl2	174.89 (3)	O4—Mn2—Cl4	85.24 (6)				

The five-coordinate Mn(II) ions are coordinated to the pyridinediimine group and two chloride ions; leaving the alcohol groups uncoordinated. The coordination geometry of the five-coordinate Mn(II) ions can be best described as distorted trigonal bipyramidal with two chloride and one pyridine nitrogen atoms in the trigonal plane and two imine nitrogen atoms in the axial postions. Hydrogen bonding parameters are given in Table 2-9. The two seven-coordinate units (molecules A and B) are linked through hydrogen bonding (O-H···Cl) and these hydrogen bonded units (A-B) are linked together by a five-coordinate molecule (C) (O-H···Cl). However there is no hydrogen bond contact between five-coordinate units. The five-coordinate molecule (D) makes one intramolecular and one intermolecular hydrogen bond. All molecules are linked *via* hydrogen bonding forming a 1D hydrogen bond chain along the *a* axis (Figure 2-40).

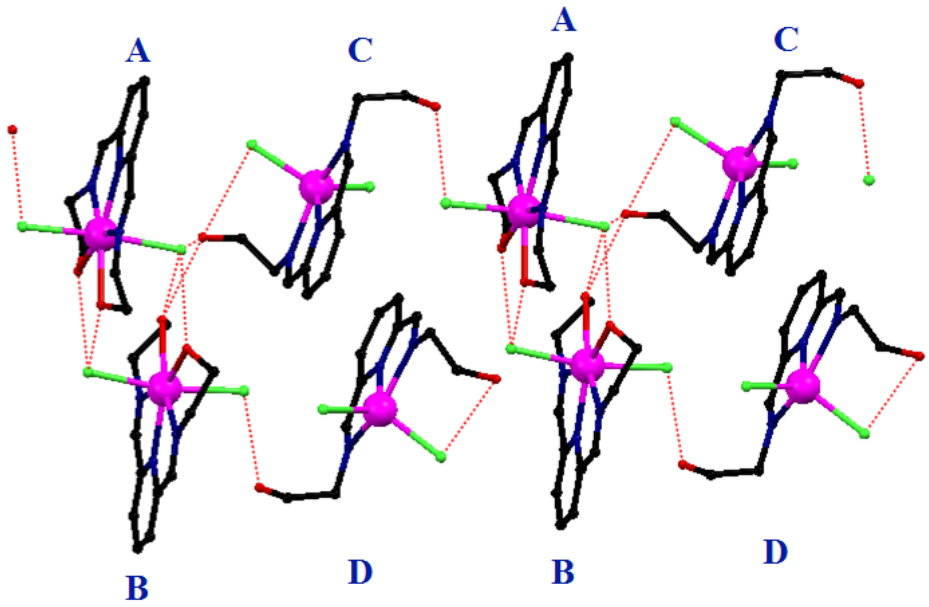

Figure 2-40 1D hydrogen bond chain along the a axis in complex (7).

Table 2-9 Hydrogen bond parameters for (7) [Å and °].

D—H···*A*	*D*—H	H···*A*	*D*···*A*	*D*—H···*A*
O8-H8····Cl3^{i}	0.85	2.31	3.126(2)	160.4
O6-H6A····Cl2^{ii}	0.85	2.30	3.126(2)	165.5
O1-H1····Cl4	0.85	2.31	3.099(2)	153.7
O2-H2····Cl4	0.85	2.53	3.248(2)	143.0
O4-H4····Cl1	0.85	2.19	3.021(2)	164.7
O7-H7A····Cl7	0.85	2.59	3.286(3)	140.1
O5-H5A····Cl1	0.85	2.80	3.273(2)	117.1
O5-H5A····Cl5	0.85	2.75	3.446(2)	140.4
O3-H3A····O5	0.85	2.08	2.819(3)	144.7
O3-H3A····Cl1	0.85	2.99	3.601(2)	130.1

Symmetry codes: (i) *x*-1, *y*, *z*; (ii) *x*+1, *y*, *z*.

Hydrogen bonded chains are connected by stacking interactions within the structure and molecular packing is determined by hydrogen bonding and π-π interactions (Figure 2-41).

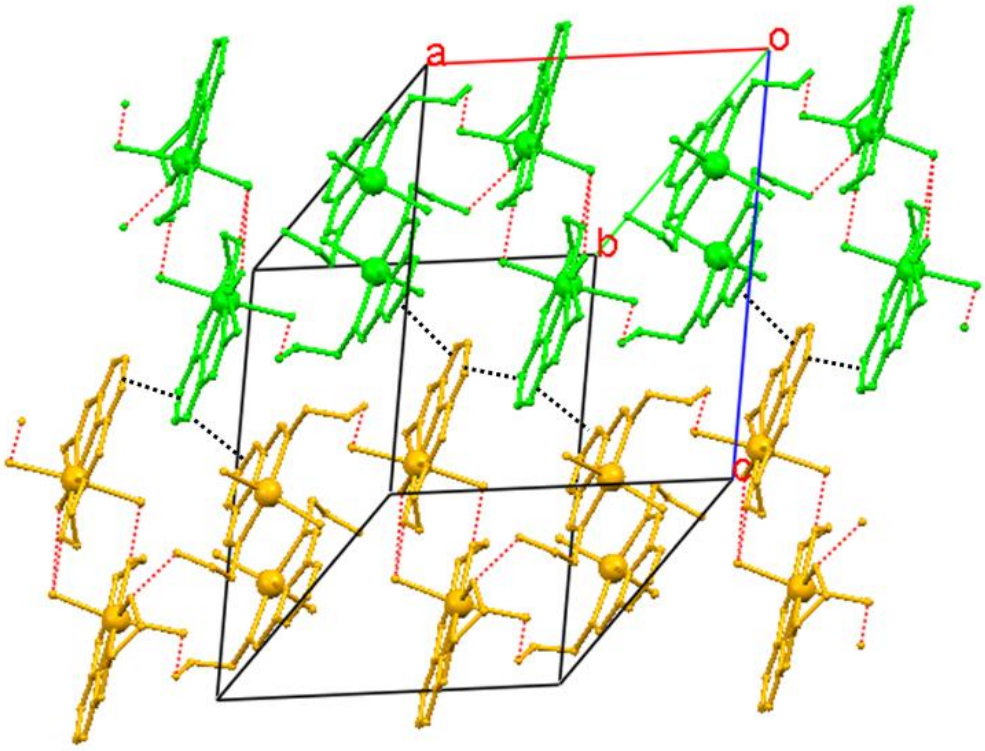

Figure 2-41 Packing diagram of (7). Hydrogen bonded chains are shown in green and yellow colours. Hydrogen bonding and π-π stacking are shown as red and black dotted lines and hydrogen atoms are omitted for clarity.

The structure of $[Mn_2(H_2L_4)_2(NCS)_4]$ (8) consists of centrosymmetric dimers; one alcohol from each ligand is an axial donor to the manganese ion of the adjacent unit (Figure 2-42). The manganese(II) ions have approximate pentagonal bipyramidal geometry in which donors in the pentagonal plane are three nitrogen atoms and one oxygen atom of one ligand and one N-bonded thiocyanate ion; a second N-bonded thiocyanate ion and one oxygen atom of the neighbouring ligand are bound in axial positions. Mn-N(pyridinediimine) and Mn-O distances are longer than Mn-NCS distances.

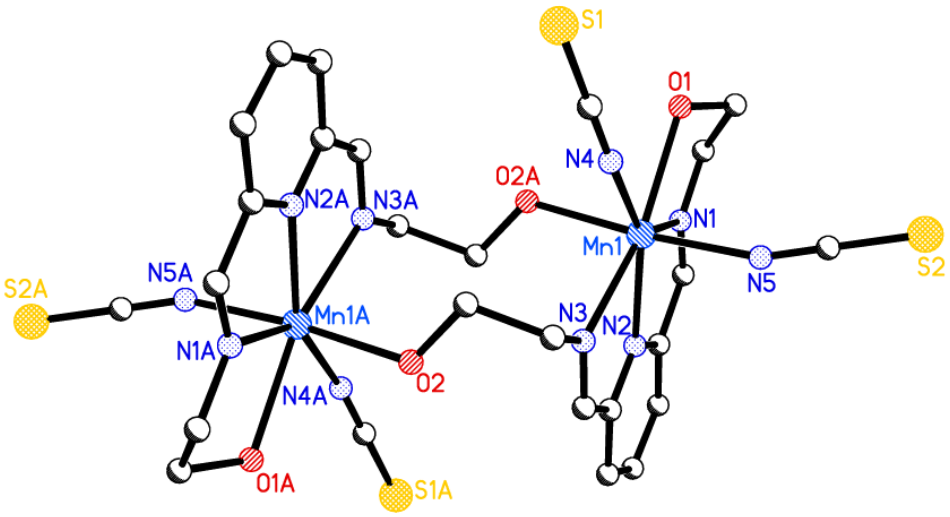

Figure 2-42 Perspective view of (8).

Selected bond lengths and angles for (8) are given in Table 2-10. The axial Mn-N, O and Mn-NCSeq distances are relatively shorter than the rest of Mn donor distances. All of the equatorial angles deviate significantly from the ideal value of pentagonal bipyramidal geometry (72º). The angles between the axial bonds and the equatorial ones range between 84.86(8)º and 95.90(9)º.

The dimeric units are linked into 2D sheets by intermolecular hydrogen bonding (Figure 2-43) between O1-H10···S2 and O2-H20···S1 (symmetry operations x, ½-y, ½ +z and -1-x, 1-y, -z respectively) with an O···S separation of 3.270(2) and 3.357(2) Å, respectively (Table 2-11). There is no evidence of significant π-π stacking interactions in the structure.

Table 2-10 Selected bond lengths and angles for (8) (Å, º).

Mn1—N1	2.374 (2)	N2—Mn1—N3	67.51 (8)
Mn1—N2	2.341 (2)	N2—Mn1—N4	150.50 (9)
Mn1—N3	2.426 (2)	N2—Mn1—N5	91.24 (8)
Mn1—N4	2.224 (2)	N2—Mn1—O1	133.86 (8)
Mn1—N5	2.154 (2)	N2—Mn1— $O2^{i}$	89.96 (7)
Mn1—O1	2.418 (2)	N3—Mn1—N4	83.27 (8)
Mn1—$O2^{i}$	2.264 (2)	N3—Mn1—N5	95.83 (8)
		N3—Mn1—O1	158.36 (8)
N1—Mn1—N2	67.44 (8)	N3—Mn1— $O2^{i}$	91.19 (7)
N1—Mn1—N3	134.76 (8)	N4—Mn1—N5	95.90 (9)
N1—Mn1—N4	141.04 (9)	N4—Mn1—O1	75.14 (8)
N1—Mn1—N5	89.04 (8)	N4—Mn1—$O2^{i}$	86.50 (8)
N1—Mn1—O1	66.43 (8)	N5—Mn1—O1	87.91 (9)
N1—Mn1— $O2^{i}$	84.86 (8)	N5—Mn1—$O2^{i}$	172.80 (9)
		$O2^{i}$—Mn1—O1	86.15 (8)

Symmetry code: (i) *-x*, *-y*+1, *-z*.

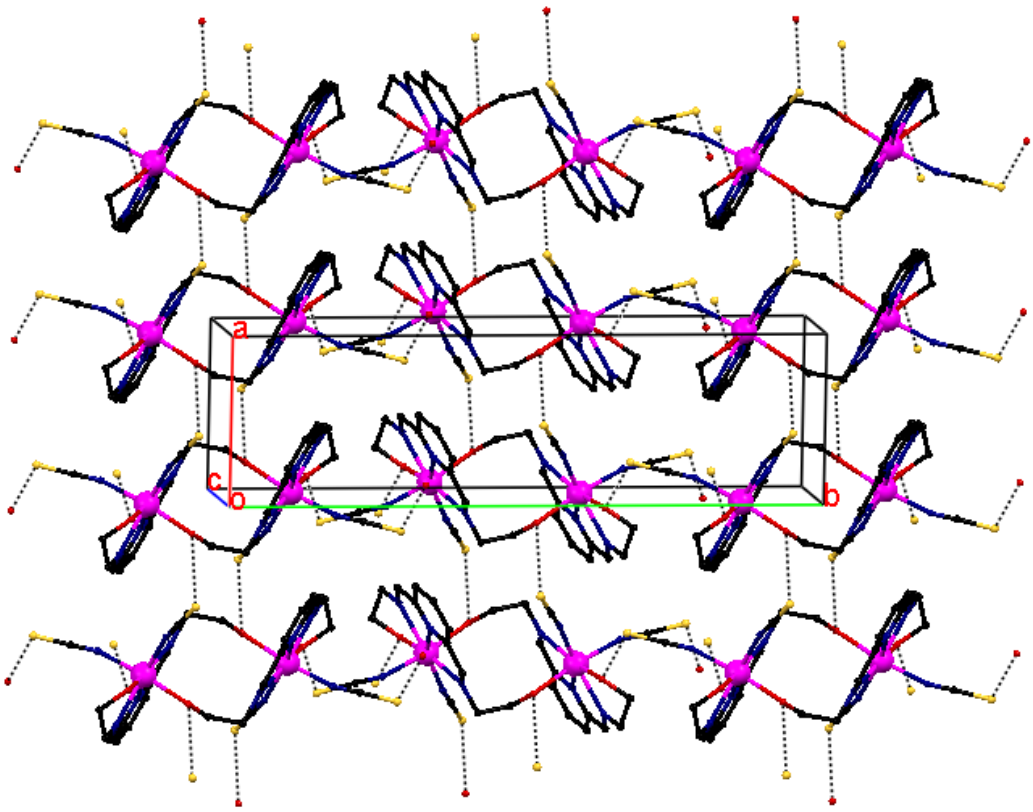

Figure 2-43 Packing plot of (8), hydrogen bonding is shown as dotted lines.

Table 2-11 Hydrogen-bond geometry of (8) (Å, °).

D—H···*A*	*D*—H	H···*A*	*D*···*A*	*D*—H···*A*
O1-H10····S2^{i}	0.85	2.44	3.270(2)	167.2
O2-H20····S1^{ii}	0.85	2.55	3.359(2)	158.6

Symmetry codes: (i) *x*, -*y*+½, *z*+½; (ii) -*x*-1, -*y*+1, -*z*.

In the structure of (9) $[Mn_2(H_2L_4)_2(N_3)_3Cl)]$, two azide bridges give access to a dimeric structure (Figure 2-44). In contrast to complex (8), the Mn(II) ions in (9) are six-coordinate, with two imine nitrogens, one pyridyl nitrogen and one azide donor located in the equatorial plane, with two azide nitrogens in the axial positions. The azide bridged dimeric structure is supported by an intramolecular hydrogen bond O2···O2A at 2.773(3) Å producing a S(12) ring motif. One of the axial azide donors (N4,N5,N6) is disordered with chloride (Cl1) which is modelled as 0.55 Cl and 0.45 azide. One of the alcohol groups shows some disorder and this has been modelled as a rotation about the C-C bond. Site occupancy factors were set at 0.60 C1 and O1 at 0.40 for C1' and O1'.

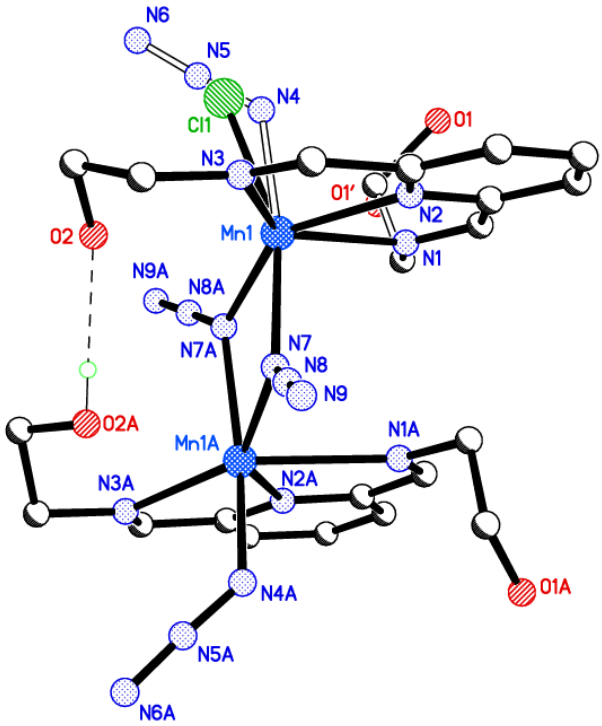

Figure 2-44 Crystal structure of (9). There is no symmetry in the dinuclear complex (9). Intramolecular hydrogen bonding shown as dashed lines, the rest of the hydrogen atoms are omitted for clarity. Disordered azide ligand (N4,N5,N6) with chloride(Cl1) and disordered alcohol group(O1) are shown in the figure.

The dimeric units are linked by a hydrogen bond network. Both components of disordered azide with chloride atom (Cl1) are involved in hydrogen bonding with one of the alcohol groups of an adjacent molecule (O1A-H···Cl1 and O1A-H···N6). The Cl1 ion also hydrogen bonds with one alcohol group of a neighbouring molecule. Intermolecular hydrogen bonding is the main factor controlling the crystal packing of (9) and intermolecular hydrogen bonding is supported by π-π (pyridyl-pyridyl) stacking with a 3.620 Å centroid-centroid separation under symmetry operation -1+x, y, z (Figures 2-45 and 2-46). Hydrogen bond information is given in Table 2-12.

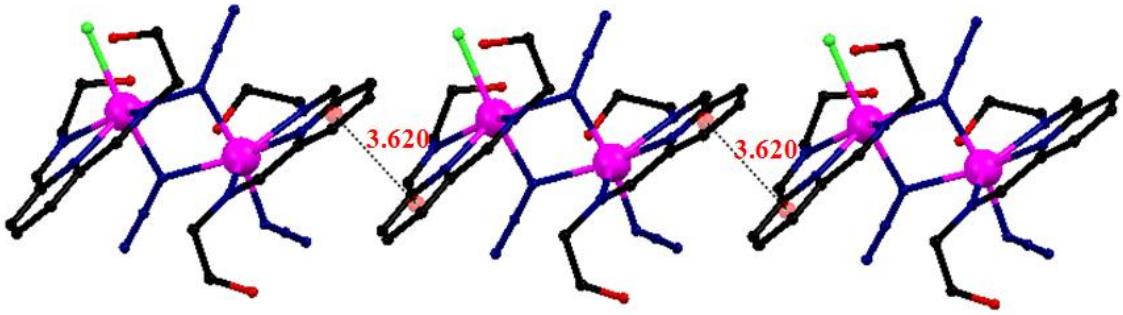

Figure 2-45 π-π stacking interactions along the c axis in complex (9).

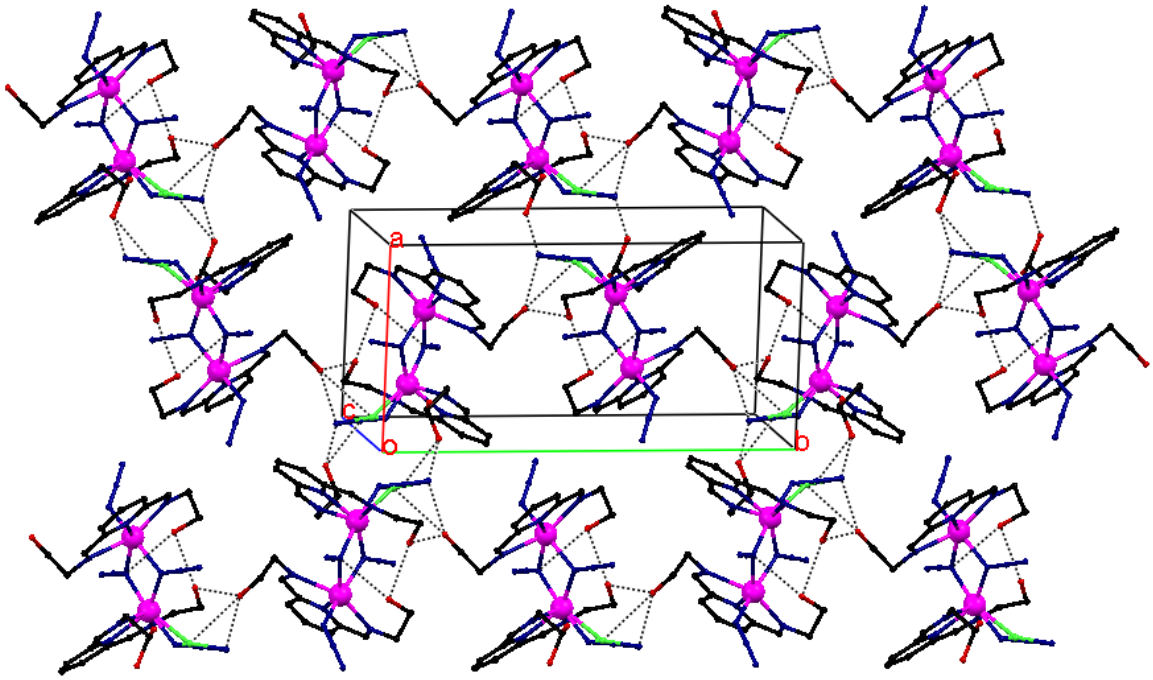

Figure 2-46 Packing diagram of (9) showing hydrogen bond network.

Table 2-12 Hydrogen bonds for (9) [Å and °].

D—H···*A*	*D*—H	H···*A*	*D*···*A*	*D*—H···*A*
O1A—H1A···N6^{i}	0.84	1.88	2.598 (7)	143.2
O1A—H1A···Cl1^{i}	0.84	2.60	3.233 (4)	133.1
O1—H1···Cl1^{ii}	0.84	2.34	3.173 (5)	171.0
O1'—H1'···N9A^{iii}	0.84	1.88	2.631 (9)	148.7
O2—H2···O1A^{iv}	0.84	1.87	2.703 (3)	170.2
O2A—H2A···O2	0.84	1.97	2.773 (3)	160.7

Symmetry codes: (i) -*x*+1, *y*+½, -*z*+½; (ii) -*x*, -*y*, -*z*; (iii) -*x*+1, -*y*, -*z*; (iv) -*x*+1, *y*-½, -*z*+½.

It is informative to compare the structures of complexes (7)-(9) with the analogous Mn(II) complex of the related ligand (H_2G) (Figure 2-47) derived from 2,6-diacetylpyridine and 2-aminoethanol with chloride,[181] thiocyanate, and azide counter ions.[182]

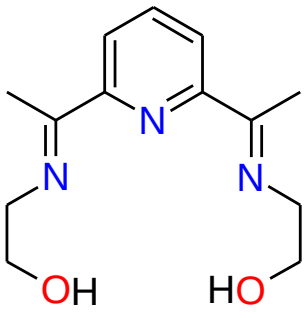

Figure 2-47 Ligand H_2G.

In contrast to the reported Mn(II) complexes derived from H_2G, we obtain different geometric arrangements in the crystal structure in each case. The reported structures of H_2G complexes are seven-coordinate and possess pentagonal byprimidal geometry; complexes of H_2L4 are range from five- to six- and seven-coordination. The azide (9) and thiocyanate (8) complexes of H_2L4 have dimeric, dinuclear structures while the chloro complex (7) shows five- and seven-coordination. In the three published complexes of H_2G, the Mn(II) ions in all three complexes are seven-coordinate; the pentagonal plane is occupied by all donor atoms from N_3O_2 type ligand and two chloride, two thiocyanates and two azides are located in the axial positions to give monomeric structures (Figure 2-48). The only difference between the two ligands is that the ligand H_2G contains methyl groups attached to the imine carbon atom and these groups in H_2G decrease the degree of the freedom and flexibility. The reason why the complexes of H_2L4 resulted in different complexes may be attributed to flexibility of ligand.

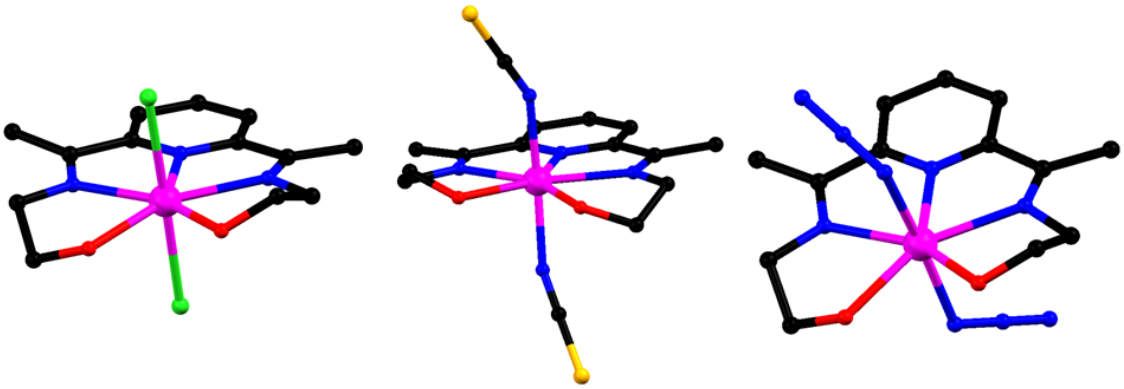

Figure 2-48 Molecular structures of Mn(II) complexes of H_2G redrawn from reference.[181,182]

2.2.11 [Mn(L5)(NCS)$_2$] (10), [Mn(L5)(N$_3$)$_2$]·MeOH (11) and [Mn(L5)Cl$_2$] (12)

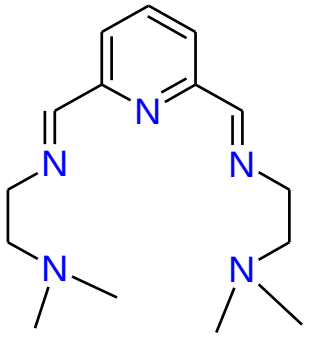

L5

In the synthesis of Mn(II) complexes (10)-(12), L5 was first prepared by Schiff base condensation of 2,6-diformylpyridine and *N*,*N*-dimethylethane-1,2-diamine in alcohol at room temperature. The ligand L5 was used directly to prepare complexes by simply mixing with Mn(II) salts in alcohol. IR spectra of complexes showed strong -C=N- stretches at 1653, 1651 and 1654 cm^{-1} for complexes (10)-(12) respectively. Thiocyanate and azide stretches in complexes (10) and (11) were observed at 2062 and 2045 cm^{-1} respectively. Yellow crystals of the chloride complex [Mn(L5)Cl$_2$] (12) turn into brown oil after several days in air possibly due to oxidation of the Mn(II) ion. However, no similar behaviour was observed for the thiocyanate (10) and azide (11) complexes and these complexes are stable in air. Therefore, the chloride complex was analysed immediately after it was synthesised.

Crystals suitable for X-ray analysis were obtained by slow diffusion of diethylether into methanol solutions of the complexes. The complex [Mn(L5)(NCS)$_2$] (10) was bright yellow while [Mn(L5)(N$_3$)$_2$](CH$_3$OH) (11) and [Mn(L5)Cl$_2$] (12) were orange. The details of the

crystal structure and refinement for (10), (11) and (12) can be found in Tables A11, A12 and A13 respectively in Appendix 2.

Perspective views of all three complexes (10)-(12) are shown in Figure 2-49. The structures of the complexes are broadly similar, differing in the ligands at the axial positions. The asymmetric unit of (10) contains two independent complex molecules with similar bond lengths and angles. Complex (11) contains a disordered methanol molecule in the asymmetric unit while complexes (10) and (12) do not have any solvent in their structures. The disordered methanol was dealt with in refinement using the squeeze procedure.[216] In each complex, the Mn(II) ion is seven-coordinate, bonded to all nitrogen atoms in the pentagonal plane and two negatively charged ligands in axial positions. Mn-N_{amine} distances are longer than Mn-N_{pyr} and Mn-N_{imine} distances in all three complexes (Table 2-13). Mn-N axial distances in complex (10) and (11) are significantly shorter than those Mn-N distances in the pentagonal planes. Additionally, Mn-D_{donor} distances in the pentagonal plane for complexes (10)–(12) are longer than Mn-D_{donor} distances in the pentagonal plane of the macrocyclic complex $[Mn_4(H_2L^*)Cl_4][MnCl_4]\cdot 4.5CH_3CN$ (see Table 2-3). Mn-Npyridine distances are 2.355(4), 2.387(12) and 2.432(17) Å for complexes (10)-(12), respectively. This may be due to mismatch of the cavity provided by the flexible acyclic ligand L5 and size of the Mn(II) ion.

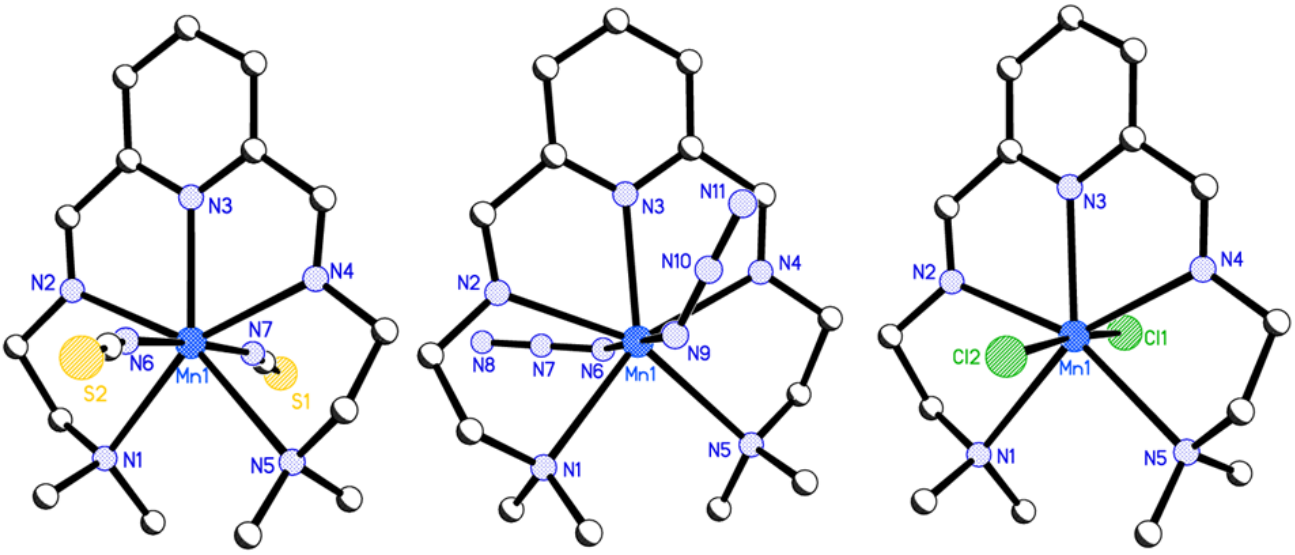

Figure 2-49 Perspective view of $[Mn(L5)(NCS)_2]$ (10)(left), $[Mn(L5)(N_3)_2]$ (11) (middle) and $[Mn(L5)Cl_2]$ (12) (left).

Table 2-13 Selected bond lengths for (10), (11) and (12) (Å).

Complex (10)		(11)		(12)	
Mn-N1	2.538(4)	Mn-N1	2.570(13)	Mn-N1	2.688(17)
Mn-N2	2.389(4)	Mn-N2	2.410(13)	Mn-N2	2.376(16)
Mn-N3	2.355(4)	Mn-N3	2. 387(12)	Mn-N3	2.432(17)
Mn-N4	2.380 (4)	Mn-N4	2.386(13)	Mn-N4	2.383(16)
Mn-N5	2.728(4)	Mn-N5	2.628(13)	Mn-N5	2.621(18)
Mn-N6	2.147(3)	Mn-N6	2.1473(10)	Mn-Cl1	2.4920(6)
Mn-N7	2.182(3)	Mn-N7	2.1531(10)	Mn-Cl2	2.4480(6)

In complex (10), two independent complex molecules show two distinct π-π interactions. First, one edge of pyridinediimine section (C5-C8) is stacked with the same section of an adjacent molecule under symmetry operation 1-x, 2-y, 1-z; C6 and C7* are separated by a distance of 3.506 Å. Second, the C7A-C8A edge of the molecule is stacked with the same egde of a neighbouring molecule under symmetry operation 2-x, 2-y, -z; C7A and C8A** are separated by a distance of 3.490 Å (Figure 2-50).

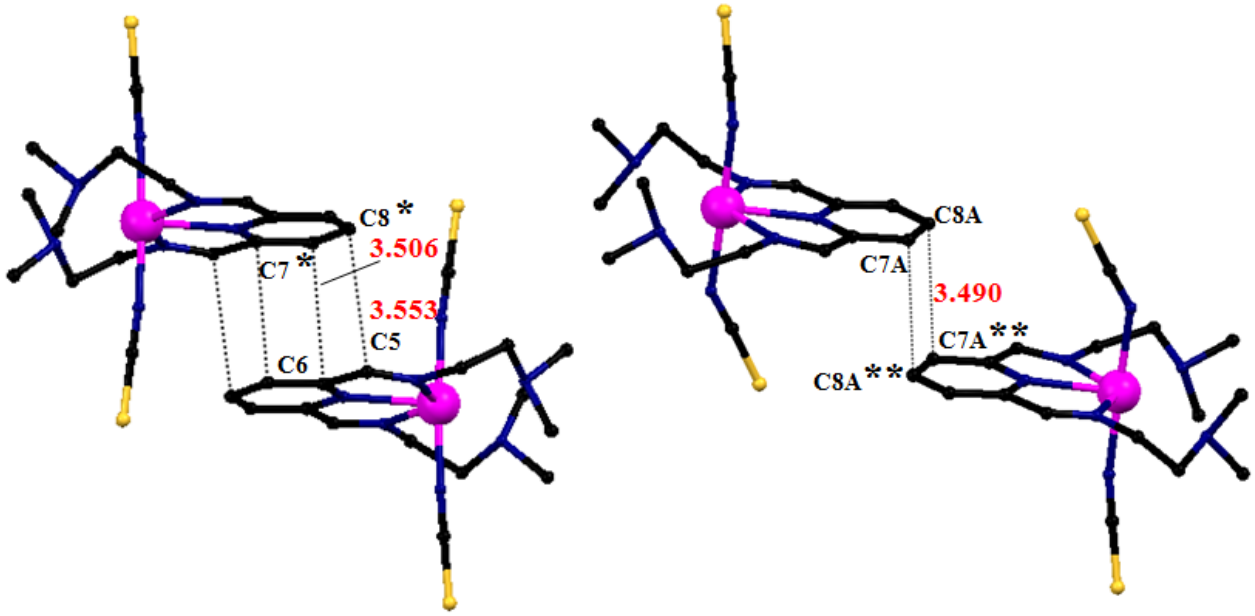

*Figure 2-50 π-π interactions in complex (10). Symmetry operations: * 1-x, 2-y, 1-z, **2-x, 2-y, -z.*

There are also some S···HC weak hydrogen bond type interactions[180] observed in the structure and, as shown in Figure 2-51. The weak CH···S hydrogen bond distances range between 2.843 and 2.960 Å.

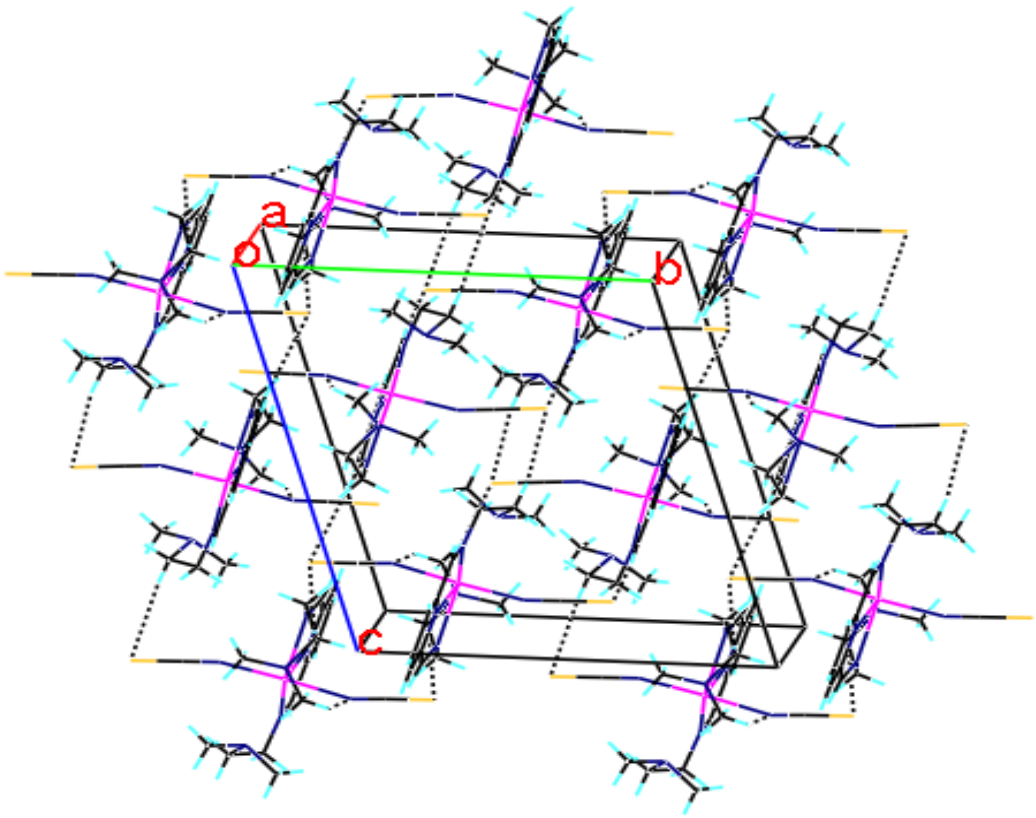

Figure 2-51 Crystal packing of (10), CH…..S hydrogen bonds are shown as dashed lines.

In complex (11), π-π edge to edge stacking was observed in the structure; one pyridinediimine edge (C5-C7) is stacked with the same section of an adjacent molecule under symmetry operation -x, 1-y, 2-z with a separation of 3.412 Å (Figure 2-52).

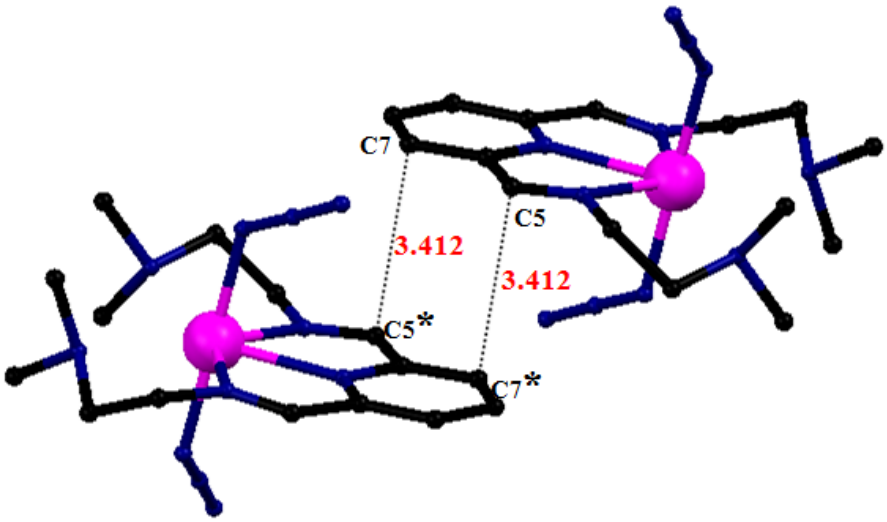

*Figure 2-52 π-π stacking interactions in (11, symmetry operation: *-x, 1-y, 2-z.*

Complex molecules are linked *via* weak CH⋯⋯N(azide) hydrogen bonds[180] (Figure 2-53, Table 2-14), this was supported by π-π stacking.

Table 2-14 Hydrogen-bond geometry (Å, º) for (11).

D—H⋯*A*	*D*—H	H⋯*A*	*D*⋯*A*	*D*—H⋯*A*
C1—H1*A*⋯N9	0.98	2.61	3.2846 (17)	126
C15—H15*B*⋯N6	0.98	2.72	3.3873 (19)	126
C3—H3*B*⋯N11^{i}	0.99	2.64	3.4764 (18)	143
C9—H9⋯N8^{ii}	0.95	2.69	3.5286 (18)	147
C11—H11⋯N8^{ii}	0.95	2.62	3.4595 (18)	147
C5—H5⋯N11^{iii}	0.95	2.57	3.4576 (17)	156

Symmetry codes: (i) *x*, *y*-1, *z*; (ii) *x*, *y*+1, *z*; (iii) -*x*, -*y*+1, -*z*+2.

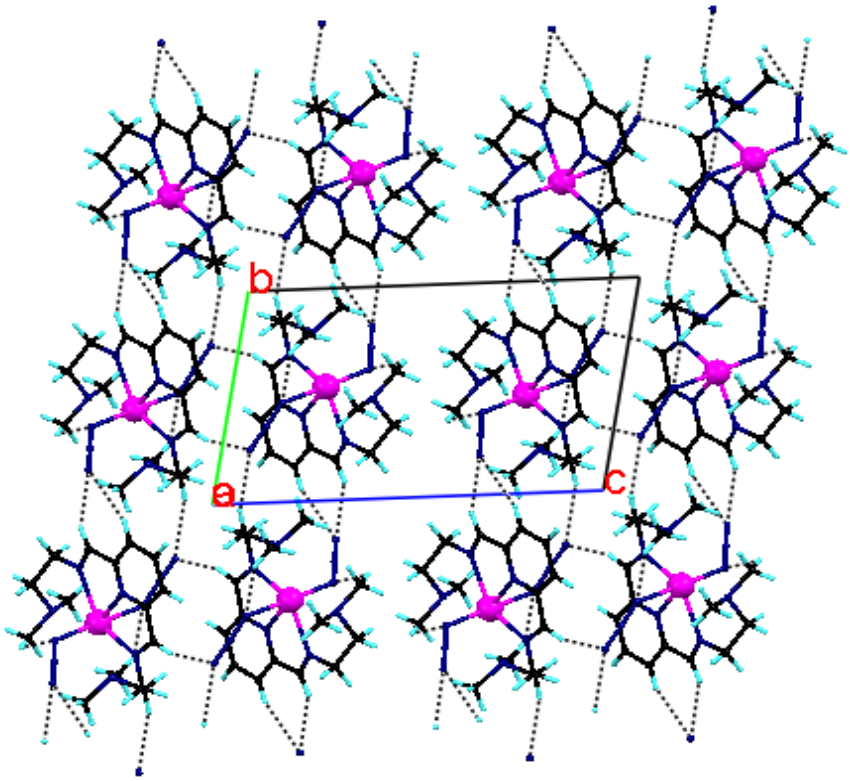

Figure 2-53 Packing diagram of (11) viewing down the a axis, CH⋯⋯N hydrogen bonds are shown as dashed lines.

In complex (12), there are CH⋯⋯Cl weak hydrogen bond interactions[180] linking molecules and this was supported by π-π stacking interactions (Table 2-15). C7-C10 atoms of the pyridine ring are stacked with C5*-C7* atoms of the neighbouring molecule under symmetry operation ½+x, y, ½-z with centroid-centroid distance of 3.813 Å; C10 and C7* are separated

by a distance of 3.194 Å which is significantly shorter than π stacking distance in graphite (3.35 Å) (Figures 2-54 and 2-55).

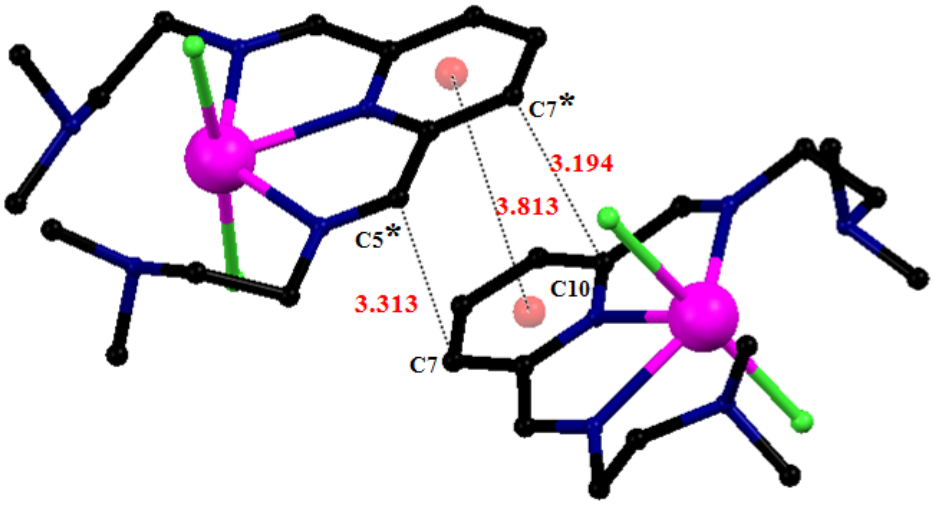

Figure 2-54 π-π interactions in (12) [Mn(L5)Cl$_2$, symmetry operation: ½+x, y, ½-z.

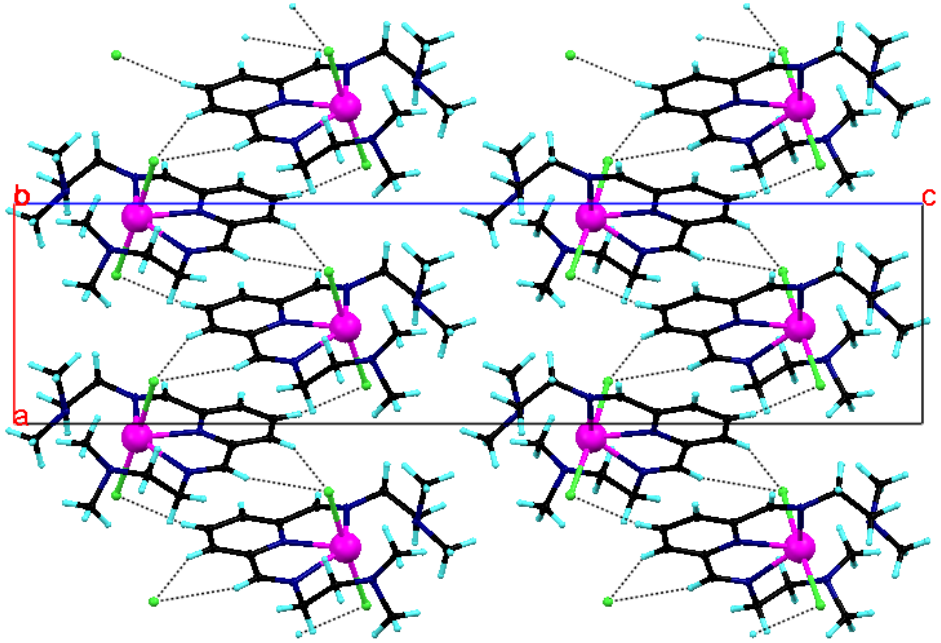

Figure 2-55 Hydrogen bond and π-π interactions in (12) [Mn(L5)Cl$_2$].

Table 2-15 Hydrogen-bond geometry (Å, º) for (12).

D—H···*A*	*D*—H	H···*A*	*D*···*A*	*D*—H···*A*
C8—H8···Cl2^{i}	0.95	2.83	3.485 (2)	127
C5—H5···Cl1^{ii}	0.95	2.87	3.708 (2)	148
C7—H7···Cl1^{ii}	0.95	2.82	3.680 (2)	151

Symmetry codes: (i) *x*-½, *y*, -*z*+½; (ii) *x*+½, *y*, -*z*+½.

2.2.12 $[Mn(H_2L6)(N_3)_2]$ (13), $[Mn(H_2L6)Cl(H_2O)]Cl\cdot(H_2O)$ (14) and $[Mn_2(H_2L6)(NCS)_2]$ (15)

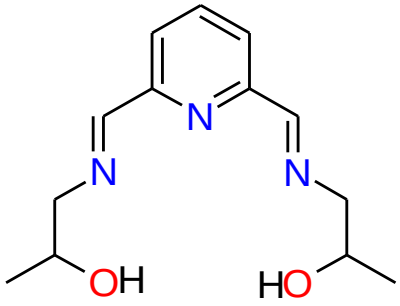

H_2L6

The reaction of H_2L6 with Mn(II) in the presence of azide, chloride and thicyanate results in mononuclear seven-coordinate complexes (13), (14) and (15). All three complexes were characterised by IR spectroscopy showing that there was no indication of primary amines or carbonyl in the sample. In the IR spectra of the complexes, strong imine stretching (C=N) vibrations were seen at 1650, 1655 and 1659 cm^{-1} for complexes (13)-(15) respectively. Thiocyanate υ(CN) and azide $\upsilon_{asym}(N_3)$ stretches in complexes (13) and (15) were observed at 2081 and 2063 cm^{-1} respectively with no splitting. In the ESI mass spectra for complexes (13), (14) and (15) peaks at 303 (100%), 309 (50%) and 362 (100%) m/z were assigned to $[Mn(HL_6)]^+$, $[Mn(H_2L_6)Cl]^+$ and $[Mn(H_2L_6)(NCS)]^+$ respectively. No crystals suitable for X-ray diffraction study were obtained in the case of complexes (13) and (15) from slow evaporation of methanol or acetonitrile and methanol-diethylether or dmf-diethylether diffusion.

Single crystals of (14) suitable for X-ray were obtained by slow diffusion of diethylether into methanolic solution of the complex. The structure of the complex was solved in the monoclinic space group $P2_1/c$. The details of the crystal structure and refinement can be found in Table A14 in Appendix 2. The structure of complex (14) cation is shown in Figure 2-56. In (14), Mn(II) ions have pentagonal bipyrimidal geometry as expected, coordinated to two imine, one pyridyl nitrogen and two alcohol oxygen atoms in the pentagonal plane, one oxygen (water) atom and one chloride ion in axial positions. The pyridinediimine head unit of the ligand provides similar N-Mn-N angles to the macrocyclic complexes (4 and 5) having pentagonal bipyramidal geometry (see section 2.2.5 Table 2-3 and section 2.2.7 Table 2-5). Selected bond lengths and angles are given in Table 2-16. An uncoordinated water molecule

and a chloride ion are also present in the asymmetric unit and are involved in hydrogen bonding.

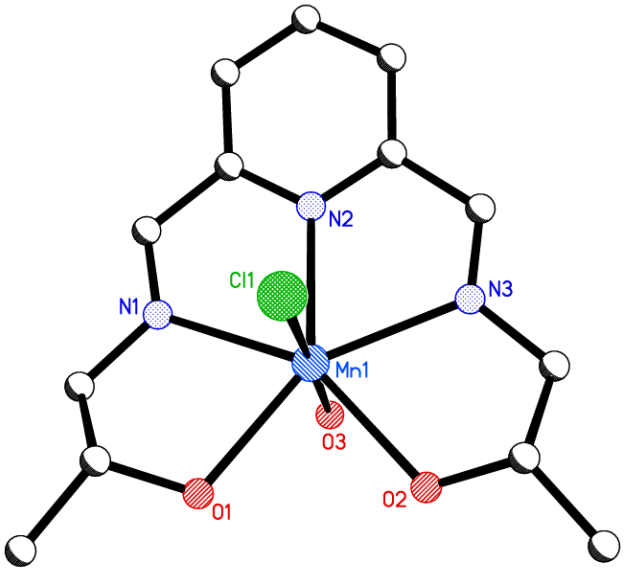

Figure 2-56 Perspective view of (14).Hydrogen atoms, an uncoordinated water molecule and an uncoordinated chloride ion are omitted for clarity.

Table 2-16 Selected bond lengths [Å] and angles [°] for (14).

Mn1—N1	2.3044 (19)	N2—Mn1—O1	139.24 (7)
Mn1—N2	2.281 (2)	O2—Mn1—O1	82.19 (6)
Mn1—N3	2.3209 (19)	N1—Mn1—O1	70.10 (7)
Mn1—O1	2.3059 (16)	O3—Mn1—N3	89.98 (7)
Mn1—O2	2.2899 (17)	N2—Mn1—N3	68.86 (7)
Mn1—O3	2.190 (2)	O2—Mn1—N3	69.62 (7)
Mn1—Cl1	2.5098 (8)	N1—Mn1—N3	137.79 (7)
		O1—Mn1—N3	151.81 (7)
O3—Mn1—N2	92.86 (7)	O3—Mn1—Cl1	178.65 (5)
O3—Mn1—O2	82.57 (7)	N2—Mn1—Cl1	88.30 (6)
N2—Mn1—O2	138.21 (7)	O2—Mn1—Cl1	97.02 (6)
O3—Mn1—N1	87.91 (7)	N1—Mn1—Cl1	91.87 (6)
N2—Mn1—N1	69.15 (8)	O1—Mn1—Cl1	91.97 (5)
O2—Mn1—N1	151.18 (7)	N3—Mn1—Cl1	91.07 (6)
O3—Mn1—O1	86.71 (7)		

The uncoordinated water molecule (O4) and chloride ion (Cl2) link the molecule ions into a 3D hydrogen bonded network (Table 2-17). Cl2 is involved in hydrogen bonding with coordinated (O3-H⋯Cl2) and uncoordinated (O4-H⋯Cl2) water molecules resulting in a

$R^4_6(12)$ hydrogen bonding motif. Cl2 also makes hydrogen bonds with alcohol groups of the ligand (O1-H····Cl2 and O2-H····Cl2) producing a $R^1_2(6)$ hydrogen bonding motif. The coordinated chloride ion (Cl1) forms hydrogen bonds with the uncoordinated water molecule (O4-H····Cl1). The hydrogen bond network and a packing diagram are shown in Figures 2-57 and 2-58. There is no evidence of π-π stacking interactions in the structure; the packing is determined by the hydrogen bond network.

Table 2-17 Hydrogen bond information for (14).

D—H···*A*	*D*—H	H···*A*	*D*···*A*	*D*—H···*A*
O4—H4*B*···Cl2^{i}	0.85	2.24	3.083 (2)	170
O3—H3*C*···Cl2^{ii}	0.85	2.30	3.1266 (19)	166
O4—H4*A*···Cl1^{i}	0.85	2.30	3.143 (2)	173
O1—H1′···Cl2	0.85	2.31	3.1103 (19)	158
O2—H2′···Cl2	0.85	2.24	3.0743 (18)	169
O3—H3*D*···O4	0.85	1.83	2.678 (3)	171

Symmetry codes: (i) *x*, -*y*+½, *z*+½; (ii) -*x*, *y*-½, -*z*+$^3/_2$.

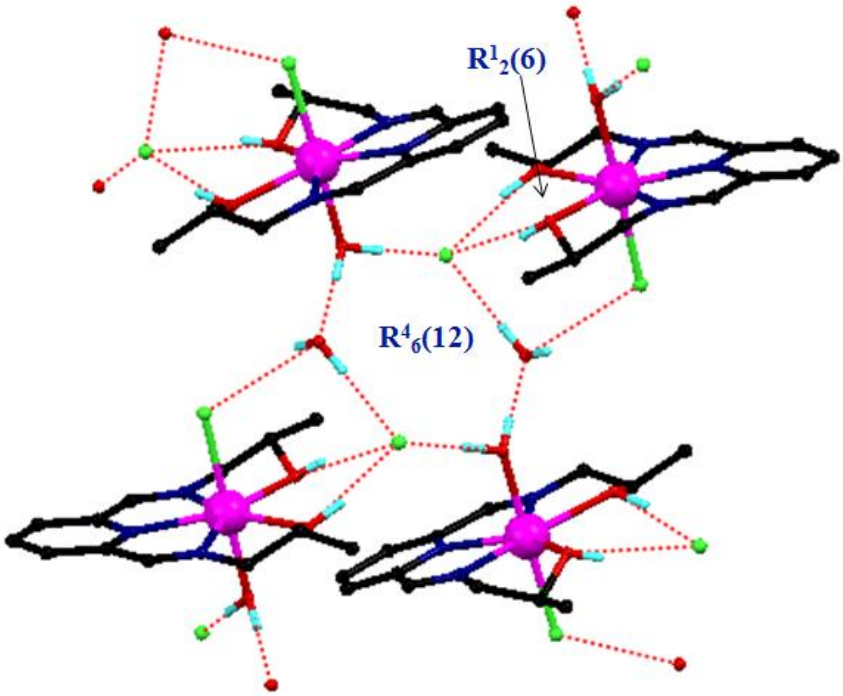

Figure 2-57 Hydrogen bond network in (14).

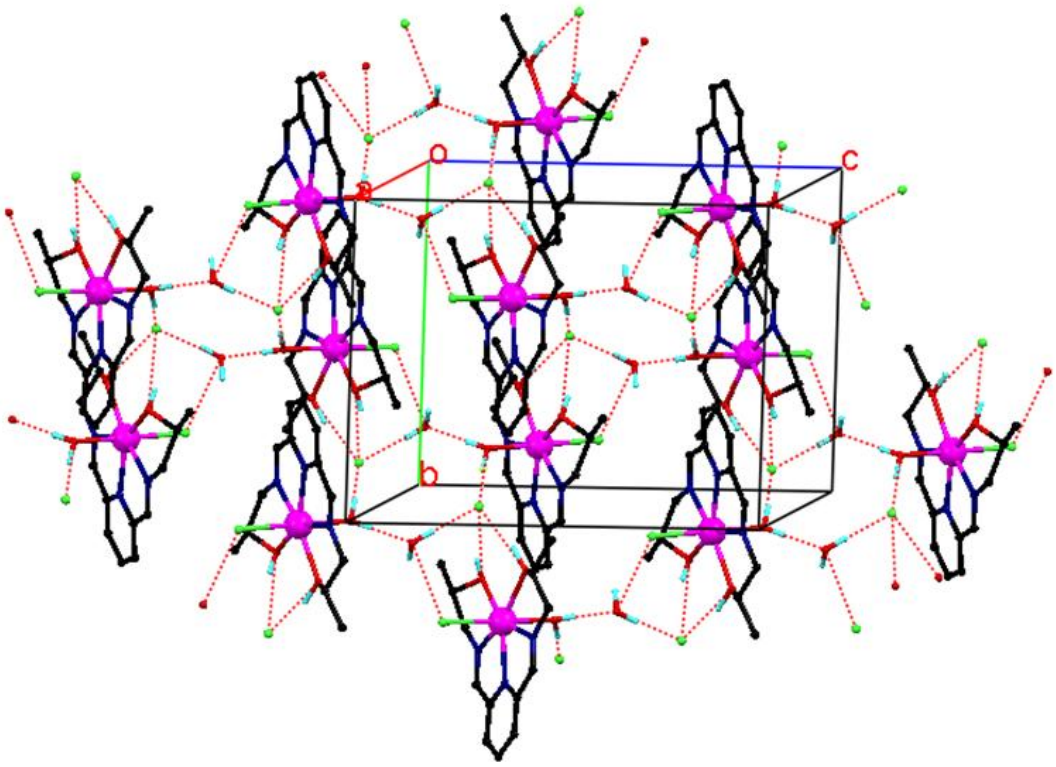

Figure 2-58 Packing plot of (14). Hydrogen bonds are shown as dashed lines.

2.2.13 [Mn(H$_2$L7)(NCS)$_2$] (16) and [Mn(H$_2$L7)Cl$_2$(H$_2$O)]·H$_2$O (17)

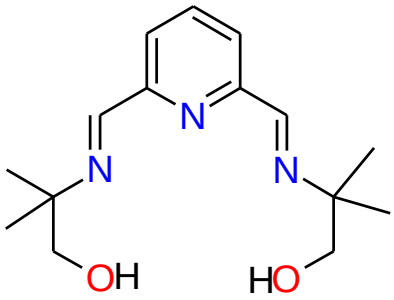

H$_2$L7

The reaction between one equivalent of H$_2$L7 and one equivalent of manganese(II) chloride in refluxing methanol gives a yellow powder (complex 17). Complex (16) was obtained by the same method except that two equivalents of sodium thiocyanate were added to the refluxing solution mixture. An orange precipitate formed when the solution was cooled to room temperature which was collected and washed with diethylether. IR spectra of the powder products showed strong -C=N- stretches at 1654 and 1642 cm^{-1} for (16) and (17) respectively. The thiocyanate stretch in complex (16) was seen at 2073 cm^{-1}. The ESI mass spectra of complexes (16) and (17) were recorded in methanol and peaks at 390(100%) and

367(70%) m/z were assigned to complex cations $[Mn(H_2L7)(NCS)]^+$ and $[Mn(H_2L7)Cl]^+$ respectively.

Single crystals of (16) were obtained *via* vapour diffusion of diethylether into a dmf solution of the complex and complex (16) crystallises as (16)·dmf. Methanol-diethylether and acetonitrile-diethylether vapour diffusion were also tried to get single crystals, but yellow powder products were obtained in each case. Single crystals of (17) were obtained *via* vapour diffusion of diethylether into an acetonitrile solution of the complex.

The details of the crystal structure and refinement for (16) and (17) can be found in Tables A15 and A16 respectively in Appendix 2. Crystal structure of (16) is shown Figure 2-59.

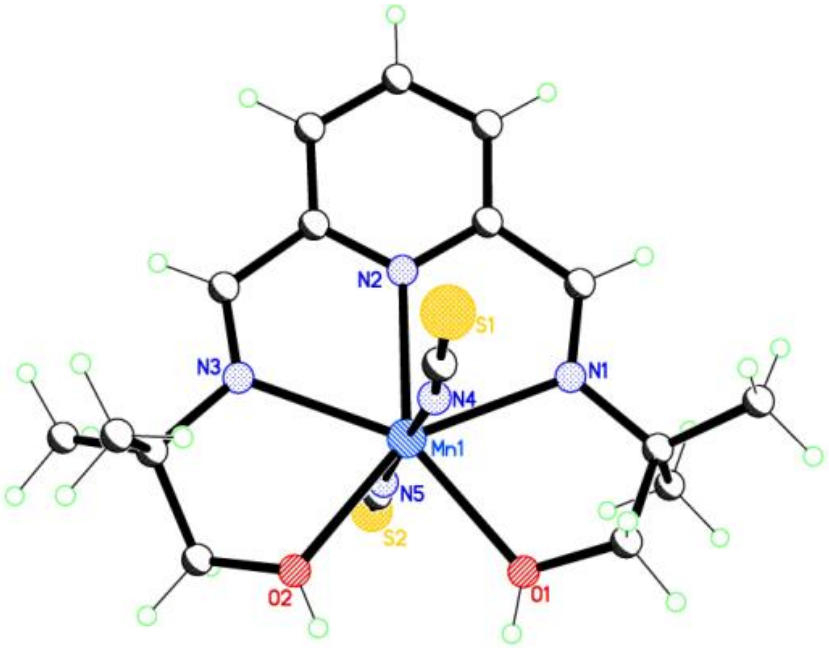

Figure 2-59 Crystal structure of (16). The uncoordinated dmf molecule is removed for clarity.

The asymmetric unit of (16) contains the mononuclear Mn(II) complex and an uncoordinated dmf molecule. The Mn(II) ion is seven-coordinate, bonded to the pyridinediimine unit and alcohol oxygen atoms (N_3O_2) of the ligand in the pentagonal plane, and to two N-bound thiocyanate ions at the axial positions. The uncoordinated dmf molecule is hydrogen bonded to two alcohol groups of the complex forming $R^1_2(6)$ hydrogen bonding motif. The pyridine diimine head unit of the ligand provides bite angles of 69.41(5)° (N1-Mn1-N2) and 69.37(5)° (N2-Mn1-N3) which are distorted from a regular pentagonal plane of 72°. The axial ligands with an angle of 176.70(70)° (N4-Mn1-N5) are slightly bent away from the ideal linear angle of 180°. Mn1-N_{axial} distances are shorter than the Mn1-$N_{pentagonal}$ and Mn1-O distances.

Selected bond lengths and angles for (16) are given in Table 2-18. Hydrogen bond parameters are given in Table 2-19.

Table 2-18 Selected bond lengths [Å] and angles [°] for (16).

Mn1—N1	2.3315 (15)	N5—Mn1—O2	89.51 (6)
Mn1—N2	2.2733 (15)	N4—Mn1—O2	88.23 (6)
Mn1—N3	2.3257 (15)	N2—Mn1—O2	139.60 (5)
Mn1—N4	2.2095 (17)	O1—Mn1—O2	81.89 (5)
Mn1—N5	2.1988 (17)	N5—Mn1—N3	86.34 (6)
Mn1—O1	2.2778 (15)	N4—Mn1—N3	95.15 (6)
Mn1—O2	2.2883 (14)	N2—Mn1—N3	69.37 (5)
		O1—Mn1—N3	151.14 (5)
N5—Mn1—N4	176.70 (7)	O2—Mn1—N3	70.34 (5)
N5—Mn1—N2	90.76 (6)	N5—Mn1—N1	93.70 (6)
N4—Mn1—N2	92.52 (6)	N4—Mn1—N1	87.12 (6)
N5—Mn1—O1	85.71 (6)	N2—Mn1—N1	69.41 (5)
N4—Mn1—O1	91.59 (6)	O1—Mn1—N1	69.48 (5)
N2—Mn1—O1	138.40 (5)	O2—Mn1—N1	150.83 (5)
N3—Mn1—N1	138.78 (5)		

Table 2-19 Hydrogen bonds for (16) [Å and °].

D—H···*A*	*D*—H	H···*A*	*D*···*A*	*D*—H···*A*
O1-H1····O3	0.85	1.93	2.7023(17)	150.5
O2-H2····O3	0.85	1.90	2.7252(17)	164.5

In (16), molecules are linked by π-π interactions in the structure (Figure 2-60 and 2-61). The C6-C8 edge of one of the complex molecule is stacked with the same section of an adjacent molecule under symmetry operation 1-x, -y, -z; C6 and C8* are separated by a distance of 3.406 Å (Figure 2-60).

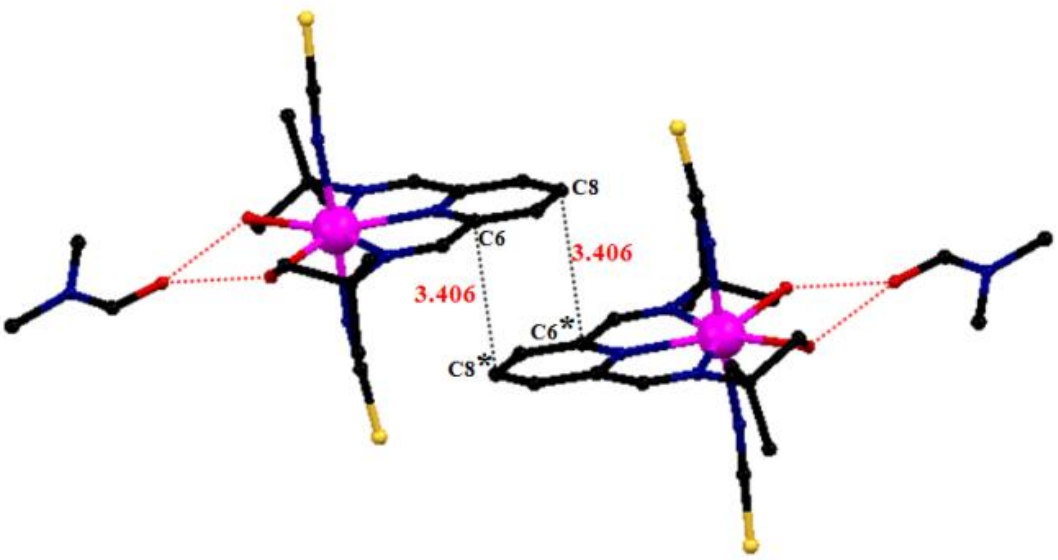

*Figure 2-60 π-π linked pairs of molecules in (16). Hydrogen bonding is shown as red dashed lines. Symmetry operation: * 1-x, -y, -z.*

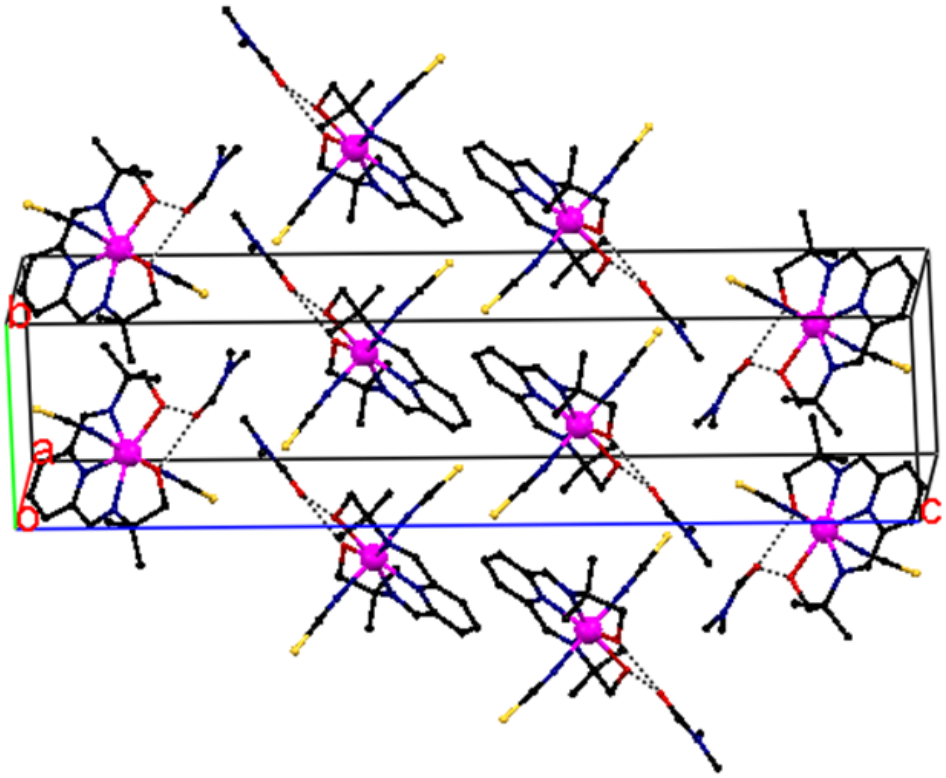

Figure 2-61 Packing diagram of (16). Hydrogen atoms are omitted for clarity and hydrogen bonds are shown as dashed lines.

In complex (17), the coordination sphere of Mn(II) comprises three nitrogen atoms from the pyridinediimine unit of the ligand, two chloride ions and the oxygen of water to give a six-coordinate Mn(II) complex (Figure 2-62). Three pyridinediimine nitrogen atoms and one chloride atom are located in the equatorial plane and one chloride and one water molecule are located at the axial positions. The axial ligands provide an angle of 172.93(3)° which is slightly bent away from the ideal value of 180° (Table 2-21). This distortion from the ideal value is quite likely due to the hydrogen bonding in which the axial ligand is involved. One of the alcohol groups is disordered in the structure and this was modelled over two positions in a 0.70:0.30 occupancy C1O1:C1'O1'. One of the methyl groups (C3) shows some disorder and this has been modelled as a rotation about the C-C bond. Site occupancy factors were set at 0.70 C3 at 0.30 for C3'.

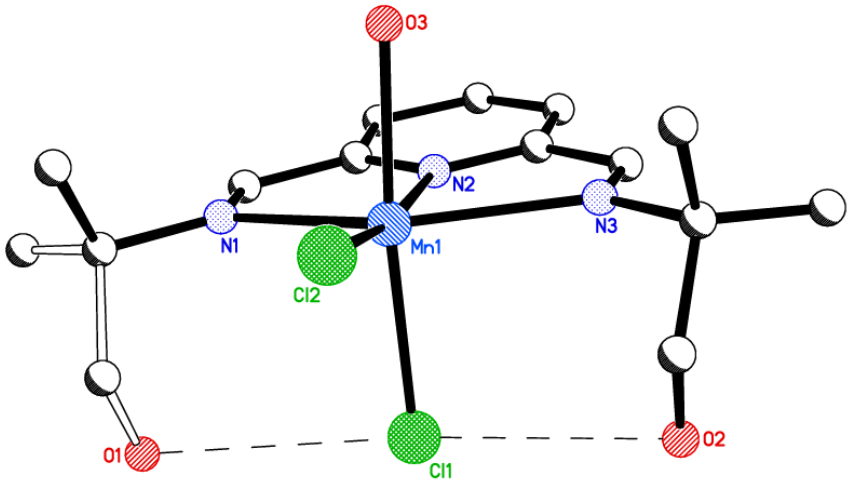

Figure 2-62 Structure of (17), alcohol and methyl group disorder are not shown in the structure. Hyroden atoms are removed for clarity. Hydrogen bonds are shown as dashed lines.

In complex (17), two alkoxy oxygen atoms pointed out from the coordination plane and remained uncoordinated while in complex (16) these two oxygen atoms are bound to Mn(II) centre. The reason why these two alkoxy oxygen atoms are not coordinated may be because of hydrogen bonding competition to stabilise the structure. There is also an uncoordinated, partially occupied water molecule (30% occupancy) which is involved in hydrogen bonding in the asymmetric unit. Six-coordinate Mn(II) complex cations are linked to each other *via* a hydrogen bond network and hydrogen bond parameters are given in Table 2-20. The chloride atom at the axial position (Cl1) forms a bifurcated hydrogen bond with one of the alcohol groups (O2-H···Cl1) and the uncoordinated water molecule (O4-H···Cl1). The uncoordinated water molecule makes three hydrogen bonds (two as donor to the axial

chloride O4-H···Cl1 and one of the alcohol groups O4-H···O2 and as acceptor from the other alcohol group O1-H···O4. The coordinated water molecule forms a bifurcated hydrogen bond (as donor) with the chloride atom in the equatorial plane (O3-H···Cl2) and one of the alcohol groups (O3-H···O1). These hydrogen bonds produce several hydrogen bonding motifs shown in Figure 2-63.

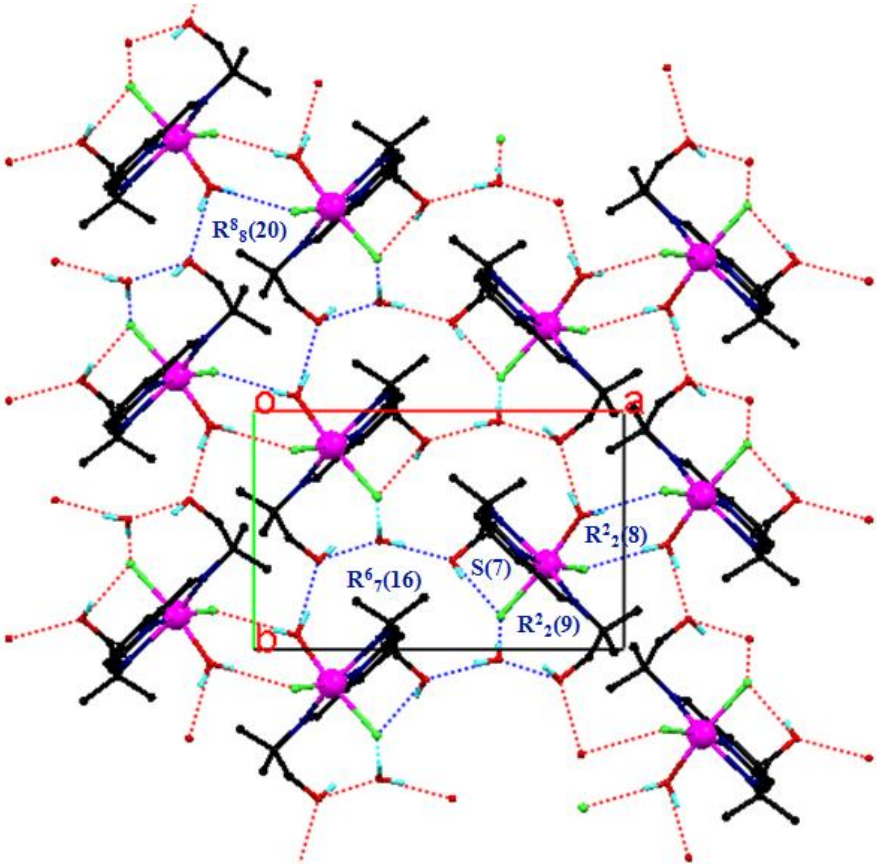

Figure 2-63 Hydrogen bond network in (17). Hydrogen atoms bonded to carbon atoms are removed for clarity. Hydrogen bonds are shown as dashed lines and hydrogen bonding motifs are shown in blue.

Table 2-20 Hydrogen bonds for (17) [Å and °].

D—H···*A*	*D*—H	H···*A*	*D*···*A*	*D*—H···*A*
O2—H2···Cl1	0.85	2.32	3.1236 (12)	157.5
O1—H1···Cl1	0.85	2.50	3.272 (2)	151.2
O1'—H1'···O4	0.85	1.90	2.744 (6)	172.4
O4—H4E···Cl1	0.85	2.19	3.038 (4)	171.7
O3—H3E···Cl2^{i}	0.85	2.40	3.2280 (11)	166.0
O3—H3D···O1'^{ii}	0.85	1.80	2.575 (4)	151.1
O3—H3D···O1'^{ii}	0.85	1.80	2.575 (4)	151.1

Symmetry codes: (i) -*x*+1, *y*+½, -*z*+½; (ii) -*x*, -*y*, -*z*; (iii) *x*, *y*-1, *z*.

Table 2-21 Selected bond lengths [Å] and angles [°] for (17).

Mn1—N1	2.3858 (11)	O3—Mn1—N3	84.66 (4)
Mn1—N2	2.2018 (11)	N1—Mn1—N3	142.72 (4)
Mn1—N3	2.3953 (11)	N2—Mn1—Cl2	170.65 (3)
Mn1—Cl1	2.5392 (4)	O3—Mn1—Cl2	88.48 (3)
Mn1—Cl2	2.4253 (4)	N1—Mn1—Cl2	108.52 (3)
Mn1—O3	2.2390 (10)	N3—Mn1—Cl2	108.47 (3)
		N2—Mn1—Cl1	91.86 (3)
N2—Mn1—O3	82.18 (4)	O3—Mn1—Cl1	172.95 (3)
N2—Mn1—N1	71.58 (4)	N1—Mn1—Cl1	89.83 (3)
O3—Mn1—N1	91.83 (4)	N3—Mn1—Cl1	89.87 (3)
N2—Mn1—N3	71.17 (4)	Cl2—Mn1—Cl1	97.485 (13)

2.2.14 [Mn(H_2L8)($NCS)_2$] (18)

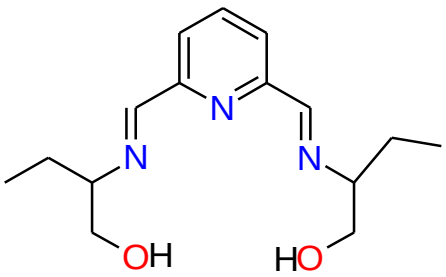

H_2L8

Complex (18) was prepared by the reaction of one equivalent of H_2L8 and one equivalent of manganese(II) chloride in the presence of two equivalents of thiocyanate in methanol. A yellow powder was obtained on reducing the solvent volume. The yellow powder was characterised by CHN analysis, IR and mass spectrometry. IR spectra of the powder product showed a strong -C=N- stretches at 1638 cm^{-1}. Peaks at 2059 (strong) and 3432 (broad) cm^{-1} can be assigned to thiocyanate and O-H stretch respectively. ESI mass spectra of the complex showed three major peaks at 390.08(100%), 331.10(60%) and 166.05(17%) attributed to $\{[Mn(H_2L8)(NCS)]\}^+$, $\{[Mn(HL8)]\}^+$ and $\{[Mn(H_2L8)]\}^{2+}$ respectively. Single crystals of the complex were obtained *via* vapour diffusion of diethylether into a dmf solution of the complex. Complex (18) was found to crystallise as $[Mn(H_2L8)(NCS)_2(dmf)]\cdot dmf$. Attempts to crystallise from methanol-diethylether, acetonitrile-diethylether and ethanol-diethylether resulted in powder products.

The complex was found to crystallise in the monoclinic space group $P2_1/c$, details of the crystal structure and refinement can be found in Table A17 in Appendix 2. The structure of complex (18) is shown in Figure 2-64. The asymmetric unit contains one mononuclear Mn(II) complex and two dmf molecules, one of which is coordinated to the Mn(II) centre. The Mn(II) ions are six-coordinate, bonded to three nitrogen atoms of the pyridinediimine unit, two thiocyanate ions (N-bound) and one oxygen atom of a dmf molecule.

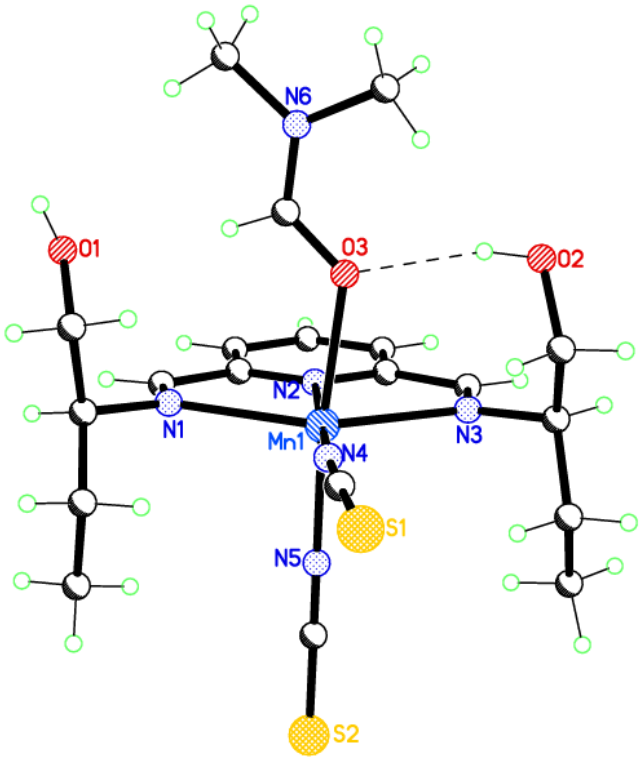

Figure 2-64 Crystal structure of [Mn(H_2L8)($NCS)_2$(dmf)]·dmf. The uncoordinated dmf is removed for clarity and hydrogen bonding is shown as dashed lines.

Three pyridinediimine nitrogen donors of the ligand and one nitrogen atom of thiocyanate are located in a plane and one oxygen atom of a dmf molecule and one thiocyanate ion are located perpendicular to this. Selected bond lengths and angles are presented in Table 2-22.

Table 2-22 Selected bond lengths [Å] and angles [°] for [Mn(H_2L8)($NCS)_2$(dmf)]·dmf

Mn1—N1	2.3861 (19)	N5—Mn1—O3	172.17 (7)
Mn1—N2	2.2090 (19)	N2—Mn1—O3	85.90 (6)
Mn1—N3	2.3485 (19)	N4—Mn1—N3	109.25 (8)
Mn1—N4	2.103 (2)	N5—Mn1—N3	91.28 (7)
Mn1—N5	2.173 (2)	N2—Mn1—N3	71.60 (7)
Mn1—O3	2.2839 (16)	O3—Mn1—N3	81.36 (6)
		N4—Mn1—N1	107.57 (8)

N4—Mn1—N5	96.24 (8)	N5—Mn1—N1	91.19 (7)
N4—Mn1—N2	174.43 (8)	N2—Mn1—N1	71.10 (7)
N5—Mn1—N2	89.22 (7)	O3—Mn1—N1	93.02 (6)
N4—Mn1—O3	88.79 (7)	N3—Mn1—N1	142.57 (7)

The coordinated dmf molecule is involved in hydrogen bonding with one of the alcohol groups of the ligand (O2H···O3) forming an S(7) hydrogen bonding motif and the uncoordinated dmf makes a hydrogen bond with the other alcohol group. Hydrogen bond parameters are given in Table 2-23. Although no π-π stacking interactions were observed, there are some S···π interactions in the structure; S2 interacts with the pyridine ring under symmetry operation x, ½-y, ½+z with a distance of 3.505 Å (Figure 2-65). The molecules are linked *via* weak S···HC hydrogen bonds[180] (Table 2-23). A packing diagram of the complex is shown in Figure 2-66.

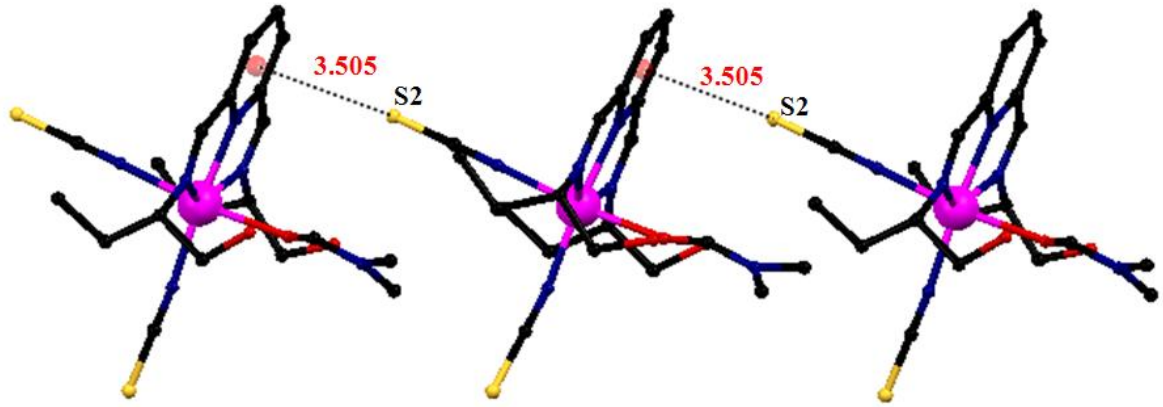

Figure 2-65 S···π interactions in [Mn(H$_2$L8)(NCS)$_2$(dmf)]·dmf

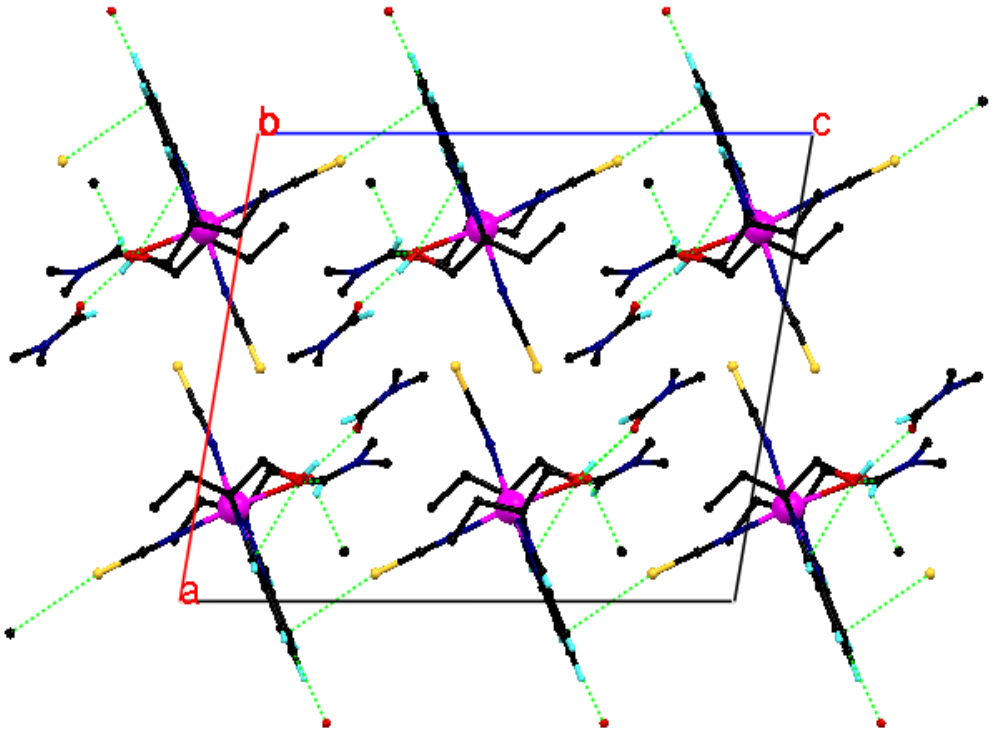

Figure 2-66 Packing plot of [Mn(H$_2$L8)(NCS)$_2$(dmf)]·dmf viewing down b axis, where hydrogen bonds and S···HC and S···π interactions are shown as dashed lines.

Table 2-23 Hydrogen bond parameters for [Mn(H$_2$L8)(NCS)$_2$(dmf)]·dmf [Å and °].

D—H···*A*	*D*—H	H···*A*	*D*···*A*	*D*—H···*A*
O2—H2A···O3	0.84	2.05	2.861 (2)	161.6
O1—H1···O4^{i}	0.84	1.86	2.695 (3)	170.6
C9—H9···O1^{ii}	0.95	2.68	3.323 (3)	125.8
C11—H11···S2^{iii}	0.95	2.89	3.800 (2)	160.1
C5—H5···S2^{iv}	0.95	2.84	3.742 (2)	158.0
C21—H21···O2^{v}	0.95	2.61	3.468 (4)	149.9
C8—H8···O2^{vi}	0.95	2.51	3.249 (3)	134.9
C18—H18···O1	0.95	2.47	3.299 (3)	145.3

Symmetry codes: (i) -*x*+1, -*y*+1, -*z*; (ii) -*x*, *y*-½, -*z*-½; (iii) -*x*, -*y*, -*z*; (iv) -*x*, -*y*+1, -*z*; (v) -*x*+1, -*y*, -*z*; (vi) -*x*, *y*+½, -*z*-½.

2.2.15 Ligands H_2L9 (19) and H_2L10 (20)

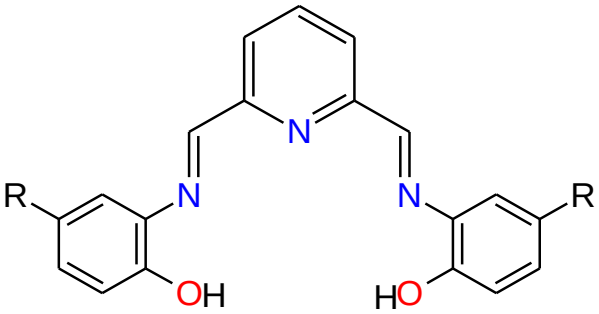

H_2L9 R=H
H_2L10 R=-CH_3

Ligands H_2L9 (19) and H_2L10 (20) were prepared according to reported methods[183,184] by reacting one equivalent of 2,6-diformylpyridine with two equivalents of 2-amino-4-methylphenol or 2-aminophenol in ethanol, the yellow products were obtained after stirring for 30 min at room temperature. Both compounds are stable at room temperature in the solid state without decomposition and are soluble in most organic solvents. Each molecule has two imine groups and two 4-methylphenol or phenol units, one each side of the pyridine. Elemental analysis results are given in the experimental chapter and are in good agreement with the calculated values. The ^{1}H and ^{13}C NMR spectra of the ligands were also recorded in $CDCl_3$, and the spectral data are given in the experimental chapter. ^{1}H NMR spectra of both compounds are displayed in Figure 2-67 and 2-68 and proton assignments are given in Figure 2-69. Both ligands show mirror symmetry in solution. In the ^{1}H NMR spectrum of H_2L9, all aromatic protons were seen in the range of δ 6.86–8.79 ppm as multiplets. A singlet peak at δ 8.84 ppm can be attributed to azomethine protons (–N=CH–). Additionally, three signals, one of which is broad, were observed at δ 3.65 (*q*), 1.68(*br*) and 1.16(*t*) ppm. Integration of peaks suggests the compound contains one ethanol molecule per molecule of H_2L9 and this is supported by CHN analysis. The ^{1}H-NMR spectrum of the H_2L10 displays a singlet at δ 2.25 ppm corresponding to the protons of the methyl groups (C-CH_3), a singlet at δ 8.77 ppm is assigned to azomethine protons (–N=CH–), one broad signal at δ 10.12 ppm assigned to phenolic protons (-C-OH). The broad signal at the δ 1.69 ppm corresponding to water protons is indicative of the presence of water in the compound, as confirmed by CHN analysis and single crystal X-ray diffraction.

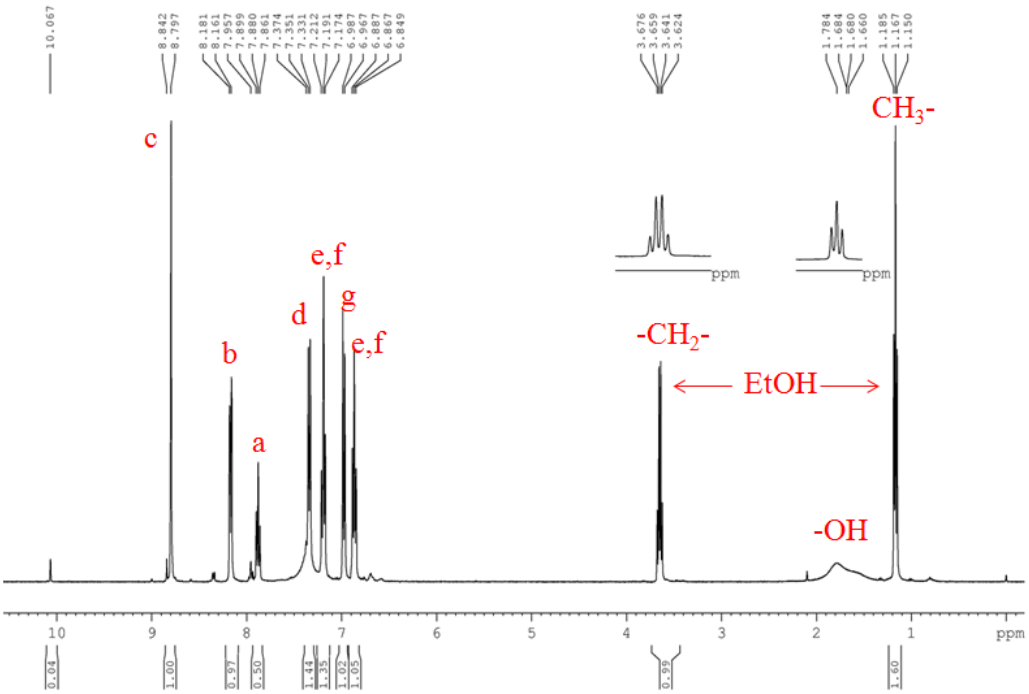

Figure 2-67 ^{1}H NMR spectrum of $H_2L9 \cdot EtOH$

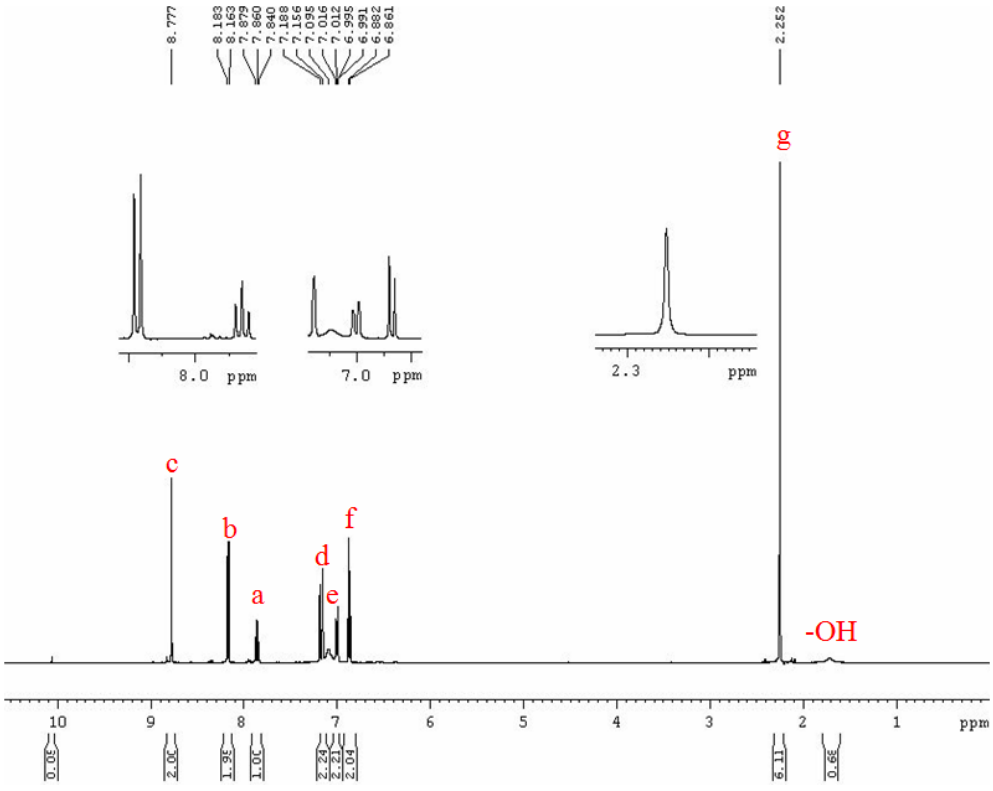

Figure 2-68 ^{1}H NMR spectrum of $H_2L10 \cdot H_2O$

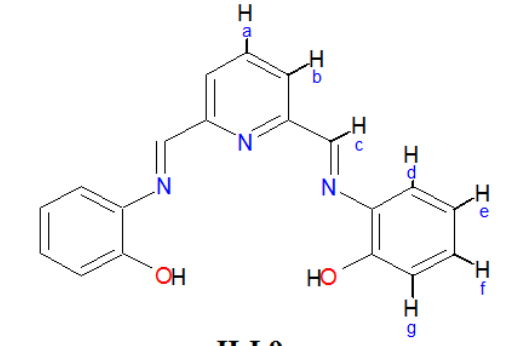

H_2L9

Peak(ppm)	Assignment	Integration
8.84	c	*s* 2H
8.79	b	*d* 2H
8.18	a	*t* 1H
7.88	d	*d* 2H
7.37, 6.86	e, f	*t* *2H*
6.98	g	*d* 2H
3.65	-CH_2- (EtOH)	*q* 2H
1.68	-OH (EtOH)	*b* 1H
1.16	CH_3- (EtOH)	*t* 3H

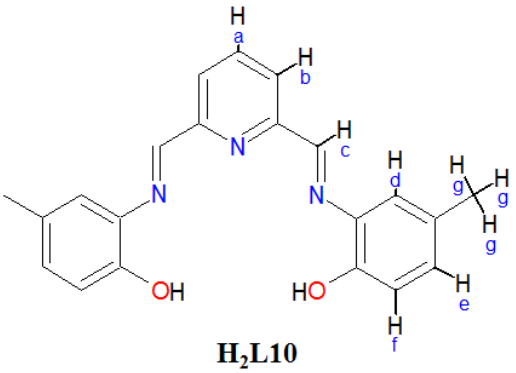

H_2L10

Peak(ppm)	Assignment	Integration
8.77	c	*s* 2H
8.17	b	*d* 2H
7.55	a	*t* 1H
7.09	d	*s* 2H
6.99	e	*d* *2H*
6.87	f	*d* 2H
2.25	g	*s* 6H
1.69	-OH (H_2O)	*b* 1H

Figure 2-69 ^1H NMR assignments for H_2L9 and H_2L10.

The ESI mass spectra of the ligands were recorded in methanol solution. In H_2L9, molecular ions were observed at m/z 673.19(5%), 372,13(25%), 340.11(100%), 318.09(15%) attributed to $\{[(H_2L9)_2]Na\}^+$, $\{[(H_2L9)](CH_3OH)H\}^+$, $\{[(H_2L9)]Na\}^+$, $\{[(H_2L9)]H\}^+$. In H_2L10 signals at m/z 346 (40%), 368(100%) and 386(7%) are assigned to $\{[(H_2L9)]H\}^+$, $\{[(H_2L9)]Na\}^+$ and $\{[(H_2L9)](H_2O)Na\}^+$ respectively.

The infrared spectra of the compounds showed an imine $\nu_{(CH=N)}$ vibrations at 1628 and 1630 cm^{-1} for H_2L9 and H_2L10 respectively. Broad bands attributed to the $\nu_{(O-H)}$ stretch were seen at around 3100 – 3400 cm^{-1}.

Single crystals for H_2L10 suitable for X-ray diffraction were obtained from slow evaporation of acetonitrile solution of the compound. However, only micro crystals were obtained for H_2L9 and were too small for X-ray diffraction study.

Crystal structure of H_2L10 was solved in the monoclinic space group *C*2/*c*, details of the crystal structure and refinement can be found in Table A18 in Appendix 2. H_2L10 crystallizes as the dimer $(H_2L10)_2 \cdot H_2O$, assembled by hydrogen bonding around a water molecule (Figure 2-70).

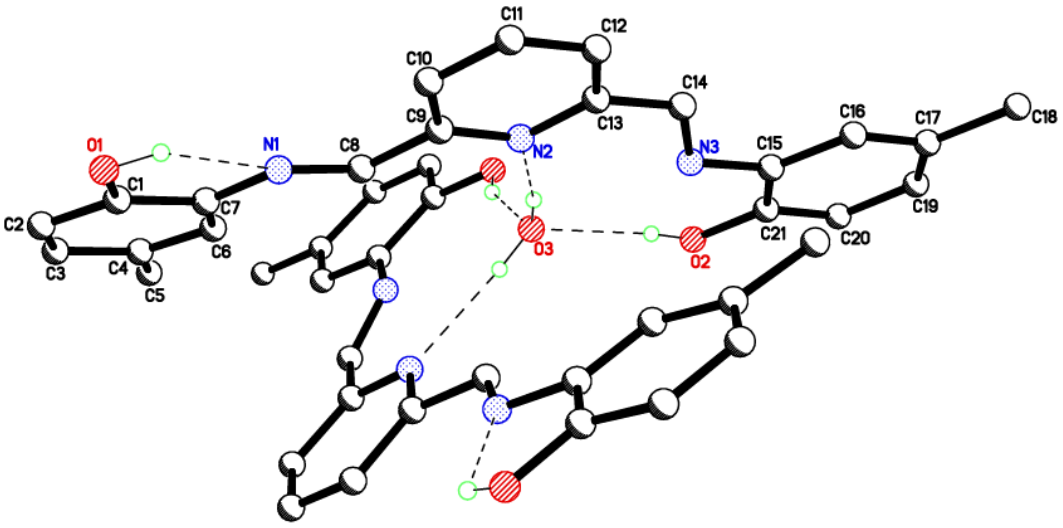

Figure 2-70 Crystal structure of H_2L10.

The water molecule sits on a two-fold axis which also relates the two identical Schiff base molecules. The water makes four strong hydrogen bonds, as donor to the pyridine nitrogen atoms, and as acceptor from the phenol groups (Table 2-24) producing a $R^2_2(10)$ motif. There are also weaker hydrogen bond interactions with one of the imine nitrogen atoms of each molecule. Additionally, there are phenol-imine intramolecular hydrogen bonds in each molecule resulting in a S(6) hydrogen bonding motif. All bond lengths and angles are within the normal ranges. The Schiff base molecule has lost the mirror symmetry indicated from solution spectra, the geometry is *cis* at the C8=N1 imine group and *trans* at the C14=N3 group. The Schiff base molecule is close to planar with interplanar angles between the pyridine and phenol groups, 11.46(8)° and 2.06(8)° for the rings containing O1 and O2 respectively.

The hydrogen bond geometry at the water molecule is approximately tetrahedral but the angle between the two H-bonded Schiff base molecules is not close to the ideal 90°; the angle between the N2-O3-O2 plane and its equivalent under two-fold rotation is 60.52(4)°. This is possibly a consequence of the intermolecular interactions in the lattice. The Schiff base molecules show two sets of interactions with neighbouring dimeric units. On the more open face (that nearest to the H-bonded phenol of the second molecule), there is a π-π interaction involving the pyridine ring and the phenolimine group H-bonded to the central water molecule. The average interplanar distance between this section and its neighbour under symmetry operation 1-x, -y, -z is 3.354(1) Å, and the phenol-pyridine centroid-centroid

distance is 3.707(2) Å. On the other face (partially blocked by the non-bonded phenol of the second molecule), there is a less extensive edge to edge interaction from C10 to C11 of a neighbouring dimer under symmetry operation 1-x, 1-y, -z is 3.392(2) Å. These result in columns formed by alternating π-π and edge to edge interactions extending through the lattice (Figure 2-71).

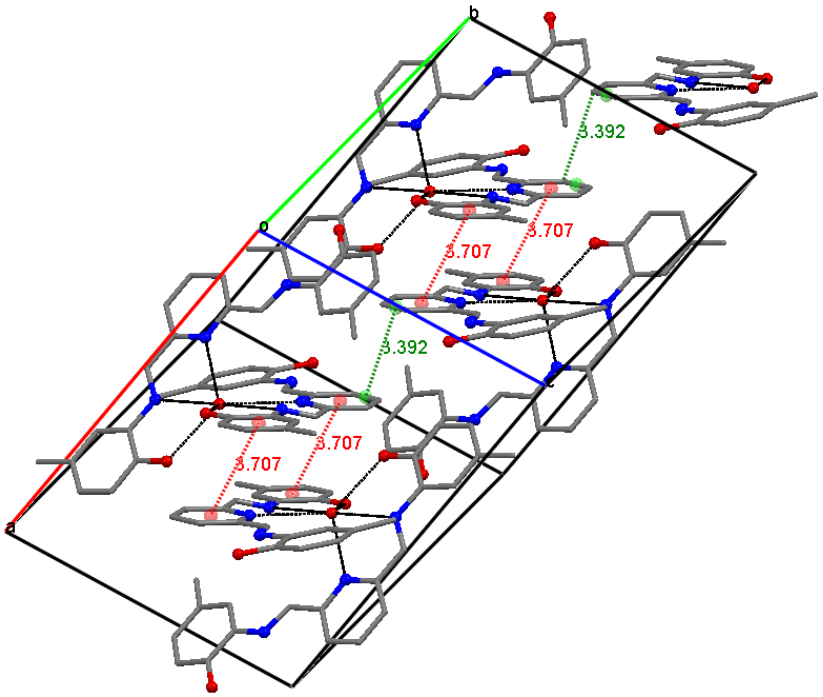

Figure 2-71 Packing diagram of H_2L10 showing π-π interactions; hydrogen atoms are removed for clarity.

Table 2-24 Hydrogen bonds for H_2L10 [Å and °].

D–H···A	*d(D–H)*	*d(H···A)*	*d(D···A)*	*<(DHA)*
O2–H2A ···O3	0.836(17)	1.960(17)	2.7592(12)	159.6(15)
O2–H2A ···N3	0.836(17)	2.347(15)	2.7624(12)	111.3(12)
O1–H1A···N1	0.86(2)	2.120(19)	2.6722(13)	121.7(16)
O3–H3D···N2	0.812(16)	2.187(16)	2.9865(12)	168.0(16)
O3–H3D···N3	0.812(16)	2.569(16)	3.0142(9)	115.9(14)

2.2.16 [Mn(H_2L9)Cl_2]·MeOH (19a)

Complex (19a) was prepared by Paul Goring (undergraduate student) and characterised by CHN, IR and mass spectrometry. The IR spectrum of the complex showed a strong peak at 1638 cm^{-1} assigned to a -C=N- stretch; the phenolic OH stretch was observed at 3432 cm^{-1} as a broad peak.

Single crystals suitable for X-ray diffraction were obtained by slow diffusion of diethylether into a methanol solution of the complex. The complex was found to crystallise in the monoclinic space group $P2_1/c$, details of the crystal structure and refinement can be found in Table A19 in Appendix 2. The structure is shown Figure 2-72, the asymmetric unit of (19a) contains a mononuclear Mn(II) complex and an uncoordinated methanol molecule. The Mn(II) ions have the expected seven-coordinate pentanogal bipyramidal geometry with two chloride ions at the axial positions.

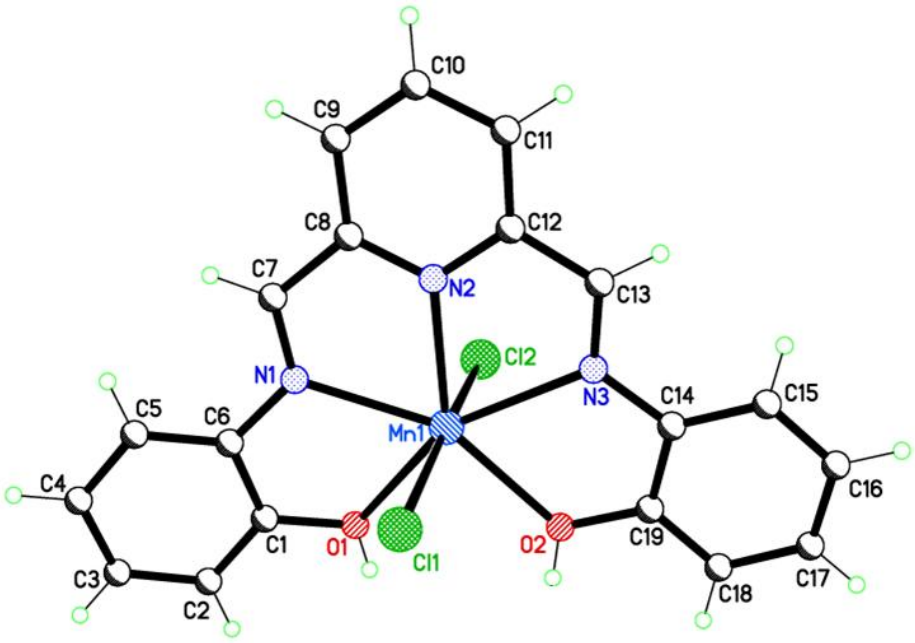

Figure 2-72 Molecular structure of (19a).

Selected bond lengths and angles are given in Table 2-26. The pyridinediimine unit of the ligand provides bite angles of 69.71(6)° (N1-Mn1-N2) and 68.78(6)° (N2-Mn1-N3) which are slightly distorted from a regular pentagonal angle of 72°. The axial ligands (Cl1-Mn1-Cl2 angle is 176.7(7)°) are bent away from the ideal value of 180°. This bending is probably because one of the axial chloride ions is involved in hydrogen bonding with both a neighbouring complex molecule and a methanol molecule.

One of the axial chloride ions is hydrogen bonded to one of the phenolic protons (O1-H1*A*···Cl2) of an adjacent complex molecule and the solvate methanol molecules make two hydrogen bonds (one as acceptor from a phenol group and one as donor to an axial chloride ion) resulting in a hydrogen bonded dimer with a $R^2_3(8)$ motif (Figure 2-73). Hydrogen bond parameters are given in Table 2-25.

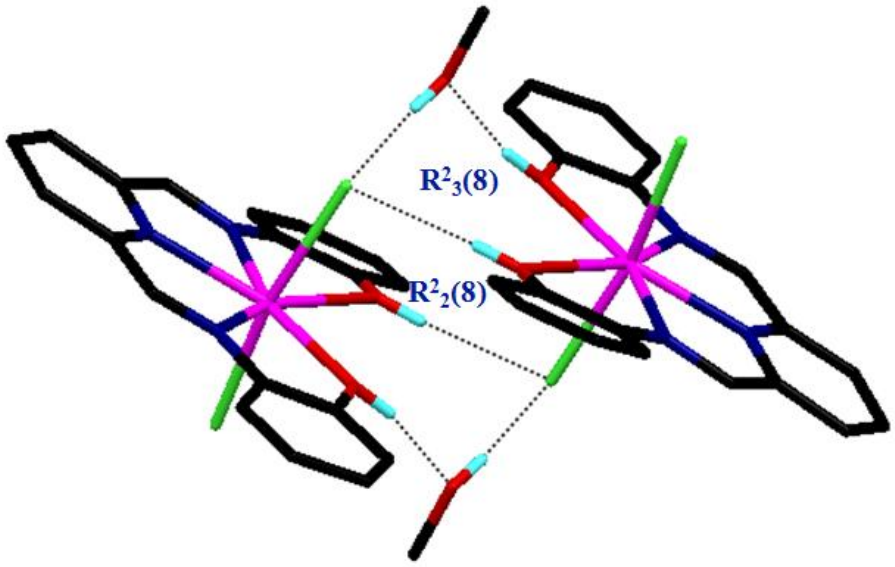

Figure 2-73 Hydrogen bonding in (19a), hydrogen atoms bonded to carbon atoms are removed for clarity.

Hydrogen bonded dimers are linked *via* π-π edge to edge interactions. The C9-C16 edge of one of the complex is stacked with the same section of an adjacent molecule under symmetry operation 1-x, -y, 1-z; C13 and C13* are separated by a distance of 3.312 Å (Figure 2-74).

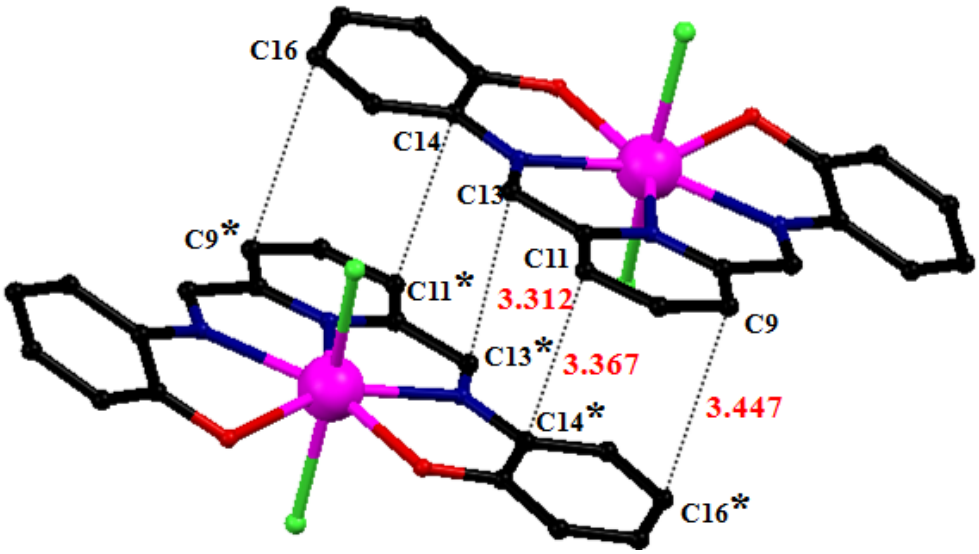

*Figure 2-74 π-π interactions in (19a), hydrogen atoms are removed for clarity. Symmetry operation: * 1-x, -y, 1-z.*

Table 2-25 Hydrogen bonds for (19a) [Å and °].

D—H···*A*	*D*—H	H···*A*	*D*···*A*	*D*—H···*A*
O1-H1A····Cl2^{i}	0.85	2.32	3.1680(16)	173.2
O3-H3A····Cl2^{i}	0.85	2.19	3.0334(18)	175.8
O2-H2A····O3	0.85	1.71	2.545(2)	168.1

Symmetry code: (i) -*x*+2, -*y*, -*z*+1

Table 2-26 Selected bond lengths [Å] and angles [°] for (19a).

Mn1—N2	2.2701 (18)	O2—Mn1—O1	84.67 (6)
Mn1—O2	2.2863 (16)	N1—Mn1—O1	68.21 (6)
Mn1—N1	2.3160 (18)	N3—Mn1—O1	152.02 (6)
Mn1—N3	2.3562 (18)	N2—Mn1—Cl1	101.44 (5)
Mn1—O1	2.4255 (16)	O2—Mn1—Cl1	89.85 (5)
Mn1—Cl1	2.4849 (7)	N1—Mn1—Cl1	86.26 (5)
Mn1—Cl2	2.5465 (7)	N3—Mn1—Cl1	100.95 (5)
		O1—Mn1—Cl1	86.95 (4)
N2—Mn1—O2	137.34 (6)	N2—Mn1—Cl2	88.56 (5)
N2—Mn1—N1	69.71 (6)	O2—Mn1—Cl2	85.38 (5)
O2—Mn1—N1	152.75 (6)	N1—Mn1—Cl2	93.56 (5)
N2—Mn1—N3	68.78 (6)	N3—Mn1—Cl2	86.32 (5)
O2—Mn1—N3	68.71 (6)	O1—Mn1—Cl2	83.00 (4)
N1—Mn1—N3	138.48 (6)	Cl1—Mn1—Cl2	169.23 (2)
N2—Mn1—O1	136.35 (6)		

2.2.17 $[Mn_3(L9)_2(OAc)_2(MeOH)_2]\cdot 2MeOH$ (21)

The reaction of one equivalent of H_2L9 with one equivalent of manganese chloride resulted in mononuclear complex (19a) as discussed above. When one equivalent of H_2L9 reacts with 1.5 equivalents of manganese acetate in refluxing methanol, a tri-nuclear Mn(II) complex was obtained. The complex was characterised by CHN analysis, IR and mass spectrometry. The ESI mass spectrum in methanol showed several fragments corresponding to mono, di and trinuclear species in solution, however, a molecular complex cation was observed at m/z 854.03(30%) assigned to $\{[Mn_3(L9)_2(OAc)]\}^{+}$.

Single crystals suitable for X-ray study were obtained from slow diffusion of diethylether into a MeOH solution of the complex. The complex was found to crystallise in the monoclinic space group $P2_1/c$, details of the crystal structure and refinement can be found in Table A20 in Appendix 2 and the structure is shown in Figure 2-75. The tri-nuclear complex

consists of two mononuclear acyclic units linked by a central Mn(II) ion. Mn1 and Mn3 are seven-coordinate with approximate pentagonal bipyramidal geometry with one oxygen atom from methanol and one oxygen atom from an acetate ion as axial donors. The central ion, Mn2, is six-coordinate, bonded to four phenolate groups and two acetate anions which bridge to Mn1 and Mn3. Phenolate oxygen atoms are deprotonated and serve to bridge two Mn(II) centres. Mn1-Mn2 and Mn2-Mn3 distances are 3.3206(5) and 3.3552(5) Å respectively. Selected bond lengths and angles are given in Table 2-28.

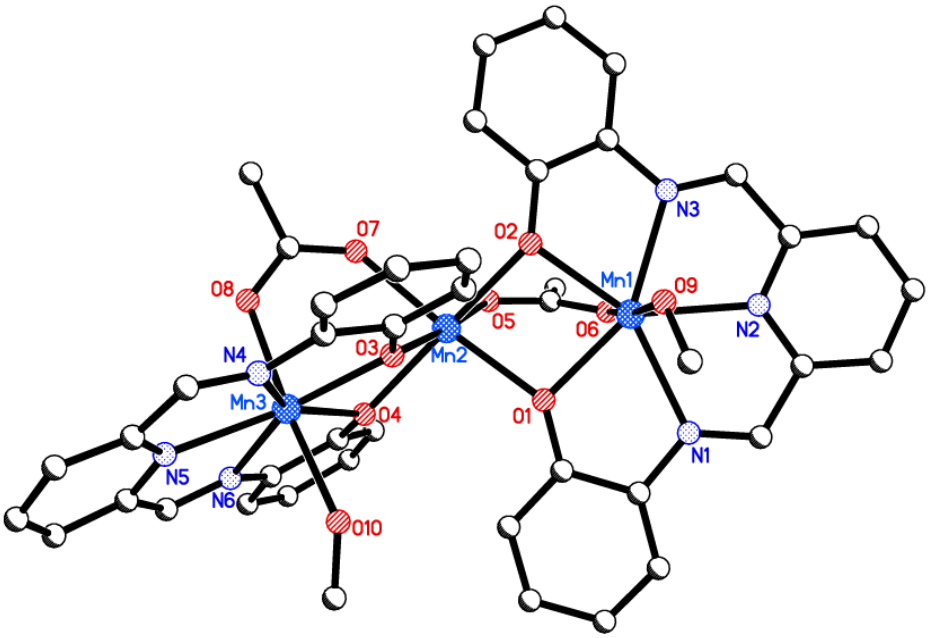

Figure 2-75 Crystal structure of (21), hydrogen atoms and 2 MeOH of crystallisation are omitted for clarity.

Each oxygen atom of a carboxylate ion has two lone pair electrons, one pair directed away from the R group is called the *syn* pair and the other is *anti*.[185] Through these lone pairs, carboxylate ions (RCO_2^-) such as acetate (CH_3COO^-) can bridge metals ions in a number of ways as a bridging bidentate ligand in a *syn-syn* (A), syn-anti (B) or *anti-anti* (C) configuration or as a monatomic bridging ligand (D), either alone, with additional bridging (E), or in arrangements involving chelation and bridging (F, G) as illustrated in Figure 2-76.[185] The binding mode of both acetate ligands in the tri-nuclear complex (21) described here is classified as *syn-syn* with three atoms bridging; each acetate ligand links (Mn1-Mn2 and Mn2-Mn3) two manganese ions.

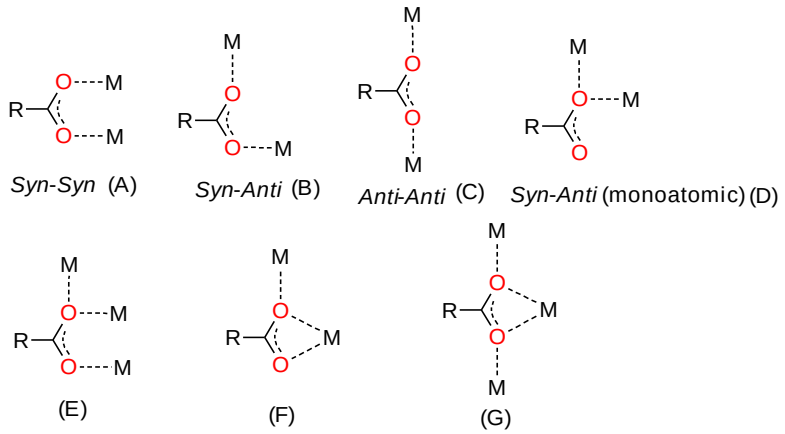

Figure 2-76 Different bridging modes for carboxylate ligands.

There are two uncoordinated methanol molecules in the asymmetric unit, which are involved in hydrogen bonding. One is hydrogen bonded with the acetate group (O11-H···O8), the other makes two hydrogen bonds with one of the coordinated acetate groups (as donor, O12-H···O5) and one of the coordinated methanol molecules of an adjacent complex (as acceptor, O9-H···O12) resulting 1D hydrogen bonded chains (Figure 2-78). Hydrogen bonding information is presented in Table 2-27.

The chains are linked by two sets of π-π stacking interactions. First, the edge of the one of the pyridine phenol units (C24-C27) is stacked with the same edge of the neighbouring molecule under symmetry operation -x, 1-y, -z, and second, one of the pyridine units (C8-N2) is stacked with one of the phenol rings (C1-C6)** under symmetry operation 1-x, -½+y, ½-z with a centroid-centroid distance of 3.658 Å (Figure 2-77).

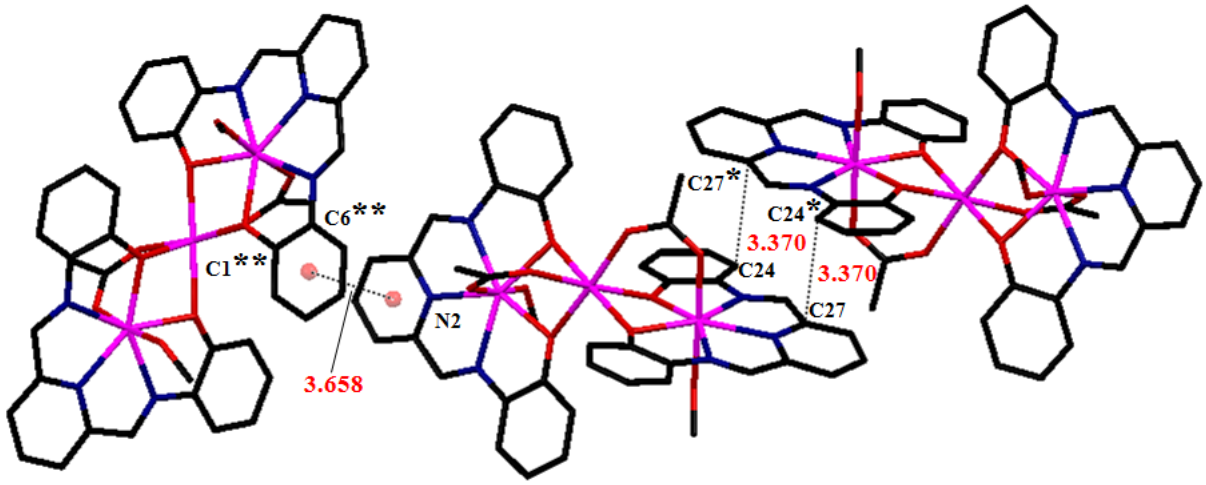

*Figure 2-77 π-π interactions in (21). Hydrogen atoms and 2 MeOH of crystallisation are omitted for clarity. Symmetry operations: * -x, 1-y, -z, ** 1-x, -½+y, ½-z.*

Table 2-27 Hydrogen bonds for (21) [Å and °].

D—*H*···*A*	*D*—*H*	*H*···*A*	*D*···*A*	*D*—*H*···*A*
O9—H9*A*···O12	0.85	1.89	2.724 (2)	165
O11—H11*A*···O8	0.85	1.97	2.817 (3)	172
O12—H12···O5^{i}	0.85	2.03	2.861 (2)	164

Symmetry codes: (i) *x*, -*y*+½, *z*-½.

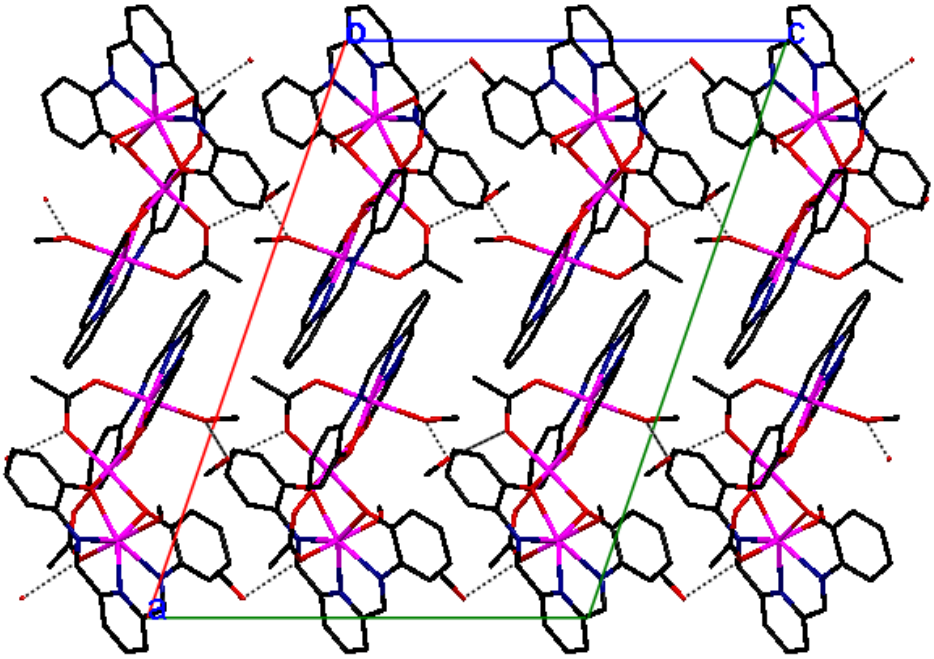

Figure 2-78 Packing diagram of (21). Hydrogen bonds are shown as dashed lines.

Table 2-28 Selected bond lengths [Å] and angles [°] for (21).

Mn1—N1	2.3506 (19)	N2—Mn1—N1	67.87 (7)
Mn1—N2	2.3072 (19)	O3—Mn2—O7	86.46 (6)
Mn1—N3	2.3057 (19)	O3—Mn2—O1	93.21 (6)
Mn1—O1	2.1780 (15)	O7—Mn2—O1	175.34 (6)
Mn1—O2	2.2100 (15)	O3—Mn2—O2	99.56 (6)
Mn1—O6	2.1809 (16)	O7—Mn2—O2	96.83 (6)
Mn1—O9	2.2923 (16)	O1—Mn2—O2	78.64 (6)
Mn2—O1	2.1879 (15)	O3—Mn2—O4	76.92 (6)
Mn2—O2	2.2115 (15)	O7—Mn2—O4	84.38 (6)
Mn2—O3	2.1772 (15)	O1—Mn2—O4	100.08 (6)
Mn2—O4	2.2223 (15)	O2—Mn2—O4	176.22 (6)
Mn2—O5	2.2364 (16)	O3—Mn2—O5	175.49 (6)

Mn2—O7	2.1796 (16)	O7—Mn2—O5	89.38 (6)
Mn3—N4	2.3128 (19)	O1—Mn2—O5	91.08 (6)
Mn3—N5	2.3052 (18)	O2—Mn2—O5	82.64 (6)
Mn3—N6	2.3293 (18)	O4—Mn2—O5	100.97 (6)
Mn3—O3	2.1825 (15)	O8—Mn3—O3	91.25 (6)
Mn3—O4	2.1962 (16)	O8—Mn3—O4	89.38 (6)
Mn3—O8	2.1588 (16)	O3—Mn3—O4	77.36 (6)
Mn3—O10	2.2936 (16)	O8—Mn3—O10	174.19 (6)
		O3—Mn3—O10	83.28 (6)
O1—Mn1—O6	87.48 (6)	O4—Mn3—O10	91.33 (6)
O1—Mn1—O2	78.88 (6)	O8—Mn3—N5	95.66 (6)
O6—Mn1—O2	91.23 (6)	O3—Mn3—N5	140.96 (6)
O1—Mn1—O9	98.92 (6)	O4—Mn3—N5	140.89 (6)
O6—Mn1—O9	173.04 (6)	O10—Mn3—N5	87.42 (6)
O2—Mn1—O9	87.35 (6)	O8—Mn3—N4	91.71 (6)
O1—Mn1—N3	151.12 (6)	O3—Mn3—N4	72.73 (6)
O6—Mn1—N3	87.68 (6)	O4—Mn3—N4	150.08 (6)
O2—Mn1—N3	72.78 (6)	O10—Mn3—N4	84.80 (6)
O9—Mn1—N3	85.38 (6)	N5—Mn3—N4	68.70 (6)
O1—Mn1—N2	139.67 (7)	O8—Mn3—N6	95.20 (6)
O6—Mn1—N2	96.05 (6)	O3—Mn3—N6	149.09 (6)
O2—Mn1—N2	140.87 (7)	O4—Mn3—N6	72.53 (6)
O9—Mn1—N2	80.87 (6)	O10—Mn3—N6	90.51 (6)
N3—Mn1—N2	69.18 (7)	N5—Mn3—N6	68.39 (7)
O1—Mn1—N1	71.80 (6)	N4—Mn3—N6	137.00 (7)
O6—Mn1—N1	95.41 (6)	Mn1—O1—Mn2	99.03 (6)
O2—Mn1—N1	149.56 (6)	Mn1—O2—Mn2	97.36 (6)
O9—Mn1—N1	89.23 (6)	Mn2—O3—Mn3	100.64 (6)
N3—Mn1—N1	137.03 (7)	Mn3—O4—Mn2	98.81 (6)

2.2.18 $[Mn_2Ca(L9)_2(OAc)_2(MeOH)_2]\cdot 2MeOH$ (22)

In complex (21), a trinuclear Mn(II) complex was obtained *via* bridging two seven-coordinate Mn(II) centres with a six-coordinate Mn(II) ion. From this it was decided to change bridging Mn(II) centre with Ca(II) to obtain a heteronuclear complex. The oxygen evolving complex (OEC) of photosystem II that catalyzes the oxidation of two molecules of water to dioxygen contains Mn_4Ca in its active site. Preparation of similar MnCa complexes is of interest because of its role in photosystem II.

Heteronuclear Mn_2Ca complex (22) was prepared by the reaction of one equivalent of the ligand H_2L9 and one equivalent of manganese acetate and half an equivalent of calcium acetate in methanol. The structure of the complex was determined by CHN analysis, IR and mass spectrometry. The ESI mass spectrum in methanol showed several fragments in methanol solution, however no molecular complex cation was observed.

Single crystals suitable for X-ray study were obtained from slow diffusion of diethylether into a MeOH solution of the complex. The complex was found to crystallise in the triclinic space group $P\bar{1}$, details of the crystal structure and refinement can be found in Table A21 in Appendix 2. The structure of (22) is shown in Figure 2-79. The calcium ion lies on an inversion centre so the asymmetric unit contains half of the complex molecule and one uncoordinated methanol molecule. The heteronuclear complex consists of two mononuclear acyclic units bridged by a six-coordinate Ca(II) ion. Two acetate ligands bridge Mn(II) and Ca(II) centres in *syn-syn* mode. The Mn(II) ions are seven-coordinate with approximate pentagonal bipyramidal geometry bonded to three nitrogen and two phenolate oxygen atoms of the acyclic ligand in the equatorial plane and one oxygen atom from methanol and one oxygen atom from an acetate ion in axial positions. The bridging Ca(II) ion is six-coordinate bonded to four phenolate oxygen atoms from two acyclic ligands and two oxygen atoms from acetate ions. Selected bond lengths and angles are given in Table 2-29.

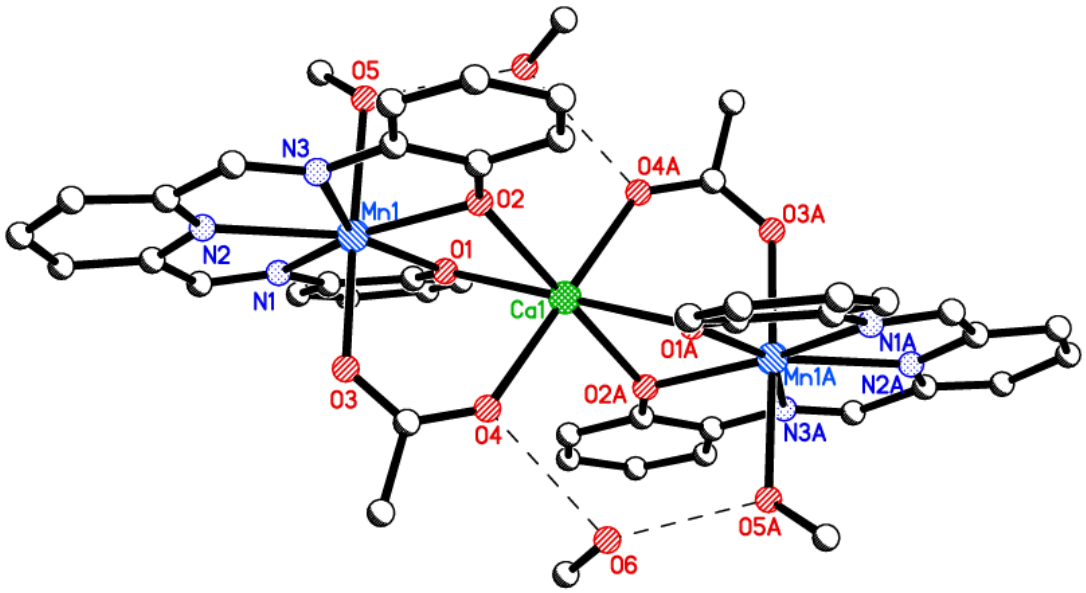

Figure 2-79 Crystal structure of (22). Hydrogen atoms have been removed for clarity; hydrogen bonds are shown as dashed lines.

Table 2-29 Selected bond lengths [Å] and angles [°] for (22).

Mn1—N1	2.326 (3)	O1—Mn1—N1	72.28 (9)
Mn1—N2	2.319 (3)	O5—Mn1—N1	90.17 (9)
Mn1—N3	2.327 (3)	N2—Mn1—N1	67.95 (10)
Mn1—O1	2.237 (2)	O3—Mn1—N3	91.84 (10)
Mn1—O2	2.214 (2)	O2—Mn1—N3	72.45 (9)
Mn1—O3	2.176 (3)	O1—Mn1—N3	151.50 (9)
Mn1—O5	2.301 (3)	O5—Mn1—N3	86.99 (9)
Ca1—O1	2.342 (2)	N2—Mn1—N3	68.08 (10)
Ca1—O1^{i}	2.342 (2)	N1—Mn1—N3	135.53 (10)
Ca1—O2	2.346 (2)	O1—Ca1—O1^{i}	180.0
Ca1—O2^{i}	2.346 (2)	O1—Ca1—O4	88.37 (8)
Ca1—O4	2.345 (2)	O1^{i}—Ca1—O4	91.63 (8)
Ca1—O4^{i}	2.345 (2)	O1—Ca1—O4^{i}	91.63 (8)
		O1^{i}—Ca1—O4^{i}	88.37 (8)
O3—Mn1—O2	95.17 (9)	O4—Ca1—O4^{i}	180.0
O3—Mn1—O1	93.34 (9)	O1—Ca1—O2	74.44 (8)
O2—Mn1—O1	79.17 (8)	O1^{i}—Ca1—O2	105.56 (8)
O3—Mn1—O5	177.81 (9)	O4—Ca1—O2	84.19 (8)
O2—Mn1—O5	82.72 (9)	O4^{i}—Ca1—O2	95.81 (8)
O1—Mn1—O5	86.83 (9)	O1—Ca1—O2^{i}	105.56 (8)
O3—Mn1—N2	86.66 (10)	O1^{i}—Ca1—O2^{i}	74.44 (8)
O2—Mn1—N2	140.53 (9)	O4—Ca1—O2^{i}	95.81 (9)
O1—Mn1—N2	140.20 (9)	O4^{i}—Ca1—O2^{i}	84.19 (8)
O5—Mn1—N2	94.61 (10)	O2—Ca1—O2^{i}	180.0
O3—Mn1—N1	91.96 (10)	Mn1—O1—Ca1	97.53 (8)
O2—Mn1—N1	150.91 (9)	Mn1—O2—Ca1	98.04 (9)

Symmetry code: (i) -*x*+1, -*y*+1, -*z*+1.

The uncoordinated methanol molecules are involved in hydrogen bonding with the coordinated acetate ligand (as donor) and coordinated methanol molecule (as acceptor) forming a $R^2_2(7)$ graph set motif. Hydrogen bond information is given in Table 2-30.

Table 2-30 Hydrogen bonds for (22) [Å and °].

D—H···*A*	*D*—H	H···*A*	*D*···*A*	*D*—H···*A*
O5—H5A···O6^{i}	0.85	1.84	2.680 (3)	169.1
O6—H6···O4	0.85	1.90	2.717 (4)	159.5

Symmetry code: (i) -*x*+1, -*y*+1, -*z*+1.

The principal interactions between heteronuclear complex molecules are π-π edge-edge stacking interactions. There are two sets in the structure (Figure 2-80); first, the C6-C9 edge of the complex is stacked with the same section of an adjacent complex under symmetry operation 1-x, 1-y, 2-z (the shortest contact is between C7 and C7 atoms with a distance of 3.156 Å), second, the C11-C14 edge of the complex is stacked with the same section of a neighbouring molecule under symmetry operation 2-x, 2-y, 2-z (the shortest contact is between C13 and C13 with a distance of 3.325 Å).

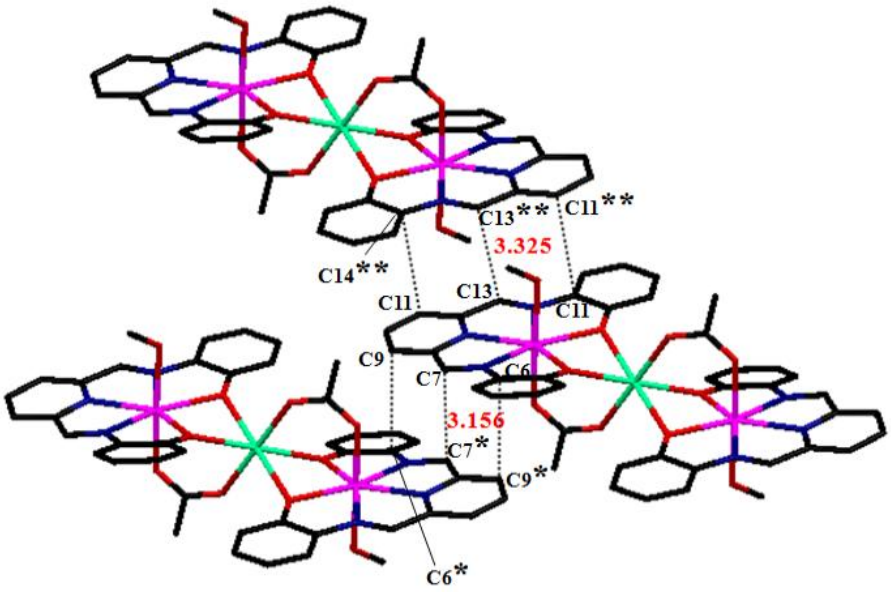

*Figure 2-80 π-π stacking interactions for (22). Symmetry operations: *1-x, 1-y, 2-z, **2-x, 2-y, 2-z*

The packing diagram of complex (22) is shown in Figure 2-81. The packing of the structure is determined by π-π stacking interactions.

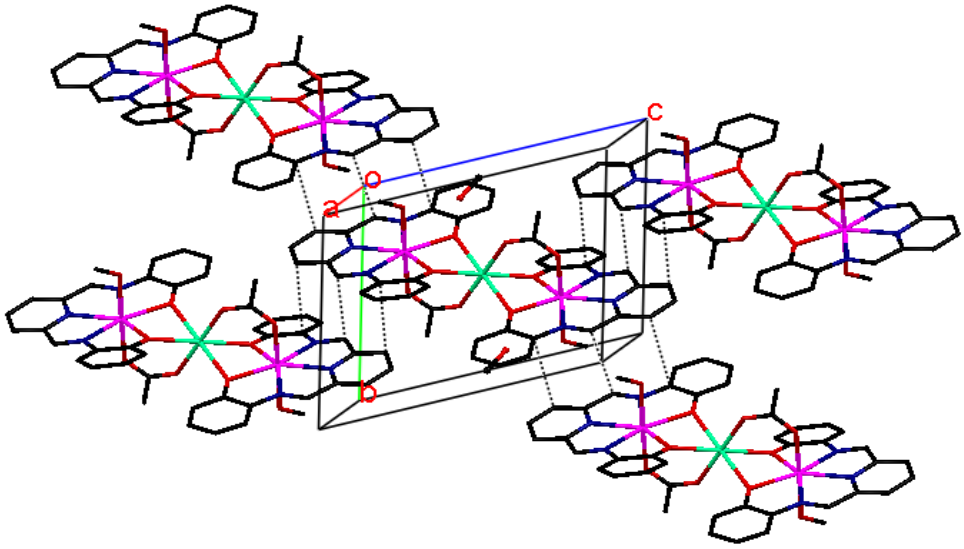

Figure 2-81 Packing diagram of complex (22) showing π-π stacking interactions.

2.2.19 $[Mn(H_2L10)(NCS)_2]\cdot H_2O$ (23) and $[Mn(H_2L10)(N_3)_2]$ (24)

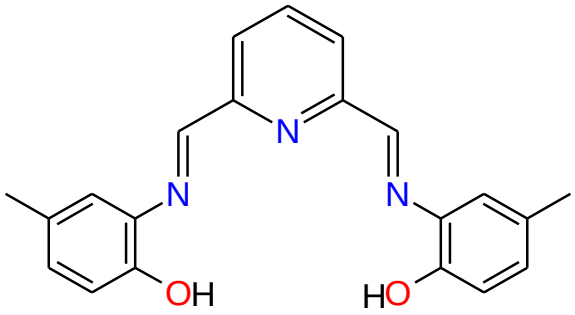

H_2L10

Complexes $[Mn(H_2L10)(NCS)_2]\cdot H_2O$ (23) and $[Mn(H_2L10)(N_3)_2]$ (24) were obtained by the reaction of one equivalent of H_2L10 with one equivalent of manganese perchlorate in the presence of two equivalents of sodium thiocyanate or azide in methanol. The complexes were characterised by CHN, IR and mass spectrometry. In the IR spectra of the complexes, the strong band at at 1624 cm^{-1} due to imine bond stretch (C=N) shifted to lower waver number (1620 cm^{-1} for (23) and 1599 cm^{-1} for (24)). Thiocyanate υ(CN) and azide $\upsilon_{asym}(N_3)$ vibrations were observed at 2072 and 2043 cm^{-1} for (23) and (24) respectively. The ESI mass spectra of both complexes showed a peak at m/z 393(100%) assigned to $\{[Mn(HL10)]\}^+$.

For both complexes, attempts to obtain single crystals *via* slow evaporation of methanol or acetonitrile and methanol-diethylether or dmf-diethylether diffusion failed and each time

powder was obtained. The molecular formulae of the complexes were found to be $[Mn(H_2L10)(NCS)_2]\cdot H_2O$ (23) and $[Mn(H_2L10)(N_3)_2]$ (24) by CHN analysis.

In conclusion, in most cases, the acyclic ligands prepared from 2,6-diformylpyridine (DFP) and several monoaminoalcohols maintained seven-coordination *via* an N_3O_2 donor set with two axial ligands. However, some six-coordinate and dimeric complexes were also obtained. Deprotonation of alcohol groups were not observed for any of the acyclic systems as seen in the macrocyclic system (see section 2.2.5 Figure 2.15 and 2.20) and no alcohol bridging between two manganese atoms was seen. The acyclic ligand L5 derived from DFP and *N*,*N*-dimethylethane-1,2-diamine also gave seven-coordinate Mn(II) complexes with an N_5 donor set and two axial ligands. All complexes derived from acyclic ligands are stable in air without decomposition except the complex of L5 with two axial chloride ions $[Mn(L5)Cl_2]$ (12) which turns into a brown oil after several days in air.

Acyclic ligands having phenol groups can give access to mono- and polynuclear complexes. The reaction of one equivalent of ligands H_2L9 and H_2L10 with one equivalent of Mn(II) formed seven-coordinate mononuclear complexes. A trinuclear Mn(II) complex was obtained when a 1:1.5 Mn:H_2L9 ratio was used. Additionally, a heteronuclear Mn_2Ca complex was obtained when a 1:1:0.5 Mn:H_2L9:Ca ratio was used.

Chapter 3

Manganese complexes of tripodal Schiff bases and N-alkylated benzimidazoles

3.1 Introduction

Tripodal polydentate ligands can give access to mono-[90] and polynuclear[91] complexes and can be prepared by a Schiff base condensation reaction of tripodal amines and aldehydes or ketones which are capable of forming metal complexes with transition metals. Altering the length of the ligand strands will change the geometry and flexibility around the metal centre and may bring about changes in the biological activity of the complex. Our interest, therefore, was to prepare symmetric and unsymmetric tripodal Schiff base ligands and their manganese complexes and to investigate these as potential SOD and catalase mimics. In this chapter, synthesis and characterisation of potentially heptadentate Schiff base ligands of symmetric and asymmetric tripodal amines will be discussed in detail. Manganese complexes of tripodal ligands will be explored and their molecular structure will be examined by using spectral methods and X-ray crystallography. In the second part of the chapter the synthesis and characterization of a novel N-alkylated benzimidazole ligand and its Mn(II) complexes is discussed.

3.1.1 Organic synthesis

Tripodal amines were prepared by three step reactions as their hydrochloride salts.[186,187] In the first step, iminobispropylamine and iminobisethylamine are protected by using phthalic anhydride followed by N-alkylation using 2-bromoethylphthalimide or 3-bromopropylphthalimide in the second step. Deprotection with HCl gives HCl salts of the corresponding podands in the final step (Figure 3-1). Both protection and secondary N-alkylation are performed at elevated temperature.

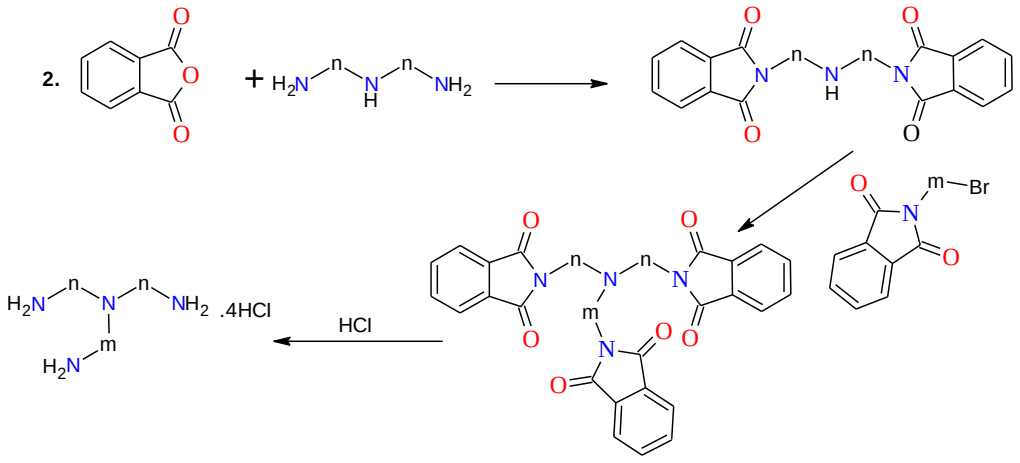

Figure 3-1 Preparation of tripod amines (n and m = -CH_2CH_2- or -$CH_2CH_2CH_2$-).[186,187]

3.1.2 Characterisation of 2-bromoethylphthalimide (25) and 3-bromopropyl-phthalimide (26)

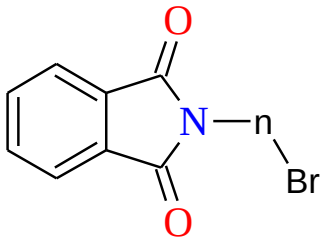

n=$(CH_2)_2$ **(25)**
n=$(CH_2)_3$ **(26)**

Compounds (25) and (26) were prepared by the reaction of one equivalent of potassium phthalimide with one equivalent of 1,2-dibromoethane or 1,3-dibromopropane in anhydrous dmf as cream colour products with high purity and yield.[186] Identities of the compounds were determined by CHN analysis, mass spectra (FAB), IR and ^{1}H NMR spectroscopy. In the ^{1}H NMR spectra, the appearance of two triplets at 3.55 (–CH_2^a–Br) and 4.05 (N-CH_2^b-) ppm in (25) and two triplets at 3.46 (CH_2^aBr) and 3.78 (N–CH_2^c–) ppm with a quintet at 2.32 (*q* 2H, C–CH_2^b–C) ppm in (26) were seen in the aliphatic region. Two aromatic signals were overlapped in the aromatic region for both compounds. ^{1}H NMR shifts for the compounds are given in Table 3-1. FAB mass spectra showed molecular ions at m/z 254(100%) and 290(100%) corresponding to {[25]H}$^+$ and {[26]Na}$^+$ respectively.

Table 3-1 ^{1}H NMR shifts for compounds (25) and (26).

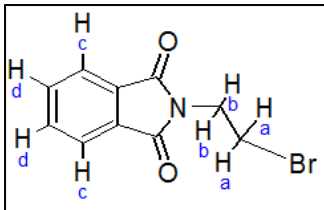

Peak(ppm)	Assignment	integration
7.70-7.86	c, d	*m* 4H
3.55	a	*t* 2H
4.05	b	*t* 2H

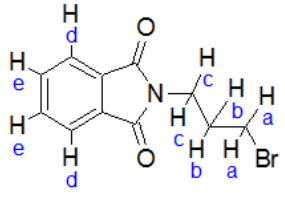

Peak(ppm)	Assignment	integration
7.77-7.85	d, e	*m* 4H
3.46	a	*t* 2H
3.78	c	*t* 2H
2.32	b	*q* 2H

m: multiplet, t: triplet, q: quintet

3.1.3 Characterisation of (27a) and (27b)

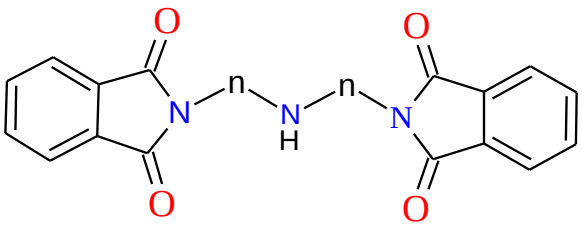

n=$(CH_2)_2$ **(27a)**
n=$(CH_2)_3$ **(27b)**

Compounds (27a) and (27b) were prepared by the reaction of two equivalents of phthalic anhydride with one equivalent of diethylenetriamine or dipropylenetriamine at elevated temperatures. The glassy products were pulverized to give powders. ^{1}H NMR of the compounds showed their symmetric nature; spectra of both compounds were simple and all protons were assigned (Table 3-2). In the ESI mass spectra of the compounds singly charged peaks at m/z 364(100%) and 392(100%) can be assigned to $\{[(27)]H\}^+$ and $\{[(28)]H\}^+$ respectively. In the IR spectra, peaks at around 1700 cm^{-1} were assigned to C=O vibrations.

Table 3-2 Chemical shifts for compounds (27a) and (27b).

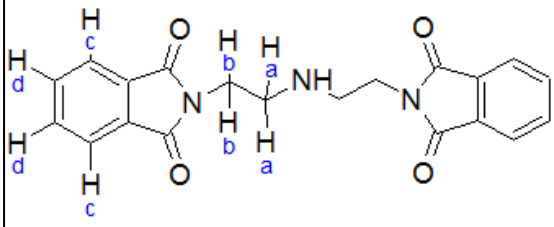

Peak(ppm)	Assignment	integration
7.64-7.80	c, d	*m* 8H
3.72	b	*t* 4H
2.94	a	*t* 4H

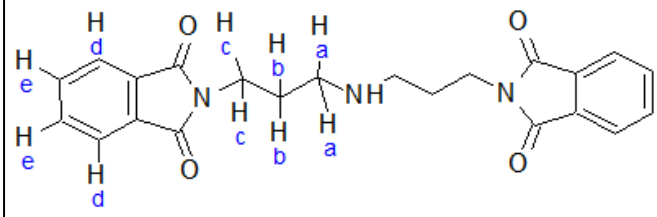

Peak(ppm)	Assignment	integration
7.74-7.78	d, e	*m* 8H
3.73	c	*t* 4H
2.65	a	*t* 4H
1.84	b	*q* 4H

m: multiplet, t: triplet, q: quintet

3.1.4 Characterisation of (28), (29) and (30)

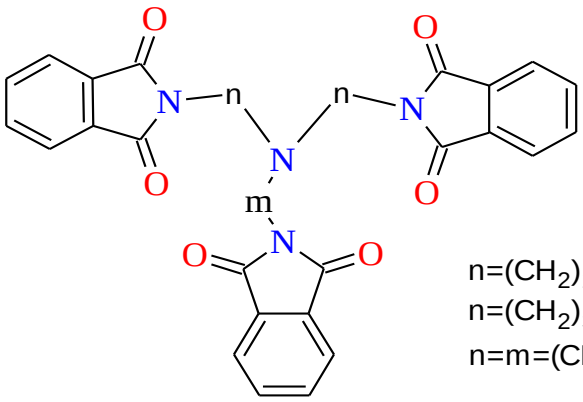

n=$(CH_2)_2$ m=$(CH_2)_3$ **(28)**
n=$(CH_2)_3$ m=$(CH_2)_2$ **(29)**
n=m=$(CH_2)_3$ **(30)**

The compounds (28), (29) and (30) were prepared by alkylation at the secondary N atom of phthalimido-protected diethylenetriamine or diproylenetriamine with 2-bromoethylphthalimide and 3-bromopropylphthalimide at elevated temperatures.[187,188] CHN analyses of three compounds agreed well with calculated values. ^{1}H NMR of compounds (28) and (29) are rather complicated and aliphatic proton signals overlapped showing the asymmetric nature of compounds. However, compound (30) shows a simple ^{1}H NMR spectrum confirming its symmetric structure. The ESI mass spectra of the compounds in methanol solution showed peaks assigned to $\{[M]H\}^+$. In the IR spectra, disappearance of the N-H stretch at around 2910 cm^{-1} supported the formation of the compounds (28)-(30).

3.1.5 Characterisation of BAEP·4HCl (31), ABAP·4HCl (32) and TRPN·4HCl (33)

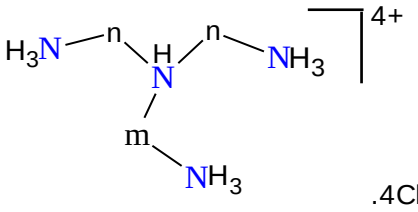

n=$(CH_2)_2$ m=$(CH_2)_3$ **BAEP·4HCl (31)**
n=$(CH_2)_3$ m=$(CH_2)_2$ **ABAP·4HCl (32)**
n=m=$(CH_2)_3$ **TRPN·4HCl (33)**

Deprotection of (28), (29) and (30) using concentrated HCl gave the salts (31), (32) and (33).[187,188] The compounds were recrystallised from an ethanol-water mixture to give hygroscopic products. In the ^{1}H NMR spectra of the compounds, the disappearance of signals of aromatic protons confirmed completion of reactions. The IR spectra of compounds showed that all three compounds contain water; this was confirmed by elemental analysis given in the experimental chapter.

3.1.6 Characterisation of Schiff base ligands with salicylaldehyde, H_3L13 (34), H_3L14 (35), H_3L12 (36) and H_3L11 (37)

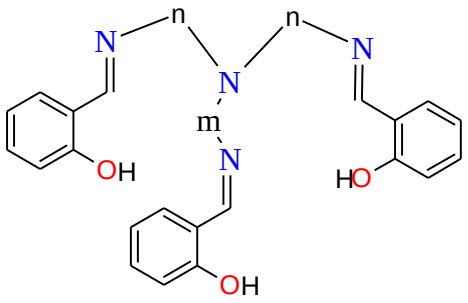

n=m=$(CH_2)_2$	**H_3L11**
n=m=$(CH_2)_3$	**H_3L12**
n=$(CH_2)_2$ m=$(CH_2)_3$	**H_3L13**
n=$(CH_2)_3$ m=$(CH_2)_2$	**H_3L14**

Schiff base ligands of unsymmetric tripodal amines with salicylaldehyde were simply prepared by addition of three equivalents of salicylaldehyde to the stirring solution of one equivalent of tetrachloride salt and four equivalents of base (NaOH) in absolute ethanol. The ligand H_3Saltren (H_3L11) was prepared *via* direct condensation of neutral amine with salicylaldehyde forming a yellow solid in ethanol.

Ligands (34), (35) and (36) were obtained as yellow oils and did not form solid products even under reduced pressure. In the ESI mass spectra of the ligands, molecular ions $\{[H_3L12]H\}^+$, $\{[H_3L13]H\}^+$ and $\{[H_3L14]H\}^+$ were seen at 472, 487 and 501 m/z respectively. IR spectra showed no indication of primary amines or carbonyls. The formation of the imine bonds was confirmed by the C=N stretch at around 1630-1670 cm^{-1}.

In the first attempts to form the neutral tripodal ligands from the tetrachloride salts, triethylamine was used as a base in order to neutralize the tripod hydrochloride salt but when the solvent was removed, triethylamine hydrochloride salt remained as an impurity in the sample. Therefore the product was dissolved in acetone in order to remove triethylaminehydrochloride and the neutral ligands were obtained as yellow oils. NaOH was later used as a base in absolute ethanol due to the lower solubility of NaCl in ethanol. All Schiff base reactions were carried out in absolute ethanol.

The ligand H_3L11 (H_3Saltren) was obtained as yellow crystals suitable for single X-ray diffraction study. The structure of H_3Saltren was previously reported by Gunduz and co-workers; the structure was solved in the monoclinic space group $P2_1/c$ with R=0.073 .[189]

The ligand prepared here was found to crystallise in the same space group and unit cell parameters with better R value (0.0345). The details of the crystal structure and refinement can be found in Table A22 in Appendix 2. Three arms attached to the amine (N4) have a

similar conformation and the molecule has approximate (non-crystallograhic) threefold symmetry (Figure 3-2). There are three intra-molecular hydrogen bonds between phenolic hydrogens and the imine nitrogens of the same strand (Table 3-3) and the interplanar angles between phenol rings (C1-C6/C13-C18, C13-C18/C22-C27, C1-C6/C22-C27) are 49.50(5), 70.76(4), 61.45(4)° respectively.

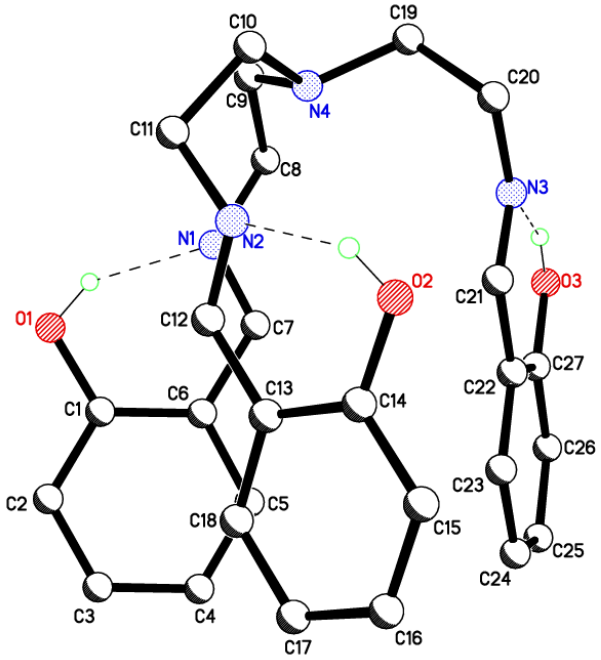

Figure 3-2 Perspective view of (37). Hydrogen atoms bonded to carbon atoms are removed for clarity.

Table 3-3 Hydrogen bond parameters for (37) [Å and °].

D–H···A	*D-H*	*H···A*	*D···A*	*<(DHA)*
O1-H1···N1	0.84	1.81	2.5623(15)	147.6
O2-H2A···N2	0.84	1.82	2.5722(14)	147.4
O3-H3A···N3	0.84	1.85	2.5956(16)	147.7

3.1.7 Characterisation of Mn(III) complexes, [Mn(L11)] (38), [Mn(L12)] (39) and [Mn(L13)] (40)

Tripodal Schiff base complexes of manganese were prepared by refluxing the neutral ligand and manganese(II) salts in methanol or ethanol to give dark green solutions. The solutions were left to stand in air and, on partial evaporation of solvents, dark green products were formed. The colour change of the solutions from yellow to reddish to green black colour over time suggest the Mn(II) is oxidised to Mn(III). This was observed for the other manganese complexes derived from Schiff base ligands of tren in the literature.[90,190,191] On oxidation of Mn(II) to Mn(III), the phenolic oxygens are deprotonated to give neutral complexes. Deprotonation of phenolic oxygens was confirmed by IR spectra which show no O-H stretch at around 3000-3500 cm^{-1}. The ESI mass spectra of the complexes show the molecular ion peaks. In the mass spectra of [Mn(L11)] and [Mn(L12)], main peaks were seen at 407(100%) and 421(100%) were assigned as shown in Table 3-4, similar fragmentation was observed in all three complexes.

Table 3-4 The ESI mass spectra assignments for complexes (38), (39) and (40).

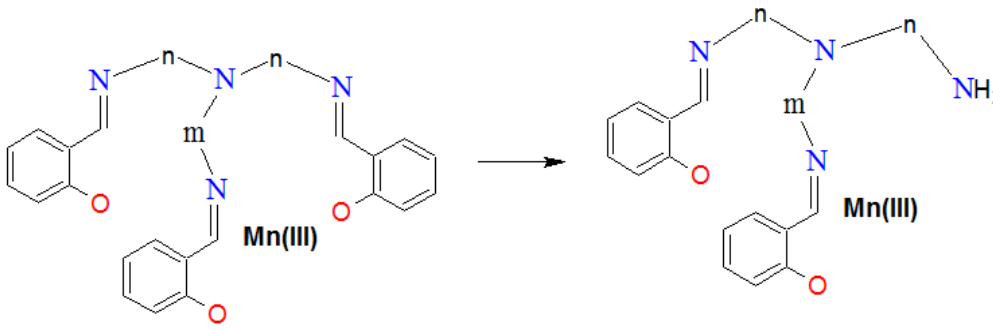

Molecular ion peaks observed in mass spect.

Complexes	Assignment	Mass (m/z)Found
[Mn(L11)] (38)	$\{[Mn(L11)]H\}^+$	510(20%)
[Mn(L12)] (39)	$\{[Mn(L12)]H\}^+$	525(15%)
[Mn(L13)] (40)	$\{[Mn(L13)]H\}^+$	539(100%)

Fragmentation peaks observed in mass spect.

Complexes	Assignment	Mass (m/z)Found
[Mn(L11)] (38)	$\{[Mn(C_{20}H_{24}N_4O_2)]\}^+$	407(100%)
[Mn(L12)] (39)	$\{[Mn(C_{21}H_{26}N_4O_2)]\}^+$	421(100%)
[Mn(L13)] (40)	$\{[Mn(C_{22}H_{28}N_4O_2)]\}^+$	435(10%)

Single crystals of complex (38) were obtained from methanol solution over a long time (5 weeks). Attempts to grow crystals for complexes (39) and (40) failed in all organic solvents tried, resulting black-green powder each time. This may be due to lack of symmetry in the molecules.

A mononuclear manganese(III) complex (38) was crystallised using the method previously reported[90] and washed with diethylether to give dark green crystals. The [Mn(L11)] crystallises in the space group $P2_1/n$ with unit cell parameters (7.8372(15), 25.541(5), 11.609(2) Å(a,b,c), β=96.737(3)º) and the structure of the complex was reported with same space group and unit cell parameters (7.906(2), 25.609(5), 11.736(2) Å, β=96.55(3)º).[190] The structure has also been reported as a methanol solvate [Mn(L11)]·MeOH with the same space group and different unit cell parameters (10.826(5), 14.821(9), 16.348(9) Å, β=95.10(4)º)[191] and (10.790(3), 14.742(3), 16.252(4) Å, β=94.98(2)º)[90] in the literature.

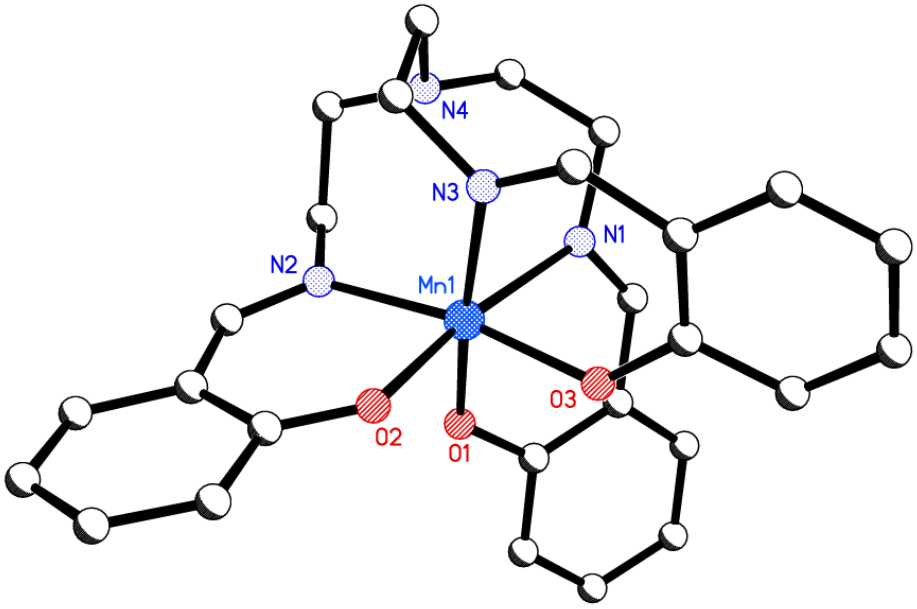

Figure 3-3 A perspective view of [Mn(L11)] (38).

The details of the crystal structure and refinement can be found in Table A23 in Appendix 2. The asymmetric unit contains a mononuclear six-coordinate manganese(III) ion. Mn1-O bond distances are shorter than Mn-N distances. Crystal data of complex (38) and the one in the literature[190] showed that there was no solvent molecule in the crystal lattice although reported structures[90,191] have methanol solvent in the crystal lattice. A perspective view of the compound is shown in Figure 3-3. The crystal structure showed that the ligand is coordinated to three phenolate and three imine nitrogen donors while the central amine nitrogen atom stays free (Figure 3-3). The hydroxyl groups of the phenol rings are deprotonated and the manganese is oxidised to manganese(III). Selected bond distances and angles are given in Table 3-5. Mn1-O2 and Mn1-N1 distances of 2.089(2) and 2.336(3) Å respectively are significantly longer the other Mn-O and Mn-N distances. This longer bond distances are

consistent with Jahn-Teller distortion for typical of the d^4 Mn(III) system.[191] Phenolate-imine groups provide bite angles of 83.67(9), 86.30(9) and 88.41(9)° for O1-Mn1-N1, O2-Mn1-N2 and O3-Mn1-N4 respectively. Both the methanol solvate complex [Mn(L11)]·MeOH[90] and the non-solvated complex [Mn(L11)] have similar bond lengths and angles (Table 3-5).

There is weak intermolecular hydrogen bonding[180] (C15-H···O1) with a distance of 3.657 Å (D···A)(under symmetry operation ½+x, ³⁄₂-y, ½+z) and this is supported by π···H stacking within the structure (H16···centroid (C1-C6) distance is 2.860 Å). The packing diagram is shown in Figure 3-4.

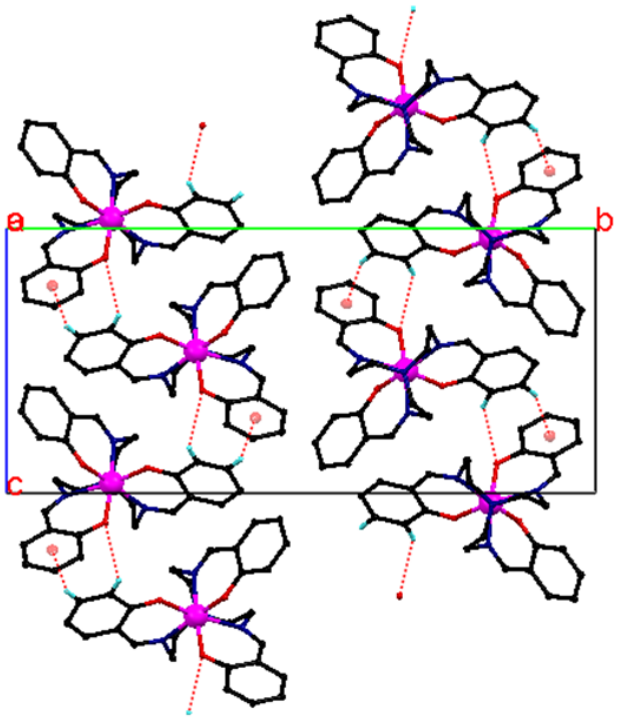

Figure 3-4 Packing diagram of [Mn(L11)] viewing down the a axis. Hydrogen atom attached to carbon atoms except H15 and H16 are omitted for clarity.

Table 3-5 Selected bond lengths [Å] and angles [°] for [Mn(L11)].

[Mn(L11)]		*[Mn(L11)]·MeOH[90]*	
Mn1—O1	1.918 (2)	Mn1—O2	1.901 (4)
Mn1—O2	2.089 (2)	Mn1—O1	2.118 (3)
Mn1—O3	1.925 (2)	Mn1—O3	1.893(3)
Mn1—N1	2.336 (3)	Mn1—N4	2.326 (4)
Mn1—N2	2.095 (3)	Mn1—N2	2.084 (5)
Mn1—N3	2.099 (3)	Mn1—N3	2.051(4)

O1—Mn1—O3	90.02 (9)	O2—Mn1—O3	89.5 (1)
O1—Mn1—O2	98.43 (9)	O1—Mn1—O3	97.4 (1)
O3—Mn1—O2	88.84 (9)	O1—Mn1—O2	87.1 (1)
N2—Mn1—N3	99.85 (10)	N2—Mn1—N3	98.1 (2)
N2—Mn1—N1	103.25 (10)	N2—Mn1—N4	102.7 (7)
N3—Mn1—N1	90.30 (10)	N3—Mn1—N4	91.6 (2)

3.1.8 Characterisation of Mn(II) complexes $[Mn(L15)](ClO_4)_2$ (41), $[Mn(L18)](ClO_4)_2$ (42), $[Mn(L16)](ClO_4)_2$ (43) and $[Mn(L17)](ClO_4)_2$ (44) derived from tripodal amines and 2-pyridinecarboxaldehyde

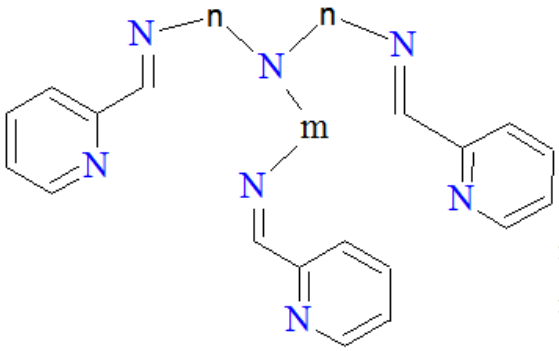

$n=m=(CH_2)_2$	**L15**
$n=(CH_2)_2$ $m=(CH_2)_3$	**L16**
$n=(CH_2)_3$ $m=(CH_2)_2$	**L17**
$n=m=(CH_2)_3$	**L18**

Ligands L16, L17 and L18 were prepared according to the method used for H_3L12-H_3L14 except using 2-pyridinecarboxaldehyde in place of salicylaldehyde. The neutral ligands were obtained as brown oils and used directly in complexation without further purification. Ligand L15 was obtained by Schiff base condensation of three equivalents of 2-pyridinecarboxaldehyde and one equivalent of tren in MeOH. Mn(II) complexes were prepared by mixing one equivalent of the ligand and one equivalent of manganese(II) chloride followed by addition of two equivalents of sodium perchlorate in a refluxing solution of ethanol. On cooling, yellow-brown products formed and were collected and analysed. Yellow crystals formed in the case of $[Mn(L15)](ClO_4)_2$ on cooling the ethanol solution. Single crystals for Mn(II) complexes of $[Mn(L16)](ClO_4)_2$ and $[Mn(L18)](ClO_4)_2$ were obtained by vapour diffusion of diethylether into dmf solutions of the complexes. However, attempts to get single crystals for the complex $[Mn(L17)](ClO_4)_2$ failed and yellow-brown powder was obtained from most organic solvents and diffusion methods.

The unit cell information for the $[Mn(L15)](ClO_4)_2$ crystals were collected and matched those on the Cambridge Structural database (CSD),[192] therefore whole dataset was not collected. X-ray data were collected for Mn(II) complexes of L16 and L18. The details of the crystal structure and refinement for complexes $[Mn(L16)](ClO_4)_2$ and $[Mn(L18)](ClO_4)_2$ can be found in Tables A24 and A25 respectively in Appendix 2.

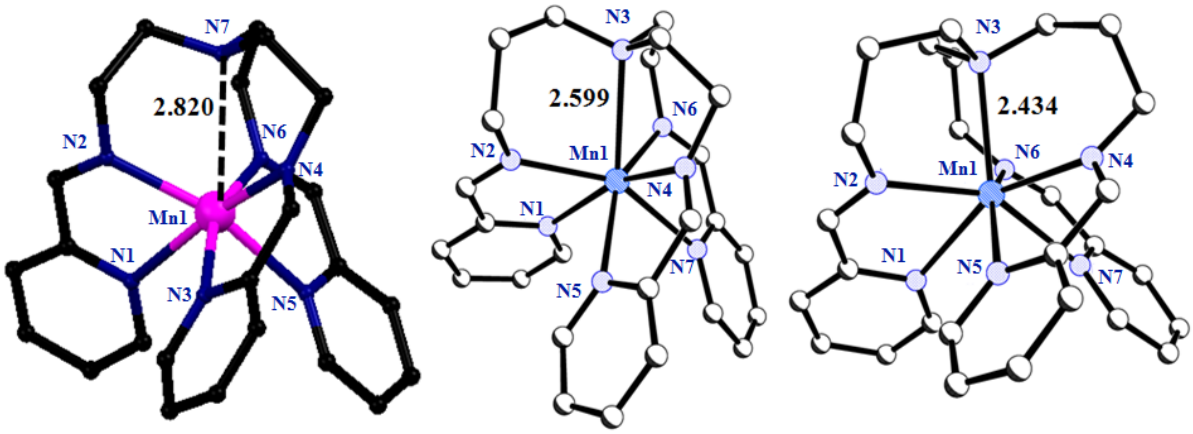

Figure 3-5 Structures of complex cations $[Mn(L15)]^{2+}$(left)[192], $[Mn(L16)]^{2+}$(middle) and $[Mn(L18)]^{2+}$(right). Perchlorate ions are omitted for clarity.

The structures of the complex cations $[Mn(L15)]^{2+}$, $[Mn(L16)]^{2+}$ and $[Mn(L18)]^{2+}$ are shown in Figure 3-5. Selected bond lengths and angles are given in Table 3-6. All three complexes are mononuclear and the structures contain Mn(II) complex cations and uncoordinated perchlorate ions. In the published structure of $[Mn(L15)](ClO_4)_2$, the long $Mn\text{-}N_{bridgehead}$ distance (2.820 Å) showed that the bridgehead nitrogen atom remained uncoordinated, strain in the alkyl arms possibly prevents the bridgehead nitrogen atom approaching the metal centre for coordination. However, when an extra carbon atom was introduced to one arm of L15 ligand to give the asymmetric ligand L16, the $Mn\text{-}N_{bridgehead}$ distance (2.599 Å) shortens and the bridgehead nitrogen atom approaches the metal centre for coordination. Additionally, when an extra carbon atom was added to each arm to give symmetric ligand L18, the $Mn\text{-}N_{bridgehead}$ distance is even shorter than the $Mn\text{-}N_{bridgehead}$ distance in complex (43). In all three complexes, pyridine-imine sections provide bite angles at the metal ranging from 69 to 73° and these bite angles do not change upon changing the arm sizes.

The complexes $[Mn(L16)](ClO_4)_2$ and $[Mn(L18)](ClO_4)_2$ are seven-coordinate bonded to seven nitrogen atoms from a single tripodal ligand. The coordination polyhedron of these complexes can be described as a monocapped antitrigonal prism of $[MnN_7]$. In all three

complexes, the cations are linked by weak $O_3ClO\cdots HC$ hydrogen bond type interactions.[180] No π-π stacking interactions were observed in any of the three complexes.

Table 3-6 Selected bond lengths [Å] and angles [°] for [Mn(L15)](ClO$_4$)$_2$, [Mn(L16)](ClO$_4$)$_2$ and [Mn(L18)](ClO$_4$)$_2$.

[Mn(L15)](ClO$_4$)$_2$		[Mn(L16)](ClO$_4$)$_2$		[Mn(L17)](ClO$_4$)$_2$	
Mn1—N1	2.357(4)	Mn1-N1	2.360(3)	Mn1-N1	2.4630(18)
Mn1—N2	2.223(4)	Mn1-N2	2.245(3)	Mn1-N2	2.255(2)
Mn1—N3	2.367(4)	Mn1-N5	2.402(3)	Mn1-N5	2.3984(17)
Mn1—N4	2.206(4)	Mn1-N4	2.215(3)	Mn1-N4	2.3020(19)
Mn1—N5	2.294(4)	Mn1-N7	2.408(2)	Mn1-N7	2.3596(18)
Mn1—N6	2.228(4)	Mn1-N6	2.218(3)	Mn1-N6	2.2697(17)
Mn1—N7$_{bridgehead}$	2.820	Mn1-N3 $_{bridgehead}$	2.599(2)	Mn1-N3$_{bridgehead}$	2.4339(18)
N1—Mn1—N2	72.22 (13)	N1—Mn1—N2	70.73 (10)	N1—Mn1—N2	69.81 (7)
N1—Mn1—N3	86.50 (13)	N1—Mn1—N5	82.33 (8)	N1—Mn1—N5	90.99 (6)
N1—Mn1—N4	157.35 (14)	N1—Mn1—N4	153.57 (10)	N1—Mn1—N4	154.06 (6)
N1—Mn1—N5	86.65 (13)	N1—Mn1—N7	91.00 (10)	N1—Mn1—N7	83.89 (6)
N1—Mn1—N6	93.23 (14)	N1—Mn1—N6	82.61 (10)	N1—Mn1—N6	77.90 (6)
N2—Mn1—N3	89.95 (13)	N2—Mn1—N5	90.45 (9)	N2—Mn1—N5	78.71 (7)
N2—Mn1—N4	101.62 (14)	N2—Mn1—N4	107.70 (10)	N2—Mn1—N4	120.62 (8)
N2—Mn1—N5	158.56 (14)	N2—Mn1—N7	161.62 (9)	N2—Mn1—N7	149.74 (7)
N2—Mn1—N6	104.12 (14)	N2—Mn1—N6	107.15 (10)	N2—Mn1—N6	115.54 (7)
N3—Mn1—N4	71.51 (15)	N4—Mn1—N5	71.25 (10)	N4—Mn1—N5	69.90 (7)
N3—Mn1—N5	92.38 (14)	N5—Mn1—N7	85.04 (9)	N5—Mn1—N7	87.32 (6)
N3—Mn1—N6	165.15 (15)	N5—Mn1—N6	151.47 (10)	N5—Mn1—N6	156.52 (6)
N4—Mn1—N5	99.32 (14)	N4—Mn1—N7	87.72 (10)	N4—Mn1—N7	78.02 (7)
N4—Mn1—N6	109.41 (15)	N4—Mn1—N6	121.57 (10)	N4—Mn1—N6	112.81 (7)
N5—Mn1—N6	72.80 (15)	N6—Mn1—N7	71.14 (10)	N6—Mn1—N7	71.11 (6)
		N1—Mn1—N3	128.16 (10)	N1—Mn1—N3	128.06 (6)
		N2—Mn1—N3	70.09 (9)	N2—Mn1—N3	79.76 (8)
		N4—Mn1—N3	71.94 (10)	N4—Mn1—N3	77.86 (7)
		N5—Mn1—N3	130.03 (10)	N5—Mn1—N3	123.54 (6)
		N6—Mn1—N3	77.94 (10)	N6—Mn1—N3	78.82 (6)
		N7—Mn1—N3	125.72 (8)	N7—Mn1—N3	129.74 (7)

Deroche *et al.* prepared the amine analogue of $[Mn(L15)](ClO_4)_2$ (Figure 3-6), reducing imine to amine, increased the C-N bond distance, and reduced the strain of the tripodal chain which gives more flexibility to the bridgehead nitrogen atom to approach metal centre.[193] The short $Mn\text{-}N_{bridgehead}$ distance shows that the bridgehead nitrogen atom is coordinated to the Mn(II) centre. The crystal structure of the complex consists of seven-coordinate Mn(II) ions (bonded to all nitrogen atoms of the reduced ligand) and hexafluorophosphate anions.

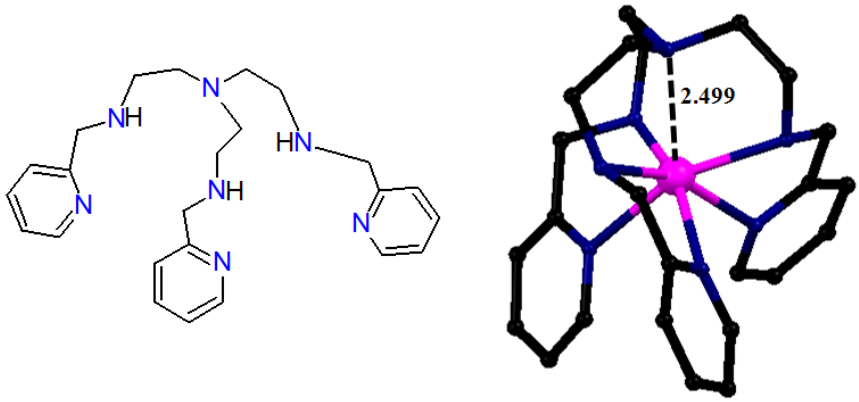

Figure 3-6 Reduced L15 ligand and its Mn(II) complex cation $[Mn(RedL15)]^{2+}$.

IR spectra of the new complexes showed C=N stretches at around 1630-1670 cm^{-1} and peaks at around ~650 and ~1050 cm^{-1} could be assigned to perchlorate stretches with no splitting. Elemental analysis data agreed with calculated values showing the purity of the complexes. ESI mass spectra of the complexes show single and doubly charged cations with high relative abundance (Table 3-7).

Table 3-7 Mass spectra of the complexes.

Complexes	Assignment	Relative Abundance	Mass (m/z)Found
$[Mn(L15)](ClO_4)_2$ (41)	$\{[Mn(L15)](ClO_4)\}^+$	100	567
$[Mn(L18)](ClO_4)_2$ (42)	$\{[Mn(L18)](ClO_4)\}^+$	100	609
$[Mn(L16)](ClO_4)_2$ (43)	$\{[Mn(L16)](ClO_4)\}^+$	100	595
$[Mn(L17)](ClO_4)_2$ (44)	$\{[Mn(L17)](ClO_4)\}^+$	100	581

3.2 Characterisation of a pyridinebenzimidazole ligand and its Mn(II) complexes

Benzimidazole derivatives and their metal complexes have received a particular attention due to them possessing a broad spectrum of biological activities. Some of the benzimidazoles have been found to possess antiviral, antibacterial, and fungicide activities.[194]Additionally, metal complexes of these ligands are of interest as a model of some biological molecules. Transition metal complexes of 2,6-bis(benzimidazol-2'-yl)pyridine (BBP) have been well studied in the literature.[195] The ligand BBP can be modified by introduction of new group through N-alkylation. The ligand L19 can be prepared by the reaction of BBP and 1-bromobutane in the presence of base. It was initially used to prepare $[Co(L19)_2](ClO_4)_2$ as a redox mediator in dye-sensitized solar cells with undergraduate project student Jagdeep Sagu. It was found that introduction of butyl groups has an effect on the oxidation-reduction potentials of the complex. The ligand L19 was later used to prepare Mn(II) complexes as potential SOD and catalase mimics.

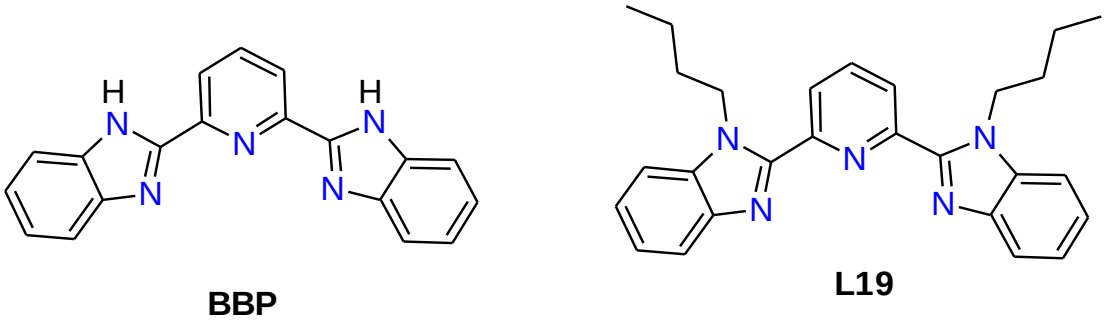

Figure 3-7 Ligands BBP and L19.

3.2.1 The ligand L19

2,6-Bis(benzimidazol-2'-yl)pyridine (BBP) (45) was prepared by the reaction of 2,6-pyridinedicarboxylic acid with *o*-phenylenediamine in syrupy phosphoric acid at 230°C (Figure 3-8).[196] Spectral data are given in experimental chapter. The alkylated ligand 2,6-bis(1-butyl-1H-benzo[d]imidazol-2-yl)pyridine (L19) was obtained as a sticky cream oil by the reaction of 2,6-bis(benzimidazol-2'-yl)pyridine)(BBP) (45) and 1-bromobutane in THF in the presence of a base (NaOH).[197] The ligand L19 is stable at room temperature without decomposition. The ligand is soluble all common organic solvents.

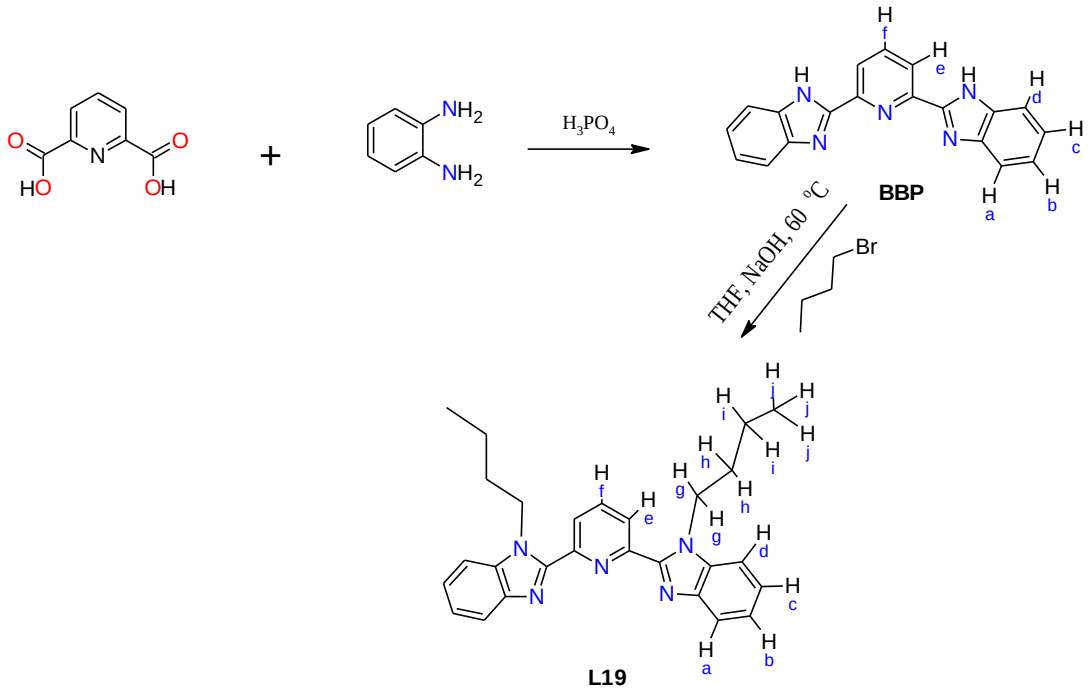

Figure 3-8 Preparation scheme of the ligand L19.

The ^{1}H- and ^{13}C-NMR spectra of the ligand (L19) were recorded in $CDCl_3$ as a solvent and are presented in Figures 3-9 and 3-10. The ligand (L19) has a symmetric nature. In the ^{1}H-NMR spectrum, the aromatic ring protons were seen in the range δ 7.28–8.02 ppm as multiplets. The pyridine protons H^e and H^f were seen at δ 8.33 and 8.06 ppm as a doublet and triplet respectively. Two doublets at δ 7.47 and 7.89 ppm were assigned to two benzimidazole protons H^d and H^a respectively. Benzimidazole protons H^b and H^c were observed as overlapped triplets at δ 7.37–7.39 ppm. The aliphatic region contains two triplets at δ 0.71 and 4.73, one sextet at δ 1.35 ppm and one quintet at δ 1.72 ppm assigned to H^j, H^g, H^i and H^h respectively. The ^{13}C-NMR spectrum was also investigated and exhibited signals due to the presence of aromatic and butyl carbons. Four signals between δ 13.48 – 44.64 ppm were observed and assigned to aliphatic C atoms in the butyl chain. All other aromatic carbon shifts were observed in the range of δ 110.39 – 150.57 ppm. Both ^{1}H and ^{13}C NMR spectra of the ligand confirmed that there was no significant organic impurity in the sample.

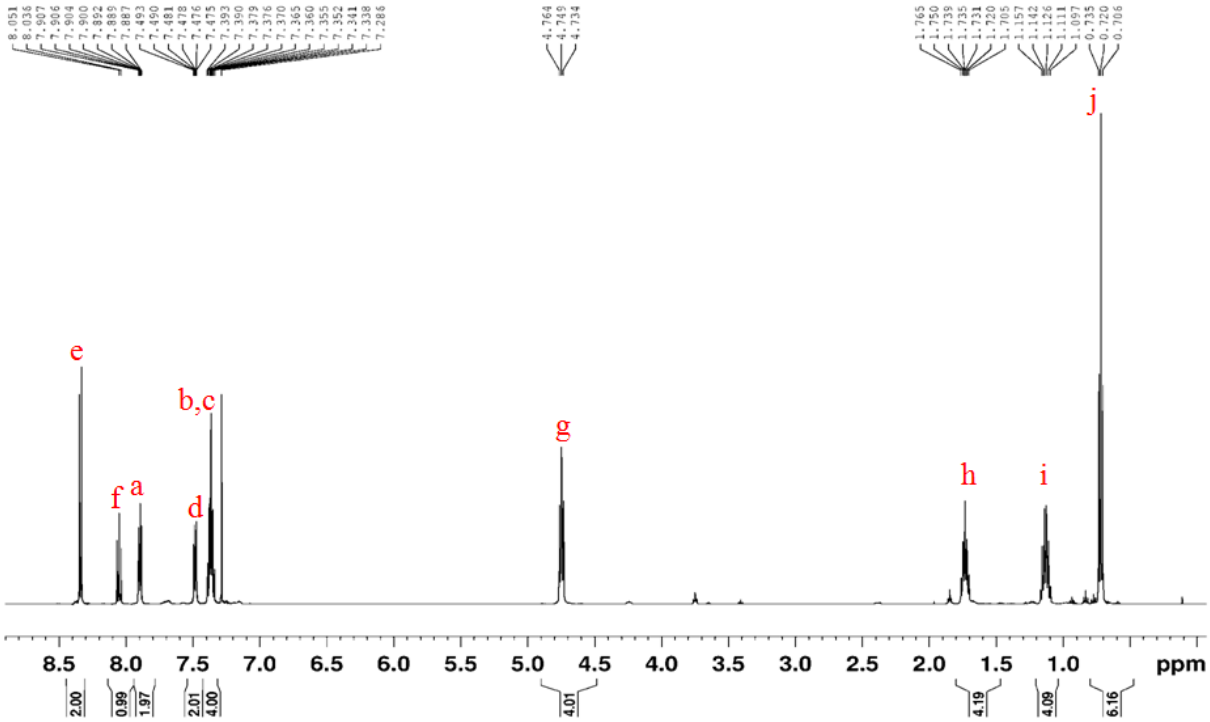

Figure 3-9 ^{1}H NMR spectrum of the ligand L19.

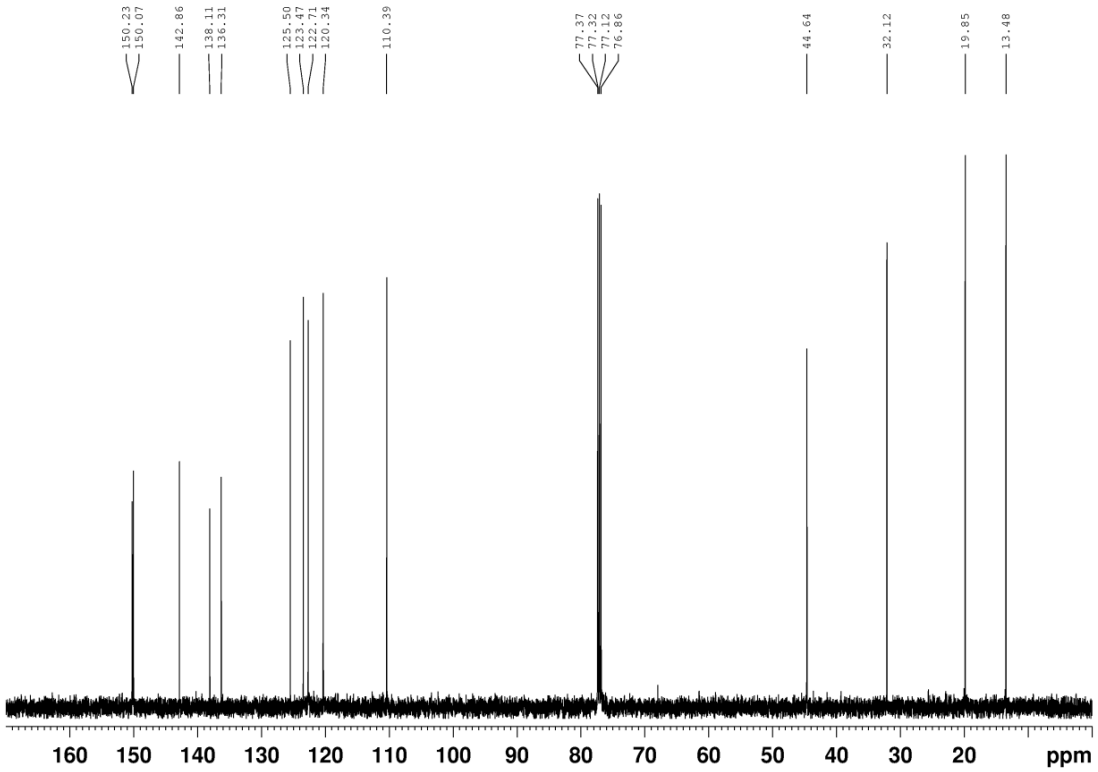

Figure 3-10 ^{13}C NMR of the ligand L19.

The ESI mass spectrum of (L19) showed signals at m/z 424(40%) and 446(100%) assigned to $\{[L19]H\}^+$, $\{[L19]Na\}^+$ respectively. There are two higher mass peaks at m/z 847(40%) and 869(25%) assigned to $\{[L19]_2H\}^+$ and $\{[L19]Na\}^+$ respectively. The ESI spectrum of ligand (L19) is shown in Figure 3-11.

N-alkylation of benzimidazole ring was confirmed by the disappearance of a broad band at 3193 cm^{-1} in the IR spectrum assigned to the ν(N-H) group of the benzimidazole ring (BBP) and appearance of a band at 2956 cm^{-1} assigned to ν(C-H)(alkyl).

3.2.2 Mn(II) complexes of L19; $[Mn(L19)Cl_2]$ (47), $[Mn(L19)(NCS)_2]$ (48), $[Mn(L19)_2](ClO_4)_2$ (49), $[Mn(L19)(NO_3)_2]$ (50) and $[Mn(L19)_2](PF_6)_2$ (51)

Reactions of Mn(II) with (L19) in the presence of Cl^-, SCN^- and NO_3^- in MeOH yield 1:1 (metal:ligand ratio) complexes, while in the presence of ClO_4^- and PF_6^- yield only 1:2 (M: Ligand) complexes. All complexes are air-stable at room temperature without decomposition and are soluble in dmf and dmso. $[Mn(L19)Cl_2]$ (47), $[Mn(L19)(NCS)_2]$ (48), $[Mn(L19)_2](ClO_4)_2$ (49) and $[Mn(L19)(NO_3)_2]$ (50) are slightly soluble in MeOH and EtOH and insoluble in CH_3CN, H_2O and nonpolar organic solvents such as Et_2O, $CHCl_3$, CH_2Cl_2, *etc*. The complex $[Mn(L19)_2](PF_6)_2$ (51) is soluble in MeOH, EtOH and CH_3CN but insoluble in non-polar organic solvents.

The complexes $[Mn(L19)Cl_2]$ (47) and $[Mn(L19)(NO_3)_2]$ (50) were obtained by the reaction of one equivalent of the ligand with one equivalent of the corresponding manganese(II) salt in MeOH. Similarly, $[Mn(L19)_2](ClO_4)_2$ (49) was obtained in MeOH but with a 1:2 metal-ligand ratio. $[Mn(L19)(NCS)_2]$ (48) and $[Mn(L19)_2](PF_6)_2$ (51) were obtained by addition of two equivalents of NaNCS and KPF_6 respectively to the mixture of the ligand and $Mn(II)(OAc)_2{\cdot}4H_2O$.

The IR spectra of the complexes are similar and distinguished by counterion vibrations. In the IR spectrum of the thiocyanate complex (48), the strong thiocynate stretch was observed at 2049 cm^{-1}. In the IR spectrum of nitrate complex (50), nitrate stretches were observed at 1484, 1281 and 1025 cm^{-1}. These three stretches suggest that at least one of two nitrate ions coordinates to metal as bidentate ligand. X-ray structure analysis showed that both of the nitrate ions bind to the metal as a bidentate chelating ligands. The IR spectrum of the perchlorate complex (49) shows two strong stretches at 1088 and 622 cm^{-1} with no splitting, suggesting that these ions are not coordinated. This was further confirmed by X-ray

crystallography. In the hexaflorophoshate complex (51), two strong ν(P-F) stretches were observed at 839 and 557 cm^{-1}.

In ESI mass spectra, Mn(II) complex cations were observed for all complexes. These are listed in the experimental chapter. From the mass spectra of $[Mn(L19)(X)_2]$ complexes (where X= Cl^-, NCS^-, NO_3^-), some of the complex molecules dissociate in solution and form the new complexes $[Mn(L19)_2](X)_2$. This was confirmed by the appearance of peaks corresponding to $\{[Mn(L19)_2]\}^{2+}$ and $\{[Mn(L19)_2]X\}^+$. However, X-ray diffraction studies showed that these complexes only exist as $[Mn(L19)(X)_2]$ in the solid state. In the mass spectrum of $[Mn(L19)_2](X)_2$ (where X= PF_6^-, ClO_4^-), complexes exist as $[Mn(L19)_2](X)_2$ in both solution and solid state. Mass spectra of chloride and perchlorate complexes are shown in Figure 3-11.

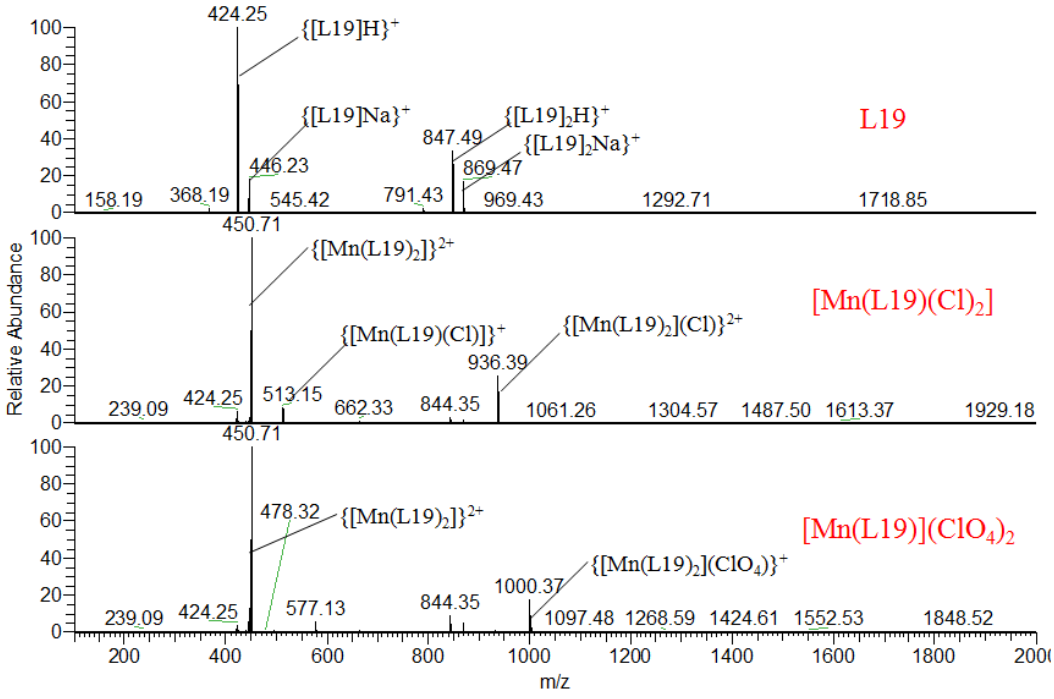

Figure 3-11 ESI mass spectra of Ligand L19, $[Mn(L19)Cl_2]$ and $[Mn(L19)_2](ClO_4)_2$.

Single crystals of (47), (48), (49) and (50) suitable for X-ray diffraction study were obtained by slow diffusion of diethylether into dmf solutions of the complexes. Single crystals of complex (51) were also obtained *via* the vapour diffusion method but, due to very weak diffraction, the data set was not collected. Therefore, the formula of this complex was determined *via* CHN analysis, IR and mass spectrometry techniques.

3.2.3 Crystal structures of [Mn(L19)Cl_2] (47) and [Mn(L19)$(NCS)_2$] (48)

The details of the crystal structure and refinement for (47) and (48) can be found in Tables A26 and A27 respectively in Appendix 2. Crystal structures of [Mn(L19)Cl_2] (47) and [Mn(L19)$(NCS)_2$] (48) with atom numbering are shown in Figure 3-12 and selected bond lengths and angles are given in Table 3-8. The asymmetric units each contain one neutral molecule. One of the butyl chains (C1-C4) in [Mn(L19)Cl_2] is disordered and this was modelled over two positions in a 65:35 ratio (C(1)-C(4):C(1)'-C(4)'), the structures of [Mn(L19)Cl_2] (47) and [Mn(L19)$(NCS)_2$] (48) are broadly similar. The Mn(II) ions are five-coordinate in both complexes. The coordination sphere of Mn(II) in [Mn(L19)Cl_2] (47) comprises three nitrogen atoms from the tridentate ligand and two chloride ions (Cl1, Cl2). The two chloride ions are replaced by two N-bonded thiocynate ions in [Mn(L19)$(NCS)_2$] (48).

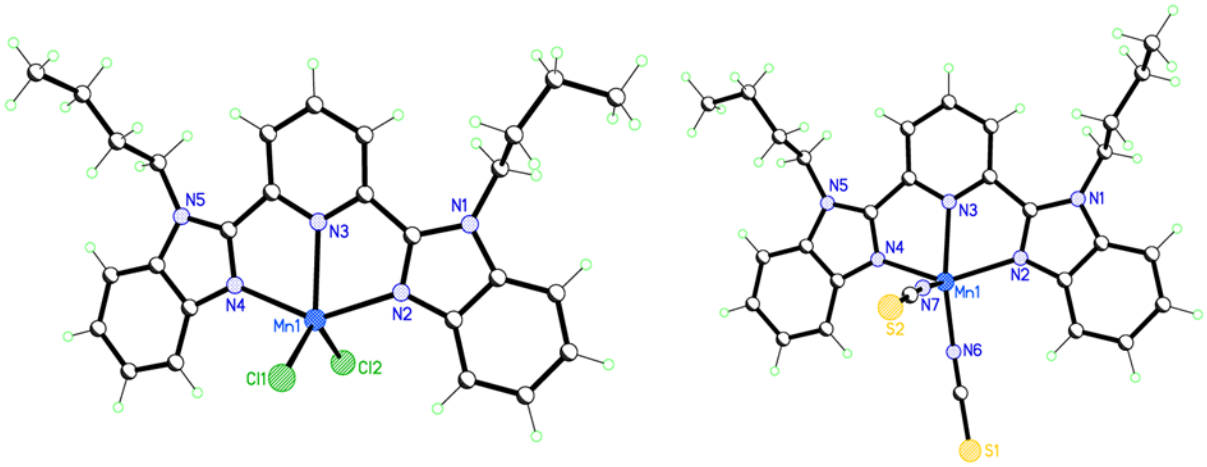

Figure 3-12 Molecular structures of (47) and (48).

Table 3-8 Selected bond lengths [Å] and angles [°] for (47), (48) and [Mn(BBP)Cl_2].[192]

[Mn(L19)Cl_2] (47)		[Mn(L19)$(NCS)_2$] (48)		[Mn(BBP)Cl_2][192]	
Mn1—N2	2.237 (2)	Mn1—N2	2.2019 (14)	Mn1—N1	2.276 (3)
Mn1—N3	2.299 (2)	Mn1—N3	2.2465 (14)	Mn1—N3	2.229 (3)
Mn1—N4	2.211 (2)	Mn1—N4	2.2073 (14)	Mn1—N5	2.258 (3)
Mn1—Cl1	2.3684 (9)	Mn1—N6	2.0772 (17)	Mn1—Cl1	2.340 (1)
Mn1—Cl2	2.3554 (9)	Mn1—N7	2.0703 (17)	Mn1—Cl2	2.385 (2)
N2—Mn1—N3	70.93 (8)	N2—Mn1—N3	71.76 (5)	N1—Mn1—N3	71.3 (1)
N3—Mn1—N4	70.68 (8)	N3—Mn1—N4	71.96(5)	N1—Mn1—N5	71.1 (1)
N2—Mn1—N4	141.59 (8)	N2—Mn1—N4	142.29 (5)	N3—Mn1—N5	140.7 (1)

Cl1—Mn1—Cl2	120.41(3)	N6—Mn1—N7	106.85 (7)	Cl1—Mn1—Cl2	112.92 (5)
N2—Mn1—Cl1	100.36 (6)	N2—Mn1—N6	101.98 (6)	N1—Mn1—Cl1	141.1 (2)
N3—Mn1—Cl1	121.09 (6)	N3—Mn1—N6	147.94 (6)	N3—Mn1—Cl1	101.44 (9)
N4—Mn1—Cl1	98.23 (6)	N4—Mn1—N6	103.18 (6)	N5—Mn1—Cl1	100.07 (8)
N2—Mn1—Cl2	97.82 (6)	N3—Mn1—N7	105.20 (6)	N2—Mn1—Cl2	105.9 (1)
N3—Mn1—Cl2	118.49 (6)	N4—Mn1—N7	100.01 (6)	N3—Mn1—Cl2	99.9 (1)
N4—Mn1—Cl2	101.23 (6)	N2—Mn1—N7	99.02 (6)	N5—Mn1—Cl2	101.5 (1)

The coordination polyhedron about the manganese ion in [Mn(L19)Cl_2] (47) can be regarded as a distorted trigonal bipyramid. The equatorial positions are occupied by the two chlorides and the pyridine nitrogen atom (N3) and the apical positions are occupied by two imidazol nitrogen atoms (N2 and N4). The three angles in the equatorial plane are close to the ideal value of 120º. The Cl(2)–Mn–Cl(1) angle 120.41(3) slightly deviates from the ideal value of 120º. The apical to equatorial angles deviate considerably from the ideal value of 90º. It is informative to compare crystal structures of [Mn(L19)Cl_2] with the Mn(II) complex of BBP prepared from 2,6-bis(benzimidazol-2'-yl)pyridine and $MnCl_2 \cdot 6H_2O$. The [Mn(BBP)Cl_2] complex was synthesised and structurally characterised by Shuangxi *et al.*[198] In both the complex [Mn(L19)Cl_2] and the published structure [Mn(BBP)Cl_2], the Mn(II) ions are five-coordinate and they both have similar Mn-donor distances. However, the Cl-Mn-Cl angle in [Mn(BBP)Cl_2], 112.92(5)º is smaller than the same angle of the complex [Mn(L19)Cl_2], 120.41(3)º. This smaller Cl-Mn-Cl angle could be attributed to a hydrogen bond between NH(imidazol)⋯Cl in the [Mn(BBP)Cl_2]. There is also an uncoordinated hydrogen bonded dmf molecule in the asymmetric unit of [Mn(BBP)Cl_2]; no solvent of crystallisation was included in the complex [Mn(L19)Cl_2].

There are π-π stacking interactions observed in both [Mn(L19)Cl_2] (47) and [Mn(L19)$(NCS)_2$] (48) structures. In (47), one edge of a benzimidazole ring is stacked with the same section of an adjacent molecule under symmetry operation -x, 2-y, 1-z; C23 and C23* are separated by a distance of 3.313 Å shorther than π stacking distance (3.35 Å) in graphite (Figure 3-13). There are two sets of π-π stacking interactions in (48); first, one edge of the pyridinebenzimidazole of one of the complex molecules is stacked with the same section of a neighbouring molecule under symmetry operation 2-x, 1-y, -z, second, one edge of the benzene ring (C8-C10) is stacked with the same section of an adjacent molecule under

symmetry operation 2-x, 1-y, 1-z; C8 and C10* are separated by a distance of 3.392 Å (Figure 3-14).

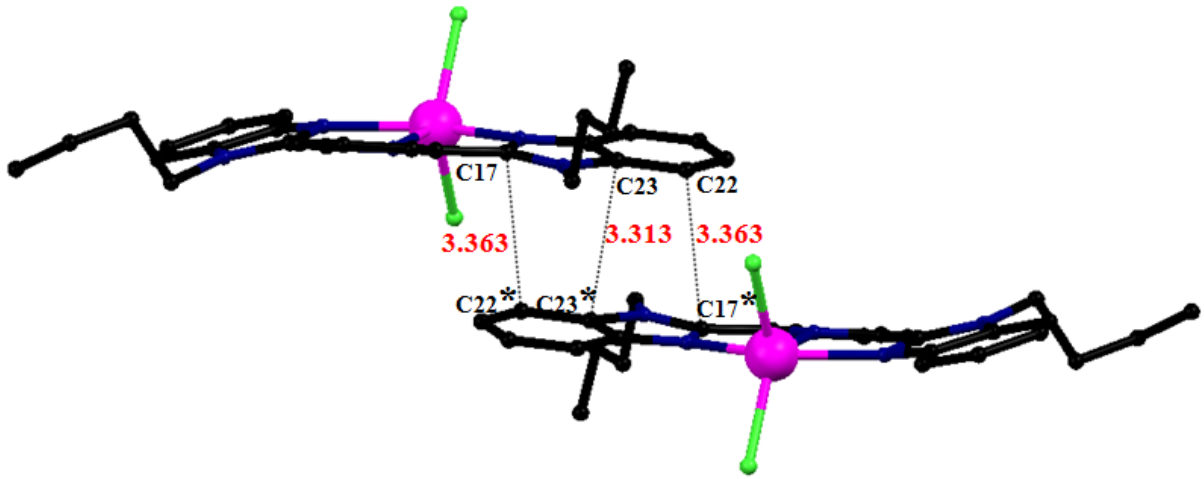

*Figure 3-13 π-π interactions in [Mn(L19)Cl$_2$] (47). Symmetry operation: *-x, 2-y, 1-z.*

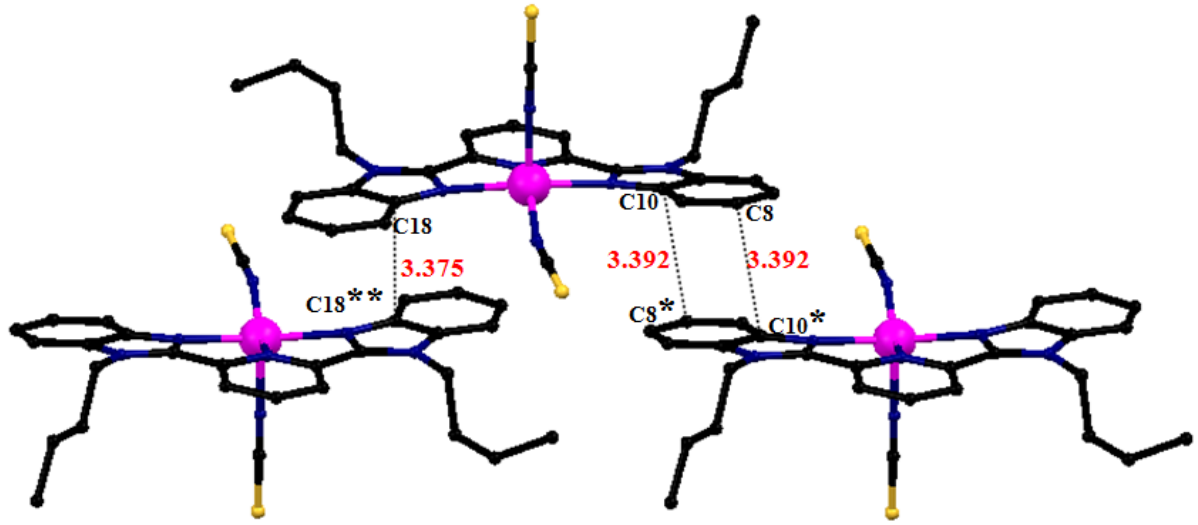

*Figure 3-14 π-π interactions in [Mn(L19)(NCS)$_2$] (48). Symmetry operations: *2-x, 1-y, 1-z, **2-x, 1-y, -z.*

Packing is determined by CH···Cl and π-π stacking interactions in (47), CH···S and π-π stacking interactions in (48). Packing diagrams are shown in Figure 3-15 and 3-16.

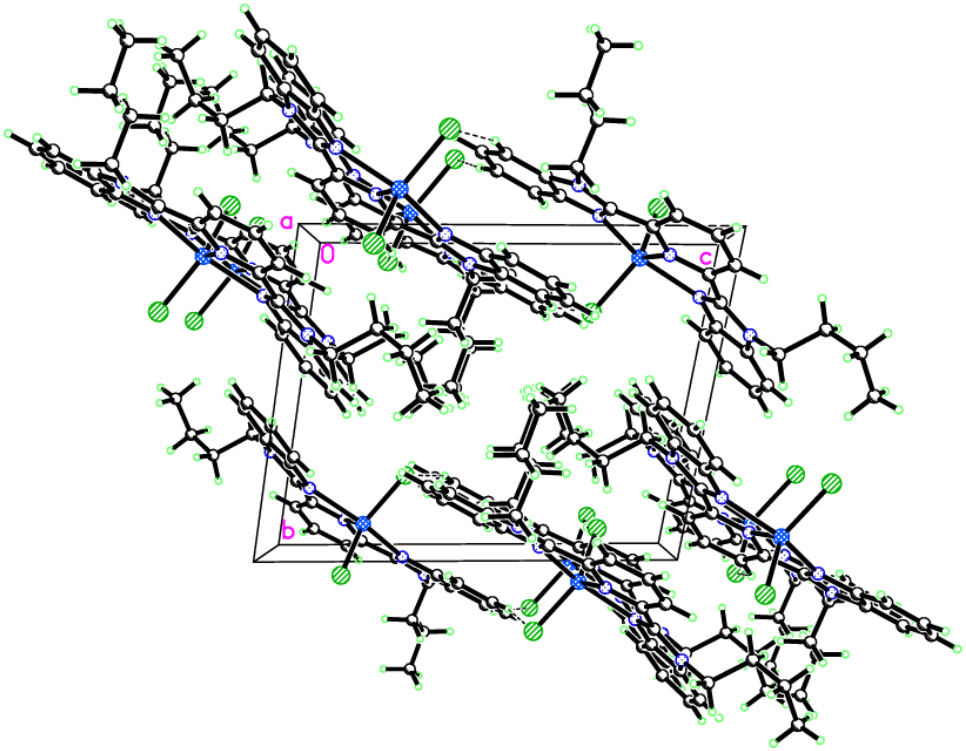

Figure 3-15 Packing diagram of (47) viewing down a axis.

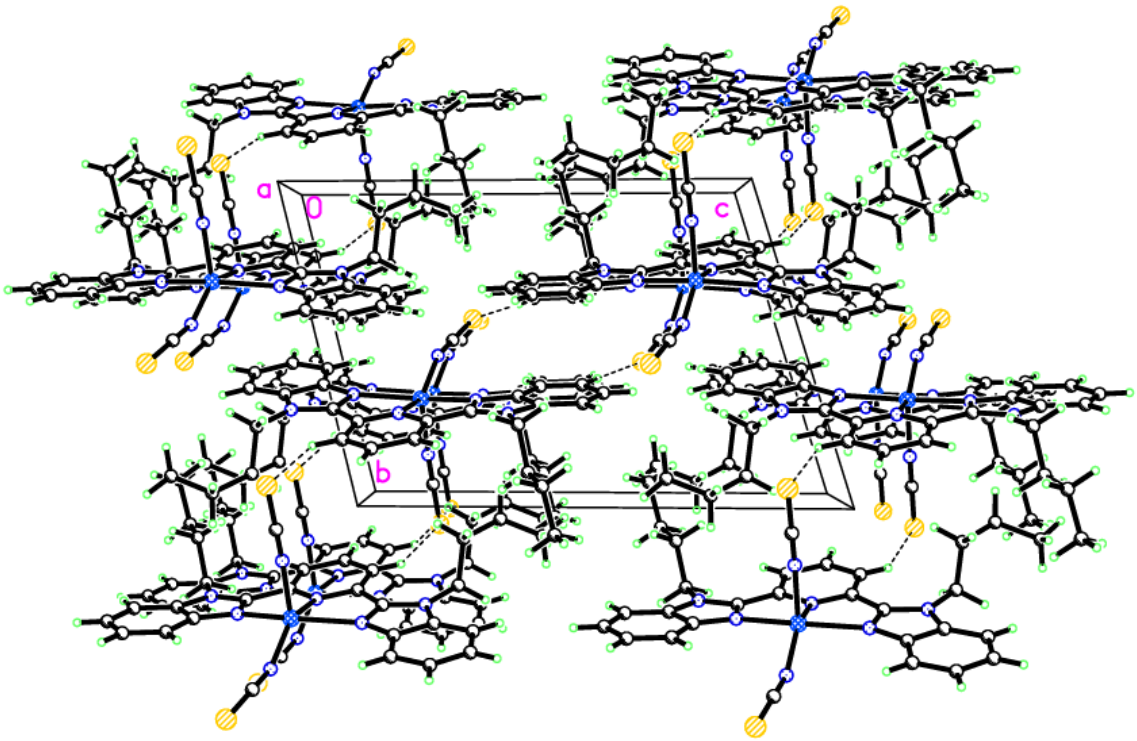

Figure 3-16 Packing diagram of (48). CH····S interactions are shown as dashed lines (C15-H15····S2 distance is 2.943 Å).

3.2.4 Crystal structure of [Mn(L19)$(NO_3)_2$] (50)

The complex was found to crystallise in the triclinic space group $P\bar{1}$. Details of the crystal structure and refinement can be found in Table A28 in Appendix 2.

The structure of the complex is depicted in Figure 3-17. [Mn(L19)$(NO_3)_2$] has a seven-coordinate Mn(II) centre, however, the geometry around the Mn(II) ion is not pentagonal bipyramidal as found for the seven coordinate Mn(II) ions. The coordination sphere of manganese consists of three nitrogen atoms of the ligand L19 and four oxygen atoms of two bidentate chelating nitrate ligands.

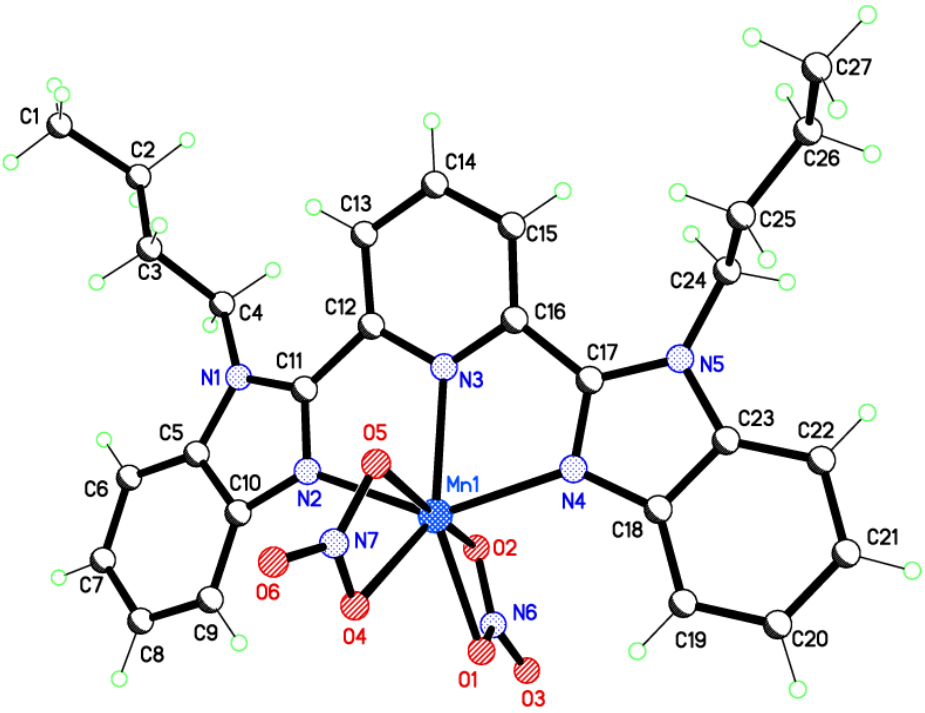

Figure 3-17 Crystal structure of (50).

The two bidentate nitrate groups are asymmetrically bound (Mn1-O1 and Mn1-O2 distances are 2.2455(13) and 2.3062(13) Å respectively and Mn1-O4 and Mn1-O5 distances are 2.2041 (11) and 2.3968 (12) Å respectively.

Table 3-9 Selected bond lengths [Å] and angles [°] for (50).

Mn1—N2	2.2041 (11)	N3—Mn1—O1	144.18 (5)
Mn1—N3	2.2083 (12)	N3—Mn1—O2	91.11 (5)
Mn1—N4	2.2352 (13)	N3—Mn1—O4	135.73 (4)
Mn1—O1	2.2455 (13)	N3—Mn1—O5	83.99 (4)
Mn1—O2	2.2760 (12)	N4—Mn1—O1	93.91 (5)
Mn1—O4	2.3062 (13)	N4—Mn1—O2	92.47 (5)
Mn1—O5	2.3968 (12)	N4—Mn1—O4	119.86 (5)
		N4—Mn1—O5	90.09 (4)
N2—Mn1—N3	71.46 (4)	O1—Mn1—O2	55.91 (5)
N2—Mn1—N4	143.44 (5)	O1—Mn1—O4	79.99 (5)
N2—Mn1—O1	115.56 (5)	O1—Mn1—O5	129.89 (5)
N2—Mn1—O2	87.36 (5)	O2—Mn1—O4	127.51 (5)
N2—Mn1—O4	87.80 (5)	O2—Mn1—O5	173.49 (4)
N2—Mn1—O5	87.02 (4)	O4—Mn1—O5	55.52 (4)
N3—Mn1—N4	71.99 (4)		

There is evidence of π–π stacking interactions in the structure; one of the benzimidazole groups is stacked with the same section of an adjacent complex molecule under symmetry operation 1-x, 1-y, -z; C17 and C21 are separated by a distance of 3.502 Å (Figure 3-18). In the structure, π–π stacking and $CH\cdots ONO_2$ weak hydrogen bond type interactions[180] are the principal interactions in crystal packing. The packing diagram of the structure (50) is shown in Figure 3-19.

Table 3-10 Hydrogen-bond geometry (Å, º) for (50).

D—H···*A*	*D*—H	H···*A*	*D*···*A*	*D*—H···*A*
C15—H15···O4^{i}	0.95	2.52	3.2177 (19)	130.6
C15—H15···O6^{i}	0.95	2.70	3.414 (2)	132.2
C24—H24A···O4^{i}	0.99	2.58	3.4200 (19)	143.1
C26—H26A···O4^{i}	0.99	2.65	3.487 (2)	142.6
C20—H20···O1^{ii}	0.95	2.60	3.394 (2)	141.5
C22—H22···O2^{iii}	0.95	2.61	3.341 (2)	134.0
C22—H22···O3^{iii}	0.95	2.66	3.611 (2)	176.6
C26—H26B···O3^{iii}	0.99	2.51	3.434 (2)	155.4
C13—H13···O5^{iv}	0.95	2.51	3.1786 (19)	127.5
C6—H6···O2^{v}	0.95	2.37	3.253 (2)	154.9

Symmetry codes: (i) *x*+1, *y*, *z*; (ii) -*x*, -*y*+1, -*z*; (iii) -*x*+1, -*y*+1, -*z*; (iv) -*x*+1, -*y*+1, -*z*+1; (v) -*x*+1, -*y*+2, -*z*+1.

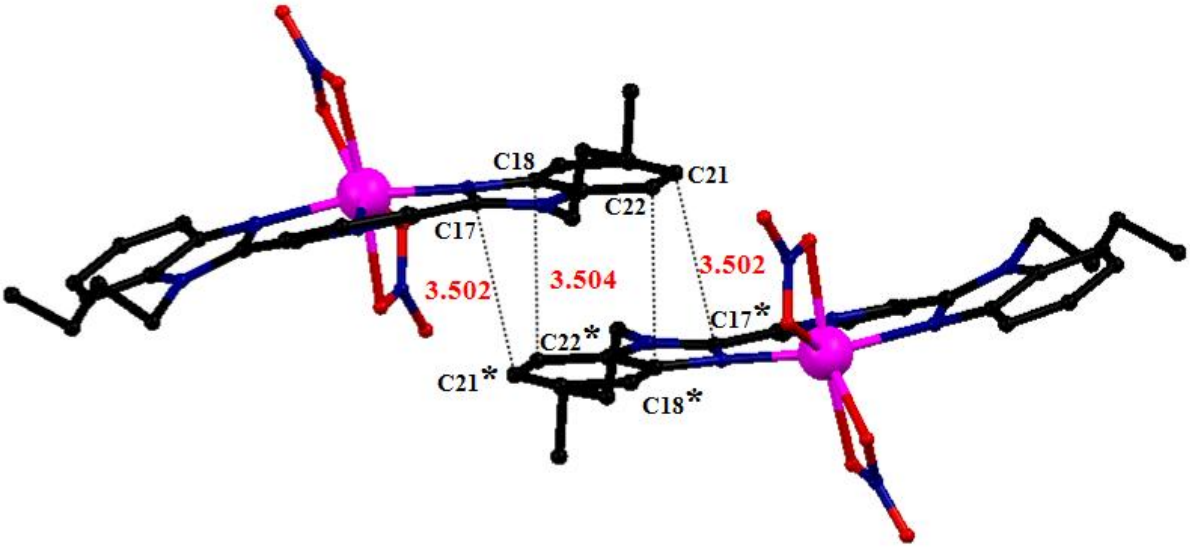

Figure 3-18 π–π stacking interactions in (50). Symmetry operation: 1-x, 1-y, -z.*

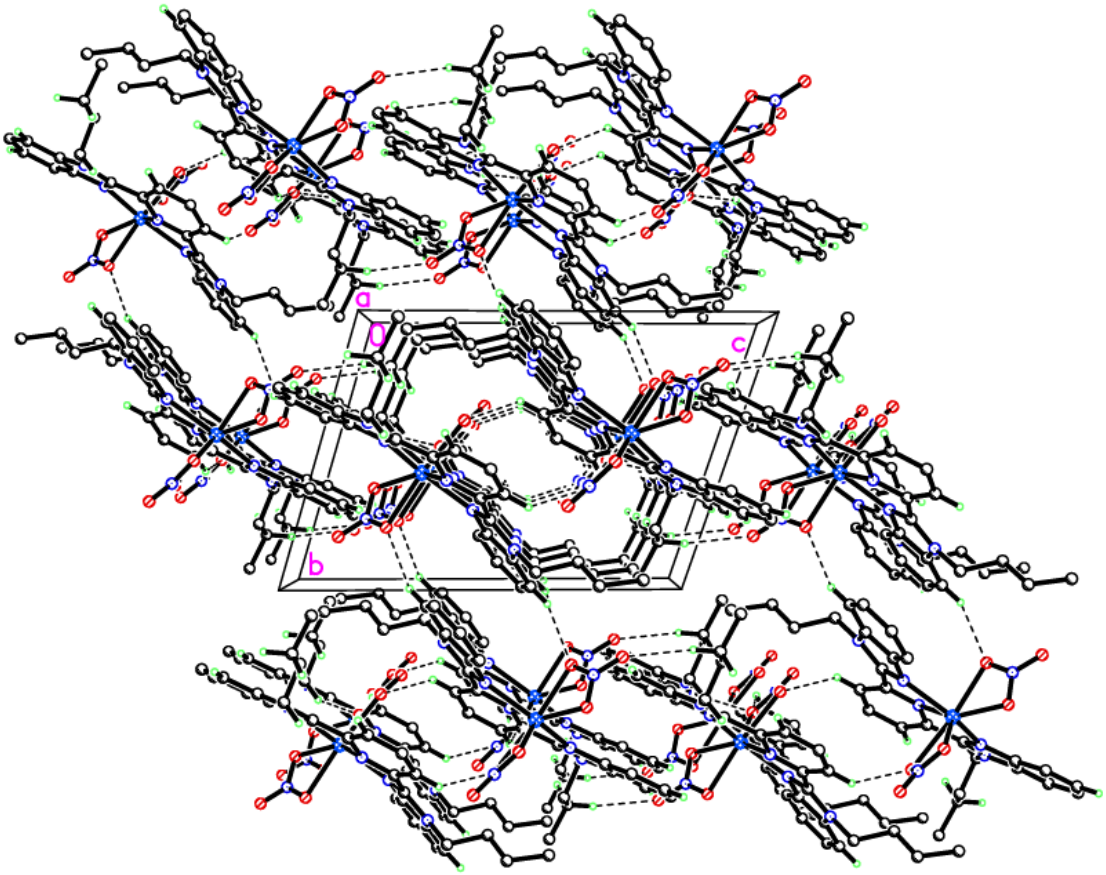

Figure 3-19 Packing diagram of (50). Hydrogen atoms which are not involved in hydrogen bonding are removed for clarity.

3.2.5 Crystal structure of $[Mn(L19)_2](ClO_4)_2$ (49)

Good quality crystals for X-ray diffraction study were obtained by slow diffusion of diethylether into dmf solution of the complex which crystallised as $[Mn(L19)_2](ClO_4)_2 \cdot dmf$. The structure was solved in the monoclinic space group *P*2/*c* and details of the crystal structure and refinement can be found in Table A29 in Appendix 2. The asymmetric unit contains half of the complex cation and an uncoordinated percholarate ion. The structure of the complex cation is shown in Figure 3-20. It contains a single six-coordinate Mn(II) ion that is coordinated to six nitrogen atoms of two benzimidazole ligands. One of the butyl chains (C24-C27) is disordered and this was modelled over two positions in a 60:40 ratio (C24-C27:C24'-C27'). There is a partial occupancy disordered dmf molecule which was dealt with by the squeeze procedure (see details Appendix 2 Table A29).

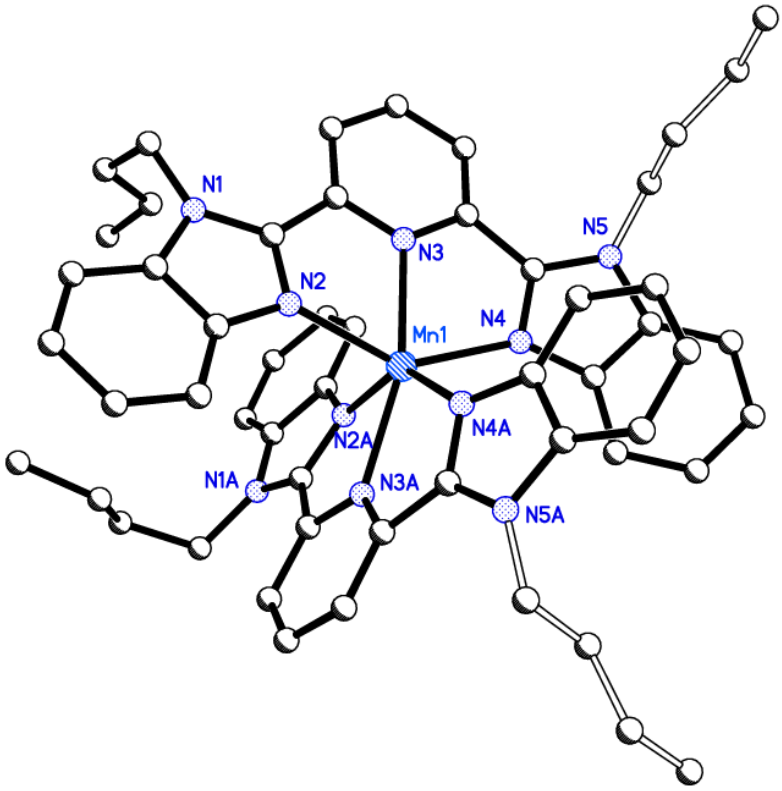

Figure 3-20 X-ray structure of complex (49) cation $[Mn(L19)_2]^{2+}$. Hydrogen atoms and uncoordinated perchlorate ions are omitted for clarity. Symmetry code: A -x+1, y, -z+½.

Complex cations are linked *via* π–π edge-edge stacking interactions; one edge of the ligand is stacked with the same section of an adjacent complex under symmetry operation 1-x, -y, -z with a centroid-centroid (C12-N3)-(C5-C10) distance of 3.764 Å (Figure 3-21).

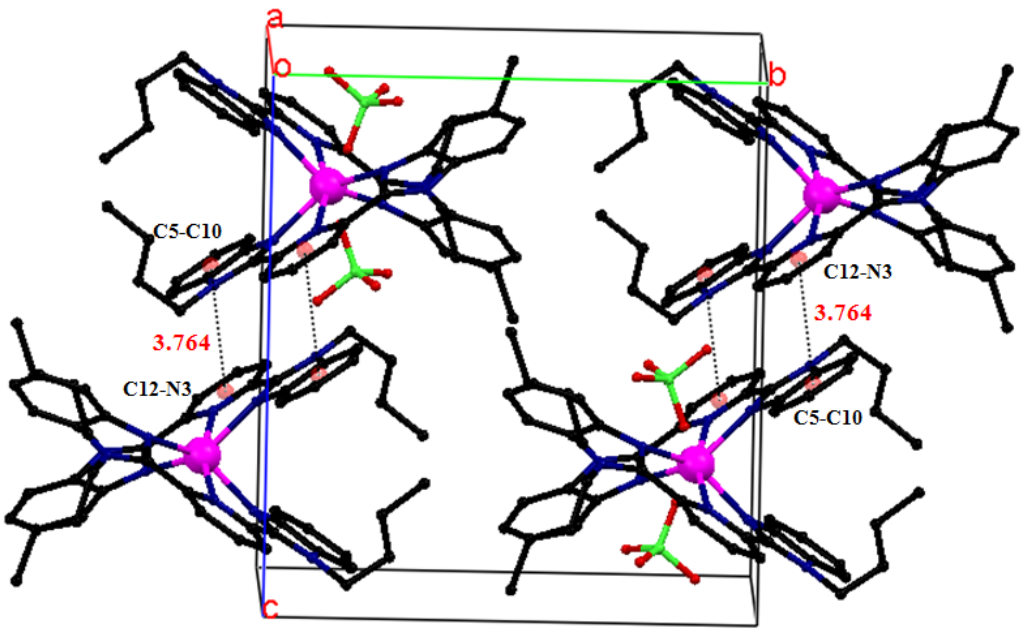

Figure 3-21 Packing diagram of (49) showing π-π interactions. Pink dots are ring centroids.

Table 3-11 Selected bond lengths [Å] and angles [°] for (49)·dmf.

Mn1—N2	2.2309 (19)	Mn1—N2^{i}	2.2309 (19)
Mn1—N3	2.2544 (18)	Mn1—N3^{i}	2.2544 (18)
Mn1—N4	2.197 (2)	Mn1—N4^{i}	2.197 (2)
N2—Mn1—N3	71.28 (7)	N3—Mn1—N4^{i}	121.02 (7)
N2—Mn1—N4	141.78 (7)	N4—Mn1—N2^{i}	101.32 (7)
N2—Mn1—N2^{i}	94.11 (10)	N4—Mn1—N3^{i}	121.02 (7)
N2—Mn1—N3^{i}	97.00 (7)	N4—Mn1—N4^{i}	87.78 (10)
N2—Mn1—N4^{i}	101.32 (7)	N2^{i}—Mn1—N3^{i}	71.28 (7)
N3—Mn1—N4	72.26 (7)	N4^{i}—Mn1—N2^{i}	141.77 (7)
N3—Mn1—N2^{i}	97.00 (7)	N4^{i}—Mn1—N3^{i}	72.26 (7)
N3—Mn1—N3^{i}	163.20 (10)	Symmetry code: (i) -*x*+1, *y*, -*z*+½.	

The reaction of N-alkylated pyridinebenzimidazole ligand L19 with Mn(II) produced mononuclear complexes [Mn(L19)Cl_2] (47), [Mn(L19)$(NCS)_2$] (48), [Mn$(L19)_2$]$(ClO_4)_2$ (49), [Mn(L19)$(NO_3)_2$] (50) and [Mn$(L19)_2$]$(PF_6)_2$ (51) in high yield and purity. In the presence of strongly binding counter ions Cl^-, SCN^- and NO_3^-, 1:1 (Mn:L19) complexes were obtained and in those complexes counter ions are coordinated to Mn(II). In the presence of weakly binding ClO_4^- or PF_6^-, 1:1 or 1:2 Mn:L19 reactions yield only 1:2 (M:Ligand) complexes and the counter ions remain uncoordinated.

Chapter 4

Catalytic studies

4.1 Introduction

In this chapter, catalase and superoxide dismutase activity of the complexes will be introduced. In the first part, catalase activity of the complexes and experimental details will be discussed and then comparisons will be made between similar complexes. The structure and activity relations will also be examined in detail. In the second part, direct and indirect techniques used to measure superoxide dismutase activity will be introduced and advantages and disadvantages of these techniques will be discussed. The experimental details of the techniques used to test complexes in this thesis will also be explained and results will be categorised according to structural similarities.

4.2 Catalase activity of complexes

Catalase activity was carried out volumetrically *via* the measurement of oxygen evolution. The equipment was set up for oxygen collection using two upturned 1000 cm^3 measuring cylinders containing water in a water bath. The temperature of the water bath was maintained at 25 °C (Figure 4-1).

Figure 4-1 Equipment used for measuring catalase activity.

Once the equipment was set up, the temperature of the water tank was allowed to equilibrate to 25 °C for 1 hr. A sample of complex (1 mg) was placed into a three necked round bottom flask and followed by addition of methanol (1 ml). The solution was stirred and the flask was sealed. Hydrogen peroxide (2 ml) was then introduced through a rubber septum into the sealed round bottom flask and oxygen evolution was monitored every ten seconds for ten minutes. Each complex was tested with and without the addition of base triethylamine. In the cases where base was used, 0.010 g was added to the flask before the hydrogen peroxide was introduced. The addition of base during catalase testing has previously been shown to enhance the catalytic activity.[199,200] Pecoraro *et al.* suggested that base deprotonates the hydrogen peroxide to initiate the reaction of binding to manganese ions.[160]

The hydrogen peroxide used in tests was standardised by titration with potassium permanganate. From the calculations, the hydrogen peroxide was found to have a concentration of 7.28 ± 0.08 mol L^{-1}. When all of the hydrogen peroxide (2 ml) was broken down, a maximum of 163 ml of oxygen (based on ideal gas behaviour) would be expected to be produced at 25 °C when the reaction is complete. However, the volume of the oxygen released was often higher that calculated. This may due to the exothermic nature of the reaction as an increase in heat would cause the volume of gas to expand.

Initial tests were then carried out on the catalase mimic, *cis*-$[Mn(phen)_2Cl_2]$, originally studied by McCann *et al.*[155] to check the equipment before testing the new complexes. Each *cis*-$[Mn(phen)_2Cl_2]$ was shown to turnover 5382 hydrogen peroxide for each manganese atom during the first minute.[155] In the test this complex breaks down 5345 hydrogen peroxide molecules during the first minute. McCann *et al.* also showed that a simple $MnCl_2$ broke down 918 hydrogen peroxide molecules during the first minute.[155]

Calculation of turnover number:

$$2H_2O_2 \xrightarrow{\text{Mangenese complex}} O_2 + 2H_2O$$

From the reaction, 1 mole of O_2 is produced when 2 moles of hydrogen peroxide are broken down. Assuming ideal gas behaviour, 1 mole of O_2 occupies 22400 ml and 1ml then contains ($1/22400 = 4.5 \times 10^{-5}$ moles of O_2). Therefore 9.0×10^{-5} moles of hydrogen peroxide are consumed for every 1 ml of oxygen produced. This is equal to ($9.0 \times 10^{-5} \times (N_A)$) $= 5.42 \times 10^{19}$ molecules of hydrogen peroxide broken down for every 1 ml of oxygen produced.

The number of molecules of complex that are present in the sample (1 mg) is equal to (Mass(g)/RMM) x N_A where mass=1 mg, RMM=relative molecular mass of complex and N_A= Avagadro`s constant= 6.022×10^{23} mol^{-1}.

For each tested compound, turnover number was calculated *via* the following equation;

5.42×10^{19} x Rate (ml/s^{-1}) / Number of molecules of complex present

The rate of the reaction during the fastest part of the reaction has been taken from the maximum slope of the graph during catalase activity.

Three different tests were carried out for all complexes. In the first test, catalase activity of the complex was measured in the presence of base. Most of the complexes prepared in this thesis showed catalase activity in the presence of base. In the second test, no base was used. Only one complex showed catalase activity in the absence of base. The third test was carried out to see if base itself has any catalase activity in the absence of complex. It was found that in the presence of base no oxygen evolution was observed.

Table 4-1 Catalase test procedure.

	Complex	Methanol	Base (triethylamine)	Hydrogen peroxide
Test 1	1 mg	1 ml	0.010 g	2 ml
Test 2	1 mg	1 ml	No base	2 ml
Test 3	No complex	1 ml	0.010	2 ml

* Glassware precision: 1 ml pipette ±0.006, analytical balance ±0.0002 for two readings.

The results that are obtained for catalase activity are subject to errors, therefore the turnover number that is calculated is an approximate figure in which the error is difficult to estimate due to the set-up of the equipment, changes in temperature that may occur, cylinder readings and possible gas leaking. However, at least three tests were repeated to obtain concordant results and average values were used in calculations. Test results showed that those results were reproducible. An electronic copy of the full catalase activity results is given in the Appendix CD.

4.2.1 Catalase activity of macrocyclic complexes

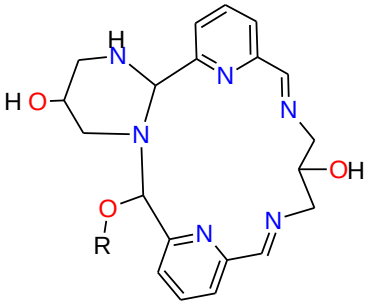

H_3L2 R= -CH_3
H_3L3 R= -CH_2CH_3

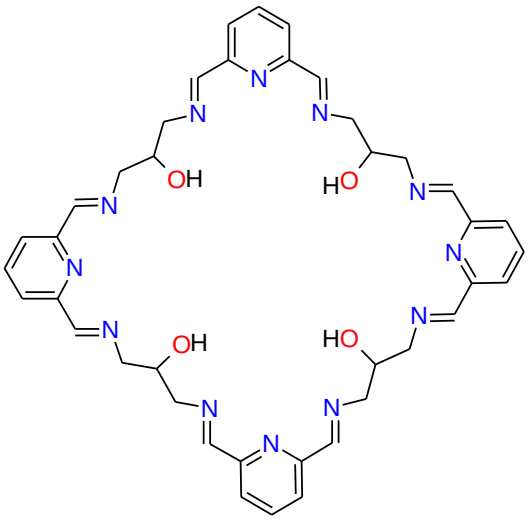

H_4L^*

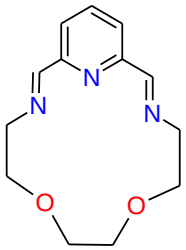

L4

Macrocyclic Mn(II) complexes have been compared to investigate the effect of different axial ligands and ligand structure on catalase acitivity. Five macrocyclic complexes, two poly nuclear complexes $[Mn_4(H_2L^*)Cl_4][MnCl_4]$ (4) and $[Mn_4(H_2L^*)Cl_4][ClO_4]$ (4a) and three mononuclear complexes, were tested with and without base. None of the complexes showed any catalase activity without base. The results of the catalase activity are illustrated in Figure 4-2 and Table 4-2. The graph shows the catalase activity for complexes with base and demonstrates differences observed for catalase activity. The results have been used to calculate the number of H_2O_2 molecules disproportionated by one molecule of complex (known as turnover number) both after one minute and the fastest part of the reaction. The turnover number after one minute, was then calculated to show those complexes which have an induction period.

At the end of the catalase reactions, the colour of the solutions remained light yellow; this indicates these complexes enhance catalytic disproportion of hydrogen peroxide and no formation of insoluble manganese dioxide was observed.

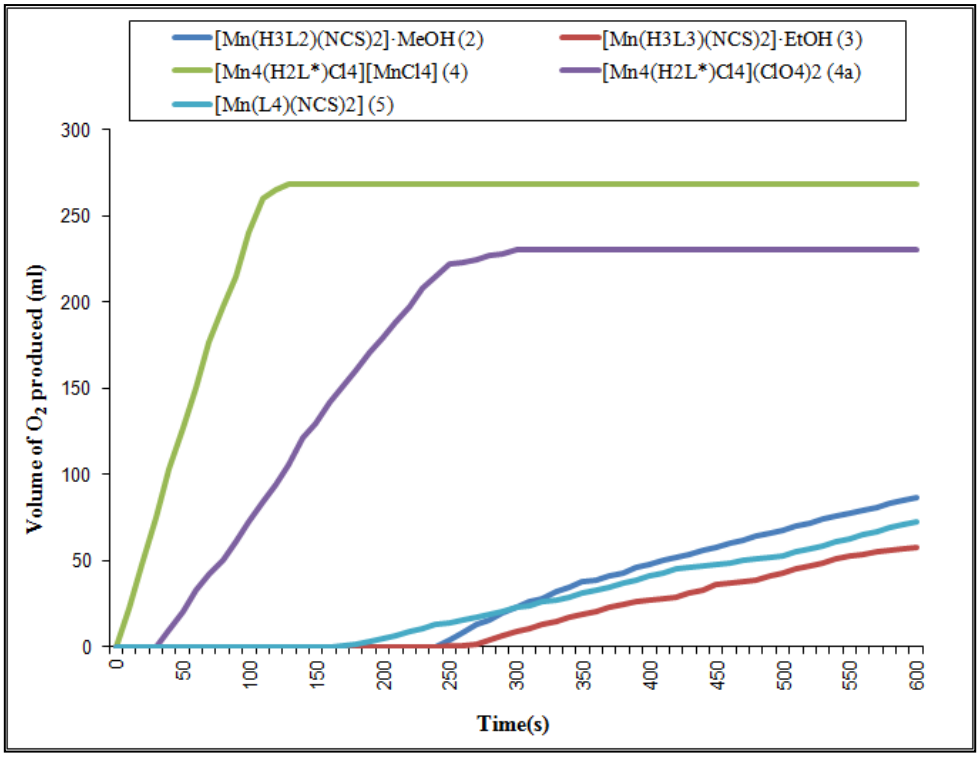

Figure 4-2 Catalase activity for macrocyclic complexes.

Table 4-2 Rates and turnover numbers for macrocyclic complexes.

Complex		Fastest rate(ml/s)	Turnover Number*[a]	B	C
$[Mn(H_3L2)(NCS)_2]$	(2)	0.31	18	0	4793
$[Mn(H_3L3)(NCS)_2]$	(3)	0.13	8	0	3347
$[Mn_4(H_2L^*)Cl_4][MnCl_4]$	(4)	3.70	437	17731	31680
$[Mn_4(H_2L^*)Cl_4](ClO_4)_2$	(4a)	1.73	205	3904	27208
$[Mn(L4)(NCS)_2]$	(5)	0.13	5	0	2747
$[Mn_2(HA)Cl_2]_2(ClO_4)_2$		1.1	130	7807	-
$[Mn_2(HA)(N_3)_2]_2(ClO_4)_2$		1.1	49	7830	-
$[Mn_2(RedHA)Cl_2]_2[MnCl_4]$		2.7	328	21302	-
$[Mn_2(RedHA)(N_3)_2]_2(ClO_4)_2$		6.1	867	52006	-

* = turnover number = maximum number of molecules of hydrogen peroxide converted to oxygen per molecule of complex[155,199] a = per second during the fastest part of the reaction, B = Number of H_2O_2 broken down after 60 seconds per complex, C = Total number of H_2O_2 broken down per molecule of complex after 10 min.

Initial observations indicated that complex (4) is the most efficient catalase mimic with the fastest rate observed at 3.70 ml/s and approximately 437 molecules of H_2O_2 broken down per second for each complex at the fastest rate of activity and approximately 31680 molecules of H_2O_2 broken down for each complex after completion of the reaction. Complex (4a) showed slower catalase activity when compared to complex (4) with the fastest rate of 1.73 ml/s and approximately 205 molecules of H_2O_2 broken down per second for each complex during the fastest rate. The structures of complexes (4) and (4a) contain the same macrocyclic tetranuclear Mn(II) cations and different counter ions. Complex (4) contains $[MnCl_4]^{2-}$ as counter ion while complex (4a) contains perchlorate as counter ions. Higher catalase activity of the complex can then be attributed to an extra manganese atom present in the structure.

The mononuclear complexes $[Mn(H_3L2)(NCS)_2]$ (2), $[Mn(H_3L3)(NCS)_2]$ (3) and $[Mn(L4)(NCS)_2]$ (5) showed limited catalase activity with a long induction period, and once catalase activity starts the rate is slow. Slow catalase activity of these complexes could be explained by their structure. Complexes (2), (3) and (5) contain seven-coordinate Mn(II) ions with approximate pentagonal bipyramidal geometry and the axial positions are occupied by two N-bound thiocyanate ions. In ring-contracted complexes (2) and (3), formation of the ring within the ligand system may prevent access of hydrogen peroxide to the manganese centre for catalytic reaction (steric effect). The axial ligands that are bound to the manganese centres also have some impact on the observed activity. Low activity of these complexes may be due to the strength that the axial ligand is bound to the manganese.

For catalytic dismutation of hydrogen peroxide by mononuclear seven-coordinate complexes we proposed a catalytic mechanism (Figure 4-3).

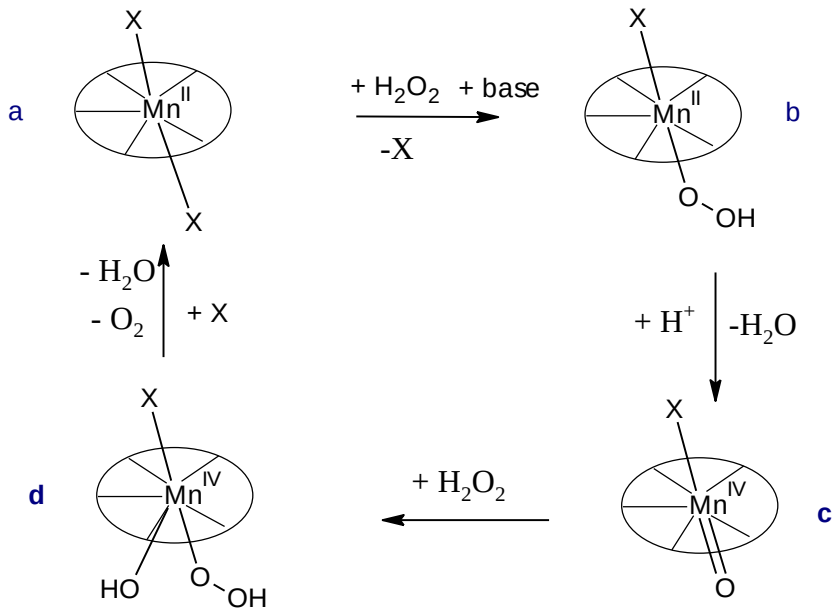

Figure 4-3 Proposed mechanism for dismutation of H_2O_2 by mononuclear seven-coordinate complexes (where X is axial ligands H_2O,Cl^-, NCS^- etc.).

In the proposed catalytic mechanism, the Mn(II) ion oscillates between oxidation states of two and four. In step a→b, hydrogen peroxide is deprotonated and displaces one of the axial ligands. In step b→c, bond cleavage of the hydroperoxide occurs by coupling protonation of the terminal hydroperoxide with Mn(II) oxidation to give the (O)=Mn(IV) species and releasing a free water molecule. The next step c→d involves binding and deprotonation of the second hydrogen peroxide molecule by the bound oxo group to give a terminally bound hydroperoxide anion species. In the final step d→a involves two-electron oxidation of the hyrdroperoxide to re-form the starting species and release the product O_2 molecule and a water molecule, completing the catalytic cycle. In the catalytic cycle, the axial ligands and presence of base have an important role. Deprotonation of hydrogen peroxide increases its donor ability to bind to a metal centre.[160] Dismukes *et al.* previously suggested that the binding of strong donors to the metal centre may affect the activation of the substrates.[168] Labile axial ligands such as water and chloride require less energy than less labile axial ligands such as thiocyanate and azide to be removed before the catalase reaction can begin.

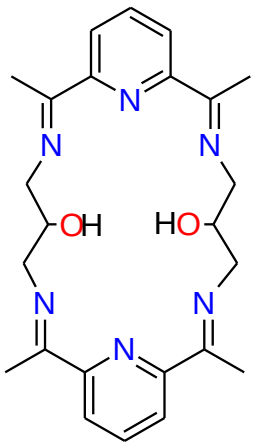

H_2A

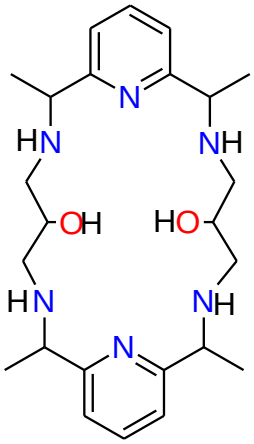

Red-H_2A

The catalase activity of the macrocyclic Mn(II) complexes derived from DAP have been tested previously by Leanne James using the same experimental procedure.[201] It was found that none of the complexes derived from H_2A showed any catalase activity in the absence of base (Table 4-2). Mn(II) complexes of H_2A with chloride and azide are similar with the fastest rate of 1.1 ml/s and approximately 7807 and 7830 molecules of H_2O_2 broken down after 60 seconds for each complex during the fastest rate of the activity, respectively. Mn(II) complexes of H_2A showed slower catalase activity than Mn(II) complexes of H_4L^*. As discussed in section 2.2.6, Mn(II) complexes of H_2A with chloride and azide have tetranuclear dimeric structures with pentagonal bipyramidal geometry around Mn(II) ions. The structures of the Mn(II) complexes of H_4L^* (complexes (4) and (4a)) are similar to chloride and azide complexes of H_2A and contain a tetranuclear macrocyclic unit with pentagonal bipyramidal geometry. Although, the geometry around Mn(II) centers for complexes derived H_2A and H_4L^* are same, Mn(II) complexes of H_2A showed higher catalase activity. Complex (4) contains $[MnCl_4]^{2-}$ as counter ion and shows higher catalase activity may be due to an extra manganese ion present in the structure. A significant increase in catalase activity was observed upon reduction of the imine bond in the H_2A macrocycle. The Mn(II) complex of red-H_2A with azide $[Mn_2(RedHA)(N_3)_2]_2(ClO_4)_2$ showed higher catalase activity than with chloride $[Mn_2(RedHA)Cl_2]_2[MnCl_4]$ although the chloride complex contains an extra manganese as a counter ion in the structure, $[MnCl_4]^{2-}$.

4.2.2 Catalase activity of acyclic Mn(II) complexes

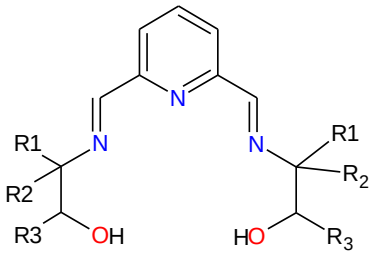

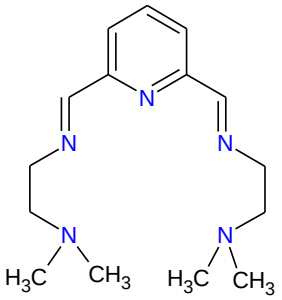

L5

H_2L4 $R_1=R_2=R3=H$

H_2L6 $R_1=R_2=H$ $R_3=CH_3$

H_2L7 $R_1=R_2=CH_3$ $R_3=H$

H_2L8 $R_1=CH_2CH_3$ $R_2=R_3=H$

Catalase activity of the complexes derived from acyclic ligands is illustrated in Figure 4-4 and Table 4-3. The results indicate that the mononuclear complex $[Mn(H_2L4)Cl_2]$ (7) shows the highest catalase activity with a rate of 6.67 ml/s during the fastest rate and approximately 5315 molecules of H_2O_2 broken down after one minute for each complex molecule. The complex which showed the least catalase activity was the dinuclear complex $[Mn_2(H_2L4)_2(NCS)_4]$ (8) with approximately 35 molecules of H_2O_2 broken during the fastest rate and no oxygen evolution was observed after one minute.

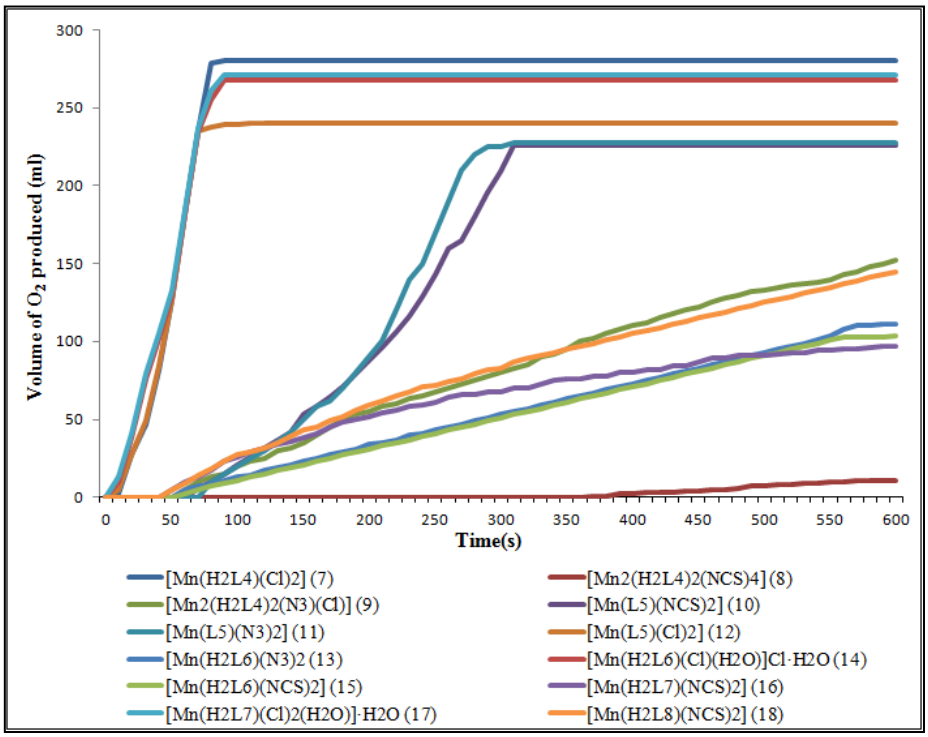

Figure 4-4 Catalase activity for acyclic complexes.

To explain why manganese complexes of H_2L4 show different catalase activity, structural details should be taken into account. Complexes $[Mn(H_2L4)Cl_2]$ (7), $[Mn_2(H_2L4)_2(NCS)_4]$ (8) and $[Mn_2(H_2L4)_2(N_3)_3Cl]$ (9) derived from H_2L4 ligand have different structures. Complex (7) is mononuclear containing five and seven-coordinate Mn(II) centres in the structure while complexes (8) and (9) are dinuclear, bridged by two H_2L4 ligands. The lower catalase activity of these two complexes could be attributed to less flexibility of the complex to form a required geometry for a catalase reaction. Another possibility for lower catalase activity may be due to strongly coordinated thiocyanate (8) and azide ligands (9).

Table 4-3 Rates and turnover numbers for acyclic complexes.

Complex		Fastest rate(ml/s)	Turnover Number*[a]	B	C
$[Mn(H_2L4)Cl_2]$	(7)	6.67	260	5315	14756
$[Mn_2(H_2L4)_2(NCS)_4]$	(8)	0.11	35	0	745
$[Mn_2(H_2L4)_2(N_3)_3Cl]$	(9)	0.57	7	0	9319
$[Mn(L5)(NCS)_2]$	(10)	2.21	89	0	9074
$[Mn(L5)(N_3)_2]$	(11)	2.52	94	0	8498
$[Mn(L5)Cl_2]$	(12)	6.31	227	4573	8642
$[Mn(H_2L6)(N_3)_2]$	(13)	5.12	191	0	9899
$[Mn(H_2L6)Cl(H_2O)]Cl{\cdot}H_2O$	(14)	0.33	23	0	7754
$[Mn(H_2L6)(NCS)_2]$	(15)	5.10	188	4798	9892
$[Mn(H_2L7)(NCS)_2]$	(16)	0.43	16	0	3932
$[Mn(H_2L7)Cl_2(H_2O)]{\cdot}H_2O$	(17)	0.45	18	202	3912
$[Mn(H_2L8)(NCS)_2]$	(18)	6.53	257	5245	10986

* = turnover number = maximum number of molecules of hydrogen peroxide converted to oxygen per molecule of complex[155,199] a = per second during the fastest part of the reaction, B = Number of H_2O_2 broken down after 60 seconds per complex, C = Total number of H_2O_2 broken down per molecule of complex after 10 min.

The mononuclear structures of the complexes of L5 are similar and the only difference is the axial ligands. The complex with axial chloride ligands (12) showed faster catalase activity than those complexes with thiocyanate (10) and azide (11) axial ligands which are more strongly coordinated to the Mn(II) centres than chloride ligands. As discussed in section 4.2.1 (see Figure 4-3) removal of the axial thiocyanate or azide ligands or at least one axial ligand

before the catalase reaction can take place requires more energy than removing the axial chloride ions. During the catalase activity of Mn(II) complexes of L5, reaction solutions became brown-red and at the end of reactions brown-black precipitates were observed. Brown-black precipitate may be due to decomposition of complexes and formation of insoluble manganese dioxide however no analysis was performed on brown-black material due to insufficient amount of the sample. In all other acyclic complexes formation of brown-black precipitate was not observed and reaction solutions remained yellow.

The structures of the complexes $[Mn(H_2L4)Cl_2]$ (7) and $[Mn(H_2L6)Cl(H_2O)]Cl{\cdot}H_2O$ (14) are quite similar; they both contain mononuclear seven-coordinate Mn(II) centres with approximate pentagonal bipyramidal geometry. The pentagonal planes comprise the N_3O_2 of the acyclic ligands and the axial positions are occupied by two chloride ions in complex (7) and one chloride ion and one water molecule in complex (14). Another difference is that one of the protons attached to the alcohol carbon atom in the ligand H_2L4 is replaced by methyl group in the ligand H_2L6. Both complex (7) and (14) showed catalase activity, but complex (7) has higher catalase activity than (14). Addition of two methyl groups in complex (14) may cause a steric effect and prevent the acces of hydrogen peroxide for the catalytic reaction and lead lower catalase activity.

Two complexes derived from H_2L7 differ in axial ligation. Complex $[Mn(H_2L7)(NCS)_2]$ (16) contains a seven-coordinate Mn(II) ion with approximate pentagonal bipyramidal geometry; the pentagonal plane consists of N_3O_2 donor atoms from the ligand. Axial positions are occupied by two thiocyanate ions. Complex $[Mn(H_2L7)Cl_2(H_2O)]{\cdot}H_2O$ (17) has a six-coordinate Mn(II) ion, coordinated to two three nitrogen atoms from the ligand, two chloride ions and one water molecule. Complex (17) shows higher catalase activity than complex (16). The reason for this may be due to fact that the coordinated chloride and water molecule are more labile than the thiocyanate ligand and require less energy to be removed before the catalase reaction can begin.

Overall, the mononuclear Mn(II) complexes derived from acyclic ligands containing coordinated exogenous water or chloride ligands show higher catalase activity than those with exogenous thiocyanate or azide ligands. Dinuclear Mn(II) complex $[Mn_2(H_2L4)_2(NCS)_4]$ (8) shows least catalase activity amongst these sets of complexes.

4.2.3 Catalase activity of Mn(II) complexes of H_2L9 and H_2L10

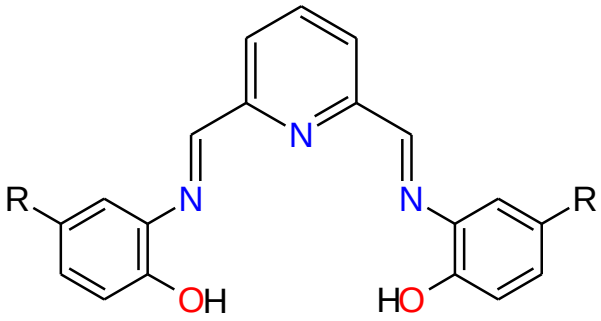

H_2L9 R=H

H_2L10 R=-CH_3

The catalase activities of Mn(II) complexes of H_2L9 and H_2L10 are illustrated in Figure 4-5 and Table 4-4. The graph displayed in Figure 4-5 shows the catalase activity for complexes with base and demonstrates differences in the curves obtained for catalase activity. The complexes do not show any catalase activity in the absence of base.

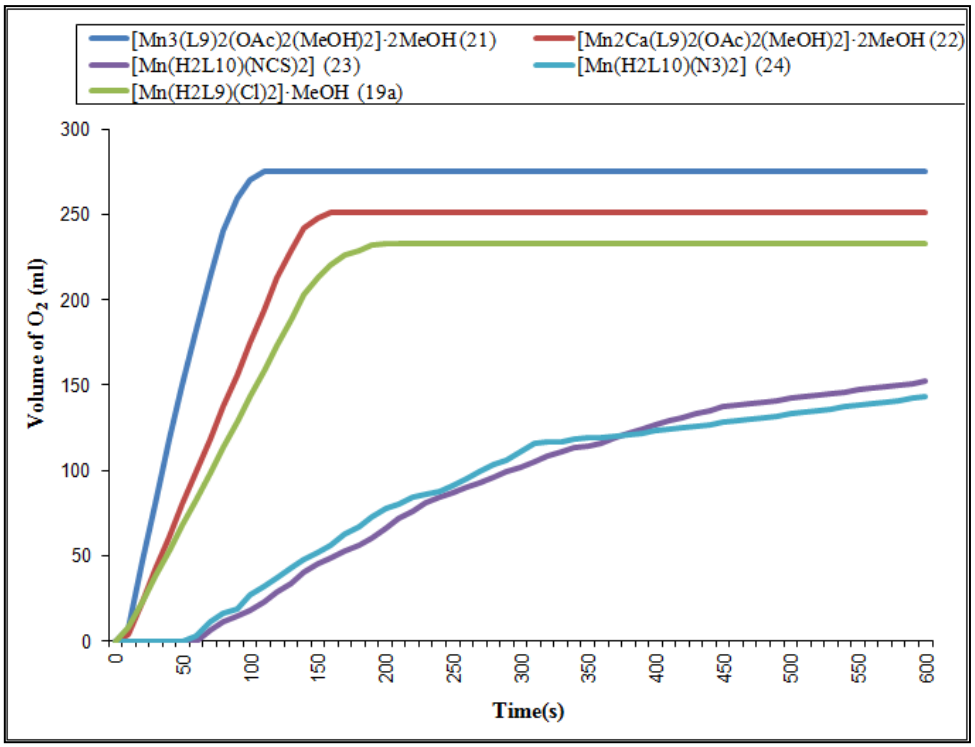

Figure 4-5 Catalase activity of complexes derived from H_2L9 and H_2L10.

Initial observations showed that the polynuclear complexes $[Mn_3(L9)_2(OAc)_2(MeOH)_2]\cdot 2MeOH$ (21) and $[Mn_2Ca(L9)_2(OAc)_2(MeOH)_2]\cdot 2MeOH$ (22) are more active than those mononuclear complexes $[Mn(H_2L10)(NCS)_2]$ (23),

$[Mn(H_2L10)(N_3)_2]$ (24) and $[Mn(H_2L9)Cl_2]\cdot MeOH$ (19a). The trinuclear complex (21) is the most efficient complex catalase mimic of the tested macrocyclic complexes with the fastest rate observed 5.33 ml/s and approximately 500 molecules of H_2O_2 broken down per second for each complex during the fastest rate of activity and approximately 17069 molecules of H_2O_2 broken down for each complex after completion of the reaction. The heteronuclear complex (22) showed slower catalase activity when compared to the trinuclear complex (21) with the fastest rate of 3.17 ml/s and approximately 293 molecules of H_2O_2 broken down per second for each complex during the fastest rate of the activity. The structures of complexes (21) and (22) are similar; the only difference is the central six-coordinate Mn(II) ion is replaced by a Ca(II) ion. Higher catalase activity of complex (21) can then be attributed to an extra manganese atom present in the structure. Neither complex showed an induction period; as soon as hydrogen peroxide was introduced to the reaction flask, oxygen gas evolution was observed.

Table 4-4 Rates and turnover numbers for the complexes of H_2L9 and H_2L10.

Complex		Fastest rate(ml/s)	Turnover Number*[a]	B	C
$[Mn_3(L9)_2(OAc)_2(MeOH)_2]\cdot 2MeOH$	(21)	5.33	500	17069	25791
$[Mn_2Ca(L9)_2(OAc)_2(MeOH)_2]\cdot MeOH$	(22)	3.17	293	9152	23204
$[Mn(H_2L9)Cl_2]\cdot MeOH$	(19a)	2.52	108	3551	9969
$[Mn(H_2L10)(NCS)_2]$	(23)	0.95	44	0	7068
$[Mn(H_2L10)(N_3)_2]$	(24)	1.01	44	131	6236

* = turnover number = maximum number of molecules of hydrogen peroxide converted to oxygen per molecule of complex[155,199] a = per second during the fastest part of the reaction, B = Number of H_2O_2 broken down after 60 seconds per complex, C = Total number of H_2O_2 broken down per molecule of complex after 10 min.

The structure of complexes (19a), (23) and (24) are similar, they are all mononuclear seven-coordinate Mn(II) complexes containing chloride, thiocyanate and azide located at the axial positions, respectively. Catalase test results showed that the axial ligands bound to the manganese centre have some impact on the observed rates. Complex (19a) showed highest catalase activity amongst these three mononuclear complexes with the fastest rate of 2.52 ml/s and approximately 108 molecules of H_2O_2 broken down per second during the fastest part of the reaction. Catalase activity was dramatically reduced in the presence of thiocyanate

and azide ligands at the axial positions. This trend would be anticipated due to the strength with which the axial ligand is bound to the manganese centre. Thiocyanate and azide ligands are more strongly bound to the manganese centre than chloride.

An expanded plot of the catalase data was generated to see more clearly how the induction period changes for different complex systems (Figure 4-6). The delay for complexes (23) and (24) may be due to a removal of the axial ligands or at least one axial ligand before the catalase reaction takes place. However, in the cases of complexes (21), (22) and (19a), immediate reactions were observed for each complex. Complexes (21) and (22) contain two methanol molecules that are coordinated to manganese centres at the axial positions and complex (19a) has two chloride ions that are coordinated to manganese at the axial positions. Removal of methanol and chloride ligands is much easier than removing thiocyanate and azide ligands.

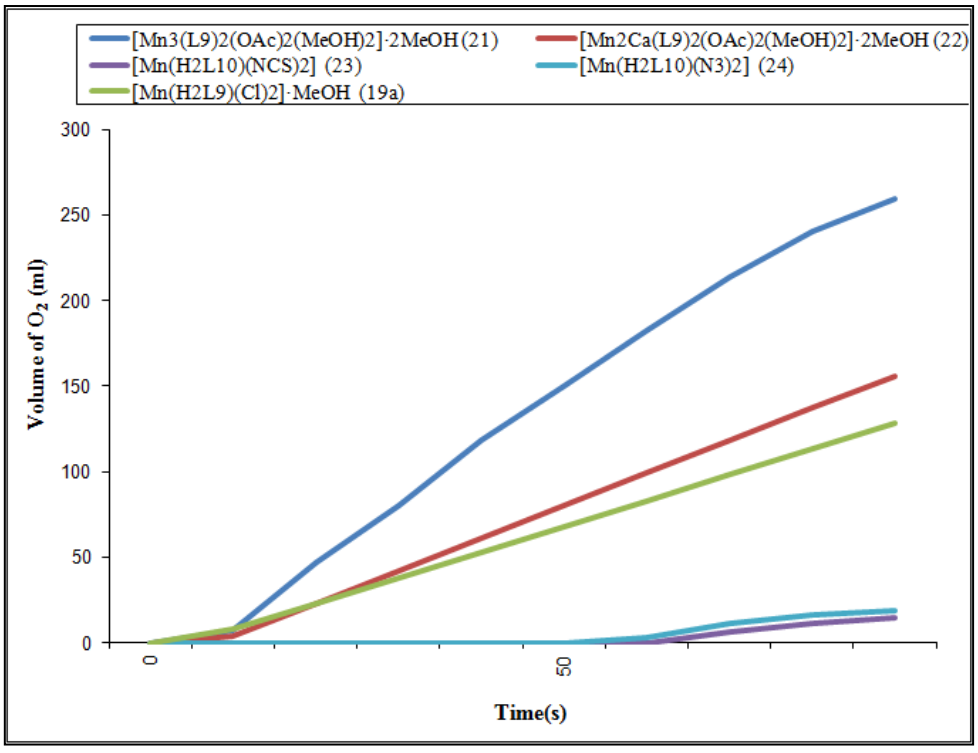

Figure 4-6 Induction period for catalase activity observed for complexes of H_2L9 and H_2L10.

4.2.4 Catalase activity of tripodal ligand complexes

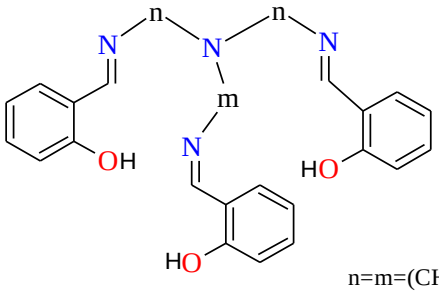

n=m=$(CH_2)_2$ **H_3L11**
n=$(CH_2)_2$ m=$(CH_2)_3$ **H_3L12**
n=$(CH_2)_3$ m=$(CH_2)_2$ **H_3L13**

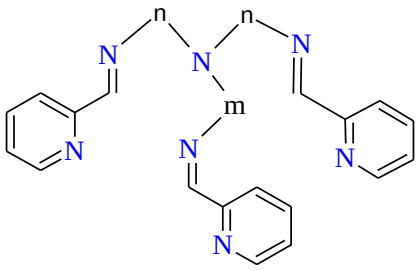

n=m=$(CH_2)_2$ **L15**
n=$(CH_2)_2$ m=$(CH_2)_3$ **L16**
n=$(CH_2)_3$ m=$(CH_2)_2$ **L17**
n=m=$(CH_2)_3$ **L18**

The catalase activity data for the manganese complexes of tripodal ligands are illustrated in Figure 4-7 and Table 4-5. The complex [Mn(L18)]$(ClO_4)_2$ (42) is the most efficient catalase mimic of those tripodal complexes and has been calculated to break down approximately 15935 molecules of hydrogen peroxide per molecule of complex. The complex [Mn(L15)]$(ClO_4)_2$ (41) is the least efficient catalyst amongst these tripodal manganese complexes which broke down 7255 molecules of hydrogen peroxide. Complex (42) was the only tripodal complex to show any catalase activity without base.

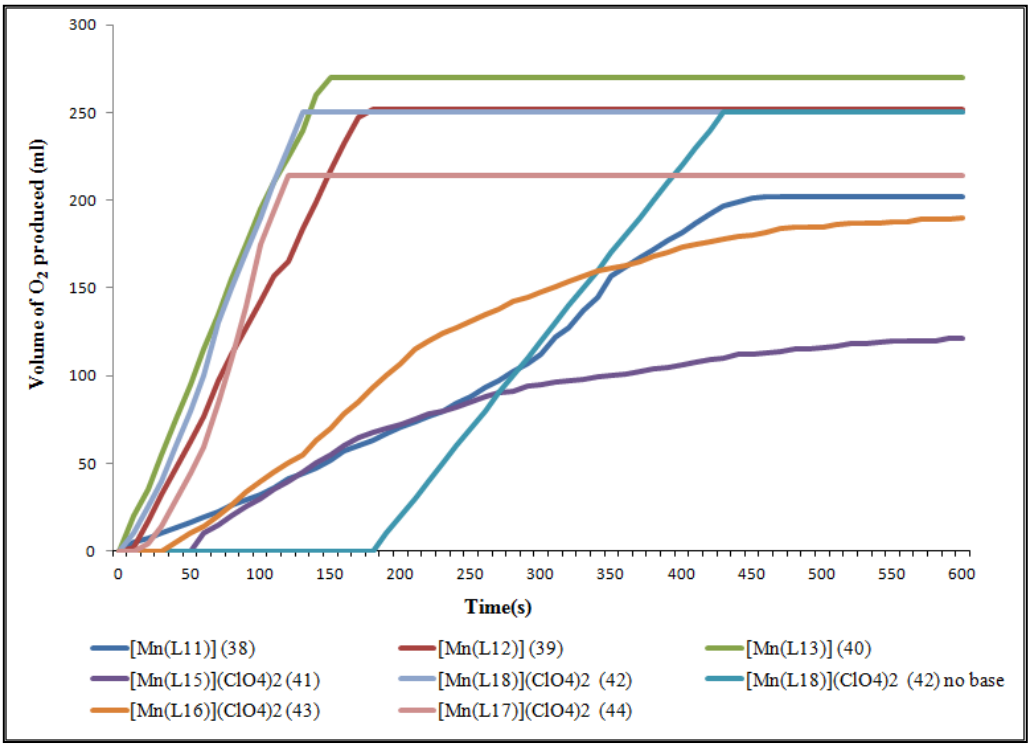

Figure 4-7 Catalase activity of tripodal ligand complexes.

Complexes (38)-(40) consist of tripodal Schiff base ligand derived from tripodal amines and salicyladehyde. The ligands coordinate to the metal centre *via* three imine nitrogen and three phenolate oxygen atoms. Complex (38) contains a symmetric Schiff base ligand with two carbon atoms in each arm of the tripod while (39) and (40) are asymmetric; the ligand in (39) with two arms containing a two carbon chain and the third arm has a three carbon chain; in (40) two arms contain two a three carbon chain and the third arm contains a two carbon chain. Complexes (38), (39) and (40) do not contain any counter ions and the mangenese ion has oxidation state of +3. From the catalase data, changing the arm size in those complexes has an effect on catalase activity. The symmetric complex (38) has the reaction rate of 1.16 ml/s and when one additional carbon atom introduced into one of the arms (complex 39), the rate increased more than 100% (2.66 ml/s). When one carbon atom was added to each of two arms (complex 40), an even higher reaction rate was obtained (3.16 ml/s).

Table 4-5 Rates and turnover numbers for tripodal ligand complexes.

Complex		Fastest rate(ml/s)	Turnover Number*[a]	B	C
[Mn(L11)]	(38)	1.16	53	872	9275
[Mn(L12)]	(39)	2.66	126	3632	11888
[Mn(L13)]	(40)	3.16	136	5570	13077
$[Mn(L15)](ClO_4)_2$	(41)	0.82	49	0	7255
$[Mn(L18)](ClO_4)_2$	(42)	3.66	240	6374	15935
$[Mn(L16](ClO_4)_2$	(43)	1.16	71	857	11632
$[Mn(L17)] (ClO_4)_2$	(44)	4.30	269	3686	13371
$[Mn(L18)](ClO_4)_2$ **	(42)	1.66	106	0	15932

* = turnover number = maximum number of molecules of hydrogen peroxide converted to oxygen per molecule of complex[155,199] a = per second during the fastest part of the reaction, B = Number of H_2O_2 broken down after 60 seconds per complex, C = Total number of H_2O_2 broken down per molecule of complex after 10 min., ** = no base added.

In the literature, Mn(III) complexes derived from tripodal tetraamine (tren) and several substituted salicyaldeyde derivatives have been tested for laundry bleaching applications. In laundry, bleach serves mainly to clean unwanted stains on fabric to achieve the intended cleaning effect.[202] Bleach may also be applied to destroy dyestuff in solution in order to prevent discoloration of fabrics by migrating dyestuff from coloured textiles (dye transfer

inhibition DTI). Laundry detergent usually contains percarbonate and perborate salts as bleach. These peroxy salts produce H_2O_2 when they are dissolved in washing liquor and the bleach activity of hydrogen peroxide is only sufficient at temperatures above 60 ºC. The research has been focused on catalytic systems being able to effectively activate hydrogen peroxide at low temperatures. Several granulated substituted manganese(III)saltren complexes have been incorporated in bleach booster and a powder detergent. Activated by peroxide, the catalyst has been found to be the most effective, bleaching between 30 and 60 ºC. These complexes bleach fabric and also fugitive dyes in solution. These tripodal Mn(III) complexes have been patented in US patent literature.[202] Asymmetric tripodal Mn(III) complexes [Mn(L12)] (39) and [Mn(L12)] (40) showed higher catalase activity than [Mn(L11)] (38) and these complexes can be applied in laundry bleaching processes.

Complexes (41)-(44) contain tripodal Schiff base ligands derived from tripodal amines and 2-pyridinecarboxaldeyde. Complexes (41) and (42) consists of symmetric tripodal ligands with two carbon atoms in each arm and three carbon atoms in each arm respectively while complexes (43) and (44) have asymmetric tripodal ligands. In complexes (41)-(44), perchlorate ions present in their structure balance the complex cations. As seen from the series (38)-(40), increasing the arm size of the tripodal ligands improved the catalase activity significantly. Complex (41) has a fastest rate of 0.82 ml/s, however, when one carbon atom was added to each arm, the rate increased significantly to 3.66 ml/s.

An expanded view of the induction periods shows some delay for each complex tested and no immediate reaction was observed for any of the complexes (Figure 4-8). The delay that is observed for each complex may be due to some rearrangement that is taking place within the ligand before catalase activity begins.

Complex (42) $[Mn(L18)](ClO_4)_2$ showed catalase activity without addition of base with a long induction period (Figure 4-9), but once catalytic activity occurs, it continues at a rate of 1.66 ml/s. The reason why this complex shows catalase activity and the others not without base could be attributed to the structure of the complex. The structures of complexes (41)-(44) are quite similar; however, the numbers of carbon atoms in the arms are different (Figure 3-5). Complex (42) has three carbon atoms in each arm in the ligand. This provides more flexibility for catalase activity. The arm size of the tripodal ligands can give rise to different geometry and coordination number around the metal centre. For example, while the Mn(II) complex of L15 is six-coordinate, Mn(II) complexes of L16 and L18 are

seven-coordinate. Changes in geometry and coordination number would affect catalase activity.

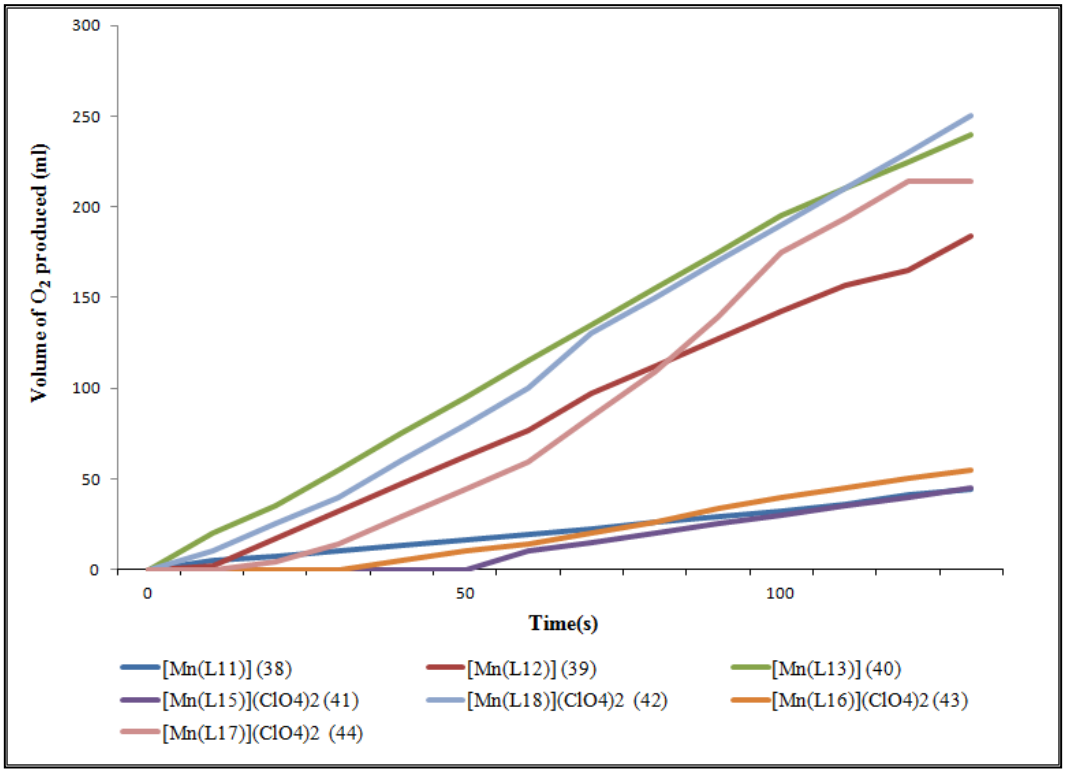

Figure 4-8 Delay for catalase activity observed of tripodal complexes.

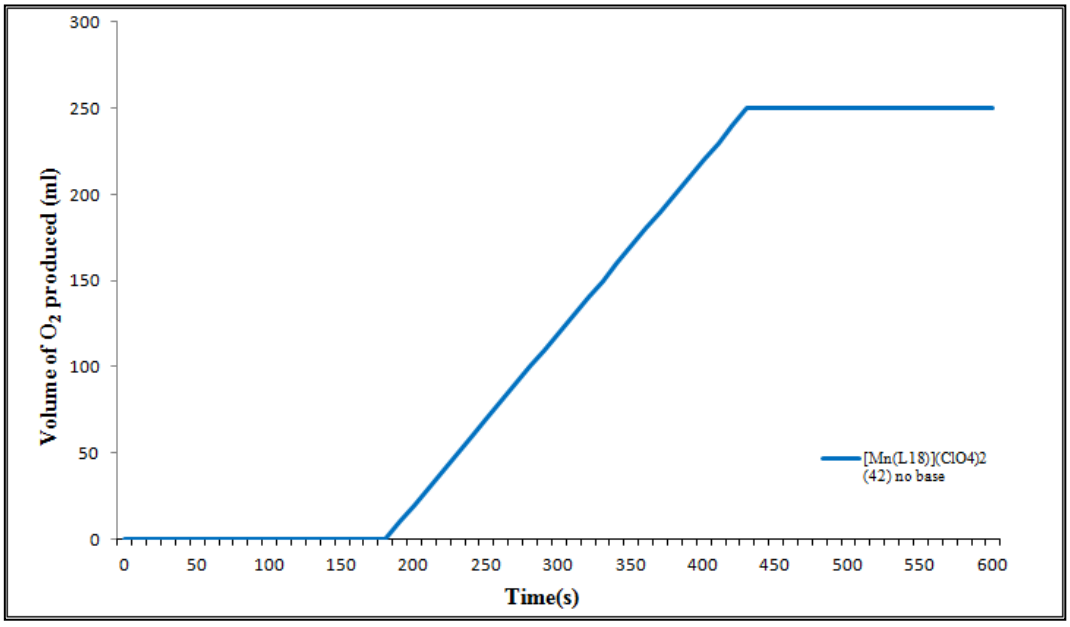

Figure 4-9 Catalase activity of complex (42) with no base.

4.2.5 Catalase activity of Mn(II) complexes of L19

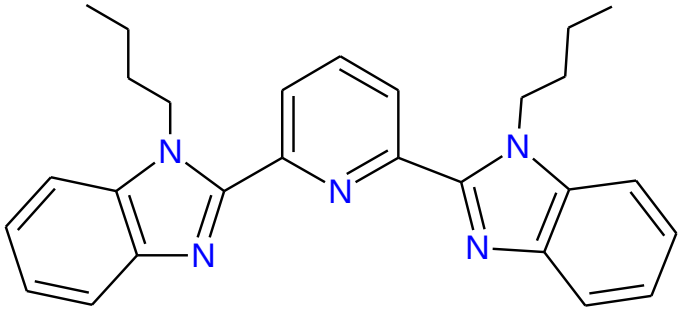

L19

Catalase activities of the manganese complexes of L19 are illustrated in Figure 4-10 and Table 4-6. Complex (47) $[Mn(L19)Cl_2]$ is the most efficient catalase mimic amongst the Mn(II) complexes prepared from the ligand L19 with a total of 12659 molecules of hydrogen peroxide broken down per complex molecule and the fastest rate of 1.34 ml/s^{-1}. During the first minute, 3263 molecules of hydrogen peroxide are broken down by complex (47). Complexes (48) $[Mn(L19)(NCS)_2]$ and (50) $[Mn(L19)(NO_3)_2]$ showed similar activity with totals of 11567 and 11553 molecules of hydrogen peroxide broken down per complex molecule, respectively. However, during the first minute, the number of hydrogen peroxide molecules broken down by complexes (48) and (50) are significantly less than complex (47). This could be attributed to strong binding of thiocyanate and chelate binding of nitro groups which do not allow hydrogen peroxide to approach the metal centre for the catalase reaction. Complexes (49) $[Mn(L19)_2](ClO_4)_2$ and (51) $[Mn(L19)_2](PF_6)_2$ do not show any activity during the first minute. Nevertheless, these two complexes show considerable catalase activity. During and after reactions with peroxide, all solutions remained light yellow. This indicates that these complexes both enhance catalytic disproportion of hydrogen peroxide and inhibit the formation of insoluble manganese dioxide.

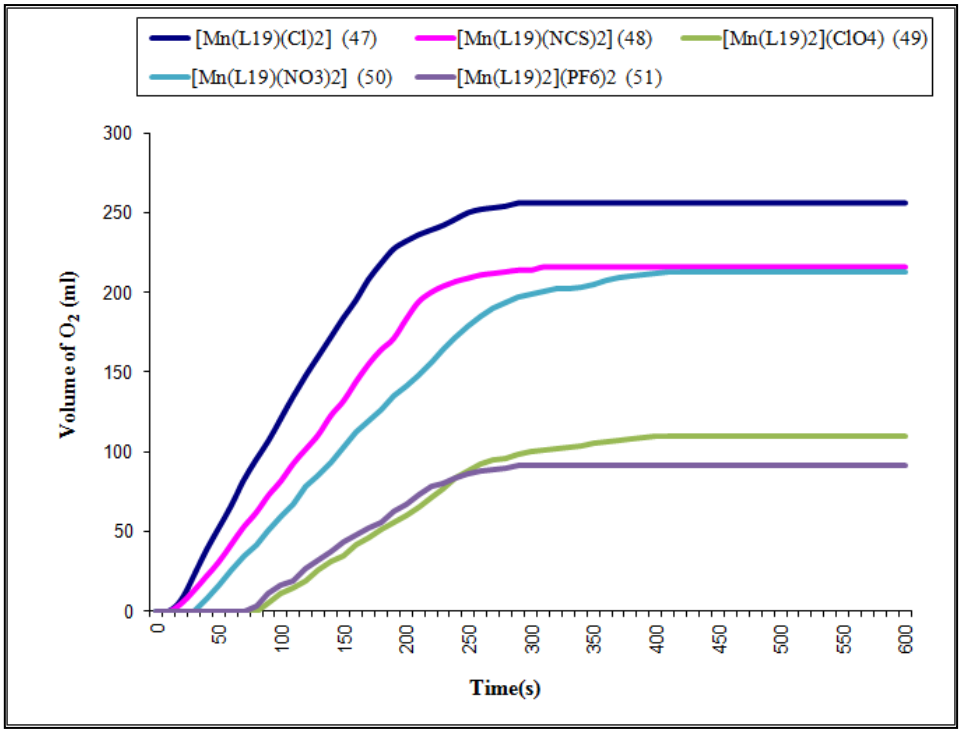

Figure 4-10 Catalase activity of complexes of L19.

Table 4-6 Rates and turnover numbers for complexes of L19.

Complex		Fastest rate(ml/s)	Turnover Number*[a]	B	C
$[Mn(L19)Cl_2]$	(47)	1.34	68	3263	12659
$[Mn(L19)(NCS)_2]$	(48)	1.01	56	2249	11567
$[Mn(L19)_2](ClO_4)_2$	(49)	0.52	53	0	5451
$[Mn(L19)(NO_3)_2]$	(50)	0.69	39	1410	11553
$[Mn(L19)_2](PF_6)_2$	(51)	0.52	58	0	4882

* = turnover number = maximum number of molecules of hydrogen peroxide converted to oxygen per molecule of complex[155,199] a = per second during the fastest part of the reaction, B = Number of H_2O_2 broken down after 60 seconds per complex, C = Total number of H_2O_2 broken down per molecule of complex after 10 min.

The diagram in Figure 4-11, clearly shows that there is some delay for each complex tested. The delay that is observed for these complexes may be due to some re-arrangement that is taking place within the structure before catalytic reactions take place. Complexes (49) and (51) showed the longest delays and this may be explained by the structures of these complexes. In the structure of complexes (49) and (51), Mn(II) centres are six-coordinate; bound to six nitrogens of two tridentate ligand L19. Before the catalytic reaction takes place,

there may be slow dissociation of the complex which causes the delay. Additionally, for complexes (49) and (51) catalase activity stopped after five minutes although there is still some hydrogen peroxide in the reaction solution. At the end of 30 mins, there was no sign of insoluble manganese dioxide formation and reaction solutions remained pale yellow. The reason why the catalase reaction stopped may be that the remaining hydrogen peroxide oxidises the ligand in the complex structure. Repeating catalase reactions for complexes (49) and (51) gave similar results.

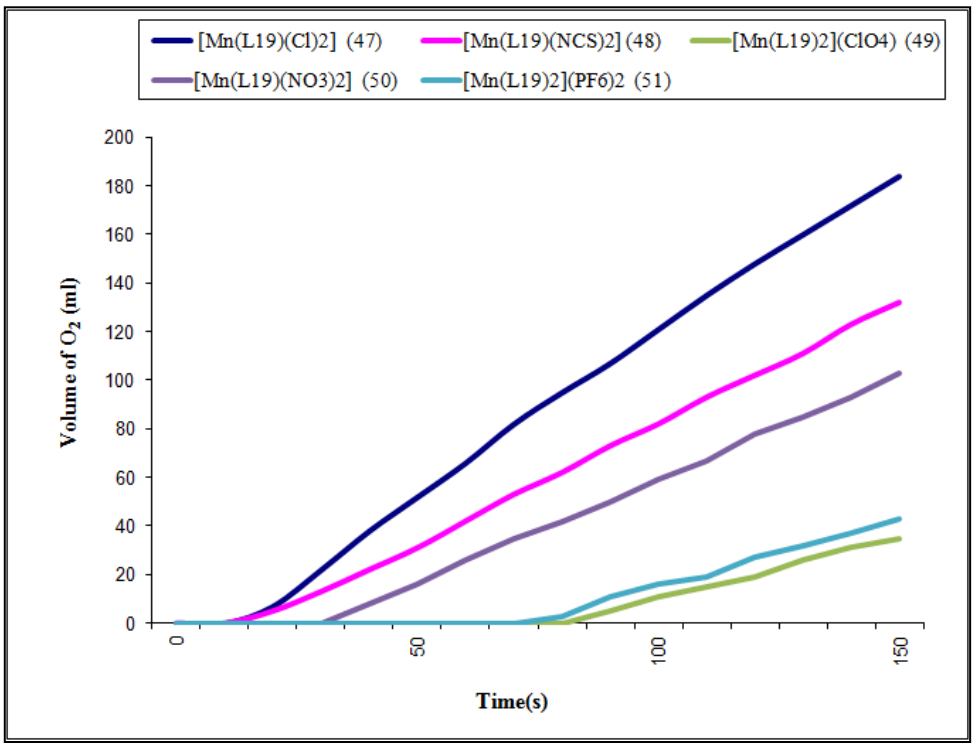

Figure 4-11 Delay for catalase activity observed for complexes of L19.

4.2.6 Conclusions for catalase activity

The catalase activity results of macrocyclic and acyclic ligands showed the effect that different ligands produced. Results also indicated that an increase in the number of manganese centres proves to be important. In addition to the structure of the ligand being important, there were similar complexes differing only in the type of axial ligands, suggesting that the dissociation constants of axial ligands are important and maybe the axial ligands are removed before hydrogen peroxide can be broken down. Most macrocyclic and acyclic complexes tend to show an induction period before oxygen was evolved from the reaction and this delay suggest that there is some rearrangement before catalase activity can begin.

The tripodal complexes showed high rates of catalase activity and the different arm lengths of the tripodal complexes result in different rates of activity. Changes in the arm size support the idea that the geometry of the complex is important for the catalase reaction. Generally, increase in the arm length of the tripodal complexes enhanced the catalytic rate of the reactions.

Most of the catalase mimics in the literature are based on dinuclear manganese complexes. It is informative to compare the catalytic rates of the complexes with the rates of other previously published complexes. Some turnover numbers for catalase activity obtained from the literature are given in Table 4-7.

Table 4-7 Catalase activity results of the reported in the literature.[160]

Complex	Turnover Number*
MnCat (*T. thermophilus*)	$2.6x10^5$
$Mn(ClO_4)_2 \cdot 6H_2O$	0.006
$[Mn_2(salpn)_2O_2]$	250
$[Mn(bpia)(\mu\text{-}OAc)]_2(ClO_4)_2$	1070
$[Mn_2(benzimpn)(\mu\text{-}OAc)](ClO_4)_2$	0.23
Mn_2(anthracenediporphyrine) complexes	1.5-6.1

* = turnover number = maximum number of molecules of hydrogen peroxide converted to oxygen per molecule of complex per second during the fastest part of the reaction.

MnCat from *T. thermophilus* has been found to show catalytic rates with turnover number $2.6x10^5$ and there is no synthetic complex having similar catalase activity to this natural enzyme. The most efficient catalase mimic to date was prepared by Pecoraro *et al.* This

complex contains a dinuclear Mn(II) centre and has a turnover number of 1070. The simple manganese perchlorate salt shows very low catalase activity with turnover number of 0.006.[160]

Catalase activities of the complexes described in this thesis shows turnover number between 5 and 500 and are a lot higher than simple manganese salts. The trinuclear acyclic complex $[Mn_3(L9)_2(OAc)_2(MeOH)_2]\cdot 2MeOH$ derived from 2,6-diformylpyridine and 2-aminophenol was found to be the most efficient catalase mimic of the tested complexes with approximately 500 molecules of H_2O_2 broken down per second for each complex during the fastest rate of activity.

4.3 SOD Activity

4.4 Measuring SOD activity

Measuring SOD activity is rather difficult, since the $O_2^{\cdot -}$ free radical has a short half-life in neutral aqueous solution. There are many direct and indirect methods reported for measuring the SOD activity. The most commonly used methods will be described and compared.

4.4.1 Direct analysis

The direct measurement of SOD activity falls into two categories: stopped-flow kinetic analysis and pulse radiolysis.[114] These methods provide precise measurement of the rate of dismutation of superoxide by observing the spectrophotometric decay of the superoxide anion directly in buffer solution. Pulse radiolysis methods often rely on a steady-state generation of superoxide, where the initial concentration of dissolved oxygen in water (which is about 100 μM under 1 atm of air at 25°C) is the limiting factor for superoxide flux. In this method, superoxide is produced by pulse irradiation of oxygen-saturated aqueous solutions in the presence of formate. The problems associated with cost and equipment limit the widespread use of this method.[114,117]

Riley *et al.* developed stopped-flow kinetic methods for measuring superoxide decay kinetics *via* spectrophotometric absorbance of superoxide at 245-270 nm.[117] In this method uncatalyzed decay of superoxide (second-order kinetics) can be distinguished from a catalyzed decay of superoxide (first-order kinetics) in the presence of a large excess of superoxide over the complex being screened. A second order catalytic rate constant (k_{cat}) can be obtained for an agent with true catalytic SOD activity by assessing the first order decay of superoxide at various concentrations of metal complex being evaluated. Direct assessment of a true k_{cat} could compare directly the SOD activities of enzymes and mimics under given conditions. Compounds which possess catalytic rates lower than $<10^{5.5}$ M^{-1} s^{-1} (at pH ≈ 7.4) cannot be determined by the stopped-flow technique due to second order self-dismutation of superoxide.[114]

In collaboration with Dr. David Worrall, attemps were made to use the stopped-flow technique to determine rate constants for superoxide dismutation by manganese complexes. The stopped-flow equipment was coupled with a fluorimeter which was used as the light source and an oscilloscope to allow faster measurement to be made. In the stopped-flow experiment, the intenstiy of light passing through the cell was recorded at 270 nm, so when

superoxide which absorbs light at 270 nm enters the mixing cell, the intensity of light hitting the detector is reduced and a decrease in voltage is recorded on the oscilloscope. The voltage then increases back to the base level reading as the superoxide is broken down. To test the stopped-flow set up, initial results were obtained for two complexes $[Mn_2(H_2A)Cl_2]_2(ClO_4)_2$ and $[Mn_2(H_2A)(N_3)_2]_2(ClO_4)_2$ prepared by a previous PhD student (Leanne James) in different concentrations. These complexes were tested using an indirect method (NBT) and showed considerable SOD activity (K_{cat} values of $7.7x10^6$ and $3.7x10^6$ $M^{-1}s^{-1}$ for $[Mn_2(H_2A)Cl_2]_2(ClO_4)_2$ and $[Mn_2(H_2A)(N_3)_2]_2(ClO_4)_2$, respectively).

Experimental

A solution of potassium superoxide was prepared under a nitrogen atmosphere. Potassium superoxide (0.20 g) and tertiary butyl ammonium perchlorate (1.70 g) were placed into a volumetric flask and 50 ml of dmso (analytical grade) was added. The solution was then placed into an ultrasonic bath for 20-30 mins. The yellow solution was then filtered to remove any excess solid potassium superoxide. The solution was covered with aluminium foil and stored in darkness to prevent decomposition. This procedure gives ~0.002 M $O_2^{\cdot -}$ in dmso.

A solution of complexes $[Mn_2(H_2A)Cl_2]_2(ClO_4)_2$ and $[Mn_2(H_2A)(N_3)_2]_2(ClO_4)_2$ ($1x10^{-4}$ M) were prepared in dmso. Different concentrations in the range $1x10^{-5}$ M to $1x10^{-7}$ M were prepared *via* several dilutions of the complex solutions.

During analysis, the superoxide solution and the complex solution were mixed in a 1:1 ratio and results were recorded on a Lecroy waverunner LT364 500mHz ossiloscope as voltage versus time at 270 nm. However, the catalytic rate for these complexes cannot be calculated by the stopped-flow technique as there was not a significant difference in the voltage rise back to the base level. Additionally, a 1:10 (superoxide solution:complex solution) ratio to get a large excess of superoxide over metal complex was used; again no difference in the voltage rise back was observed. This may be due to the reaction being completed on a scale that is too fast for the stopped-flow set up which has a mixing time of 30 ms. Due to the limited time, no further attempts were performed for setting up the instrument for direct measurement. Instead, a known indirect method was used for measuring the SOD activity of the complexes.

4.4.2 Indirect analysis

In "indirect" methods, superoxide is produced either enzymatically or chemically to react with indicator molecules which scavenge the free radical. After Fridovich and McCord developed an assay using cyctochrome *c*,[203] a number of indirect assays based on this method have been introduced to measure SOD activity.

Cyctochrome c and nitrobluetetrazolium (NBT) are the most commonly used redox indicators in a system using xanthine/xanthine oxidase to generate steady-state (continuous) low levels of superoxide. [114,204,205] The superoxide radical reduces the indicator and this gives a spectral change. If an added reagent reacts with $O_2^{\cdot -}$ this inhibits the reduction of the indicator by reducing the concentration of superoxide and this gives a measure of SOD activity. Indirect analysis can cause false positive results for SOD activity if the tested SOD mimic inhibits the production of superoxide or reacts stoichiometrically with superoxide. Additionally, side reactions may occur and interfere with measurements. So it is often argued that a true catalytic rate cannot be determined, and no direct comparisons can be made, between the k_{cat} value and activity obtained from indirect assays.[114]

Nitrobluetetrazolium (NBT) is commonly used as an indicator molecule because of its convenience and ease of use. On the other hand, NBT has some disadvantages such as poor water solubility of the formazan dye and the interaction with the reduced form of xanthine oxidase. In collaboration with Dr. Paul Lucas, we used 2-(4-iodophenyl)-5-(2,4-disulfophenyl)-2*H*-tetrazolium, monosodium salt (WST-1) which produces a water-soluble formazan dye upon reduction by the superoxide anion. The xanthine-xanthine oxidase system was used as a source of superoxide ($O_2^{\cdot -}$).[206-208]

In this method, xanthine oxidase aerobically oxidases xanthine to urate, producing $O_2^{\cdot -}$ in the process. WST-1 scavenges the $O_2^{\cdot -}$ formed in the reaction, which causes reduction of the colourless WST-1 to the yellow WST-1 formazan as illustrated in Figure 4-12. Since WST-1 formazan has a characteristic absorbance peak at 440 nm, the quantitative reduction of WST-1 to WST-1 formazan by $O_2^{\cdot -}$ was followed spectrophotometrically at 440 nm and 25 ^{o}C for 20 min. In the presence of the complex being tested, the absorbance values of the WST-1 formazan decrease. This is because the complex competes with the WST-1 to scavenge the $O_2^{\cdot -}$.[206-208]

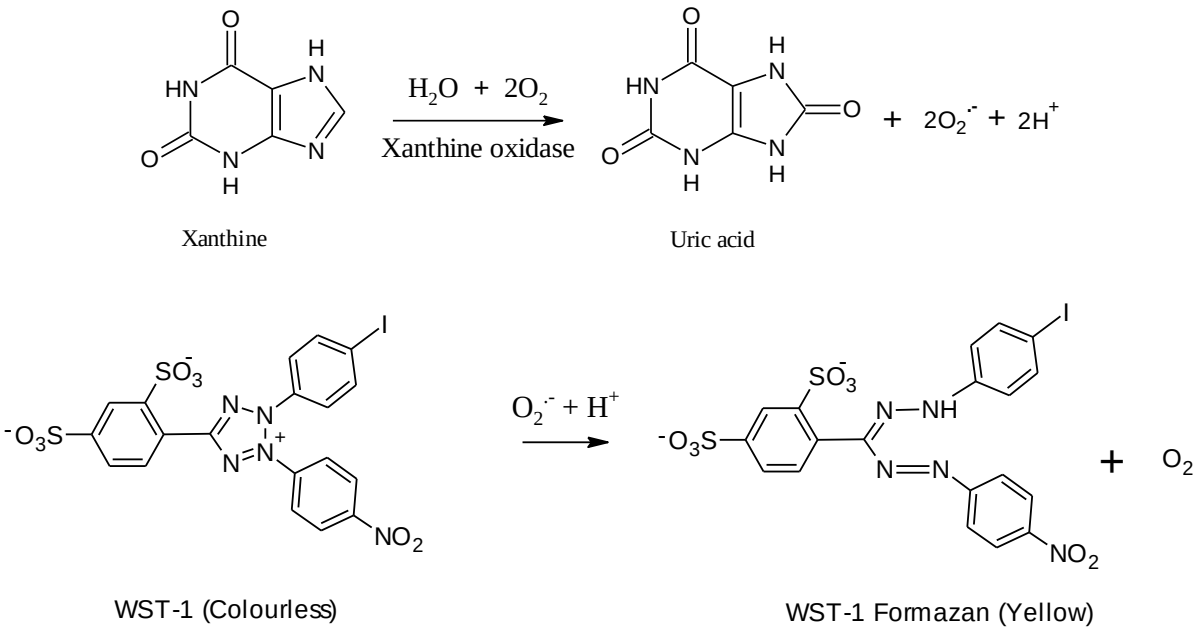

Figure 4-12 Generation of superoxide by the xanthine-xanthine oxidase system (top) and reaction of WST-1 with superoxide (bottom).[204]

The WST-1 assay is an indirect method of analysis because the extent of the reduction of the appearance of the yellow WST-1 formazan in the presence of a SOD mimic is taken as a measure of SOD activity.[202,203] This could introduce problems if side reactions occur that interfere with the measurements and then the true mechanism of the catalysis cannot be determined. On the other hand, the indirect method provides conditions that approximate better in *vivo* conditions than direct methods. The indirect method assumes that there are no side reactions occurring and that only the catalytic superoxide dismutation reaction is taking place.[114] A schematic representation of the method is illustrated in Figure 4-13.

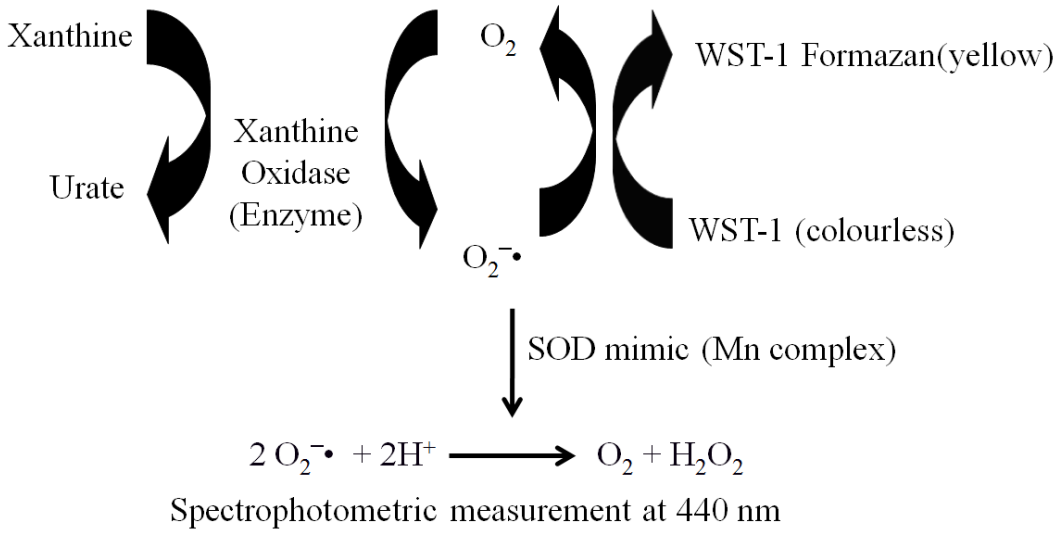

Figure 4-13 Schematic representation of the WST-1 indirect assay method.

4.5 SOD activity results&discussion

Experimental

WST SOD assay kits were purchased from Sigma-Aldrich Chemical Co. Ltd. and stored in the freezer at -80 °C. Solutions were protected from light using aluminium foil to prevent the degradation of any chemicals.

One WST assay kit contains:

- WST solution (5 ml)
- Enzyme solution (100 ml)
- Buffer solution (100 ml) (phosphate buffer pH=7.4)
- Dilution buffer (50 ml) (137 mM NaCl, 2.7 mM KCl, 1.47 mM KH_2PO_4, 8.1 mM Na_2HPO_4, pH=7.4)

Working solutions were prepared as follows:

The WST working solution was prepared daily. 1 ml of WST solution was diluted with 19 ml of buffer solution.

Enzyme working solution: The enzyme solution was centrifuged for 5 seconds and mixed by pipeting and then 15 ml of enzyme solution was diluted with 2.5 ml of dilution buffer. The

enzyme working solution was prepared daily and its activity was measured at the end of each day.

Solutions of the complexes to be tested were prepared at different concentrations ($2x10^{-4}$, $8x10^{-5}$, $6x10^{-5}$, $4x10^{-5}$ and $2x10^{-5}$ M) in dimethylsulfoxide. Dimethylsulfoxide was used as solvent since it does not affect the production of superoxide at concentrations up to 30 μM.

The prepared solutions were then added to 1 cm path length quartz cuvettes in varying amounts, as described in Table 4-8 below, using micropipettes.

Table 4-8 SOD activity test procedure.

	Sample	Blank 1	Blank 2	Blank 3
Complex solution	80 μl	-	80 μl	-
Dist. water	-	80 μl	-	80 μl
WST working solution	800 μl	800 μl	800 μl	800 μl
Enzyme working solution	80 μl	80 μl	-	-
Dilution buffer	-	-	80 μl	80 μl
Total volume (ml)	960 μl	960 μl	960 μl	960 μl

For each concentration of a tested complex, four absorbance readings (Sample, blank 1, blank 2, blank 3) were collected. **Sample**: The WST working solution was mixed with enzyme working solution followed by addition of a complex solution. The complex competes with the WST-1 to scavenge the $O_2^{\cdot -}$. Absorbance changes at 440 nm were recorded on a Shimadzo UV-Vis 1201 spectrophotometer.

Blank 1: WST working solution is mixed with enzyme working solution followed by addition of distilled water. Superoxide is produced continuously by the enzyme system and reacts with WST-1 to form yellow WST-1 formazan in the absence of metal complex.

Blank 2: WST working solution is mixed with dilution buffer followed by addition of complex solution. Superoxide is not produced since no enzyme solution was added. Blank 2 measurements are taken to see any absorbance change at 440 nm in the absence of superoxide.

Blank 3: WST working solution is mixed with dilution buffer followed by addition of distilled water. Superoxide is not produced since no enzyme solution was added. Blank 3 measurements are taken to see any absorbance change at 440 nm in the absence of superoxide or a metal complex.

A plot of absorbance values at 440 nm versus time was obtained for each tested complex at different concentrations. One example of an absorbance versus time plot is shown in Figure 4-14. All SOD testing data and calculations are given in the Appendix CD.

For the blank 1 reading, which contains no SOD mimic, the rate of the change of absorbance is 0.055 per minute, and reflects the rate of formation of superoxide ($O_2^{\cdot-}$) without any complex added. Blank 1 was then used to calculate the % inhibition of WST-1 in the presence of a complex. When the inhibition of WST is 100%, then the rate of change of absorbance is equal to 0, and when there is 0% inhibition, the rate of change of absorbance is equal to the slope of the blank 1.

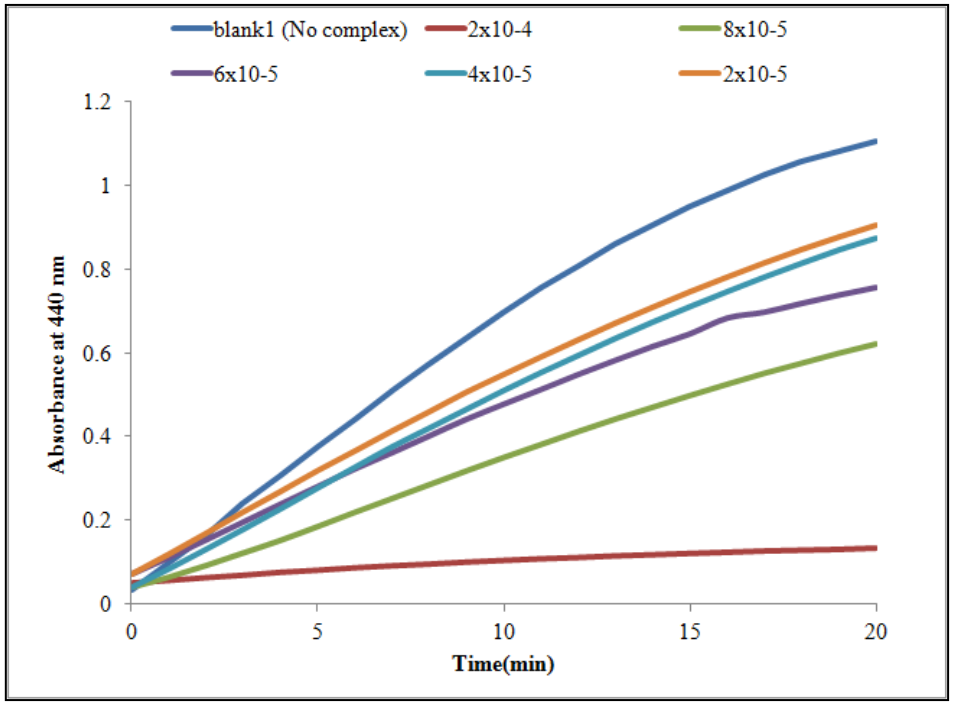

Figure 4-14 Absorbance versus time graph at 440 nm with increasing concentration of $[Mn_4(H_2L^*)Cl_4][MnCl_4]$.

The % inhibition for each concentration is then calculated as shown below:

SOD activitiy (inhibition %)= {[(S1-S3)-(SS-S2)]/(S1-S3)}x100

Where S1 = slope of blank 1, S2 = slope of blank 2, S3 = slope of blank3 and SS = slope of sample.

After calculating % inhibition for each concentration, an inhibition versus concentration graph was produced as shown in Figure 4-15. The graph is then used to calculate the half maximal inhibitory concentration referred to as IC_{50} value, which is derived from linear regression analyses and given as concentration (μM) equivalent to 1 unit of SOD activity. The IC_{50} value is calculated by using the line equation (y = mx+n, where y = % inhibition and x = concentration). Substituting a value of 50 for y and then solving for x allows calculation of what concentration of sample is equivalent to 50% inhibition. One unit of SOD activity is the concentration of the complex that causes 50% inhibition of WST-1.

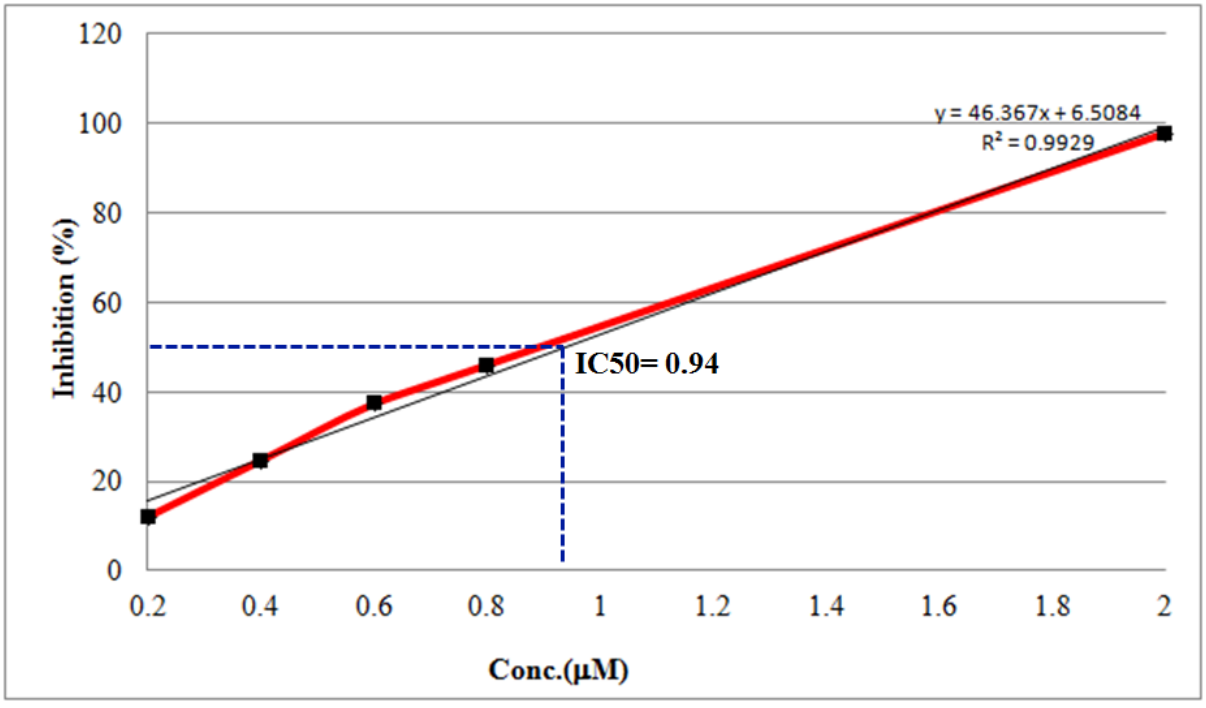

Figure 4-15 Graph of inhibition (%) versus concentration of complex $[Mn_4(H_2L^*)Cl_4][MnCl_4]$.

The IC_{50} values obtained are dependent upon the indicator used and concentration of the indicator [WST] can be used to calculate rate constant K_{cat} using the calculation proposed by McCord and Fridovich shown in the following equation.

$$K_{cat}=K_{WST\text{-}1} \text{ x } [\text{WST-1}]/IC_{50}$$

where; K_{cat}: rate constant $K_{WST\text{-}1}$: rate of WST-1 reduction: $3.7x10^{4}$ $mol^{-1}L$ s^{-1} (pH 8), [WST-1]: concentration of WST-1.[204]

K_{cat} values are independent of both the nature and concentration of indicator used. Therefore, the calculated values will be more appropriate for comparison with literature values.

4.5.1 SOD activity of macrocyclic complexes

SOD enzymes and mimic complexes catalyze the dismutation of superoxide and hydrogen peroxide in a ping-pong mechanism where the metal cycles between oxidised and reduced forms (Figure 4-16).

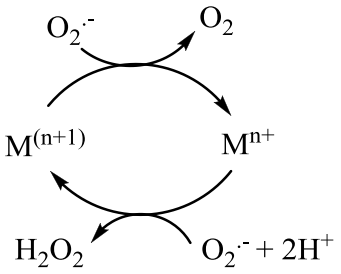

Figure 4-16 Dismutation of superoxide

As discussed in section 1.4.3, Riley *et al.* proposed the catalytic cycle for seven-coordinate Mn(II) complexes as SOD mimics shown in Figure 4-17.[147,149] Riley suggested two reaction pathways; a pH-independent inner-sphere pathway and a pH-dependent, outer-sphere pathway. In both the inner-sphere and outer-sphere pathways, formation of six-coordinate intermediate species by removing one of the axial ligands is necessary to start the catalytic reaction. Therefore, the ease of dissociation of the axial ligands is important. Weakly bound axial ligands such as chloride and water are expected to dissociate easily. However, the removal of strongly bound axial ligands such as thiocynate and azide requires more energy.

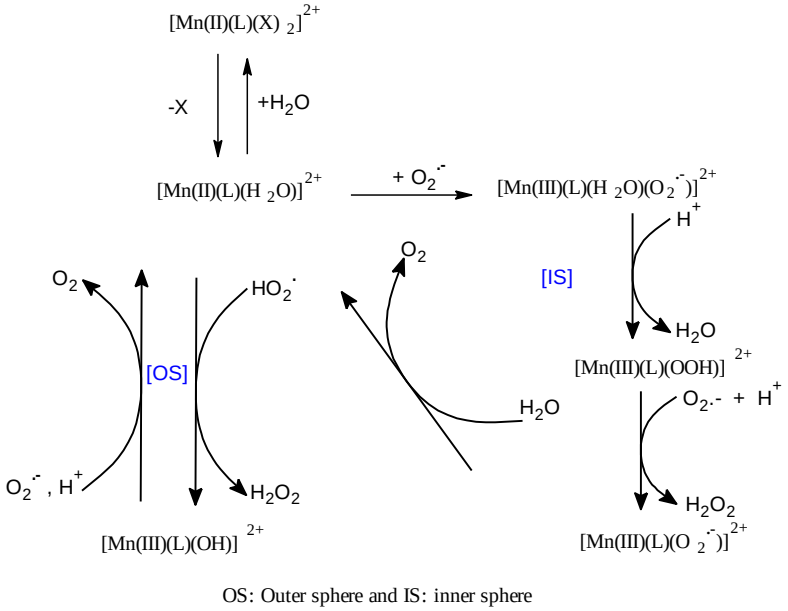

OS: Outer sphere and IS: inner sphere

Figure 4-17 Proposed catalytic cycle for synthetic SOD mimics.

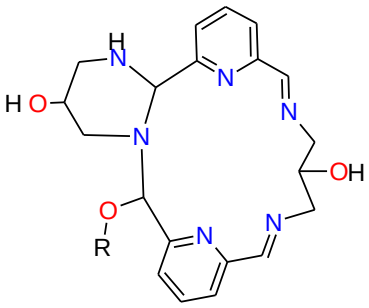

H_3L2 R= -CH_3
H_3L3 R= -CH_2CH_3

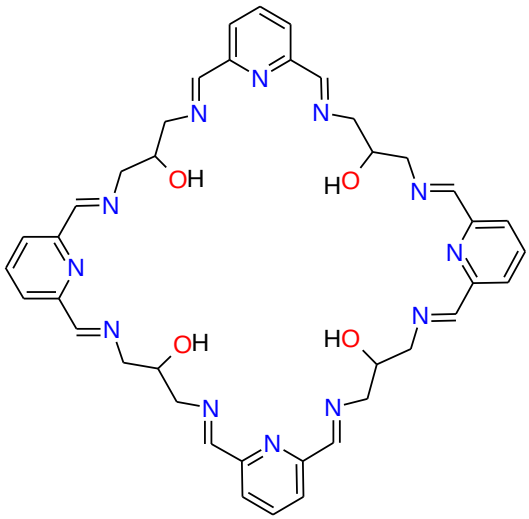

H_4L*

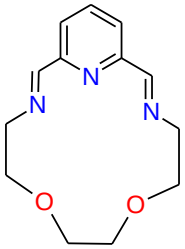

L4

Table 4-9 SOD activity results of the macrocyclic complexes.

Complex		IC_{50} (μM) (WST-1 assay)	K_{cat} (M^{-1} s^{-1})
$[Mn(H_3L2)(NCS)_2]$	(2)	1.78	$8.98x10^5$
$[Mn(H_3L3)(NCS)_2]$	(3)	1.87	$8.56x10^5$
$[Mn_4(H_2L^*)Cl_4][MnCl_4]$	(4)	0.94	$1.18x10^6$
$[Mn_4(H_2L^*)Cl_4](ClO_4)_2$	(4a)	1.13	$9.82x10^5$
$[Mn(L4)(NCS)_2]$	(5)	2.00	$1.19x10^5$

The SOD activities of the macrocyclic complexes are presented in Table 4-9. For the tested complexes, $[Mn_4(H_2L^*)Cl_4][MnCl_4]$ (4) showed the greatest activity as SOD mimic displaying an IC_{50} value of 0.94 μM which gives a calculated K_{cat} value of $1.18x10^6$ $M^{-1}s^{-1}$. The complex $[Mn_4(H_2L^*)Cl_4](ClO_4)_2$ (4a) containing the same macrocyclic structure also showed high activity with a K_{cat} value of $9.82x10^5$ $M^{-1}s^{-1}$. Higher SOD activity of $[Mn_4(H_2L^*)Cl_4][MnCl_4]$ (4) can be attributed to the extra Mn(II) ion in the structure (as a counter ion $[MnCl_4]^{2-}$). Ring-contracted complexes $[Mn(H_3L2)(NCS)_2]\cdot MeOH$ (2) and $[Mn(H_3L3)(NCS)_2]\cdot EtOH$ (3) were found to possess catalytic activity with K_{cat} values of $6.21x10^5$ and $5.90x10^5$ $M^{-1}s^{-1}$ respectively. The reason why the ring-contracted complexes showed lower rates than complexes (4) and (4a) may be attributed to the strongly bound thiocyanate axial ligand or having only one manganese ion per complex molecule. Thus results may suggest that the ease of dissociation of the axial ligands is important and the axial ligands may be substituted by the incoming superoxide ion. A thiocynate ligand binds to

manganese centres more strongly than a chloride ligand, thus a chloride ligand is expected to dissociate more readily from manganese than a thiocyanate ligand. The complex $[Mn(L4)(NCS)_2]$ (5) showed the least SOD activity amongst the macrocyclic complexes tested here, with a K_{cat} value of $1.19x10^5$ M^{-1} s^{-1}.

SOD dismutase activity of the complexes derived from DAP analogues and ring-contracted complexes have been tested previously by Dr. A. Kellet and Prof. M. Devereux at the Dublin Institue of Technology using the NBT assay (Table 4-10).[201] Kinetic rates of ring-contracted complexes using NBT assay were similar to those obtained from WST-1 assay. However, IC_{50} values are higher in the case of NBT assay; this is because the indicator concentration in the case of NBT assay was higher than WST-1 assay. As discussed in section 4.2.1, the ring-contracted complexes have been found to show limited catalase activity. However, they have shown reasonable superoxide dismutase activity by using both NBT and WST-1 assays. These compounds have the potential for use in research as anticancer compounds. All the other macrocyclic complexes have shown both catalase and superoxide dismutase activity.

Table 4-10 SOD activity results of the reported macrocyclic complexes.[201]

Complex	IC_{50} (μM) (NBT assay)	k_{cat} (M^{-1} s^{-1})
$[Mn_2(H_2A)Cl_2]_2(ClO_4)_2$	0.77	$7.7x10^6$
$[Mn_2(H_2A)(N_3)_2]_2(ClO_4)_2$	1.53	$3.7x10^6$
$[Mn_4(A^*)(ClO)_4]$	1.30	$4.6x10^6$
$[Mn(H_3L2)(NCS)_2]$	2.70	$2.2x10^6$
$[Mn(H_3L3)(NCS)_2]$	3.77	$1.6x10^6$

The SOD activity of the complexes derived from DAP analogues showed a higher catalytic rate than the complexes derived from DFP analogues prepared in this thesis. The structures of the complexes $[Mn_2(H_2A)Cl_2]_2(ClO_4)_2$ and $[Mn_2(H_2A)(N_3)_2]_2(ClO_4)_2$ contain two [2+2] macrocyclic units linked by two chloride and azide bridges between manganese centres. During the catalytic reaction these links may be broken and each macrocyclic unit is involved in the dismutation of superoxide. The Mn(II) ions in complex $[Mn_4(A^*)(ClO)_4]$ are held tightly in the cubane structure but the perchlorate ions are coordinated weakly to the Mn(II) centres and these can dissociate easily for the catalytic reaction.

4.5.2 SOD activity of acyclic Mn(II) complexes

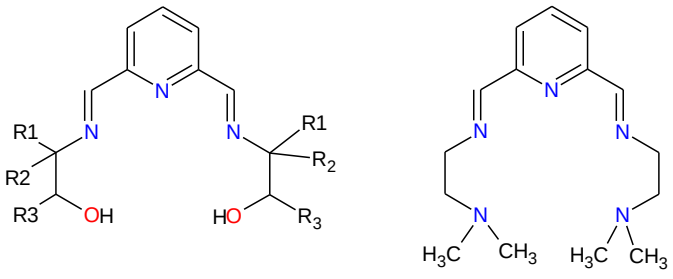

H_2L4 $R_1=R_2=R3=H$

H_2L6 $R_1=R_2=H$ $R_3=CH_3$

H_2L7 $R_1=R_2=CH_3$ $R_3=H$

H_2L8 $R_1=CH_2CH_3$ $R_2=R_3=H$

L5

The SOD test results for acyclic complexes are presented in Table 4-11. Mn(II) complexes prepared from acyclic ligands have shown high superoxide dismutase activity except for $[Mn_2(H_2L6)_2(N_3)_4]$ (13) which showed no activity. The mononuclear complex $[Mn(H_2L6)Cl(H_2O)]Cl{\cdot}H_2O$ (14) shows the highest SOD activity with a rate constant of $2.05x10^6$ $M^{-1}s^{-1}$ and the IC_{50} value of 0.78 μM. The complex which showed the lowest rate was the dinuclear complex $Mn_2(H_2L4)_2(NCS)_4$ (8) with a rate of 5.86x105 $M^{-1}s^{-1}$ and IC_{50} value of 2.04 μM. There is a slight increase in the catalytic rate observed in all complexes when chloride or water ligands coordinate to the metal centres.

The complex $[Mn(H_2L4)Cl_2]$ (7) contains five- and seven-coordinate Mn(II) centres in the structure while complexes $Mn_2(H_2L4)_2(NCS)_4$ (8) and $[Mn_2(H_2L4)_2(N_3)_3Cl]$ (9) are dinuclear complexes bridged by two H_2L4 ligands. Lower SOD activity of these two complexes could be attributed to reduced flexibility of the ligand to form a required geometry for the catalytic reaction. Removal of the axial thiocyanate or azide ligands or at least one axial ligand requires more energy than removing the axial chloride ions to form the required geometry for catalytic reaction.

Table 4-11 SOD activity results of the acyclic complexes.

Complex		IC_{50} (μM) WST-1 assay	k_{cat} (M^{-1} s^{-1})
$[Mn(H_2L4)Cl_2]$	(7)	0.87	$1.30x10^6$
$Mn_2(H_2L4)_2(NCS)_4$	(8)	2.04	$5.86x10^5$
$[Mn_2(H_2L4)_2(N_3)_3Cl]$	(9)	1.44	$8.29x10^5$
$[Mn(L5)(NCS)_2]$	(10)	1.27	$1.15x10^6$
$[Mn(L5)(N_3)_2]$	(11)	1.23	$8.99x10^5$
$[Mn(L5)Cl_2]$	(12)	0.89	$1.24x10^6$
$[Mn(H_2L6)\ (N_3)_2]$	(13)	No measuble activity	-
$[Mn(H_2L6)Cl(H_2O)]Cl{\cdot}H_2O$	(14)	0.78	$2.05x10^6$
$[Mn(H_2L6)(NCS)_2]$	(15)	2.39	$6.70x10^5$
$[Mn(H_2L7)(NCS)_2]$	(16)	1.47	$1.09x10^6$
$[Mn(H_2L7)Cl_2(H_2O)]{\cdot}H_2O$	(17)	1.13	$1.42x10^6$
$[Mn(H_2L8)(NCS)_2]$	(18)	1.21	$1.32x10^6$

The complexes of L5 showed very similar SOD activity. The structures of the complexes of L5 are similar, where the only difference is the axial ligands. Results showed that axial ligands did not have that much effect on the activity of complexes of L5. When looking closely at the structures of these complexes, Mn-N (tertiary amine) distances are rather long (2.5-2.7 Å). Dissociation of one of the Mn-N (tertiary amine) bonds may be providing extra conformational flexibility for catalytic reaction.

The complex $[Mn(H_2L6)(N_3)_2]$ (13) did not show any SOD activity. However, two other complexes $[Mn(H_2L6)Cl(H_2O)]Cl{\cdot}H_2O$ (14)and $[Mn(H_2L6)(NCS)_2]$ (15) derived from H_2L6 have been found to show considerable catalytic activity. Complex (13) contains a seven-coordinate Mn(II) centre with two azide ligands at the axial positions. The azide ligands probably have an effect on flexibility of the complex for catalytic reaction. However, complexes (14) and (15) consist of mononuclear seven-coordinate Mn(II) ions. Dissociation of one of the axial ligands provides the conformational re-arrangement for catalytic reaction. The structures of two complexes derived from H_2L7 are different from each other. The complex $[Mn(H_2L7)(NCS)_2]$ (16) contains a seven-coordinate Mn(II) ion with approximate

pentagonal bipyramidal geometry with axial two thiocyanate ions. The complex $[Mn(H_2L7)Cl_2(H_2O)]\cdot H_2O$ (17) contains a six-coordinate Mn(II) ion bound to three nitrogen atoms from the ligand, two chloride ions and one water molecule. Complex (17) shows slightly higher SOD activity than complex (16). The reason for this may be due to strongly bound thiocyanate ligands.

Overall, Mn(II) complexes derived from acyclic ligands containing coordinated exogenous water or chloride ligands show higher SOD activity than those with exogenous thiocyanate or azide ligands.

4.5.3 SOD activity of Mn(II) complexes of H_2L9 and H_2L10

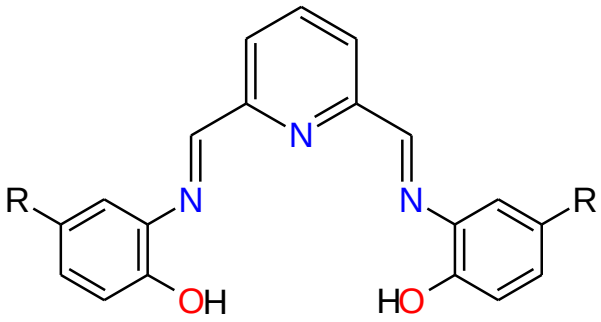

H_2L9 R=H

H_2L10 R=-CH_3

The SOD activity of the complexes of H_2L9 and H_2L10 are presented in Table 4-12. The mononuclear complex $[Mn(H_2L9)Cl_2]\cdot MeOH$ (19a) showed the greatest SOD activity with an IC_{50} value of 0.95 μM which gives a calculated K_{cat} value of $1.67x10^6$ $M^{-1}s^{-1}$. The complexes $[Mn(H_2L10)(NCS)_2]$ (23) and $[Mn(H_2L10)(N_3)_2]$ (24) do not show any measurable SOD activity. The structures of (19a), (23) and (24) are similar; they are all mononuclear and contain seven-coordinate Mn(II) centres. The only difference is axial ligands; axial positions are occupied by two chloride ions in (19a), two N-bound thiocycnate ions in (23) and two azide ions in (24). Riley *et al.* proposed a catalytic cycle (discussed in section 1.4.3) for seven-coordinate complexes. In this catalytic cycle, the loss of one of the axial ligand from a seven-coordinate complex produces a six-coordinate intermediate which enters the catalytic cycle. Thiocyanate and azide ligands coordinate to manganese centres at the axial positions more strongly than a chloride ligand, thus a chloride ligand is expected to dissociate more readily from manganese than thiocyanate and azide ligands. The H_2L10 ligand contains an extra methyl groups at the para positions of the phenol rings. This may

also change the conformational flexibility of the ligand to form a six-coordinate intermediate for the catalytic cycle.

Table 4-12 SOD activity results of the complexes of H_2L9 and H_2L10.

Complex		IC_{50} (μM) (WST-1 assay)	k_{cat} ($M^{-1}s^{-1}$)
$[Mn_3(L9)_2(OAc)_2(MeOH)_2]\cdot 2MeOH$	(21)	1.01	$9.05x10^5$
$[Mn_2Ca(L9)_2(OAc)_2(MeOH)_2]\cdot 2MeOH$	(22)	1.09	$1.47x10^6$
$[Mn(H_2L9)Cl_2]\cdot MeOH$	(19a)	0.95	$1.67x10^6$
$[Mn(H_2L10)(NCS)_2]$	(23)	No measuble activity	-
$[Mn(H_2L10)(N_3)_2]$	(24)	No measuble activity	-

Complexes (21) and (22) have been found to show similar SOD activity with the rates of $9.05x10^5$ and $1.47x10^6$ $M^{-1}s^{-1}$, respectively. The structure of complex (21) contain two seven-coordinate Mn(II) acyclic unit joined by a third six-coordinate Mn(II) ion. In complex (22) the central six-coordinate Mn(II) ion is replaced by a Ca(II) ion. In both complexes axial positions of the seven-coordinate Mn(II) ions are occupied by an oxygen atom of an acetate group and a methanol molecule. Releasing the coordinated methanol molecule for the catalytic reaction is easier than acetate groups because the acetate ligand is stronger ligand than the methanol ligand and it also bridges two metal centres. The complex containg the Ca(II) ion (22) showed a slightly higher catalytic rate than complex (21). The result indicates that the central Mn(II) ion in complex (21) is not involved in the catalytic reaction.

4.5.4 SOD activity of tripodal ligand complexes

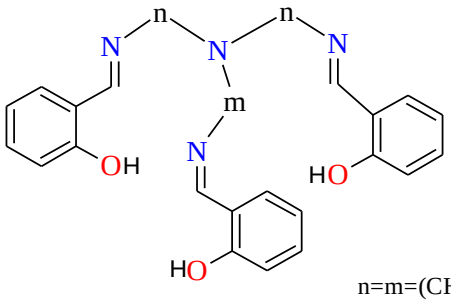

n=m=$(CH_2)_2$	**H_3L11**
n=$(CH_2)_2$ m=$(CH_2)_3$	**H_3L12**
n=$(CH_2)_3$ m=$(CH_2)_2$	**H_3L13**

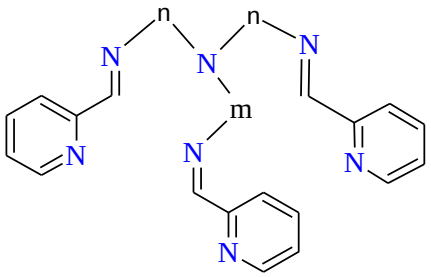

n=m=$(CH_2)_2$	**L15**
n=$(CH_2)_2$ m=$(CH_2)_3$	**L16**
n=$(CH_2)_3$ m=$(CH_2)_2$	**L17**
n=m=$(CH_2)_3$	**L18**

SOD test results of tripodal manganese complexes are presented in Table 4-13. The results indicate that the complex [Mn(L13)] (40) shows the highest SOD activity amongst the tripodal manganese complexes with a rate of $1.78x10^6$ $M^{-1}s^{-1}$ and the IC_{50} value of 0.90 μM. The complex which showed the lowest rate was the dinuclear complex $[Mn(L15)](ClO_4)_2$ (41) with a rate of $4.24x10^5$ $M^{-1}s^{-1}$ and IC_{50} value of 1.96 μM.

Table 4-13 SOD activity results of the tripodal complexes.

Complex		IC_{50} (μM) (WST-1 assay)	k_{cat} (M^{-1} s^{-1})
[Mn(L11)]	(38)	1.04	$1.54x10^6$
[Mn(L12)]	(39)	0.91	$1.76x10^6$
[Mn(L13)]	(40)	0.90	$1.78x10^6$
$[Mn(L15)](ClO_4)_2$	(41)	1.96	$4.24x10^5$
$[Mn(L18)](ClO_4)_2$	(42)	1.24	$6.74x10^5$
$[Mn(L16](ClO_4)_2$	(43)	1.28	$6.51x10^5$
$[Mn(L17)]$ $(ClO_4)_2$	(44)	1.17	$7.11x10^5$

Complexes (38)-(40) derived from tripodal amines and salicyladehyde have been found to show higher SOD activity than complexes (41)-(44) derived from tripodal amines and 2-pyridinealdeyhde. Complexes (38)-(40) are neutral, containing mononuclear Mn(III) ions while complexes (41)-(44) contain mononuclear Mn(II) ions and perchlorate counter ions. The presence of percholorate ions in (41)-(44) may be the cause of slower reaction rate than complexes (38)-(40). From the SOD data, changing the arm size in those complexes has an effect on the activity. The symmetric complex (38) has a catalytic rate of $1.54x10^6$ $M^{-1}s^{-1}$ and

when one extra carbon atom is introduced into one of the arms (39), around a 10% ($1.76x10^6$ $M^{-1}s^{-1}$) increase in the catalytic rate was observed. However, addition of a carbon atom to another arm (40) had only a very slight effect on the catalytic rate ($1.78x10^6$ $M^{-1}s^{-1}$). The same trend was observed for complexes (41)-(44). Addition of one carbon atom to one of the arms in complex (41) to give complex (42) increased the catalytic rate considerably (about 60% increase in the rate). Addition of one carbon atom to each arm enhanced the catalytic rate to $7.11x10^5$ $M^{-1}s^{-1}$. Increasing the arm size by adding carbon atoms enhance the conformational flexibility of the ligands, therefore providing a more suitable arrangement for the catalytic reaction.

4.5.5 SOD activity of Mn(II) complexes of L19

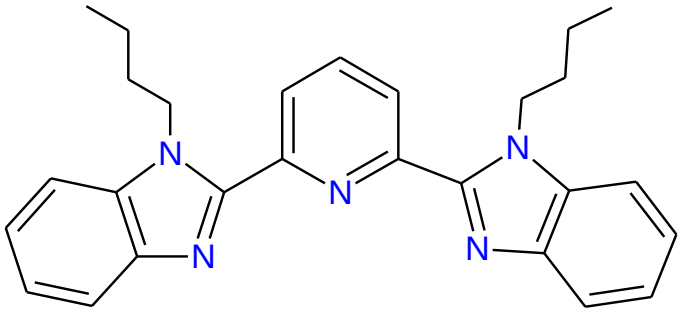

L19

The SOD activity of the complexes of L19 was not measured using WST-1 assay because of insolubility of the complexes in the aqueolex solutions were prepared in dmso and mixed with aqueous testing solution. No problems were encountered in the case of all other complexes in terms of solubility, however, when complexes of L19 were mixed with aqueous testing solution, a cloudy solution formed and the absorbance at 450 nm was fluctuating and no stable increase was observed. This may be due to low solubility of the complexes in aqueous media.

4.5.6 Conclusions for SOD activity

It is informative to compare the catalytic rates of the complexes with the rates of other previously published complexes. Some kinetic values for SOD activity obtained from the literature are given in Table 4-14.

Table 4-14 SOD activity results of the reported in the literature.

Complex	k_{cat} (M^{-1} s^{-1})	Method
$Mn(ClO_4)_2$ +EDTA[209]	$3.4x10^4$	Indirect
$Mn(ClO_4)_2$[209]	$1.3x10^6$	Indirect
M40403[152]	$1.6x10^7$	Stopped-flow
S,S-dimethyl-M40403[96]	$1.6x10^9$	Stopped-flow
MnSalen(EUK8)[114]	$8x10^5$	Stopped-flow
Mn(III) porphyrinato complex[145]	$4x10^6$	indirect
MnSOD[154]	$5.2x10^8$	indirect
CuZnSOD[210]	$2x10^9$	Pulse radiolysis

The results for SOD activity of S,S-dimethyl-M40403 have been found to show catalytic rates that exceed that of the natural MnSOD enzyme itself and this complex is the most active SOD mimic to date.[96] Simple manganese perchlorate has a high rate of catalytic activity; however, addition of EDTA reduces the catalytic rate dramatically.[209] The manganese salen complex (EUK8) has been found to show a slower reaction rate than manganese percholorate.[114] The SOD activity results that have been obtained for the complexes in this thesis have shown similar activity to those of manganese salen complex (EUK8) and manganese perchlorate, however reaction rates are much less than the rates of *S,S*-dimethyl-M40403, M40403 and natural MnSOD.

Conclusions

Several macrocyclic and acyclic Mn(II) complexes containing 2,6-diformylpyridine (DFP) as a head unit have been successfully prepared, producing a catalogue of complexes which display differences in coordination number and geometry around the metal centre.

Template assembly of macrocyclic Ba(II) complexes, formed by Schiff-base condensation of 1,3-diamino-2-propanol and 2,6-diacetylpyridine (DAP) and 2,6-diformylpyridine (DFP), are structurally similar. Transmetallation reactions of the DFP-derived Ba complex, $[Ba(H_2L1)(\mu_{1,2}\text{-}ClO_4)]_2(ClO_4)_2$, with Mn(II) ions result in both macrocyclic ring-contraction and ring-expansion depending on both the solvent and counter ion used. Two mononuclear, ring-contracted complexes (H_3L2 and H_3L3) were obtained when methanol or ethanol were used as solvents in transmetallation reactions. The macrocycle H_2L1 undergoes a ring-contraction *via* the addition of methanol or ethanol across one imine bond, followed by a nucleophilic addition of the secondary amine across an adjacent imine bond resulting in a six-membered hexahydropyrimidine. Ring-contraction reduces the size of the cavity in the macrocycle to accommodate one Mn(II) ion in the macrocycle. An equivalent ring-contraction has not been observed in Mn(II) complexes of DAP-derived macrocycle (H_2A) because methyl groups provide steric hindrance which hinders the imine groups from nucleophilic attack. Reactions with the macrocyclic tetraimine ligand (H_2L1) resulted in polynuclear, ring-expanded assemblies when acetonitrile was used as a solvent. The macrocycle (H_2L1) undergoes rearrangement from a 20-membered to a 40-membered tetranuclear Mn(II) complex on reaction with Mn(II) salts. The ring-expansion occurred in the presence of the strongly coordinating chloride or azide anions. It is likely that the initial trasmetallation product is a dimeric complex with a Mn_4Cl_4 or Mn_4N_4 core which provides a cluster template for re-organisations. The ring-expansion from DAP-derived ligand (H_2A) also occurs but this time in the presence of poorly coordinating counter ions such as the perchlorate ion. Strongly coordinating ligands such as chloride and azide result in dimeric complexes showing neither ring-contraction nor ring-expansion. The macrocyclic Mn(II) complexes presented in this thesis are seven-coordinate with approximate pentagonal bipyramidal geometry and an N_3O_2 or N_5 donor set with two axial ligands.

Non-macrocyclic ligands containing phenol groups (H_2L9 and H_2L10) always gave seven-coordinate Mn(II) complexes. However, acyclic ligands with flexible alcohol groups

did not always give seven-coordinate complexes. All macrocyclic and acyclic Mn(II) complexes are stable in air without decomposition except the complex of L5 with two axial chloride ions [Mn(L5)Cl_2] (12) which turns into a brown oil after several days in air, possibly due to oxidation of the Mn(II) ion.

A range of asymmetric and symmetric tripodal Schiff base ligands and their manganese complexes were also prepared and characterised. The structures of two new (one symmetric (L18) and one asymmetric (L16)) tripodal-pyridine derived Mn(II) complexes were determined by X-ray crystallography. These complexes are seven-coordinate bonded to seven nitrogen atoms from a single tripodal ligand.

Additionally, the reaction of the N-alkylated pyridinebenzimidazole ligand L19 with Mn(II) salts produced mononuclear complexes. In the presence of the strongly binding counter ions Cl^-, SCN^- and NO_3^-, 1:1 (Mn:L19) complexes were obtained, but weakly binding counter ions ClO_4^- or PF_6^- yield only 1:2 (M:Ligand) complexes and the counter ions remain uncoordinated.

The potential application of the complexes has been tested in two main areas: (a) as new catalase mimics and (b) as new superoxide dismutase mimics.

The catalase activity results have shown that all complexes tested are active catalysts in the presence of added base and turnover numbers are in the range 5-500. Results also indicated that an increase in the number of manganese centres proves to be important. In addition to the structure of the ligand being important, there were differences between similar complexes with different axial ligands. This suggests that the dissociation constants of axial ligands are important and maybe the axial ligands are removed before hydrogen peroxide can be broken down. The trinuclear acyclic complex, $[Mn_3(L9)_2(OAc)_2(MeOH)_2]\cdot 2MeOH$, derived from 2,6-diformylpyridine and 2-aminophenol, was found to be the most efficient catalase mimic of the tested complexes with approximately 500 molecules of H_2O_2 broken down per second for each complex during the fastest rate of activity. The tripodal complex, $[Mn(L18)](ClO_4)_2$, is the only complex to show catalase activity without added base with a long induction period.

All complexes were subjected to indirect analysis of superoxide dismutase activity using the WST-1 assay. Most of the complexes showed SOD activity with rate constants in the range 2.05×10^6-1.19×10^5 $M^{-1}s^{-1}$. Three complexes were found to have no measureable SOD activity.

The SOD results showed that the axial ligands have an effect on SOD activity; strongly bound ligands such as thiocyanate and azide generally result in lower SOD activity and overall, Mn(II) complexes derived from macrocyclic and acyclic ligands containing axial water or chloride ligands showed higher SOD activity than those with exogenous thiocyanate or azide ligands. The tripodal complexes showed high rates of SOD activity and changes in the arm size generally enhance the catalytic rate of the reactions. It was not possible to measure SOD activity of the complexes of L19 using the WST-1 assay due to insolubility of the complexes in the aqueous testing solution.

Ring-contracted complexes show high rates of superoxide dismutase activity but possess limited catalase activity and these complexes have the potential for use in research as anticancer compounds. The complexes $[Mn(H_2L6)(N_3)_2]$, $[Mn(H_2L10)(NCS)_2]$ and $[Mn(H_2L10)(N_3)_2]$ showed catalase activity but no measurable SOD activity was observed using indirect methods. All other complexes showed both catalase and SOD activity.

Further Work

To extend the research presented in this thesis, it is important to find ways to increase yields and purity of the complexes for further testing and analysis. Macrocyclic and acyclic complexes presented in this thesis contain imine groups (-C=N-) which are susceptible to hydrolysis and this reduces the stability of the complexes in aqueous media. Reduced forms of these complexes can be prepared to increase stability of the complexes.

For macrocyclic ring-contracted and ring-expanded complexes, reaction progress could be examined by ESI mass spectrometry in order to determine the reaction intermediates. Ring-contracted complexes with two axial thiocyanate ligands showed considerable SOD activity but limited catalase activity. Preparing ring-contracted complexes with different axial ligands may enhance the catalytic activity.

SOD activity of the complexes has been tested using an indirect assay (WST-1). Indirect analysis can cause false positive results for SOD activity and side reactions may occur and interfere with measurements. Further work must be continued on the setup of a direct method for analysing superoxide dismutase activity or collaborations can be made with other groups who are experts in fast reaction kinetics.

Finally, toxicity issues must be studied for each type of complex if they are to be used as pharmaceutical ingredients. The stability of the complexes must also be studied in different conditions (acidic, basic, aqueous etc.).

Chapter 5

Experimental

5.1 General conditions

5.1.1 Solvents and reagents

All starting materials were purchased from commercial sources and were used without further purification unless otherwise noted. Solvents for preparative chemistry were chemically pure grade or HPLC grade and used without further purification.

5.1.2 Physical measurements

The prepared compounds were characterised *via* NMR, IR, mass spectrometry, CHN analysis and single crystal X-ray crystallography.

IR spectra were performed using KBr pellets in the range of 4000-300 cm^{-1}on a Perkin Elmer Paragon 1000 PC Fourier Transform Spectrometer.

Elemental analyses were performed using a CE-440 Elemental analyser by Mrs Pauline King within the chemistry department.

NMR spectroscopy was performed using a Bruker Avance 400 MHz or 500MHz spectrometer. Chemical shifts [δ] in ppm are relative to $SiMe_4$.

Mass spectra were recorded on a Thermo Fisher Exactive + Triversa Nanomate mass spectrometer (ESI) within the chemistry department or by the mass spectrometry service EPSRC (FAB or ESI) at the University of Swansea.

Single crystal X-ray diffraction data were collected at 150K on a Bruker APEX2 CCD[211] diffractometer using monochromated Mo-Kα radiation (λ= 0.71073 A) within the department and data reduction was performed using Bruker SAINT.[211] Unless otherwise stated, structures were solved by direct methods and refined on F^2 using all of the reflections. SHELXTL was used to solve and refine the structures.[212] All H atoms bonded to carbon atoms were placed in geometrically calculated positions and were refined using a riding model (aryl C–H 0.95 Å, methyl C–H 0.98 Å, methylene C–H 0.99 Å. *U*iso(H) values were set to be 1.2 times *U*eq of the carrier atom for aryl CH and 1.5 times *U*eq of the carrier atom for CH_3. The crystallography graphics were produced using XP[212], Mercury 2.4[213], Ortep 3 for windows[214] or POV-Ray software.[215] Details specific to each structure are given in Appendix 2 and Cif files are in the Appendix CD.

5.1.3 Preparation of activated manganese dioxide

Activated manganese dioxide which was used to oxidise of 2,6-pyridinedimethanol was prepared from manganese(II) sulphate and potassium permanganate. 100 g of $MnSO_4$ was dissolved in 125 ml of boiling distilled water. To the stirred solution, a cold saturated solution containing 90 g of potassium permanganate in 2.5 l of water was added dropwise over 4 hrs. When the addition was complete, the MnO_2 was filtered off, washed with 3 litres of boiling water to remove all remaining $KMnO_4$ and dried in the oven over a few days (150 °C) to yield 90 g of active MnO_2.

5.1.4 Preparation of 2,6-diformylpyridine (DFP)

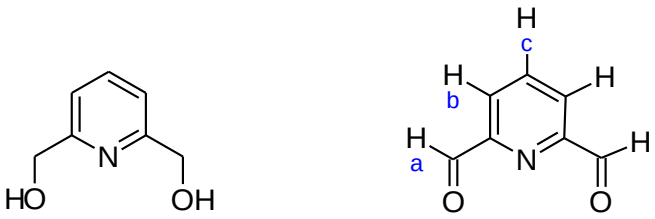

DFP

2,6-Diformylpyridine (DFP) was prepared by oxidation of 2,6-pyridinedimethanol according to the literature method.[173] The manganese dioxide (29.94 g) was supended in chloroform (300 ml) and 2,6-pyridinedimethanol (4.91 g, 3.63 mmol) was added. The solution was refluxed for 5 hrs. The MnO_2 was removed by filtration and washed with diethylether (5 x 100 ml). The filtrate and the washings were evaporated to dryness under reduced pressure to yield DFP as a cream coloured solid. Yield: 3.34 g, 62%. DFP was made several times with similar yields.

IR: $\upsilon_{(C-H)}$ 3086 , 2861 , $\upsilon_{(C=O)}$ 1714, $\upsilon_{(C=C)}$ 1593, 1349, 1260, 1210, 805, 622 cm^{-1}

Anal. (%) Found:	C = 61.37	H = 3.80	N = 10.10
Calculated for $C_7H_5NO_2$	C = 61.21	H = 3.74	N = 10.37

FAB

M/z	Rel. Abundance (%)	Assignment	Calc. Mass
136	100	$\{[C_7H_5NO_2]H\}^+$	136

NMR ($CDCl_3$, ppm, ^1H) 10.11 (*s* 2H CH^a), 8.13(*d* 2H CH^b) 7.2 (*t* H CH^c)

5.1.5 Preparation of macrocyclic complexes

5.1.6 Preparation of $[Ba(H_2L1)(ClO_4)]_2(ClO_4)_2$ (1)

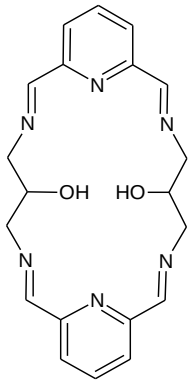

H_2L1

$[Ba(H_2L1)(ClO_4)]ClO_4$ was prepared by the template condensation of 2,6-diformylpyridine (DFP) (1.50 g, 11.1 mmol) with 1,3-diaminol) and barium(II) perchlorate (2.16 g, 5.54 mmol). 2,6-Diformylpyridine was dissolved with barium(II) perchlorate in 200 ml of dry MeOH. 1,3-Diaminopropan-2-ol was then added and the solution was stirred for 2 hrs at room temperature. The volume of the solution was reduced to 20 ml and 10 ml of EtOH was added. Colourless crystals were obtained overnight. Yield: 2.42 g, 87%.

IR: 2910, 1654, 1587, 1263, 1100, 810, 624 cm^{-1}

Anal. (%) Found: C = 33.67 H = 3.51 N = 11.80

Calculated for $[Ba(H_2L1)(ClO_4)](ClO_4)$ C = 33.16 H = 3.08 N = 11.76

ESI-MS

Found (M/z)	Rel. Abundance (%)	Assignment	Calc. Mass
515.0	34	$\{[Ba(HL1)]\}^+$	515.0
615.1	100	$\{[Ba(H_2L1)(ClO_4)]\}^+$	615.1
633.1	20	$\{[Ba(H_2L1)(ClO_4)](H_2O)\}^+$	633.1
647.1	15	$\{[Ba(H_2L1)(ClO_4)](CH_3OH)\}^+$	647.1
1229.3	2	$\{[Ba(H_2L1)(ClO_4)]_2\}^+$	1229.3

^{1}H NMR (CD_3CN, ppm) 8.32 (*s* 4H –HC=N-), 7.91(*t* 2H aromatic), 7.46 (*d* 4H aromatic), 4.94 (*s* broad 2H OH), 4.51 (*b* 2H, CH), 4.14 & 3.76 (*d* 8H $–CH_2$-)

5.1.7 Preparation of $[Mn(H_3L2)(NCS)_2]$ (2)

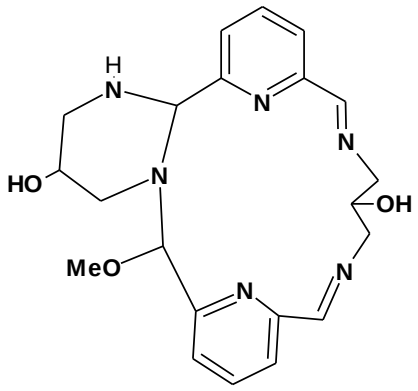

H_3L2

$[Ba(H_2L1)(ClO_4)]ClO_4$ (0.62 g, 0.87 mmol) was dissolved in MeOH (10 ml). A solution of $Mn(OAc)_2 \cdot 4H_2O$ (0.43 g, 1.7 mmol) in MeOH (30 ml) was added to a refluxing solution of the barium complex. A yellow cloudy suspension formed. The reaction mixture was refluxed for 8 hrs. On cooling, a white precipitate was removed by filtration. The filtrate was evaporated and a yellow oil resulted. The oil was dissolved in MeOH (10 ml) and Na(NCS) (0.14 g, 1.7 mmol) and the reaction solution was refluxed for a further 3 hrs. The resulting yellow solution was left to stand and the yellow powder formed was collected and analysed. Yield: 0.39 g, 79%. Single crystals suitable for X-ray diffraction were obtained from slow diffusion of diethylether into a dmf solution of the complex.

IR: 3385, 2915, 2830, 2066, 1653, 1587, 1464 cm^{-1}

Anal. (%) Found:	C = 47.42	H = 4.41	N = 18.93
Calculated for $[Mn(H_3L2)(NCS)_2]$	C = 47.51	H = 4.51	N = 19.28

ESI-MS

Found (M/z)	**Rel. Abundance (%)**	**Assignment**	**Calc. Mass**
523.11	100	$\{[Mn(H_3L2)(NCS)]\}^+$	523.11
464.13	60	$\{[Mn(H_2L2)]\}^+$	464.13

5.1.8 Preparation of $[Mn(H_3L3)(NCS)_2]$ (3)

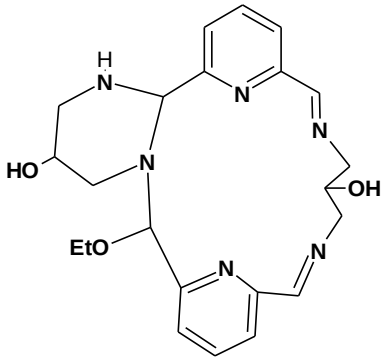

H_3L3

The ring-contracted mononuclear Mn(II) complex was prepared *via* a transmetallation reaction. $[Ba(H_2L1)(ClO_4)]ClO_4$ (0.62 g, 0.87 mmol) was dissolved in acetonitrile (25 ml). $Mn(OAc)_2 \cdot 4H_2O$ (0.43 g, 1.7 mmol) in EtOH (15 ml) was added to a refluxing solution of the barium complex. On addition of manganese acetate solution, a yellow cloudy solution formed. The reaction mixture was refluxed overnight. On cooling, a white precipitate formed and was removed by filtration. The filtrate was left to evaporate to give a yellow oil. This oily product was dissolved in acetonitrile (10 ml) and Na(NCS) (0.10 g, 1.2 mmol) in EtOH (5 ml) was added and refluxed for 3 hrs. The resulting yellow solution was left to stand and yellow crystals suitable for X-ray study grew in solution overnight. Yellow crystals were analysed. Yield: 0.41 g, 75%.

IR: 3399, 2921, 2066, 1648, 1592, 1263 cm^{-1}

Anal. (%) Found: C = 45.15 H = 4.69 N = 16.64

Calculated for $[Mn(H_3L3)(NCS)_2] \cdot 2.5(H_2O)$ C = 44.99 H = 5.31 N = 17.49

ESI-MS

Found (M/z)	**Rel. Abundance (%)**	**Assignment**	**Calc. Mass**
537.13	100	$\{[Mn(H_3L3)(NCS)]\}^+$	537.13
509.10	80	$\{[Mn(H_3L3)(NCS)](CH_3OH)\}^+$	509.10
478.15	60	$\{[Mn(H_2L3)]\}^+$	478.15

5.1.9 Preparation of $[Mn_4(H_2L^*)Cl_4][MnCl_4]$ (4)

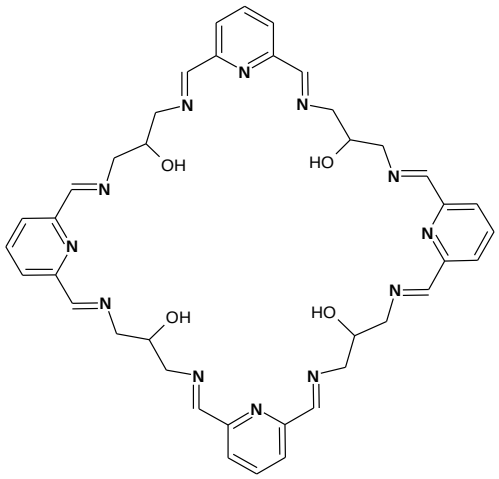

H_4L^*

The [4+4] tetranuclear Mn(II) complex was prepared *via* a transmetallation reaction. $[Ba(H_2L1)(ClO_4)]ClO_4$ (0.62 g, 0.86 mmol) was dissolved in acetonitrile (25 ml). $MnCl_2 \cdot 4H_2O$ (0.46 g, 2.3 mmol) was added to the refluxing solution of the barium complex. On addition of manganese chloride solution, a yellow cloudy solution was formed. The reaction mixture was refluxed overnight. Some white precipitate was removed by filtration and clear yellow solution cooled down to room temperature. Yellow crystals suitable for X-ray study grew in solution over 5 hrs. After isolation, crystals became powder after a few days and the powder was analysed. Yield: 0.41 g, 69%.

IR: 3391, 2899, 1655, 1591, 1263, 1114, 625 cm^{-1}

Anal. (%) Found:	C = 36.24	H = 3.44	N = 13.47
Calculated for $[Mn_4(H_2L^*)Cl_4][MnCl_4]$	C = 36.59	H = 3.22	N = 12.80

ESI-MS

Found (M/z)	**Rel. Abundance (%)**	**Assignment**	**Calc. Mass**
557.98	100	$\{[Mn_4(H_2L^*)(Cl_4)]\}^{2+}$	557.98
521.00	50	$\{[Mn_4(H_2L^*)Cl_2]\}^{2+}$	521.00
485.03	5	$\{[Mn_4(H_2L^*)]\}^{2+}$	485.03
432.10	15	$\{[Mn_2(H_2L^*)]\}^{+}$	432.10
357.00	15	$\{[Mn_4(H_2L^*)Cl_3]\}^{3+}$	357.00

347.67	60	$\{[Mn_4(H_2L^*)Cl_2]\}^{3+}$	347.67
335.68	50	$\{[Mn_4(H_2L^*)Cl]\}^{3+}$	335.68
243.01	48	$\{[Mn_4(H_2L^*)]\}^{4+}$	243.01
216.55	25	$\{[Mn(H_2L^*)]\}^{2+}$	216.55

5.1.10 Preparation of $[Mn(L4)(NCS)_2]$ (5)

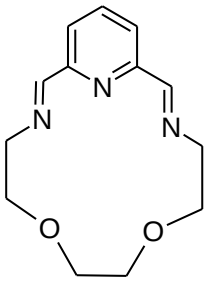

L4

2,2`-Ethylenedioxybis(ethylamine) (0.32, 2.2 mmol) in MeOH was added to a refluxing solution of DFP (0.30 g, 2.2 mmol) and $Mn(ClO_4)_2 \cdot 4H_2O$ (0.81 g, 2.2 mmol) in MeOH. The reaction mixture was refluxed for 1 hr then solid NaNCS (0.36, 4.4 mmol) was added and the mixture was refluxed for further 2 hrs. Once cooled down to room temperature, the volume was reduced to 20 ml on a rotary evaporator. The orange-yellow powder was collected, washed with diethylether and analysed. Yield: 0.75 g, 77%. Single crystals for X-ray studies were obtained from dmf-diethylether vapour diffusion.

IR: 2924, 2913, 2045 1647, 1588, 1259 cm^{-1}

Anal. (%) Found: C = 41.71 H = 4.23 N = 15.75

Calculated for $[Mn(L4)(NCS)_2] \cdot H_2O$ C = 41.28 H = 4.39 N = 16.05

ESI-MS

Found (M/z)	**Rel. Abundance (%)**	**Assignment**	**Calc. Mass**
151.03	100	$\{[Mn(L4)]\}^{2+}$	151.03
301.06	45	$\{[Mn(L4)]\}^{+}$	301.06
360.04	55	$\{[Mn(L4)(NCS)]\}^{+}$	360.04
392.07	45	$\{[Mn(L4)(NCS)](CH_3OH)\}^{+}$	392.07

5.1.11 Preparation of acyclic complexes

5.1.12 Preparation of (H_2L4) (6)

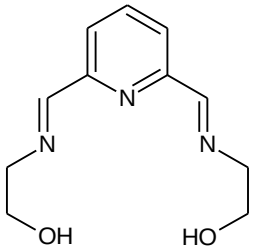

H_2L_4

Ligand H_2L4 was obtained by direct condensation of 2,6-diformylpyridine with ethanolamine in MeOH. Ethanolamine (0.45 g, 7.4 mmol) in 5 ml of MeOH was added to solution of 2,6-diformylpyridine (0.50 g, 3.7 mmol) in MeOH (10 ml). The mixture was stirred at room temperature for 30 minutes. Solvent was removed to dryness using a rotary evaporator to give the white powdery ligand (0.75 g, 3.4 mmol). The ligand was used quickly in the preparation of complexes to avoid hydrolysis of the imine bond in the free ligand. Colour: colourless, Yield: 1.52 g, 93%. Single crystals suitable for X-ray diffraction study were grown from slow evaporation of an acetonitrile solution of the compound.

IR: 3337, 2869, 1645, 1587, 1258 cm^{-1}

Anal. (%) Found:	C = 56.73	H = 6.49	N = 17.10
Calculated for $[H_2L4]\cdot CH_3OH$	C = 56.69	H = 7.40	N = 16.53

ESI-MS

Found (M/z)	**Rel. Abundance (%)**	**Assignment**	**Calc. Mass**
222.12	15	$\{[H_2L4]H]\}^+$	222.12
244.10	100	$\{[H_2L4]Na\}^+$	244.10

NMR ($CDCl_3$, ppm, ^{1}H) 3.71 (*t* 4H CH_2), 4.68(*t* 4H CH_2) 8.36 (*t* H CH aromatic) 8.02 (s 2H CH azomethine) 7.95 (*d* 2H CH aromatic)

5.1.13 Preparation of $[Mn(H_2L4)Cl_2]$ (7)

Ligand H_2L4 (0.23 g, 1.1 mmol) was dissolved in MeOH (15ml), $MnCl_2 \cdot 4H_2O$ (0.22 g, 1.1 mmol) in EtOH (5 ml) was added and the yellow reaction mixture was refluxed for 3 hrs before the volume of the solution was reduced to 10 ml. An orange-yellow product was collected within two days and analysed. Yield: 0.29 g, 76%. Suitable crystals for crystallography were obtained by slow diffusion of diethylether into a dmf solution of complex within a few days.

IR: 3285, 2950, 1659, 1591, 1287 cm^{-1}

Anal. (%) Found: C = 37.00 H = 4.18 N = 11.70

Calculated for $[Mn(H_2L4)Cl_2] \cdot ½H_2O$ C = 37.07 H = 4.49 N = 11.79

ESI-MS

Found (M/z)	**Rel. Abundance (%)**	**Assignment**	**Calc. Mass**
311.02	100	$\{[Mn(H_2L4)Cl]\}^+$	311.02
275.04	75	$\{[Mn(HL4)]\}^+$	275.04
138.02	60	$\{[MnH_2L4]]\}^{2+}$	138.02

5.1.14 Preparation of $[Mn_2(H_2L4)_2(NCS)_4]$ (8)

Ligand H_2L4 (0.23 g, 1.1 mmol) was dissolved in MeOH (15ml), $MnCl_2 \cdot 4H_2O$ (0.22 g, 1.1 mmol) in MeOH (5 ml) was added to the solution followed by addition of NaNCS (0.18 g, 2.2 mmol) in MeOH (5 ml). The reaction mixture was refluxed for 1 hr and the volume of the solution was reduced to 10 ml. On addition of diethylether (5-7 ml), a yellow product formed and was collected and analysed. Yield: 0.38, 88%. Suitable crystals for X-ray diffraction study were obtained by slow diffusion of diethylether into dmf solution of complex within a few days.

IR: 3334, 2944, 2078, 1656, 1590, 1279, 2078 cm^{-1}

Anal. (%) Found:	C = 36.61	H = 3.64	N = 15.25
Calculated for $[Mn_2(H_2L4)_2(NCS)_4] \cdot 2H_2O$	C = 36.53	H = 3.51	N = 16.39

ESI-MS

Found (M/z)	**Rel. Abundance (%)**	**Assignment**	**Calc. Mass**
275.04	100	$\{[Mn(HL4)]\}^+$	275.04
334.02	20	$\{[Mn(H_2L4)(NCS)]\}^+$	334.02
366.05	2	$\{[Mn(H_2L4)(NCS)_2]Na\}^+$	366.05

5.1.15 Preparation of $[Mn_2(H_2L4)_2(N_3)_3Cl]$ (9)

Ligand H_2L4 (0.40 g, 1.9 mmol) was dissolved in MeOH (15ml), $MnCl_2 \cdot 4H_2O$ (0.38 g, 1.9 mmol) in MeOH (5 ml) was added to the solution followed by addition of NaN_3 (0.25 g, 3.8 mmol) in MeOH (5 ml). The reaction mixture was refluxed for 1 hr and the volume of solution was reduced to 10 ml. On addition of diethylether (10 ml), orange product formed and was collected and analysed. Yield: 0.52, 76%. Suitable crystals for X-ray diffraction study were obtained from slow diffusion of diethylether into dmf solution of complex within a few days.

IR: 3381, 2925, 2055, 2042, 1648, 1590, 1279 cm^{-1}

Anal. (%) Found:	C = 36.71	H = 4.12	N = 29.20
Calculated for $[Mn_2(H_2L4)_2(N_3)_4Cl]$	C = 37.00	H = 4.24	N = 29.44

ESI-MS

Found (M/z)	**Rel. Abundance (%)**	**Assignment**	**Calc. Mass**
275.04	100	$\{[Mn(H_2L4)]\}^+$	275.04
244.10	80	$\{[H_2L4]Na\}^+$	244.10
138.02	20	$\{[Mn(H_2L4)]\}^{2+}$	138.02

5.1.16 Preparation of [Mn(L5)(NCS)$_2$] (10)

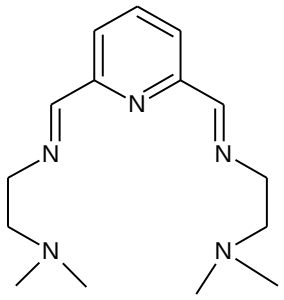

L5

2,6-Diformylpyridine (DFP) (0.26 g, 1.9 mmol) was dissolved in MeOH (20 ml) and *N*,*N*-dimethylethanediamine (0.34 g, 3.8 mmol) in MeOH (20 ml) was added dropwise. The reaction mixture was stirred at room temperature for 30 min. To the stirring solution, $MnCl_2 \cdot 4H_2O$ (0.38 g, 1.9 mmol) was added. The solution was refluxed for 2 hrs. Upon addition of NaNCS (0.31 g, 3.8 mmol), a yellow product precipitated which was collected and washed with MeOH and diethylether Yield: 0.68 g, 80%. Single crystals were grown from slow diffusion of diethylether into dmf solution of the complex.

IR: 2830, 2062, 1653, 1587, 1289 cm^{-1}

Anal. (%) Found:	C = 44.39	H = 5.58	N = 20.80
Calculated for $[Mn(L5)(NCS)_2] \cdot \frac{1}{2}H_2O$	C = 44.78	H = 5.70	N = 21.52

ESI-MS

Found (M/z)	**Rel. Abundance (%)**	**Assignment**	**Calc. Mass**
388.12	100	$\{[Mn(L5)(NCS)]\}^+$	388.12

5.1.17 Preparation of $[Mn(L5)(N_3)_2]$ (11)

2,6-Diformylpyridine (0.26 g, 1.9 mmol) was dissolved in EtOH (20 ml) and *N*,*N*-dimethylethanediamine (0.34 g, 3.8 mmol) in MeOH (20 ml) was added dropwise. The reaction mixture was stirred at room temperature for 30 min. To the stirring solution, $MnCl_2 \cdot 4H_2O$ (0.38 g, 1.9 mmol) was added followed by addition of NaN_3 (0.31 g, 3.8 mmol). The solution was refluxed for 2 hrs. The volume of the mixture was reduced to 10 ml and an orange product precipitated. The precipitate was collected, washed with diethylether and analysed. Yield: 0.65, 82%. Single crystals were grown from slow diffusion of diethylether into a MeOH solution of the complex.

IR: 2831, 2045, 1651, 1586 cm^{-1}

Anal. (%) Found:	C = 42.54	H = 5.94	N = 35.27
Calculated for $[Mn(L5)(N_3)_2] \cdot CH_3OH$	C = 43.05	H = 6.55	N = 34.51

ESI-MS

Found (M/z)	**Rel. Abundance (%)**	**Assignment**	**Calc. Mass**
298.19	70	$\{[L5]Na\}^+$	298.19
372.15	100	$\{[Mn(L5)(N_3)]\}^+$	372.15
786.32	25	$\{[Mn(L5)(N_3)]_2\}^+$	786.32

5.1.18 Preparation of [Mn(L5)Cl_2] (12)

2,6-Diformylpyridine (0.50 g, 3.7 mmol) and $MnCl_2 \cdot 4H_2O$ (0.73 g, 3.7 mmol) were dissolved in EtOH (20 ml) and *N*,*N*-dimethylmethanediamine (0.51 g, 7.4 mmol) in MeOH (20 ml) was added dropwise. The reaction mixture was refluxed for 2 hrs. The volume of the mixture was reduced to 20 ml and 10 ml of diethylether was added. Yellow crystals grew in solution overnight was collected. Yield: 0.78, 53%.

IR: 2910, 1654, 1587, 1263 cm^{-1}

Anal. (%) Found: Crystals turned to brown within a couple of days

ESI-MS

Found (M/z)	**Rel. Abundance (%)**	**Assignment**	**Calc. Mass**
365.11	100	$\{[Mn(L5)Cl]\}^{+}$	365.11
165.07	8	$\{[Mn(L5)]\}^{2+}$	165.07

5.1.19 Preparation of $[Mn_2(H_2L6)_2(N_3)_4]$ (13)

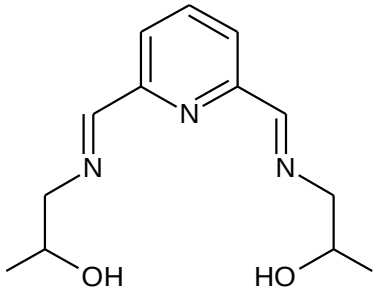

H_2L_6

2,6-Diformylpyridine (0.46 g, 3.4 mmol) was dissolved in MeOH (20 ml) and 1-aminopropan-2-ol (0.52 g, 6.8 mmol) in MeOH (15 ml) was added dropwise. The reaction mixture was stirred at room temperature for 45 min. To the stirring solution, $MnCl_2 \cdot 4H_2O$ (0.68 g, 3.4 mmol) was added followed by addition of NaN_3 (0.45 g, 6.8 mmol). The solution was refluxed for 2 hrs. The volume of the mixture was reduced to 10 ml and upon addition of diethylether an orange precipitate was obtained. The precipitate was collected and washed with diethylether. Yield: 1.02 g, 77%. No crystals were obtained from slow evaporation of MeOH, acetonitrile or by diffusion method (MeOH-diethylether, dmf-diethylether).

IR: 3391, 2912, 2063, 1650, 1591, 1263 cm^{-1}

Anal. (%) Found: C = 39.87 H = 4.88 N = 31.98

Calculated for [Mn (H_2L6) $(N_3)_2$] C = 40.21 H = 4.93 N = 32.47

ESI-MS

Found (M/z)	**Rel. Abundance (%)**	**Assignment**	**Calc. Mass**
303.07	100	$\{[Mn(HL6)]\}^+$	303.07
272.13	70	$\{[HL6]\}^+$	272.13
152.04	55	$\{[Mn(H_2L6)]\}^{2+}$	152.04

5.1.20 Preparation of $[Mn(H_2L6)Cl(H_2O)]Cl·H_2O$ (14)

2,6-Diformylpyridine (0.59 g, 4.4 mmol) was dissolved in MeOH (20 ml) and 1-aminopropan-2-ol (0.66g, 8.8 mmol) in MeOH (25 ml) was added dropwise. The reaction mixture was stirred at room temperature for 45 min. To the stirring solution, $MnCl_2.6H_2O$ (0.68 g, 3.4 mmol) was added and the reaction mixture was refluxed for 2 hrs. The volume of mixture was reduced to 10 ml to give an oily solution. Acetonitrile (30 ml) was added and the solution was allowed to evaporate to give a yellow-orange product. The precipitate was collected and analysed. Yield: 1.32 g, 70%. X-ray quality crystals were obtained from slow diffusion of diethylether into a MeOH solution of the complex.

IR: 3369, 2902, 1655, 1591, 1288 cm^{-1}

Anal. (%) Found: C = 36.98 H = 5.24 N = 10.02

Calculated for $[Mn(H_2L6)Cl(H_2O)]Cl·1½H_2O$ C = 37.15 H = 5.71 N = 10.00

ESI-MS

Found (M/z)	**Rel. Abundance (%)**	**Assignment**	**Calc. Mass**
339.05	50	$\{[Mn(H_2L6)Cl]\}^+$	339.05
303.07	33	$\{[Mn(HL6)]\}^+$	303.07
272.13	30	$\{[HL6]\}^+$	272.13
152.04	100	$\{[Mn(H_2L6)]\}^{2+}$	152.04

5.1.21 Preparation of $[Mn(H_2L6)(NCS)_2]$ (15)

2,6-Diformylpyridine (0.24 g, 1.7 mmol) was dissolved in MeOH (20 ml) and 1-aminopropan-2-ol (0.26 g, 3.5 mmol) in MeOH (25 ml) was added dropwise. The reaction mixture was stirred at room temperature for 30 min. To the stirring solution, $MnCl_2 \cdot 4H_2O$ (0.35 g, 1.7 mmol) was added and followed by addition of NaNCS (0.29 g, 3.5 mmol) then the reaction mixture was refluxed for 2 hrs. The volume of mixture was reduced to 10 ml to give an oily solution. Acetonitrile (30 ml) was added and the solution was allowed to air evaporate to give a yellow-orange product which was analysed. Yield: 0.65 g, 87%. No crystals were obtained for single X-ray diffraction.

IR: 3359, 2927, 2081, 1659, 1590, 1289 cm^{-1}

Anal. (%) Found: C = 42.17 H = 4.64 N = 14.85

Calculated for $[Mn(H_2L6)(NCS)_2]$ C = 42.80 H = 4.52 N = 15.67

ESI-MS

Found (M/z)	**Rel. Abundance (%)**	**Assignment**	**Calc. Mass**
664.12	20	$\{[Mn_2(HL6)(NCS)]\}^+$	664.12
362.05	100	$\{[Mn(H_2L6)(NCS)]\}^+$	362.05
303.07	75	$\{[Mn(HL6)]\}^+$	303.07
152.04	35	$\{[Mn(H_2L6)]\}^{2+}$	152.04

5.1.22 Preparation of $[Mn(H_2L7)(NCS)_2]$ (16)

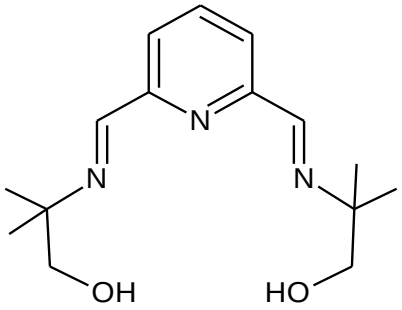

H_2L_7

2,6-Diformylpyridine (0.42 g, 3.1 mmol) was dissolved in EtOH (20 ml) and 2-amino-2-methylpropan-1-ol (0.56 g, 6.2 mmol) in EtOH (20 ml) was added dropwise. To the stirring solution, $MnCl_2 \cdot 4H_2O$ (0.62 g, 3.1 mmol) was added. The reaction mixture was refluxed at room temperature for 1 hr. The volume of solution was then reduced to 10 ml. Acetonitrile (5 ml) and diethylether (5 ml) were added. Yellow coloured precipitate was collected by filtration and analysed. Yield: 0.95, 68%. X-ray quality crystals were obtained from slow diffusion of diethylether into an acetonitrile solution of the complex.

IR: 3344, 2073, 2899, 1654, 1589, 1263, 2073 cm^{-1}

Anal. (%) Found: C = 45.02 H = 5.16 N = 15.05

Calculated for $[Mn(H_2L7)(NCS)_2]$ C = 45.53 H = 5.17 N = 15.61

ESI-MS

Found (M/z)	**Rel. Abundance (%)**	**Assignment**	**Calc. Mass**
390.08	100	$\{[Mn(H_2L7)(NCS)]\}^+$	390.08
331.10	50	$\{[Mn(HL7)]\}^+$	331.10
166.05	20	$\{[Mn(H_2L7)]\}^+$	166.05

5.1.23 Preparation of $[Mn(H_2L7)Cl_2(H_2O)]\cdot H_2O$ (17)

2,6-Diformylpyridine (0.42 g, 3.1 mmol) was dissolved in EtOH (20 ml) and 2-amino-2-methylpropan-1-ol (0.60 g, 6.2 mmol) in EtOH (20 ml) was added dropwise. To the stirring solution, $MnCl_2\cdot 4H_2O$ (0.62 g, 3.1 mmol) was added the reaction mixture was further stirred for 30 minutes. The solvent was removed by using a rotary evaporator to give an orange oil. Acetonitrile (5 ml) and diethylether (5 ml) were added to the oil and a yellow precipitate formed within 30 min and was analysed. Yield: 0.88 g, 64%. X-ray quality crystals were obtained from a dmf-acetonitrile solution of the complex by diethylether diffusion.

IR: 3386, 2935, 1642, 1590, 1287 cm^{-1}

Anal. (%) Found: C = 37.85 H = 5.19 N = 8.90

Calculated for $[Mn(H_2L7)Cl_2(H_2O)]\cdot 3H_2O$ C = 37.91 H = 5.60 N = 8.84

ESI-MS

Found (M/z)	**Rel. Abundance (%)**	**Assignment**	**Calc. Mass**
733.15	5	$\{[Mn(H_2L7)Cl]_2\}^+$	733.15
367.08	70	$\{[Mn(H_2L7)Cl]\}^+$	367.08
331.10	30	$\{[Mn(HL7)]\}^+$	331.10
166.05	100	$\{[Mn(H_2L7)]\}^{2+}$	166.05

5.1.24 Preparation of $[Mn(H_2L8)(NCS)_2]$ (18)

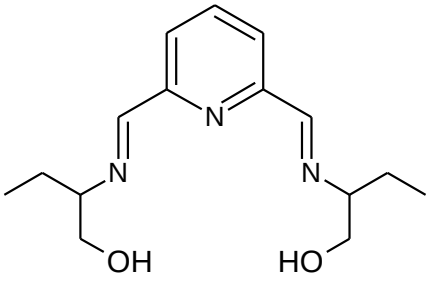

H_2L_8

2,6-Diformylpyridine (0.42 g, 3.1 mmol) was dissolved in MeOH (20 ml) and 2-amino-2-methylpropan-1-ol (0.55 g, 6.2 mmol) in MeOH (20 ml) was added dropwise. To the stirring solution, $MnCl_2 \cdot 4H_2O$ (0.62 g, 3.1 mmol) was added and the reaction mixture was further stirred for 30 minutes. The volume of the solution was reduced to 15 ml followed by addition of diethylether (5 ml) and a yellow precipitate was collected and analysed. Yield: 0.95, 70%. X-ray quality crystals were obtained from slow diffusion of diethylether into a dmf solution of the complex. Complex (18) was found to crystallise as $[Mn(H_2L8)(NCS)_2(dmf)] \cdot dmf$

IR: 3432, 2829, 2059, 1638, 1586, 1288 cm^{-1}

Anal. (%) Found: C = 44.36 H = 5.03 N = 15.30

Calculated for $[Mn(H_2L8)(NCS)_2] \cdot \frac{1}{2}H_2O$ C = 44.61 H = 5.03 N = 15.31

ESI-MS

Found (M/z)	**Rel. Abundance (%)**	**Assignment**	**Calc. Mass**
390.08	100	$\{[Mn(H_2L8)(NCS)]\}^+$	390.08
331.10	60	$\{[Mn(HL8)]\}^+$	331.10
166.05	17	$\{[Mn(H_2L8)]\}^{2+}$	166.05

5.1.25 Preparation of [H_2L9] (19)

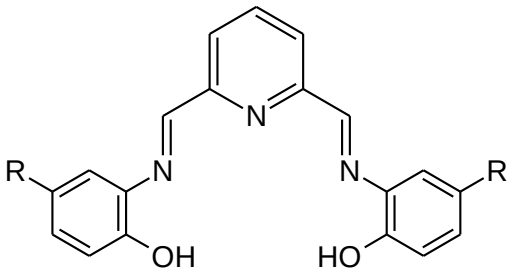

H_2L9 R=H
H_2L10 R=-CH_3

H_2L9 and H_2L10 were prepared according to the literature method.[183,184] A solution of 2,6-diformylpyridine (0.41 g, 3.0 mmol) in EtOH (15ml) was added dropwise to an EtOH solution (30ml) of 2-aminophenol (0.65 g, 5.9 mmol). A yellow colour appeared and a precipitate was formed in a few minutes. The mixture was stirred for 2 hrs, and then the yellow product was collected by filtration, washed with EtOH-diethylether mixture (1:1) and analysed. Yield: 0.86 g, 90%.

IR: 3160, 2964, 1628, 1581, 1253, 1148, 811, 739 cm^{-1}

Anal. (%) Found:	C = 65.28	H = 4.35	N = 12.01
Calculated for $[H_2L9]\cdot C_2H_5OH\cdot H_2O$	C = 66.14	H = 5.17	N = 11.62

ESI-MS

Found (M/z)	Rel. Abundance (%)	Assignment	Calc. Mass
318.09	15	$\{[H_2L9]H\}^+$	318.09
340.11	100	$\{[H_2L9]Na\}^+$	340.11
372.13	25	$\{[H_2L9](CH_3OH)H\}^+$	372.13
673.19	5	$\{[H_2L9]_2Na\}^+$	673.19

^{1}H NMR ($CDCl_3$, ppm) 10.06 (*s* OH), 8.84 (*s* 2H –HC=N-), 8.79 (*d* 2H aromatic), 8.18 (*t* 1H aromatic), 7.88 (*d* 2H aromatic), 7.37 (*t* 2H aromatic), 6.98 (*d* 2H aromatic) 6.86 (*t* 2H aromatic), 3.65 (*q* 2H EtOH), 1.68 (*b* OH), 1.16 (*t* 3H EtOH)

5.1.26 Preparation of [H_2L10] (20)

H_2L10 was obtained according to the method used for preparation of H_2L9 except using 2-amino-4-methylphenol.[183,184] Single crystals suitable for X-ray diffraction were obtained by slow evaporation of an acetonitrile solution of the compound.

Quantities: 2,6-diformylpyridine (0.42 g, 3.0 mmol), 2-amino-4-methylphenol (0.76 g, 6.2 mmol), EtOH (40 ml).

Colour: yellow. Yield: 0.85 g, 80%.

IR: 3188, 3411, 2939, 1624, 1579, 1499, 1453, 1352, 1293, 1245, 1187, 1160, 1087, 1038, 987, 960, 881, 806 cm^{-1}

Anal. (%) Found:	C = 71.03	H = 5.69	N = 11.86
Calculated for [H_2L10]·½H_2O	C = 71.17	H = 5.65	N = 11.70

ESI-MS

Found (M/z)	Rel. Abundance (%)	Assignment	Calc. Mass
346.15	40	{[H_2L10]H}$^+$	346.15
368.13	100	{[H_2L10]Na}$^+$	368.13
400.16	22	{[Na(H_2L10)](CH_3OH)} $^+$	400.16

^{1}H NMR ($CDCl_3$, ppm) 10.12 (*br*, PhOH), 8.77 (*s*, 2H, -N=CH), 8.17(*d*, 2H aromatic), 7.85 (*t*, 1H aromatic), 7.09(*s*, 2H, aromatic), 7.00 (*d*, 2H, aromatic), 6.87 (*d*, 2H, aromatic aromatic), 2.25 (*s*, 6H, C-CH_3), 1.69 (*br*, H_2O).

5.1.27 Preparation of $[Mn_3(L9)_2(OAc)_2(MeOH)_2]\cdot 2MeOH$ (21)

H_2L9 (0.32 g, 1.0 mmol) was dissolved in MeOH (20 ml). $Mn(OAc)_2\cdot 4H_2O$ (0.37 g, 1.5 mmol) was added and then the resulting clear yellow-orange solution was refluxed for 4 hrs. Upon cooling, a red precipitate formed. This was collected, washed with diethylether and analysed. Yield: 0.35 g, 67%. Single crystals suitable for X-ray study were obtained from slow diffusion of diethylether into a MeOH solution of the complex.

IR: 2923, 1694, 1559, 1533, 1471, 1404, 1315, 1268, 1146, 1032, 945, 816, 746 cm^{-1}

Anal. (%) Found: C = 52.96 H = 4.48 N = 8.11

Calculated for $[Mn_3(L9)_2(OAc)_2(MeOH)_2]\cdot 2MeOH$ C = 53.04 H = 4.64 N = 8.07

ESI-MS

Found (M/z)	Rel. Abundance (%)	Assignment	Calc. Mass
371.05	100	$\{[Mn(HL9)]\}^+$	371.05
397.51	40	$\{[Mn_3(L9)_2]\}^{2+}$	397.51
741.08	70	$\{[Mn_2(L9)_2]\}^+$	741.08
854.03	30	$\{[Mn_3(L9)_2(OAc)]\}^+$	854.03

5.1.28 Preparation of $[Mn_2Ca(L9)_2(OAc)_2(MeOH)_2]\cdot 2MeOH$ (22)

H_2L9 (0.35 g, 1.1 mmol) was dissolved in MeOH (30 ml). $Mn(OAc)_2\cdot 4H_2O$ (0.40 g, 1.1 mmol) was added followed by addition of $Ca(OAc)_2$ (0.12 g, 0.75 mmol) in MeOH (25 ml). The resulting clear, red solution was refluxed for 4 hrs. Upon cooling to room temperature, the volume was reduced to 20 ml on rotary evaporator. A red precipitate formed. This was collected, washed with diethylether and analysed. Yield: 0.33 g, 58%. Single crystals suitable for X-ray study were obtained from slow diffusion of diethylether into a MeOH solution of the complex.

IR: 2929, 1694, 1559, 1533, 1471, 1404, 1315, 1268, 1146, 1032, 945, 816, 746 cm^{-1}

Anal. (%) Found: C = 53.28 H = 4.65 N = 7.86

Calculated for $[Mn_2Ca(L9)_2(OAc)_2(MeOH)_2]\cdot 2MeOH$ C = 53.80 H = 4.71 N = 8.18

ESI-MS

Found (M/z)	**Rel. Abundance (%)**	**Assignment**	**Calc. Mass**
371.10	100	$\{[Mn(HL9)]\}^+$	371.10
741.08	70	$\{[Mn_2(L9)_2]\}^+$	741.08

5.1.29 Preparation of [Mn(H_2L10)($NCS)_2$] (23)

H_2L10 (0.21 g 0.60 mmol) was dissolved in MeOH (20 ml). $Mn(ClO_4)_2 \cdot 6H_2O$ (0.22 g, 0.60 mmol) was added followed by addition of NaNCS (0.10 g, 1.2 mmol). The resulting clear yellow-orange solution was refluxed for 4 hrs. Upon cooling, a yellow precipitate formed. This was collected, washed with diethylether and analysed. Yield: 0.23 g, 75%.

IR: 3101, 2900, 2072, 1620, 1590, 1507, 1463, 1368, 1285, 1212, 1157, 1050, 1043, 941, 806 cm^{-1}

Anal. (%) Found:	C = 51.28	H = 3.65	N = 12.40
Calculated for $[Mn(H_2L10)(NCS)_2] \cdot H_2O$	C = 51.69	H = 3.93	N = 13.11

ESI-MS

Found (M/z)	Rel. Abundance (%)	Assignment	Calc. Mass
399.08	75	$\{[Mn(HL10)]\}^+$	399.08
797.15	100	$\{[Mn_2(HL10)_2]\}^+$	797.15
1195.22	10	$\{[Mn_3(HL10)_3]\}^+$	1195.22

5.1.30 Preparation of $[Mn(H_2L10)(N_3)_2]$ (24)

The same method was used as for (**23**) except using NaN_3 in place of NaNCS.

Quantities: H_2L10 (0.21 g, 0.60 mmol), $Mn(ClO_4)_2 \cdot 6H_2O$ (0.22 g, 0.60 mmol), NaN_3 (0.081 g, 1.2 mmol)

Colour: red, Yield: 0.36 g, 65%. No suitable crystals were obtained for single X-ray diffraction study.

IR: 3100, 2920, 2043, 1599, 1527, 1483, 1282, 1262, 1208, 1148, 1094, 932, 815 cm^{-1}

Anal. (%) Found: C = 51.76 H = 3.69 N = 25.55

Calculated for $[Mn(H_2L10)(N_3)_2]$ C = 52.07 H = 3.95 N = 26.03

ESI-MS

Found (M/z)	**Rel. Abundance (%)**	**Assignment**	**Calc. Mass**
399.08	100	$\{[Mn(HL10)]\}^+$	399.08
421.06	3	$\{[Mn(H_2L10)(N_3)]\}^+$	421.06
797.15	85	$\{[Mn_2(HL10)_2]\}^+$	797.15

5.2 Preparation of tripodal ligands and their metal complexes

5.2.1 Organic synthesis

5.2.2 Preparation of compounds N-(2-bromoethyl)phthalimide (25) and N-(3-bromopropyl)phthalimide (26)

N-(2-bromoethyl)phthalimide and N-(3-bromopropyl)phthalimide were synthesised according to the reported method.[186]

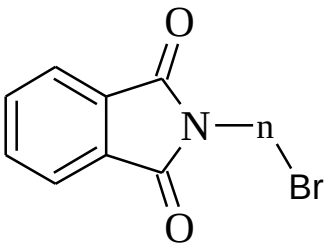

n=$(CH_2)_2$ (25)
n=$(CH_2)_3$ (26)

N-(2-bromoethyl)phthalimide (25): Potassium phthalimide (3.70 g, 20.1 mmol) and 1,2-dibromoethane (3.75 g, 20.2 mmol) were stirred in 40 ml of anhydrous dimethylformamide at room temperature for two days. The precipitated KBr was filtered off and the filtrate was concentrated using a rotary evaporator with a good vacuum. Cream coloured product formed on standing. Yield: 4.25 g, 86%.

IR 1712, 1396, 1064, 717, 509.22, 671.25 cm^{-1}

Anal. (%) Found: C = 47.25 H = 3.20 N = 5.49

Calculated for $C_{10}H_8NO_2Br$ C = 47.26 H = 3.15 N = 5.51

FAB

Found (M/z)	Rel. Abundance (%)	Assignment	Calc. Mass
254	100	$\{[C_{10}H_8NO_2Br]H\}^+$	254
321	17.19	$\{[C_{18}H_{12}N_2O_4]H\}^+$	321

NMR ($CDCl_3$, ppm, ^1H) 3.55 (*t* 2H, CH_2Br), 4.05 (*t* 2H, CH_2N), 7.70 (4H, CH Aromatic)

N-(3-bromopropyl)phthalimide (26): Compound **(26)** was prepared by the same method[186] used to prepare compound **(25)**.

Quantities: Potassium phthalimide (3.71 g, 20.0 mmol), 1,3-dibromopropane (4.05 g, 20.0 mmol).

Colour: colourless Yield: 4.10 g, 76%.

IR 1712, 1396, 1025, 736, 570.95, 639.42 cm^{-1}

Anal. (%) Found: C = 49.27 H = 3.73 N = 5.22

Calculated for $C_{11}H_{10}NO_2Br$ C = 49.05 H = 3.83 N = 5.22

FAB

Found (M/z)	**Rel. Abundance (%)**	**Assignment**	**Calc. Mass**
290	100	$\{[C_{11}H_{10}NO_2Br]Na\}^+$	290
292	97.5	$\{[C_{11}H_{10}NO_2Br]Na\}^+$	292

NMR ($CDCl_3$, ppm, ^1H) 2.32(*q* 2H, CH_2CH_2), 3.46 (*t* 2H, CH_2Br), 3.78 (*t* 2H, CH_2N), 7.77, 7.85 (4H, CH Aromatic)

5.2.3 Preparation of compounds 2,2'-Diphthalimidoethylamine (27a) and 3,3'-Diphthalimidopropylamine (27b)

2,2'-Diphthalimidoethylamine and 3,3'-diphthalimidopropylamine were synthesised according to the reported method.[80,187,188]

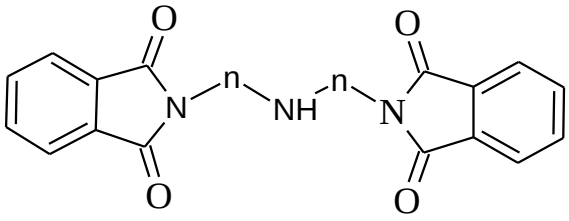

n=$(CH_2)_2$ **(27a)**
n=$(CH_2)_3$ **(27b)**

2,2'-Diphthalimidoethylamine (27a): Phthalic anhydride (7.42 g, 50.1 mmol) was melted in a beaker using an oil bath at 170 ^oC. Iminobisethylamine (2.59 g, 25.1 mmol) was added dropwise over 15 minutes with vigorous stirring to produce a brown, glassy solid on cooling. This was crushed using a pestle and mortar to give a fine, pale yellow coloured powder. The yellow product was washed with 50 ml of hot absolute EtOH and the solid product was filtered off. Yield: 8.20 g, 90%.

IR: 3325, 2947, 1774, 1712, 1396, 717 cm^{-1}

Anal. (%) Found: C = 65.82 H = 4.70 N = 11.54

Calculated for $C_{20}H_{17}N_3O_4$ C = 66.11 H = 4.68 N = 11.57

FAB

Found (M/z)	Rel. Abundance (%)	Assignment	Calc. Mass
364	100	$\{[C_{20}H_{17}N_3O_4]H\}^+$	364
365	30.47	$\{[C_{20}H_{17}N_3O_4]H\}^+$	365

NMR ($CDCl_3$, ppm, ^1H) 2.94 (*t* 2H, CH_2NH), 3.72 (2H, CH_2N), 7.64 (4H, CH Aromatic)

3,3'-Diphthalimidopropylamine (27b): Compound **(27b)** was prepared by the same method[80,187,188] used to prepare compound **(27a)**.

Quantities: Phthalic anhydrate (3.69 g, 25.1 mmol), dipropylenetriamine (1.64 g, 12.5 mmol).

Colour: orange Yield: 8.2 g, 84%.

IR: 3225, 2931, 1774, 1712, 1396, 717 cm^{-1}

Anal. (%) Found: C = 66.69 H = 5.42 N = 10.06

Calculated for $C_{22}H_{21}N_3O_4$ C = 67.50 H = 5.37 N = 10.74

FAB

Found (M/z)	**Rel. Abundance (%)**	**Assignment**	**Calc. Mass**
392	100	$\{[C_{22}H_{21}N_3O_4]H\}^+$	392
393	30	$\{[C_{22}H_{21}N_3O_4]H\}^+$	393

NMR ($CDCl_3$, ppm, ^1H) 1.84 (*q* 2H, CH_2 C), 2.65 (*t* 2H, CH_2NH), 3.73 (*t* 2H, CH_2N), 7.74, 7.78 (4H, CH Aromatic)

5.2.4 Preparation of compounds 2,2',3-triphthalimidoethylpropylamine (28) , 3,3',2-triphthalimidopropylethylamine (29) and 3,3',3-triphthalimidopropylamine (30)

2,2',3-Triphthalimidoethylpropylamine and 3,3',2-triphthalimidopropylethylamine were prepared according to the literature method.[187,188]

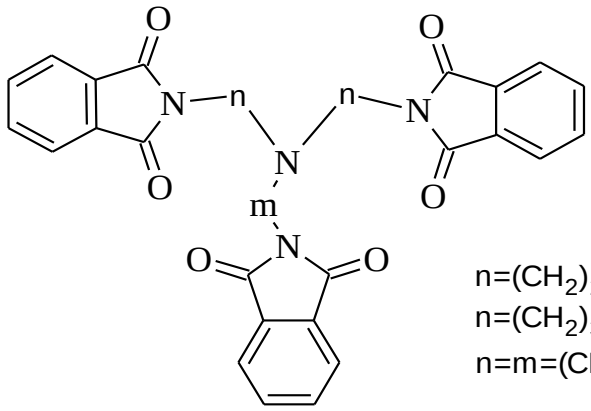

n=$(CH_2)_2$ m=$(CH_2)_3$ **(28)**
n=$(CH_2)_3$ m=$(CH_2)_2$ **(29)**
n=m=$(CH_2)_3$ **(30)**

2,2',3-Triphthalimidoethylpropylamine (28): 2, 2'-Diphthalimidoethylamine (3.64 g, 10.2 mmol) was melted in a beaker in an oil bath at 170 ^{o}C. N-(2-bromopropyl)phthalimide (2.68 g, 10.1 mmol) was added slowly over 10 minutes. On cooling, a dark brown, glassy solid was formed and crushed into powder by using a pestle and mortar, to give a finely divided, orange powder. Yield: 5.8 g, 92%.

IR 2947, 1774, 1705, 1396, 717 cm^{-1}

Anal. (%) Found: C = 66.95 H = 4.48 N = 9.56

Calculated for $C_{31}H_{26}N_4O_6$ C = 67.61 H = 4.76 N = 10.18

ESI-MS

Found (M/z)	Rel. Abundance (%)	Assignment	Calc. Mass
551	100	$\{[C_{31}H_{26}N_4O_6]H\}^+$	551
552	35	$\{[C_{31}H_{26}N_4O_6]H\}^+$	552

NMR ($CDCl_3$, ppm, ^{1}H) 1.60 (*q* 2H, CH_2), 2.40 (*t* 4H, CH_2), 3.80 (*t* 2H, CH_2), 4.14 (*t* 4H, CH_2), 7.37-8.04 (*m* 12H, CH Aromatic)

3,3',2-Triphthalimidopropylethylamine (29) and 3,3',3 triphthalimidopropylamine (30) were prepared according to the method[187,188] used to prepare (28).

3,3',2-Triphthalimidopropylethylamine (29): Quantities: 3,3'-Diphthalimidopropylamine (5.40 g, 14.2 mmol), N-(2-bromoethyl)phthalimide (3.60 g, 14.2 mmol).

Colour: orange Yield: 4.75 g, 84%.

IR 2942, 1768, 1396, 718 cm^{-1}

Anal. (%) Found: C = 67.75 H = 4.78 N = 9.66

Calculated for $C_{32}H_{28}N_4O_6$ C = 68.06 H = 5.00 N = 9.93

ESI-MS

Found (M/z)	Rel. Abundance (%)	Assignment	Calc. Mass
565	100	$\{[C_{32}H_{28}N_4O_6]H\}^+$	565
566	36	$\{[C_{32}H_{28}N_4O_6]H\}^+$	566

NMR ($CDCl_3$, ppm, ^1H) 1.36 (*q* 4H, CH_2), 2.65 (*t* 2H, CH_2), 2.70 (*t* 4H, CH_2), 3.75 (*t* 4H, CH_2), 4.25 (*t* 2H, CH_2), 7.37-7.80 (*m* 12H, CH Aromatic)

3,3',3-Triphthalimidopropylamine (30): Quantities: 3,3'-Diphthalimidopropylamine (5.55 g, 14.2 mmol), N-(3-bromopropyl)phthalimide (3.79 g, 14.2 mmol).

Colour: orange Yield: 7.46 g, 91%.

IR 2941, 1706, 1771, 1397, 719 cm^{-1}

Anal. (%) Found: C = 68.06 H = 4.92 N = 9.02

Calculated for $C_{33}H_{30}N_4O_6$ C = 68.49 H = 5.23 N = 9.69

ESI-MS

Found(M/z)	Rel. Abundance (%)	Assignment	Calc. Mass
579	100	$\{[C_{33}H_{30}N_4O_6]H\}^+$	579
580	37	$\{[C_{33}H_{30}N_4O_6]H\}^+$	580

NMR ($CDCl_3$, ppm, ^1H) 1.22 (*q* 6H, CH_2), 2.65 (*t* 6H, CH_2), 3.73 (*t* 6H, CH_2), 7.76, 7.78 (*m* 12H, CH Aromatic)

5.2.5 Preparation of compounds BAEP·4HCl (31), ABAP·4HCl (32) and TRPN·4HCl (33)

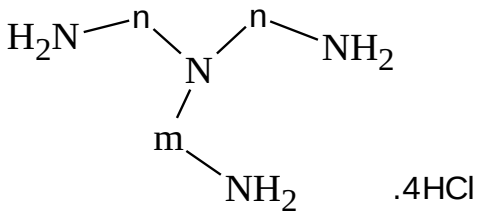

n=$(CH_2)_3$ m=$(CH_2)_2$

n=$(CH_2)_2$ m=$(CH_2)_3$

n=m=$(CH_2)_3$

BAEP·4HCl (31): 2,2',3-Triphthalimidoethylpropylamine (2.02 g, 4.00 mmol) was mixed with hydrochloric acid (30 ml, 8 M).[187,188] The mixture was heated under reflux for 19 hrs. The solid phthalic acid was removed *via* filtration and the solvent reduced to dryness leaving a green oily residue. On addition of absolute EtOH (20 ml) a white precipitate was formed. This was then stored in a desiccator. Yield: 0.51, 79%.

IR 3423, 3092, 1587, 1443 cm^{-1}

Anal. (%) Found:	C = 23.58	H = 7.72	N = 16.37
Calculated for $C_7H_{24}N_4Cl_4 \cdot 1.5(H_2O)$	C = 24.56	H = 8.11	N = 16.82

ESI-MS

Found(M/z)	Rel. Abundance (%)	Assignment	Calc. Mass
161	100	$\{[C_7H_{20}N_4]H\}^+$	161

NMR (D_2O, ppm, ^1H) 2.08 (*q* 2H, CH_2), 3.03 (*t* 2H, CH_2), 3.27 (*t* 4H, CH_2), 3.39 (*t* 4H, CH_2), 3.40 (*t* 2H, CH_2)

Compounds **(32)** and **(33)** were prepared with the same method[187,188] used to synthesise the compound **(31)**.

ABAP·4HCl (32): Quantities: 3,3',2-Triphthalimidopropylethylamine (3.5 g, 6.2 mmol), HCl (30 ml, 8M)

Colour: colourless Yield: 0.60 g, 56%.

Anal. (%) Found: C = 25.07 H = 7.57 N = 14.34

Calculated for $C_8H_{26}N_4Cl_4 \cdot 2.5H_2O$ C = 26.30 H = 7.94 N = 15.34

IR 3406, 3006, 1549, 1445 cm^{-1}

ESI-MS

Found(M/z)	**Rel. Abundance (%)**	**Assignment**	**Calc. Mass**
175	100	$\{[C_8H_{22}N_4]H\}^+$	175

NMR (D_2O, ppm, ^1H) 2.00 (*q* 4H, CH_2), 2.96 (*t* 2H, CH_2), 3.02 (*t* 4H, CH_2), 3.27 (*t* 6H, CH_2)

TRPN·4HCl (33): Quantities: 3,3',3 -Triphthalimidopropylamine (3.5 g, 6.0 mmol), HCl (30 ml, 8M)

Colour: colourless Yield: 0.90 g, 79%.

IR 3421, 2960, 1599 cm^{-1}

Anal. (%) Found: C = 31.08 H = 8.19 N = 16.00

Calculated for for $C_9H_{28}N_4Cl_4$ C = 32.33 H = 8.38 N = 16.76

ESI-MS

Found(M/z)	**Rel. Abundance (%)**	**Assignment**	**Calc. Mass**
189	100	$\{[C_9H_{24}N_4]H\}^+$	189

NMR (D_2O, ppm, ^1H) 2.10 (*q* 6H, CH_2), 3.03 (*t* 6H, CH_2), 3.28 (*t* 6H, CH_2)

5.2.6 Preparation of tripodal ligands H_3L12, H_3L13 and H_3L14

Schiff base ligands of tripods with salicylaldehyde were obtained as yellow oils (apart from H_3Saltren which is a yellow solid). NMR and mass spectra of ligands were checked before using in complexation reactions.

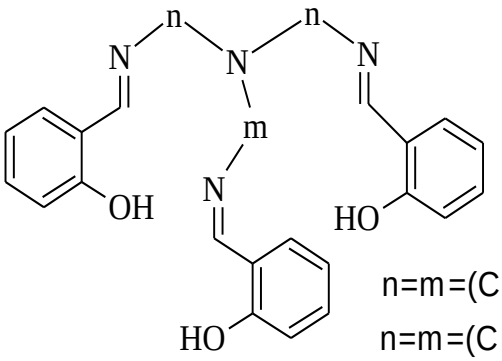

n=m=$(CH_2)_2$ **(37)**
n=m=$(CH_2)_3$ **(36)**
n=$(CH_2)_2$ m=$(CH_2)_3$ **(34)**
n=$(CH_2)_3$ m=$(CH_2)_2$ **(35)**

5.2.7 Preparation of H_3L12 (34)

BAEP.4HCl·1.5H_2O salt (0.17 g, 0.53 mmol) was placed into EtOH (20 ml) and NaOH (0.084 g, 2.1 mmol) was then added followed by salicylaldehyde (0.18 g, 1.5 mmol). The colour of the solution turned from colourless to yellow. Stirring was continued for 1 hr at room temperature. Solid NaCl was removed by filtration. The filtrate was evaporated to dryness to give a yellow oil. Yield: 0.20 g, 84%.

ESI-MS

Found (M/z)	**Rel. Abundance (%)**	**Assignment**	**Calc. Mass**
473	20	$\{[H_3L12]H\}^+$	473
495	10	$\{[H_3L12]Na\}^+$	495

NMR ($CDCl_3$, ppm, ^1H) 2.10 (*q* 2H, CH_2), 3.08 (*t* 2H, CH_2), 3.27 (*t* 4H, CH_2), 3.36 (*t* 4H, CH_2), 3.45 (*t* 2H, CH_2) 6.80- 7.74 (12H CH aromatic), 13.00-14.00 (3H OH broad)

5.2.8 Preparation of H_3L13 (35) and H_3L14 (36)

Compounds **(35)** and **(36)** were prepared by the same method used to prepare compound **(34)**.

H_3L13 (35): Quantities: ABAP.4HCl·2.5H_2O (0.18 g, 0.52 mmol), NaOH (0.084 g, 2.1 mmol), salicylaldehyde (0.18 g, 1.5 mmol).

Colour: yellow Yield: 0.19 g, 79 %.

ESI-MS

Found (M/z)	Rel. Abundance (%)	Assignment	Calc. Mass
383	100	$\{[C_{22}H_{30}N_4O_2]H\}^+$	383
487	45	$\{[H_3L13]H\}^+$	487
509	15	$\{[H_3L13]Na\}^+$	509

NMR ($CDCl_3$, ppm, ^1H) 2.05 (*q* 4H, CH_2), 2.88 (*t* 2H, CH_2), 3.01 (*t* 4H, CH_2), 3.40 (*t* 6H, CH_2) 6.65- 7.84 (12H CH aromatic), 13.00-14.00 (3H OH broad)

H_3L14 (36): Quantities: TRPN.4HCl. (0.17 g, 0.5 mmol), NaOH (0.084 g, 2.1 mmol), salicylaldehyde (0.18 g, 1.5 mmol).

Colour: yellow Yield: 0.21 g, 77%.

ESI-MS

Found (M/z)	Rel. Abundance (%)	Assignment	Calc. Mass
501	100	$\{[H_3L14]H\}^+$	501
523	10	$\{[H_3L14]Na\}^+$	523
397	95	$\{[C_{23}H_{32}N_4O_2]H\}^+$	397

NMR (CDCl3, ppm, ^1H) 1.31 (*q* 6H CH_2), 2.59 (*t* 6H CH_2) 3.59 (*t* 6H CH), 6.74-7.74 (*m* 12H CH aromatic), 13.00-14.00 (3H OH broad)

5.2.9 Preparation of compound H_3L11 (H_3Saltren)[188] (37)

Tris-(2-aminoethyl)-amine (0.30 g, 2.0 mmol) was dissolved 5 ml of MeOH and stirred. Salicylaldehyde (0.75 g, 6.1 mmol) in MeOH (5 ml) was added to the stirring solution and stirring was continued for 15 minutes. On addition of salicaldehyde, a yellow precipitate was formed. The product was dried overnight. The yellow solid was crystallized by slow evaporation of an EtOH solution of the compound to give crystals, which were collected and analysed. Yield: 0.90 g, 95%.

IR 2939, 1635, 1280 756 cm^{-1}

Anal. (%) Found:	C = 70.37	H = 6.74	N = 12.07
Calculated for [H_3L11]	C = 70.74	H = 6.55	N = 12.23

ESI-MS

Found (M/z)	**Rel. Abundance (%)**	**Assignment**	**Calc. Mass**
459	100	$\{[H_3L11]H\}^+$	459
481	16.62	$\{[H_3L11]Na\}^+$	481

NMR (CDCl3, ppm, ^{1}H) 2.76 (*t* 6H CH_2 aliphatic), 3.45 (*t* 6H aliphatic) 6.53 (*d* 3H CH aromatic), 6.87 (*d* 3H CH aromatic), 7.19 (*t* 3H CH aromatic), 7.72 (*t* 3H CH aromatic), 8.65 (*s* 3H CH=N), 13.75 (3H OH[8])

5.2.10 Preparation of [Mn(L11)] (38)

H_3Saltren (0.30 g, 0.66 mmol) was dissolved 5 ml of EtOH and stirred. To the stirring solution, the aqueous (30 ml) solution of Mn(II)$SO_4 \cdot 4H_2O$ (0.15 g, 0.66 mmol) was then added and the mixture was stirred for 5 hrs at room temperature. The mixture was set aside at room temperature in air. After a month a dark green manganese(III) complex was collected, washed with diethylether and analysed. Yield: 0.22 g, 63%.

IR 2927, 1692, 767 cm^{-1}

Anal. (%) Found:	C = 63.10	H = 5.36	N = 10.76
Calculated for [Mn(L11)]	C = 63.53	H = 5.29	N = 10.98

ESI-MS

Found (M/z)	Rel. Abundance (%)	Assignment	Calc. Mass
510.1	20	$\{[Mn(L11)]H\}^+$	510.1
407.2	100	$\{[MnC_{20}H_{24}N_4O_2]H\}^+$	407.2

5.2.11 Preparation of Mn(III) complexes (39)-(40)

5.2.12 Preparation of [Mn(L12)] (39) and [Mn(L13)] (40)

Complexes (39) and (40) were prepared by the same method used to prepare complex (38).

[Mn(L12)] (39): Quantities: H_3L12 (0.10 g, 0.21 mmol), $MnSO_4 \cdot 4H_2O$ (0.05 g, 0.23 mmol)

Colour: dark green, Yield: 0.05 g, 41%.

IR 2928, 1600, 1613, 756 cm^{-1}

Anal. (%) Found:	C = 59.49	H = 5.18	N = 9.69
Calculated for [Mn(L12)]$\cdot 2H_2O$	C = 60.82	H = 5.81	N = 9.79

ESI-MS

Found (M/z)	Rel. Abundance (%)	Assignment	Calc. Mass
525.16	15	$\{[Mn(Ll2)]\}H^+$	525.16
421.14	100	$\{[MnC_{21}H_{26}N_4O_2]H\}^+$	421.14

[Mn(L13)] (40): Quantities: H_3L13 (0.10 g, 0.21 mmol), $MnSO_4 \cdot 4H_2O$ (0.05 g, 0.23 mmol)

Colour: dark green Yield: 0.06 g, 51%.

IR 2936, 1618, 1297, 759 cm^{-1}

Anal. (%) Found:	C = 59.70	H = 5.48	N = 8.99
Calculated for $[Mn(L13)]\cdot 3H_2O$	C = 60.61	H = 6.14	N = 9.75

ESI-MS

Found (M/z)	**Rel. Abundance (%)**	**Assignment**	**Calc. Mass**
539.18	100	$\{[Mn(L13)]H\}^+$	539.18
435.15	5	$\{[MnC_{22}H_{28}N_4O_2]\}^+$	435.15

5.2.13 Preparation of L15 ligand

Tris(2-aminoethyl-amine) (0.29 g, 2.0 mmol) was dissolved in 30 ml of MeOH. To the stirring solution, 2-pyridinecarboxaldehyde (0.64 g, 6.0 mmol) was then added. The mixture was then stirred for 12 hrs at room temperature. The solution was then evaporated and dried under vacuum. Yellow brown oil was obtained. Yield: 0.63, 75%.

NMR (CDCl3, ppm, ^{1}H) 3.03 (*t* 6H CH_2[1]), 3.82 (*t* 6H CH_2 aliphatic), 7.31, 7.71, 7.91 (*m* 12H CH aromatic), 8.62 (*s* 3H CH=N)

5.2.14 Preparation of $[Mn(L15)](ClO_4)_2$ (41)

The ligand L15 (0.30 g, 0.72 mmol) was dissolved in 20 ml of MeOH. $MnCl_2 \cdot 4H_2O$ (0.14 g, 0.72 mmol) was added to the stirring solution followed by $NaClO_4$ (0.18 g). The solution was refluxed for 2 hrs. On cooling, fine yellowish crystals formed were collected and dried. Yield: 0.35, 74%.

IR 2919, 1627, 783, 623 cm^{-1}

Anal. (%) Found:	C = 42.62	H = 4.06	N = 14.31
Calculated for $[Mn(L15)](ClO_4)_2$	C = 43.18	H = 4.04	N = 14.60

ESI-MS

Found (M/z)	Rel. Abundance (%)	Assignment	Calc. Mass
567	100	$\{[Mn(L15)](ClO_4)]\}^+$	567
569	32	$\{[Mn(L15)](ClO_4)]\}^+$	569

5.2.15 Preparation of L16, L17, L18 and their Mn(II) complexes

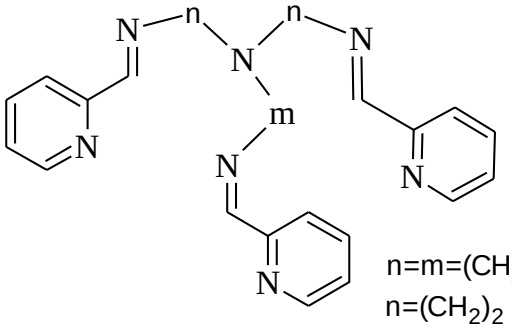

n=m=$(CH_2)_3$ **(42)** **L18**
n=$(CH_2)_2$ m=$(CH_2)_3$ **(43)** **L16**
n=$(CH_2)_3$ m=$(CH_2)_2$ **(44)** **L17**

5.2.16 Preparation of $[Mn(L18)](ClO_4)_2$ (42)

TRPN.4HCl salt (0.33 g, 1.0 mmol) was placed into EtOH (20 ml) and NaOH (0.16 g, 4.0 mmol) was then added followed by 2-pyridinecarboxaldehyde (0.31g, 1.0 mmol). The colour of the solution turned from colourless to yellow. Stirring continued for 1 hr at room temperature. Solid NaCl was removed *via* filtration. Solvent was evaporated to give an orange-brown oil. The oil was dissolved in MeOH (30 ml) followed by addition of $Mn(II)(ClO_4)_2 \cdot 6H_2O$ (0.36 g, 1.00 mmol). A yellow precipitate formed. It was collected, washed with MeOH and analysed. Yield: 0.52 g, 70%. Yellow crystals suitable for X-ray were obtained by slow diffusion of diethylether into a dmf solution of the complex.

IR 2921, 1654, 109, 622 cm^{-1}

Anal. (%) Found:	C = 45.42	H = 4.47	N = 13.69
Calculated for $[Mn(L18)](ClO_4)_2$	C = 45.69	H = 4.65	N = 13.82

ESI-MS

Found (M/z)	Rel. Abundance (%)	Assignment	Calc. Mass
609.16	100	$\{[Mn(L18)](ClO_4)\}^+$	609.16
255.10	45	$\{[Mn(L18)]\}^{2+}$	255.10

5.2.17 Preparation of $[Mn(L16](ClO_4)_2$ (43) and $[Mn(L17)](ClO_4)_2$ (44)

The same experimental procedure to form **(42)** was followed to obtain complexes **(43)** and **(44)**.

$[Mn(L16)](ClO_4)_2$ (43): Quantities: BAEP.4HCl (0.30 g, 1.0 mmol), NaOH (0.16 g, 4.0 mmol), 2-pyridinecarboxaldehyde (0.31 g, 3.0 mmol), $Mn(ClO_4)_2 \cdot 6H_2O$ (0.36 g, 1.0 mmol).

Colour: yellow-brown, Yield: 0.45 g, 65%. Yellow coloured crystals suitable for X-ray were obtained by slow diffusion of diethylether into a solution of the in dmf.

IR 2928, 1655, 1090, 623 cm^{-1}

Anal. (%) Found:	C = 44.52	H = 4.32	N = 13.73
Calculated for $[Mn(L16)](ClO_4)_2$	C = 44.89	H = 4.46	N = 14.10

ESI-MS

Found (M/z)	Rel. Abundance (%)	Assignment	Calc. Mass
595.14	100	$\{[Mn(L16)](ClO_4)\}^+$	595.14
248.10	35	$\{[Mn(L16)]\}^{2+}$	248.10

$[Mn(L17](ClO_4)_2$ (44): Quantities: ABAP.4HCl (0.32 g, 1.0 mmol), NaOH (0.16 g, 4.0 mmol), 2-pyridinecarboxaldehyde (0.31 g, 3.00 mmol), $Mn(ClO_4)_2 \cdot 6H_2O$ (0.36 g, 1.0 mmol). Colour: yellow Yield: 0.43 g, 72%.

IR 2929, 1659, 1089, 623 cm^{-1}

Anal. (%) Found:	C = 44.15	H = 4.01	N = 13.98
Calculated for $[Mn(L17)](ClO_4)_2$	C = 44.05	H = 4.25	N = 14.39

ESI-MS

Found (M/z)	Rel. Abundance (%)	Assignment	Calc. Mass
581.13	100	$\{[Mn(L17)](ClO_4)\}^+$	581.13
241.09	60	$\{[Mn(L17)]\}^{2+}$	241.09

5.3 Preparation of N-alkylated benzimidazole ligand (L19)

5.3.1 2,6-Bis(benzimidazol-2'-yl)pyridine (BBP) (45)

2,6-Bis(benzimidazol-2'-yl)pyridine was synthesised by the literature method.[196] Pyridine-2,6-dicarboxylic acid (3.35 g, 20.0 mmol) was stirred with o-phenylenediamine (4.70 g, 44.0 mmol) in syrupy phosphoric acid (40 ml) at 230 ºC for 4 hrs. The dark blue melt was poured into stirred cold water (1L). On cooling, a blue-green precipitate was collected and slurried with a 10 % aqueous solution of sodium carbonate (300 ml). The product was collected and recrystallised from MeOH to give white crystals. Yield: 4.20 g, 68%.

IR: 3193, 1601, 1573, 1318, 1278, 1230, 819, 738 cm^{-1}

Anal. (%) Found: C = 69.25 H = 4.38 N = 19.56

Calculated for $(C_{19}H_{13}N_5)\cdot CH_3OH$ C = 69.97 H = 4.96 N = 20.40

ESI-MS

Found (M/z)	Rel. Abundance (%)	Assignment	Calc. Mass
312.12	100	$\{[C_{19}H_{13}N_5]H\}^+$	312.12
334.10	32	$\{[C_{19}H_{13}N_5]Na\}^+$	334.10

NMR: (dmso as solvent, ppm, ^1H) 7.31 (*t*, 4H, CH aromatic), 7.76(*d* 4H CH aromatic), 8.16 (*t* 1H CH aromatic), 8.34 (*d* 1H CH aromatic)

5.3.2 2,6-Bis(1-butyl-1H-benzo[d]imidazol-2'-yl)pyridine (L19) (46)

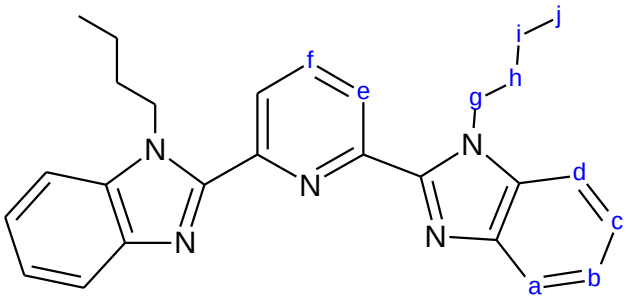

L19

N-alkylation of 2,6-bis(benzimidazol-2'-yl)pyridine was prepared slightly differently from the reported method.[197] 2,6-Bis(benzimidazol-2'-yl)pyridine (1.00 g, 3.20 mmol) and NaOH (0.50 g, 12 mmol) was stirred overnight at 60 ºC. To the stirring solution, 4-bromobutane (1.30 g, 9.60 mmol) was added and stirred for two days at 60 ºC. After two days, the solvent was removed by rotary evaporation to give a white-yellow residue. Chloroform (20 ml) was added to the residue and KBr was removed by filtration. The chloroform was removed on a rotary evaporator to give a sticky cream coloured product. Yield: 0.92 g, 68%.

IR: 2956, 1571, 1328, 1285, 823, 740 cm^{-1}

Anal. (%) Found:	C = 75.96	H = 6.55	N = 16.20
Calculated for L19	C = 76.59	H = 6.85	N = 16.54

ESI-MS

Found (M/z)	**Rel. Abundance (%)**	**Assignment**	**Calc. Mass**
424.25	100	$\{[L19]H\}^+$	424.25
446.23	60	$\{[L19]Na\}^+$	446.23
869.47	25	$\{[(L19)_2]Na\}^+$	869.47

^{1}H NMR: ($CDCl_3$ as solvent, ppm,), 0.71 (*t* 6H CH_3^j-C), 1.35 (*s* (*sextet*) 4H C-CH_2^i-C), 1.72(*q (quintet)* 4H C-CH_2^h-), 4.73 (*t* 4H CH_2^g), 7.37-7.39 (*t* 4H $CH^{b,c}$ aromatic), 7.47 (*d* 4H CH^d aromatic), 7.89(*d* 4H^a CH aromatic), 8.06 (*t* 1H CH^f aromatic), 8.33 (*d* 1H^e CH aromatic). **^{13}C NMR** ($CDCl_3$ as solvent, ppm): 13.48, 19.85, 32.12, 44.64 (aliphatic), 110.39, 120.34, 122.71, 123.47, 125.50, 136.31, 138.11, 142.86, 150.57 (aromatic)

5.3.3 Preparation of metal complexes of L19

$[Mn(L19)Cl_2]$ (**47**), $[Mn(L19)(NO_3)_2]$ (**50**) and $[Mn(L19)_2](ClO_4)_2$ (**49**) were prepared by simply mixing ligand (L19) with appropriate Mn(II) salts in MeOH. A yellow colour appeared and a precipitate was formed in a few minutes. Reaction mixtures were stirred for 2 hrs. Yellow products were collected by filtration and washed with MeOH (10 ml), EtOH (10 ml) and Et_2O (10 ml).

For the synthesis of $[Mn(L19)(NCS)_2]$ (**48**) and $[Mn(L_{19})_2](PF_6)_2$ (**51**): To a solution of L19 in CH_3OH, a solution of $Mn(OAc)_2{\cdot}4H_2O$ in CH_3OH was added dropwise with stirring at room temperature. A yellow coloured clear solution appeared. To the stirring solutions, NaNCS or KPF_6 were added in CH_3OH and a precipitate formed in a few minutes. Reaction mixtures were stirred for 2 hrs. Yellow products were collected by filtration and washed with MeOH (10 ml), EtOH (10 ml) and diethylether (10 ml) and analysed.

5.3.4 $[Mn(L19)Cl_2]$ (47)

Quatities: L19 (0.42 g, 1.00 mmol), $MnCl_2{\cdot}4H_2O$ (0.19 g, 1.0 mmol)

Colour: yellow Yield: 0.38 g, 69%.

IR: 2959, 2932, 2872, 1596, 1567, 1514, 1482, 1459, 1415, 1333, 1154, 1004, 820, 755, 433, 302 cm^{-1}

Anal. (%) Found:	C = 58.81	H = 5.34	N = 12.64
Calculated for $[Mn(L19)Cl_2]$	C = 59.03	H = 5.32	N = 12.75

ESI-MS

Found (M/z)	Rel. Abundance (%)	Assignment	Calc. Mass
450.71	100	$\{[Mn(L19)_2]\}^{2+}$	450.71
513.15	20	$\{[Mn(L19)Cl]\}^{+}$	513.15
936.39	40	$\{[Mn(L19)_2Cl]\}^{+}$	936.39

5.3.5 [Mn(L19)(NCS)$_2$] (48)

Quatities: L19 (0.42 g, 1.0 mmol), Mn(OAc)$_2$·4H$_2$O (0.25 g, 1.0 mmol), NaNCS (0.16 g, 2.0 mmol)

Colour: Yellow Yield: 0.42 g, 71%.

IR: 2960, 2930, 2871, 1599, 1572, 1515, 1483, 1459, 1420, 1332, 1088, 811, 749, 622, 429, 306 cm^{-1}

Anal. (%) Found:	C = 59.30	H = 5.22	N = 16.12
Calculated for [Mn(L19)(NCS)$_2$]	C = 58.59	H = 4.88	N = 16.49

ESI-MS

Found (M/z)	Rel. Abundance (%)	Assignment	Calc. Mass
450.71	70	{[Mn(L19)$_2$]}$^{2+}$	450.71
536.15	20	{[Mn(L19)(NCS)]}$^{+}$	536.15
959.39	100	{[Mn(L19)$_2$(NCS)]}$^{+}$	959.39

5.3.6 [Mn(L19)](ClO$_4$)$_2$ (49)

Quatities: L19 (0.42 g, 1.0 mmol), Mn(ClO$_4$)$_2$·6H$_2$O (0.19 g, 0.50 mmol)

Colour: Yellow, Yield: 0.32 g, 58%.

IR: 2960, 2930, 2871, 1599, 1572, 1515, 1483, 1459, 1420, 1332, 1088, 811, 749, 622, 429, 306 cm^{-1}

Anal. (%) Found:	C = 58.50	H = 5.34	N = 12.47
Calculated for [Mn(L19)$_2$](ClO$_4$)$_2$	C = 58.91	H = 5.31	N = 12.72

ESI-MS

Found (M/z)	Rel. Abundance (%)	Assignment	Calc. Mass
450.71	100	{[Mn(L19)$_2$]}$^{2+}$	450.71
1000.31	20	{[Mn(L19)$_2$](ClO$_4$)}$^{+}$	1000.31

5.3.7 $[Mn(L19)(NO_3)_2]$ (50)

Quatities: L19 (0.42 g, 1.0 mmol), $Mn(NO_3)_2 \cdot xH_2O$ (x= 4 or 6) (0.28 g, 1.1 mmol, based on x=4).

Color: Pale yellow, Yield: 0.54 g, 85%.

IR: 2962, 2933, 2874, 1599, 1567, 1513, 1484, 1458, 1415, 1332, 1281, 1153, 1025, 817, 752, 432, 306 cm^{-1}

Anal. (%) Found:	C = 53.18	H =4.79	N = 15.78
Calculated for $[Mn(L19)(NO_3)_2]$	C = 53.82	H = 4.73	N = 16.28

ESI-MS

Found (M/z)	Rel. Abundance (%)	Assignment	Calc. Mass
424.24	100	$\{[L19]H\}^+$	424.24
450.71	25	$\{[Mn(L19)_2]\}^{2+}$	450.71
540.16	10	$\{[Mn(L19)(NO_3)]\}^+$	540.16
847.49	28	$\{[(L19)_2]H\}^+$	847.49
963.40	24	$\{[Mn(L19)_2(NO_3)]\}^+$	963.40

5.3.8 $[Mn(L19)_2](PF_6)_2$ (51)

Quatities: L19 (0.42 g, 1.0 mmol), $Mn(OAc)_2 \cdot 4H_2O$ (0.25, 0.50 mmol), KPF_6 (0.18 g, 1.0 mmol)

Color: Yellow, Yield: 0.53 g, 76%.

IR: 2962, 2931, 2875, 1600, 1572, 1514, 1482, 1459, 1433, 1332, 1158, 1010, 839, 746, 557, 427, 306 cm^{-1}

Anal. (%) Found:	C = 53.81	H =4.76	N = 11.78
Calculated for $[Mn(L19)_2](PF_6)_2$	C = 54.41	H = 4.87	N = 11.75

ESI-MS

Found (M/z)	Rel. Abundance (%)	Assignment	Calc. Mass
446.23	100	$\{[L19]Na\}^+$	446.23
450.71	95	$\{[Mn(L19)_2]\}^{2+}$	450.71

References

1. L. F. Lindoy, *The Chemistry of Macrocyclic Ligand Complexes*, Cambridge University Press, Cambridge, 1989.
2. E. C. Constable, *Coordination Chemistry of Macrocyclic Compounds*, Oxford University Press, New York, 1999.
3. K. Gloe, *Macrocyclic Chemistry: Current Trends and Future Perspectives*, Springer, Netherlands, 2005.
4. a) N. F. Curtis, *Coord. Chem. Rev.*, 1968, **3**, 3-47. b) N. F. Curtis, *Supramolecular Chemistry*, 2012, **24**, 439-447.
5. K. S. Banu, T. Chattopadhyay, A. Banerjee, S. Bhattacharya, E. Zangrando and D. Das, *J. Mol. Cat.. A: Chemical*, 2009, **310**, 34-41.
6. V. Alexander, *Coord. Chem. Rev.,* 1995, **95**, 273-342.
7. G. T. Morgan and H. D. K. Drew, *J. Chem. Soc., Trans*, 1920, **117**, 1456-1465.
8. H. Diehl, *Chem. Rev.,* 1937, **21**, 39-111.
9. M. Calvin and K. W. Wilson, *J. Am. Chem. Soc.,* 1945, **67**, 2003-2007.
10. B. Korybut-Daszkiewicz, R. Bilewicz and K. Woźniak, *Coord. Chem. Rev.,* 2010, **254**, 1637-1660.
11. R. E. Mewis and S. J. Archibald, *Coord. Chem. Rev.,* 2010, **254**, 1686-1712.
12. D. K. Cabbiness and D. W. Margerum, *J. Am. Chem. Soc.,* 1969, **91**, 6540-6541.
13. D. K. Cabbiness and D. W. Margerum, *J. Am. Chem. Soc.,* 1970, **92**, 2151-2153.
14. F. P. Hinz and D. W. Margerum, *J. Am. Chem. Soc.,* 1974, **96**, 4993-4994.
15. F. P. Hinz and D. W. Margerum, *Inorg. Chem.,* 1974, **13**, 2941-2949.
16. M. Kodama and E. Kimura, *J. Chem. Soc., Chem. Commun.,* 1975, 326-327.
17. J. J. Christensen, D. J. Etough and R. M. Izatt, *Chem. Rev.*, 1974, **74**, 351-384.
18. M. Micheloni and P. Paoletti, *Inorg. Chim. Acta,* 1980, **43**, 109-112.
19. M. C. Thompson and D. H. Busch, *J. Am. Chem. Soc.*, 1962, **84**, 1762-1763.
20. M. C. Thompson and D. H. Busch, *J. Am. Chem. Soc.*, 1964, **86**, 213-217.
21. M. C. Thompson and D. H. Busch, *J. Am. Chem. Soc.*, 1964, **86**, 3651-3656.
22. L. T. Taylor, N. C. Rose and D. H. Busch, *Inorg. Chem.*, 1968, **7**, 785-789.
23. C. A. Root and D. H. Busch, *Inorg. Chem.,* 1968, **7**, 789-795.
24. E. L. Blinn and D. H. Busch, *Inorg. Chem.*, 1968, **7**, 820-824.

25. R. G. Pearson, *J. Am. Chem. Soc.*, 1963, **85**, 3533-3539.
26. R. G. Pearson and J. Songstad, *J. Am. Chem. Soc.*, 1967, **89**, 1827-1836.
27. R. G. Pearson, *J. Am. Chem. Soc.*, 1988, **110**, 7684-7690.
28. R. G. Pearson, *Inorg. Chem.*, 1988, **27**, 734-740.
29. H. Schiff, *Justus Liebigs Ann. Chem.*, 1864, **131**, 118-119.
30. P. Pfeiffer, E. Buchholz and O. Bauer, *J. Prakt. Chem.*, 1931, **129**, 163-177.
31. G. H. Schmid, *Organic Chemistry*, McGraw-Hill Science, 1995.
32. S. F. Lincoln, *Coord. Chem. Rev.*, 1997, **166**, 255-289.
33. S. M. Nelson, *Inorg. Chim. Acta*, 1982, **62**, 39-50.
34. A. Star, I. Goldberg and B. Fuchs, *J. Organomet. Chem.*, 2001, **630**, 67-77.
35. H. Shimakoshi, T. Kai, I. Aritome and Y. Hisaeda, *Tet. Lett.*, 2002, **43**, 8261-8264.
36. M. Salavati-Niasari, E. Zamani and M. Bazarganipour, *Appl. Clay. Sci.*, 2007, **38**, 9-16.
37. S. M. Nelson, *Pure & Appl. Chem.*, 1980, **52**, 2461-2476.
38. D. E. Fenton, *Pure & Appl. Chem.*, 1986, **58**, 1437-1444.
39. A. Aguiari, E. Bullita, U. Casellato, P. Guerriero, S. Tamburini and P. A. Vigato, *Inorg. Chim. Acta*, 1992, **202**, 157-171.
40. L. F. Lindoy, *Supramol. Chem.*, 2012, **24**, 448-461.
41. P. Guerriero, S. Tarnburini and P. A. Vigato, *Coord. Chem. Rev.*, 1995, **139**, 17-243.
42. S. R. Collinson and D. E. Fenton, *Coord. Chem. Rev.*, 1996, **148**, 19-40.
43. P. A. Vigato and S. Tamburini, *Coord. Chem. Rev.*, 2004, **248**, 1717-2128.
44. P. A. Vigato, S. Tamburini and L. Bertolo, *Coord. Chem. Rev.*, 2007, **251**, 1311-1492.
45. S. Menon, S. Jogani and Y. Agrawal, *Rev. Anal. Chem.*, 2000, **19**, 361-412.
46. P. A. Vigato, V. Peruzzo and S. Tamburini, *Coord. Chem. Rev.*, 2012, **256**, 953-1114.
47. D. A. House and N. F. Curtis, *J. Am. Chem. Soc.*, 1962, **84**, 3248-3250.
48. D. A. House and N. F. Curtis, *J. Am. Chem. Soc.*, 1964, **86**, 223-225.
49. D. A. House and N. F. Curtis, *J. Am. Chem. Soc.*, 1964, **86**, 1331-1334.
50. N. Curtis, *J. Chem. Soc. Dalton Trans.*, 1973, 863-866.
51. V. McKee, W. T. Robinson, D. McDowell and J. Nelson, *Tet. Lett.*, 1989, **30**, 7453-7456.

52. Y. Nishida, N. Tanaka, A. Yamazaki, T. Tokii, N. Hashimoto, K. Ide and K. Iwasawa, *Inorg. Chem.,* 1995, **34**, 3616-3620.
53. O. Jimenez-Sandoval, D. Ramirez-Rosales, M. del Jesus Rosales-Hoz, M. Elena Sosa-Torres and R. Zamorano-Ulloa, *J. Chem. Soc., Dalton Trans.,* 1998, 1551-1556.
54. D. Zhang, H. Wang, L. Tian, J. Jiang and Z. Ni, *Cryst. Eng. Comm.,* 2009, **11**, 2447-2451.
55. M. F. Cabral, B. Murphy and J. Nelson, *Inorg. Chim. Acta*, 1984, **90**, 169-178.
56. W. D. Carlisle, D. E. Fenton, D. C. Mulligan, P. B. Roberts, P. Alessandro Vigato and S. Tamburini, *Inorg. Chim. Acta,* 1987, **126**, 233-235.
57. M. G. B. Drew, P. C. Yates, B. P. Murphy, J. Nelson and S. M. Nelson, *Inorg. Chim. Acta*, 1986, **118**, 37-47.
58. D. E. Fenton, U. Casellato, P. A. Vigato and M. Vidali, *Inorg. Chim. Acta,* 1984, **94**, 6-11.
59. D. McDowell, J. Nelson and V. McKee, *Polyhedron,* 1989, **8**, 1143-1145.
60. A. J. Downard, V. McKee and S. S. Tandon, *Inorg. Chim. Acta,* 1990, **173**, 181-190.
61. M. G. B. Drew, C. J. Harding and J. Nelson, *Inorg. Chim. Acta,* 1996, **246**, 73-79.
62. H. Adams, D. E. Fenton and S. J. Ryan, *Inorg. Chem. Commun.,* 1999, **2**, 52-54.
63. H. Adams, N. A. Bailey, S. R. Collinson, D. E. Fenton, C. J. Harding and S. J. Kitchen, *Inorg. Chim. Acta,* 1996, **246**, 81-88.
64. H. Adams, R. Bastida, A. de Blas, M. Carnota, D. E. Fenton, A. Macias, A. Rodriguez and T. Rodriguez-Blas, *Polyhedron,* 1997, **16**, 567-572.
65. S. Brooker, *Coord. Chem. Rev.,* 2001, **222**, 33-56.
66. H. Keypour, H. Goudarziafshar, A. K. Brisdon and R. G. Pritchard, *Inorg. Chim. Acta,* 2007, **360**, 2298-2306.
67. J. Barreira-Fontecha, R. Kulmaczewski, X. Ma and V. McKee, *J. Chem. Soc. Dalton Trans.,* 2011, **40**, 12040-12043.
68. D. E. Fenton, D. H. Cook, I. W. Nowell and P. E. Walker, *J. Chem. Soc., Chem. Commun.,* 1978, 279-280.
69. D. H. Cook and D. E. Fenton, *J. Chem. Soc., Dalton Trans.,* 1979, 266-272.
70. D. H. Cook, D. E. Fenton, M. G. B. Drew, A. Rodgers, M. McCann and S. M. Nelson, *J. Chem. Soc., Dalton Trans.,* 1979, 414-419.

71. S. M. Nelson, C. V. Knox, M. McCann and M. G. B. Drew, *J. Chem. Soc., Dalton Trans.,* 1981, 1669-1677.
72. M. G. B. Drew, A. Rodgers, M. McCann and S. M. Nelson, *J. Chem. Soc., Chem. Commun.,* 1978, , 415-416.
73. V. McKee and J. Smith, *J. Chem. Soc., Chem. Commun.,* 1983, 1465-1467.
74. H. Adams, N. A. Bailey, D. E. Fenton, P. D. Hempstead and G. P. Westwood, *J. Inclusion Phenomena,* 1991, **11**, 63-69.
75. Z. Pan, Q. Luo, C. Duan and M. Shen, *Polyhedron,* 2001, **20**, 2945-2950.
76. N. A. Bailey, D. E. Fenton, I. T. Jackson, R. Moody and C. O. Rodriguez de Barbarin, *J. Chem. Soc., Chem. Commun.,* 1983, 1463-1465.
77. R. Menif, A. E. Martell, P. J. Squattrito and A. Clearfield, *Inorg. Chem.,* 1990, **29**, 4723-4729.
78. S. M. Nelson, F. S. Esho, M. G. B. Drew and P. Bird, *J. Chem. Soc., Chem. Commun.,* 1979, 1035-1037.
79. M. G. B. Drew, M. McCann and S. M. Nelson, *J. Chem. Soc., Dalton Trans.,* 1981, 1968-1978.
80. A. G. Blackman, *Polyhedron,* 2005, **24**, 1-39.
81. N. J. Lundin, I. G. Hamilton and A. G. Blackman, *Polyhedron,* 2004, **23**, 97-102.
82. E. Ristenpart, *Berichte der Deutschen Chemischen Gesellschaft,* 1896, **29**, 2526-2533.
83. F. G. Mann and W. J. Pope, *Proc. Roy. Soc. of London. Series A,* 1925, **109**, 444-458.
84. A. E. Martell, R. D. Hancock and R. J. Motekaitis, *Coord. Chem. Rev.,* 1994, **133**, 39-65.
85. J. Costes, A. Dupuis, G. Commenges, S. Lagrave and J. Laurent, *Inorg. Chim. Acta,* 1999, **285**, 49-54.
86. P. Wei and D. A. Atwood, *J. Organomet. Chem.,* 1998, **563**, 87-93.
87. P. Bhattacharyya, J. Parr and A. M. Z. Slawin, *Inorg. Chem. Comm.* 1999, **2**, 113-115.
88. A. Mustapha, K. Busch, M. Patykiewicz, A. Apedaile, J. Reglinski, A. R. Kennedy and T. J. Prior, *Polyhedron,* 2008, **27**, 868-878.
89. H. Keypour, S. Salehzadeh and R. V. Parish, *Molecules,* 2002, **7**, 140-144.

90. M. G. B. Drew, C. J. Harding, V. McKee, G. G. Morgan and J. Nelson, *J. Chem. Soc., Chem. Commun.*, 1995, 1035-1038.
91. a) C. Gedye, C. Harding, V. McKee, J. Nelson and J. Patterson, *J. Chem. Soc., Chem. Commun.*, 1992, 392-394. b) S. Chandra, P. Chakraborty and A. Chakravorty, *J. Chem. Soc. Dalton Trans.*, 1993, 863-869.
92. G. Anderegg and F. Wenk, *Helv. Chim. Acta*, 1967, **50**, 2330-2332.
93. K. D. Karlin, J. C. Hayes, J. P. Hutchinson, J. R. Hyde and J. Zubieta, *Inorg. Chim. Acta*, 1982, **64**, 219-220.
94. J. S. Valentine, in *Biological Inorganic Chemistry Structure and Reactivity*, Eds. I. Bertini, H. B. Gray, E. I. Stiefel and J. S. Valentine, University Science Books, California, 2007, 319-353.
95. S. Stohs and D. Bagchi, *Free Radic. Biol. Med.*, 1995, **18**, 321-336.
96. K. Aston, N. Rath, A. Naik, U. Slomczynska, O. F. Schall and D. P. Riley, *Inorg. Chem.*, 2001, **40**, 1779-1789.
97. K. Kahlos, *PhD thesis*, University of Oulu, 1999. (web access)
98. a) R. J. Pace, R. Stranger and S. Petrie, *J. Chem. Soc. Dalton Trans.*, 2012, **41**, 7179-7189. b) O. Iranzo, *Bioorg. Chem.*, 2011, **39**, 73-87.
99. I. Fridovich, *J. Biol. Chem.*, 1989, **264**, 7761-7764.
100. I. Fridovich, *Annu. Rev. Biochem.*, 1995, **64**, 97-112.
101. I. Fridovich, *Ann. N. Y. Acad. Sci.*, 1999, **893**, 13-18.
102. D. Flint, J. Tuminello and M. Emptage, *J. Biol. Chem.*, 1993, **268**, 22369-22376.
103. H. Yanagisawa, M. Sato, M. Nodera, O. Wada and *J. Hypertens.*, 2004, **22**, 543-550.
104. M. Kurzelewski, E. Czarnowska and A. Beresewicz, *J. Physio.& Pharm.*, 2005, **56**, 163-178.
105. P. A. Kocatürk, M. C. Akbostanci, F. Tan and G. Ö. Kavas, *Pathophysiology*, 2000, **7**, 63-67.
106. Y. Ihara, M. Chuda, S. Kuroda and T. Hayabara, *J. Neurol. Sci.*, 1999, **170**, 90-95.
107. M. E. De Leo, S. Borrello, M. Passantino, B. Palazzotti, A. Mordente, A. Daniele, V. Filippini, T. Galeotti and C. Masullo, *Neurosci. Lett.*, 1998, **250**, 173-176.
108. S. L. Marklund, R. Adolfsson, C. G. Gottfries and B. Winblad, *J. Neurol. Sci.*, 1985, **67**, 319-325.

109. Y. Toh, S. Kuninaka, M. Mori, T. Oshiro, Y. Ikeda, H. Nakashima, H. Baba, S. Kohnoe, T. Okamura and K. Sugimachi, *Oncology*, 2000, **59**, 223-228.
110. R. H. Burdon, *Free Radical Biology and Medicine*, 1995, **18**, 775-794.
111. A. Miller, *Curr. Opin. Chem. Biol.*, 2004, **8**, 162-168.
112. J. Wuerges, J. Lee, Y. Yim, H. Yim, S. Kang and K. Carugo, *Proc. Natl. Acad. Sci. U. S. A.*, 2004, **101**, 8569-8574.
113. T. Jackson and T. Brunold, *Acc. Chem. Res.*, 2004, **37**, 461-470.
114. D. Riley, *Chem. Rev.*, 1999, **99**, 2573-2587.
115. D. Barondeau, C. Kassmann, C. Bruns, J. Tainer and E. Getzoff, *Biochem.*, 2004, **43**, 8038-8047.
116. R. Kachadourian, I. Batinic-Haberle and I. Fridovich, *Inorg. Chem.*, 1999, **38**, 391-396.
117. D. P. Riley, W. J. Rivers and R. H. Weiss, *Anal. Biochem.*, 1991, **196**, 344-349.
118. R. W. Strange, S. Antonyuk, M. A. Hough, P. A. Doucette, J. A. Rodriguez, P. J. Hart, L. J. Hayward, J. S. Valentine and S. S. Hasnain, *J. Mol. Biol.*, 2003, **328**, 877-891.
119. P. Carloni, P. E. Blochl and M. Parrinello, *J. Phys. Chem.*, 1995, **99**, 1338-1348
120. M. Ferraroni, W. R. Rypniewski, B. Bruni, P. Orioli and S. Mangani, *J. Biol. Inorg. Chem.*, 1998, **3**, 411-422.
121. J. Tainer, E. Getzoff, J. Richardson and D. Richardson, *Nature*, 1983, **306**, 284-287.
122. M. Fontecave and J. Pierre, *Coord. Chem. Rev.*, 1998, **170**, 125-140.
123. W. C. Stallings, K. A. Pattridge, R. K. Strong and M. L. Ludwig, *J. Biol. Chem.*, 1984, **259**, 695-699.
124. R. Edwards, H. Baker, M. Whittaker, J. Whittaker, G. Jameson and E. Baker, *J. Biol. Inorg. Chem.*, 1998, **3**, 161-171.
125. G. E. O. Borgstahl, M. Pokross, R. Chehab, A. Sekher and E. H. Snell, *J. Mol. Biol.*, 2000, **296**, 951-959.
126. D. J. Kliebenstein, R. A. Monde and R. L. Last, *Plant Physiol.*, 1998, **118**, 637-650.
127. M. R. N. Murthy, T. J. Reid III, A. Sicignano, N. Tanaka and M. G. Rossmann, *J. Mol. Biol.*, 1981, **152**, 465-499.
128. C. Bull, E. Niederhoffer, T. Yoshida and J. Fee, *J. Am. Chem. Soc.*, 1991, **113**, 4069-4076.

129. M. Pick, J. Rabani, F. Yost and I. Fridovic, *J. Am. Chem. Soc.*, 1974, **96**, 7329-7333.
130. S. Liochev and I. Fridovich, *IUBMB Life*, 1999, **48**, 157-161.
131. D. Salvemini, D. Riley and S. Cuzzocrea, *Nat. Rev. Drug Discov.*, 2002, **1**, 367-374.
132. C. Muscoli, S. Cuzzocrea, D. Riley, J. Zweier, C. Thiemermann, Z. Wang and D. Salvemini, *Br. J. Pharmacol.*, 2003, **140**, 445-460.
133. P. Quint, R. Reutzel, R. Mikulski, R. McKenna and D. Silverman, *Free Radic. Biol. Med.*, 2006, **40**, 453-458.
134. G. Liu, M. Filipovic, F. W. Heinemann and I. Ivanovic-Burmazovic, *Inorg. Chem.*, 2007, **46**, 8825-8835.
135. T. Nagano, *J. Synth. Org. Chem. Jpn.*, 1989, **47**, 843-854.
136. J. R. Sorenson, *Prog. Med. Chem.*, 1989, **26**, 437-568.
137. D. Klugroth and J. Rabani, *J. Phys. Chem.*, 1976, **80**, 588-591.
138. R. H. Weiss and D. P. Riley, *Drugs of the Future*, 1996, **21**, 383-389.
139. M. Baudry, S. Etuenne, A. Bruce, M. Palucki, E. Jacobsen and B. Malfroy, *Biochem. Biophys. Res. Commun.*, 1993, **192**, 964-968.
140. S. R. Doctrow, K. Huffman, C. B. Marcus, W. Musleh, A. Bruce, M. Baudry and B. Malfroy, *Adv. Pharmacol.*, 1997, **38**, 247-269.
141. B. Malfroy-Camine and S. R. Doctrow, *Synthetic catalytic free radical scavengers useful as antioxidants for prevention and therapy of disease*, 5696109, US, 1993.
142. R. Boggess, J. Hughes, W. Coleman and L. Taylor, *Inorg. Chim. Acta*, 1980, **38**, 183-189.
143. A. Bruce, B. Malfroy and M. Baudry, *Proc. Natl. Acad. Sci. U. S. A.*, 1996, **93**, 2312-2316.
144. R. F. Pasternack, A. Banth, J. M. Pasternack and C. S. Johnson, *J. Inorg. Biochem.*, 1981, **15**, 261-267.
145. K. Faulkner, S. Liochev and I. Fridovich, *J. Biol. Chem.*, 1994, **269**, 23471-23476.
146. I. Batinić-Haberle, S. I. Liochev, I. Spasojević and I. Fridovich, *Arch. Biochem. Biophys.*, 1997, **343**, 225-233.
147. D. Riley and R. Weiss, *J. Am. Chem. Soc.*, 1994, **116**, 387-388.

148. D. Riley, S. Henke, P. Lennon, R. Weiss, W. Neumann, W. Rivers, K. Aston, K. Sample, H. Rahman, C. Ling, J. Shieh, D. Busch and W. Szulbinski, *Inorg. Chem.*, 1996, **35**, 5213-5231.
149. D. Riley, P. Lennon, W. Neumann and R. Weiss, *J. Am. Chem. Soc.*, 1997, **119**, 6522-6528.
150. K. Aston, N. Rath, A. Naik, U. Slomczynska, O. Schall and D. Riley, *Inorg. Chem.*, 2001, **40**, 1779-1789.
151. D. P. Riley, S. L. Henke, P. J. Lennon and K. Aston, *Inorg. Chem.*, 1999, **38**, 1908-1917.
152. D. Salvemini, Z. Wang, J. Zweier, A. Samouilov, H. Macarthur, T. Misko, M. Currie, S. Cuzzocrea, J. Sikorski and D. P. Riley, *Science*, 1999, **286**, 304-306.
153. A. Dees, A. Zahl, R. Puchta, N. J. R. v. E. Hommes, F. W. Heinemann and I. Ivanovic-Burmazovic, *Inorg. Chem.*, 2007, **46**, 2459-2470.
154. G. Liu, M. Filipovic, F. W. Heinemann and I. Ivanovic-Burmazovic, *Inorg. Chem.*, 2007, **46**, 8825-8835.
155. S. McCann, M. McCann, M. Casey, M. Jackman, M. Devereux and V. McKee, *Inorg. Chim. Acta*, 1998, **279**, 24-29.
156. H. Dunford, *Coord. Chem. Rev.*, 2002, **233**, 311-318.
157. Y. Abashkin and S. Burt, *Inorg. Chem.*, 2005, **44**, 1425-1432.
158. Y. Kono and I. Fridovich, *J. Biol. Chem.*, 1983, **258**, 3646-3648.
159. D. Christianson, *Prog. Biophys. Mol. Biol.*, 1997, **67**, 217-252.
160. a) A. Wu, J. Penner-Hahn and V. Pecoraro, *Chem. Rev.*, 2004, **104**, 903-938. b) E. Larson and V. Pecoraro, *J. Am. Chem. Soc.*, 1991, **113**, 7809-7810.
161. S. V. Antonyuk, V. R. Melik-Adamyan, A. N. Popov, V. S. Lamzin, P. D. Hempstead, P. M. Harrison, P. J. Artymyuk and V. V. Barynin, *Crystallography Reports*, 2000, **45**, 105-116.
162. V. Barynin, M. Whittaker, S. Antonyuk, V. Lamzin, P. Harrison, P. Artymiuk and J. Whittaker, *Structure*, 2001, **9**, 725-738.
163. M. Whittaker, V. Barynin, S. Antonyuk and J. Whittaker, *Biochemistry (N. Y.)*, 1999, **38**, 9126-9136.
164. S. Signorella and C. Hureau, *Coord. Chem. Rev.*, 2012, **256**, 1229-1245.
165. Y. Naruta, M. Sasayama and T. Sasaki, *Angew. Chem. Int. Edit. Engl.*, 1994, **33**, 1839-1841.

166. P. J. Pessiki and G. C. Dismukes, *J. Am. Chem. Soc.*, 1994, **116**, 898-903
167. P. J. Pessiki, S. V. Khangulov, D. M. Ho and G. C. Dismukes, *J. Am. Chem. Soc.*, 1994, **116**, 891-897.
168. A. Boelrijk and G. Dismukes, *Inorg. Chem.*, 2000, **39**, 3020-3028.
169. a) M. Triller, W. Hsieh, V. Pecoraro, A. Rompel and B. Krebs, *Inorg. Chem.*, 2002, **41**, 5544-5554. b) M. Etter, *Acc. Chem. Res.*, 1990, **23**, 120-126. c) M. Etter, J. Macdonald and J. Bernstein, *Acta Cryst.*, 1990, **B46**, 256-262.
170. G. Tojo and M. Fernandez, *Oxidation of Alcohols to Aldehydes and Ketones: A Guide to Current Common Practice*, Springer, New York; 2006.
171. S. Ball, T. Goodwin and R. Morton, *Biochem. J.*, 1948, **42**, 516-523.
172. I. Goldman, *J. Org. Chem.*, 1969, **34**, 3289-3295.
173. E. P. Papadopolous, A. Jarrar and C. H. Issadorides, *J. Org. Chem.*, 1966, 31, 615-616.
174. H. Adams, N. A. Bailey, D. E. Fenton, R. J. Good, R. Moody, de Barbarin and Cecilia O. Rodriguez, *J. Chem. Soc., Dalton Trans.*, 1987, 207-218.
175. C. Harding, D. McDowell, J. Nelson, S. Raghunathan, C. Stevenson and M. G. B. Drew, P. Yates, *J. Chem. Soc., Dalton Trans.*, 1990, 2521-2533.
176. R. Dennett, L. James and V. McKee, *Acta Cryst.*, 2007, **E63**, 1720-1721.
177. S. Brooker and V. McKee, *J. Chem. Soc., Chem. Commun.*, 1989, 619-620.
178. S. Brooker, V. McKee and T. Metcalfe, *Inorg. Chim. Acta*, 1996, **246**, 171-179.
179. S. Brooker, V. McKee, W. B. Shepard and L. K. Pannell, *J. Chem. Soc., Dalton Trans.*, 1987, 2555-2562.
180. a) M. G. B. Drew, A. H. bin Othman, P. D. A. Mcllroy and S. M. Nelson, *J. Chem. Soc., Dalton Trans.*, 1977, 1173-1180. b) D. Zhang, H. Wang, Y. Chen, Z. Ni, L. Tian and J. Jiang, *Inorg. Chem.*, 2009, **48**, 5488-5496. c) D. Zhang, H. Wang, L. Tian, J. Jiang and Z. Ni, *Cryst. Eng. Comm.*, 2009, **11**, 2447-2451. c) G. R. Desiraju and T. Steiner, *The Weak Hydrogen Bond In Structural Chemistry and Biology*, Oxford University Press Inc, New York.
181. S. Brooker and V. McKee, *J. Chem. Soc., Dalton Trans.*, 1990, 2397-2401.
182. S. Brooker and V. McKee, *Acta Cryst.*, 1993, **C49**, 441-445.
183. X. X. Sun, C. M. Qi, S. L. Ma, H. B. Huang, W. Zhu and Y. C. Liu, *Inorg. Chem. Commun.*, 2006, **9**, 911-914.
184. A. Gonzalez, E. Gomez, A. Cortes-Lozada, S. Hernandez, T. Ramirez-Apan and A. Nieto-Camacho, *Chem. Pharm. Bull.*, 2009, **57**, 5-15.

185. G. B. Deacon and R. J. Phillips, *Coord. Chem. Rev.*, 1980, **33**, 227-250.
186. M. Streater, P. Taylor, R. Hider and J. Porter, *J. Med. Chem.*, 1990, **33**, 1749-1755.
187. R. Fanshawe and A. Blackman, *Inorg. Chem.*, 1995, **34**, 421-423.
188. H. Keypour and S. Salehzadeh, *Transit. Met. Chem.*, 2000, **25**, 205-208.
189. N. Gunduz, T. Gunduz, M. Hursthouse, H. Parkes, L. Shaw, R. Shaw and M. Tuzun, *J. Chem. Soc., Perkin Trans. 2*, 1985, 899-902.
190. S. Steinhauser, F. Bachmann, M. Hazenkamp, U. Heinz, J. Dannacher and K. Hegetschweiler, *Z. Krist. New Cryst. Struct.*, 2004, **219**, 325-326.
191. a) S. Chandra and A. Chakravorty, *Inorg. Chem.*, 1991, **30**, 3795-3796. b) F. Benetollo, V. Peruzzo, S. Tamburini and P. A. Vigato, *Inorg. Chem. Commun.*, 2012, **15**, 84-87.
192. S. N. Li, Y. W. Ren, J. Li, F. X. Zhang and M. C. Hu, *Acta Cryst., 2006*, **E62**, 498-499.
193. A. Deroche, I. MorgensternBadarau, M. Cesario, J. Guilhem, B. Keita, L. Nadjo and C. HoueeLevin, *J. Am. Chem. Soc.*, 1996, **118**, 4567-4573.
194. W. Roderick, R. Appell, A. Esch and C. Nordeen, *J. Med. Chem.*, 1972, **15**, 655-658.
195. S. Mylonas, A. Valavanidis, K. Dimitropoulos, M. Polissiou, A. S. Tsiftsoglou and I. S. Vizirianakis, *J. Inorg. Biochem.*, 1988, **34**, 265-275.
196. A. W. Addison and P. J. Burke, *J. Heterocycl. Chem.*, 1981, **18**, 803-805.
197. V. McKee, M. Zvagulis, J. V. Dagdigian, M. G. Patch and C. A. Reed, *J. Am. Chem. Soc.*, 1984, **106**, 4765-4772.
198. W. Shuangxi, Z. Ying, Z. Fangjie, W. Qiuying and W. Liufang, *Polyhedron*, 1992, **11**, 1909-1915.
199. M. Devereux, M. McCann, M. Casey, M. Curran, G. Ferguson, C. Cardin, M. Convery and V. Quillet, *J. Chem. Soc., Dalton Trans.*, 1995, 771-776.
200. J. Kaizer, T. Csay, P. Kovari, G. Speier and L. Parkanyi, *J. Mol. Catal. A-Chem.*, 2008, **280**, 203-209.
201. L. James, *PhD thesis*, Loughborough University, 2010.
202. F. Bachmann, J. Dannacher, M. Hazenkamp, G. Schlingloff, G. Richter, H. Dbaly and R. H. Traber, *Metal complexes of tripodal ligands (patent)*, C07F/1502; C07F/1300; C11D/900, US, 2001.
203. J. M. Mccord and I. Fridovic, *J. Biol. Chem.*, 1969, **244**, 6049-6055.

204. S. Goldstein and G. Czapski, *Free Radic. Res. Commun.*, 1991, **12-3**, 5-10.
205. S. Goldstein and G. Czapski, in *Free Radicals*, Eds. P. Neville and K. Frank, Oxford University Press, Oxford, 1996, 241-255.
206. A. V. Peskin and C. C. Winterbourn, *Clinica Chimica Acta*, 2000, **293**, 157-166.
207. A. S. Tan and M. V. Berridge, *J. Immunol. Methods*, 2000, **238**, 59-68.
208. J. Y. Zhou and P. Prognon, *J. Pharm. Biomed. Anal.*, 2006, **40**, 1143-1148.
209. S. Durot, C. Policar, F. Cisnetti, F. Lambert, J. Renault, G. Pelosi, G. Blain, H. Korri-Youssoufi and J. Mahy, *Eur. J. Inorg. Chem.*, 2005, 3513-3523.
210. D. Klugroth, I. Fridovic and J. Rabani, *J. Am. Chem. Soc.*, 1973, **95**, 2786-2790.
211. Bruker, 1998, APEX2 and SAINT. Bruker AXS Inc., Madison, Wisconsin, USA.
212. G. M. Sheldrick, *Acta Cryst.*, 2008, **A64**, 112-122.
213. I. J. Bruno, J. C. Cole, P. R. Edgington, M. Kessler, C. F. Macrae, P. McCabe, J. Pearson and R. Taylor, *Acta Cryst.*, 2002, **B58**, 389-397.
214. L.J. Farrugia, *J. Appl. Cryst.*, 1997, **30**, 565-566.
215. Persistence of Vision Pty. Ltd. 2004, Persistence of Vision (TM) Raytracer, Persistence of Vision Pty. Ltd., Williamstown, Victoria, Australia, http://www.povray.org/.
216. A. L. Spek, *Acta Cryst.*, 2008, **D65**, 148-155.
217. Sheldrick, G. M., 2008, *CELL_NOW*, University of Göttingen, Germany.
218. Sheldrick, G. M., 2008, *TWINABS*, University of Göttingen, Germany.

Appendix 1

Published Papers to date

1. M. Dolaz, V. McKee, M. Kose, A. Golcu, M. Tumer, *Spectrochimica Acta Part A-Molecular and Biomolecular Spectroscopy*, 2010, **77**, 219-225.
2. L. James, M. Kose, T. Metcalfe, V. McKee, *J. Chem. Cryst.*, 2011, **41**, 577-581.
3. M. Kose, V. McKee, *Acta Cryst.*, 2011, **E67**, O3193-U180.
4. M. Kose, V. McKee, *Acta Cryst., 2011*, **E67**, M149-U404.
5. C. Celik, V. McKee, M. Kose, M. Aslantas, M. Tumer, *J. Mol. Struct.*, 2011, **985**, 167-172.
6. G. Ceyhan, M. Kose, V. McKee, S. Uruş, A. Golcu, M. Tumer, *Spectrochimica Acta Part A: Molecular and Biomolecular Spectroscopy*, 2012, **95**, 382-398.
7. G. Ceyhan, M. Tumer, M. Kose, V. McKee, *J. Lumin.*, 2012, **132**, 850-857.
8. G. Ceyhan, M. Tümer, M. Kose, V. McKee, S. Akar, *J. Lumin*, 2012, **132**, 2917-2928.

Conferences Attended

1. Structural characterisation and superoxide dismutase activity of manganese(II) Macrocyclic Complexes, M. Kose, L. James, M. Devereux, A. Kellett, V. McKee**,** *Macrocyclic and Supramolecular Chemistry Group Annual Meeting*, Cambridge University, Cambridge, UK 15-19 December 2009.
2. Macrocyclic and acyclic manganese (II) complexes and their catalase activities, M. Kose, V. McKee, *Meeting of the RSC Coordination Chemistry Discussion Group*, University of Bath, Bath, UK 1-2 July 2010.
3. Seven-coordinate tetranuclear (4+4) and ring-contracted Mn(II) complexes, their SOD activities and catalysts for the disproportion of hydrogen peroxide, M. Kose, V. Mckee, *First EuCheMS Inorganic Chemistry Conference (EICC-1)*, Manchester University, Manchester, UK 11-14 April 2011.
4. Rearrangement of Schiff-base macrocyclic ligands from (2+2) to (4+4) or ring-contracted systems *via* transmetallation reactions, M. Kose, V. McKee, *6th International Symposium on Macrocyclic and Supramolecular Chemistry (6-ISMSC)*, University of Sussex, Brighton, UK 3 – 7 July 2011.
5. Towards 40 and 16 membered macrocycles from 20 membered macrocycle *via* transmetallation reactions with Mn(II), M. Kose, V. McKee, *7th International*

Symposium on Macrocyclic and Supramolecular Chemistry (7-ISMSC), University of Otago, Dunedin, New Zealand 29 Jan – 2 Feb 2012.

6. Macrocyclic and acyclic manganese(II) complexes as SOD mimics, structure-activity relationship Study, M. Kose, V. McKee, P. Lucas, *Dalton Division Joint Interest Groups Meeting***,** University of Warwick, Coventry, UK 3–5 April 2012.
7. Cobalt-based redox mediators for dye-sensitized solar cells, J. S. Sagu, M. Kose, U. Wijayantha, V. McKee, *Great Western Electrochemistry Meeting*, University of Bath, UK 18 June 2012 (1. Poster Prize).
8. Cobalt-based redox mediators for dye-sensitized solar cells, J. S. Sagu, M. Kose, U. Wijayantha, V. McKee, *Midland Electrochemistry Group (MEG) Meeting***,** University of Birmingham, UK 27 June 2012.
9. Structural approach to Mn(II) complexes as SOD and catalase mimics, M. Kose, V. McKee, P. Lucas, *40 International Conference on Coordination Chemistry* (ICCC40), University of Valencia, Spain 9-13 September 2012.

Invited Lectures

Seven-Coordinate Mn(II) Complexes and Biomimetic Studies, M. Kose, Kahramanmaras Sutcuimam University, Chemistry Department, K.Maras, Turkey 27 May 2011.

Appendix 2

Table A1 Crystal data and structure refinement for $[Ba(H_2L1)(ClO_4)]_2(ClO_4)_2$.

Identification code	mk11	
Chemical formula	$C_{20}H_{22}BaCl_2N_6O_{10}$	
Formula weight	714.68	
Temperature	150(2) K	
Radiation, wavelength	MoKα, 0.71073 Å	
Crystal system	Triclinic	
Space group	P-1	
Unit cell parameters	a = 8.4587(9) Å	α = 79.7858(15)°
	b = 8.7360(9) Å	β = 88.7803(15)°
	c = 17.7722(19) Å	γ = 83.0476(15)°
Cell volume	1283.0(2) $Å^3$	
Z	2	
Calculated density	1.850 g/cm^3	
Absorption coefficient μ	1.823 mm^{-1}	
F(000)	708	
θ range for data collection	2.33 to 26.43°	
Index ranges	h −10 to 10, k −10 to 10, l −22 to 22	
Completeness to θ = 26.43°	99.1 %	
Intensity decay	0%	
Reflections collected	11122	
Independent reflections	5225 (R_{int} = 0.0239)	
Reflections with $F^2>2\sigma$	4846	
Min. and max. transmission	0.5148 and 0.8830	
Structure solution	direct methods	
Refinement method	Full-matrix least-squares on F^2	
Weighting parameters a, b	0.0396, 7.1829	
Data / restraints / parameters	5225 / 0 / 353	
Final R indices [$F^2>2\sigma$]	R1 = 0.0433, wR2 = 0.1142	
R indices (all data)	R1 = 0.0471, wR2 = 0.1157	
Goodness-of-fit on F^2	1.193	
Extinction coefficient	0.0019(6)	
Largest and mean shift/su	0.001 and 0.000	
Largest diff. peak and hole	1.351 and −1.069 e $Å^{-3}$	

Hydrogen atoms bonded to oxygen atoms (O1 and O2) were located from difference maps and positions were refined. *U*iso(H) values were set to be 1.5 times *U*eq of the carrier atoms for O1 and O2.

Table A2 Crystal data and structure refinement for $[Mn(H_3L2)(NCS)_2]\cdot$½dmf

Identification code	sora1	
Empirical formula	$C_{24.50}H_{29.50}MnN_{8.50}O_{3.50}S_2$	
Formula weight	618.13	
Temperature	150(2) K	
Wavelength	0.6884 Å	
Crystal system	Triclinic	
Space group	P-1	
Unit cell dimensions	a = 13.1104(16) Å	a= 99.3666(15)°
	b = 14.9066(18) Å	b= 97.5598(14)°
	c = 14.9514(18) Å	g = 101.8728(14)°
Volume	2779.8(6) $Å^3$	
Z	4	
Density (calculated)	1.477 Mg/m^3	
Absorption coefficient	0.671 mm^{-1}	
F(000)	1284	
Crystal size	0.52 x 0.19 x 0.18 mm^3	
Crystal description	Orange block	
Theta range for data collection	1.36 to 30.75°.	
Index ranges	-17<=h<=18, -21<=k<=22, -22<=l<=14	
Reflections collected	21514	
Independent reflections	15633 [R(int) = 0.0416]	
Completeness to theta = 30.75°	81.9 %	
Absorption correction	Semi-empirical from equivalents	
Max. and min. transmission	0.8887 and 0.7216	
Refinement method	Full-matrix least-squares on F^2	
Data / restraints / parameters	15633 / 0 / 716	
Goodness-of-fit on F^2	0.879	
Final R indices [I>2sigma(I)]	R1 = 0.0556, wR2 = 0.1122	
R indices (all data)	R1 = 0.1477, wR2 = 0.1487	
Largest diff. peak and hole	0.863 and -0.483 e.$Å^{-3}$	

X-ray data were collected at Daresbury Laboratory using synchrotron light source. Hydrogen atoms bonded to oxygen atoms (O1, O2, O4 and O5) and nitrogen atoms (N1 and N9) were located from difference maps and positions were refined. *U*iso(H) values were set to be 1.5 times *U*eq of the carrier atoms.

Table A3 Crystal data and structure refinement for $[Mn(H_3L3)(NCS)_2]\cdot$½EtOH.

Identification code	mk101	
Empirical formula	$C_{50}H_{62}Mn_2N_{16}O_7S_4$	
Formula weight	1237.28	
Temperature	150(2) K	
Wavelength	0.71073 Å	
Crystal system	Triclinic	
Space group	P-1	
Unit cell dimensions	a = 8.8964(8) Å	α= 99.1707(14)°
	b = 9.8223(9) Å	β= 99.0238(14)°
	c = 17.2709(16) Å	γ = 90.3701(14)°
Volume	1470.7(2) $Å^3$	
Z	1	
Density (calculated)	1.397 Mg/m^3	
Absorption coefficient	0.634 mm^{-1}	
F(000)	644	
Crystal size	0.44 x 0.38 x 0.08 mm^3	
Crystal description	yellow block	
Theta range for data collection	2.10 to 26.42°.	
Index ranges	-11<=h<=11, -12<=k<=12, -21<=l<=21	
Reflections collected	13121	
Independent reflections	6027 [R(int) = 0.0154]	
Completeness to theta = 26.42°	99.5 %	
Absorption correction	Semi-empirical from equivalents	
Max. and min. transmission	0.9487 and 0.7674	
Refinement method	Full-matrix least-squares on F^2	
Data / restraints / parameters	6027 / 72 / 383	
Goodness-of-fit on F^2	1.074	
Final R indices [I>2sigma(I)]	R1 = 0.0513, wR2 = 0.1647	
R indices (all data)	R1 = 0.0595, wR2 = 0.1732	
Largest diff. peak and hole	1.209 and -0.325 $e.Å^{-3}$	

Hydrogen atoms bonded to oxygen atoms (O1, O2, O2S and O2S') and nitrogen atom (N1) were located from difference maps and positions were refined. *U*iso(H) values were set to be 1.5 times *U*eq of the carrier atoms. There is a half occupancy disordered ethanol molecule in the structure and this was modelled over two positions in a 30:20 ratio (C4SC3SO2S)-(C4S'C3S'O2S').

Table A4 Crystal data and structure refinement for $[Mn_4(H_2L^*)Cl_4][MnCl_4]\cdot 4.5CH_3CN$

Identification code	mk139	
Empirical formula	$C_{49}H_{55.50}Cl_8Mn_5N_{16.50}O_4$	
Formula weight	1497.90	
Temperature	150(2) K	
Wavelength	0.71073 Å	
Crystal system	Orthorhombic	
Space group	$Pna2_1$	
Unit cell dimensions	a = 15.450(2) Å	α= 90°
	b = 30.464(5) Å	β= 90°
	c = 13.573(2) Å	γ = 90°
Volume	6388.2(17) $Å^3$	
Z	4	
Density (calculated)	1.557 Mg/m^3	
Absorption coefficient	1.351 mm^{-1}	
F(000)	3032	
Crystal size	0.38 x 0.33 x 0.19 mm^3	
Crystal description	yellow irregular	
Theta range for data collection	1.64 to 26.37°.	
Index ranges	-19<=h<=19, -38<=k<=37, -16<=l<=16	
Reflections collected	54026	
Independent reflections	13037 [R(int) = 0.0296]	
Completeness to theta = 26.37°	99.8 %	
Absorption correction	Semi-empirical from equivalents	
Max. and min. transmission	0.7834 and 0.6313	
Refinement method	Full-matrix least-squares on F^2	
Data / restraints / parameters	13037 / 855 / 825	
Goodness-of-fit on F^2	1.064	
Final R indices [I>2sigma(I)]	R1 = 0.0351, wR2 = 0.0978	
R indices (all data)	R1 = 0.0379, wR2 = 0.0997	
Absolute structure parameter	0.073(11)	
Largest diff. peak and hole	0.761 and -0.684 e.$Å^{-3}$	

The number of the hydrogen atoms in the unit cell instruction and atom list did not match, because the hydrogen atoms bonded to O1 or O3 and O2 or O4 were not located. The structure contains four full occupancy (two of them disordered) and one half occupancy acetonitrile solvate per molecule of complex. The tetrahedral tetrachloromanganese anion is also disordered and this was modelled over two positions. Site occupancy factors were set at 0.80 Mn5-Cl8 at 0.20 for Mn5'-Cl8'.

Table A5 Crystal data and structure refinement for $[Mn_4(H_2L^*)(N_3)_4](ClO_4)\cdot 3CH_3CN$

Identification code	mk170→sadsq	
Empirical formula	$C_{48}H_{52}Cl_2Mn_4N_{28}O_{12}$	
Formula weight	1503.84	
Temperature	150(2) K	
Wavelength	0.71073 Å	
Crystal system	Tetragonal	
Space group	I4/m	
Unit cell dimensions	a = 17.733(4) Å	α= 90°
	b = 17.733(4) Å	β= 90°
	c = 22.782(6) Å	γ = 90°
Volume	7164(2) $Å^3$	
Z	4	
Density (calculated)	1.394 Mg/m^3	
Absorption coefficient	0.835 mm^{-1}	
F(000)	3064	
Crystal size	0.48 x 0.30 x 0.25 mm^3	
Crystal description	orange Block	
Theta range for data collection	1.46 to 24.97°.	
Index ranges	-20<=h<=20, -20<=k<=21, -27<=l<=26	
Reflections collected	24877	
Independent reflections	3221 [R(int) = 0.0597]	
Completeness to theta = 24.97°	99.6 %	
Absorption correction	Semi-empirical from equivalents	
Max. and min. transmission	0.812 and 0.748	
Refinement method	Full-matrix least-squares on F^2	
Data / restraints / parameters	3221 / 284 / 200	
Goodness-of-fit on F^2	1.120	
Final R indices [I>2sigma(I)]	R1 = 0.0787, wR2 = 0.2359	
R indices (all data)	R1 = 0.0984, wR2 = 0.2492	
Largest diff. peak and hole	0.876 and -0.836 $e.Å^{-3}$	

This was weak high angle data set, but the structure was solved and refined. The number of the atoms in the unit cell instruction and atom list did not match, because the intensity contribution of disordered acetonitrile solvates was removed by SQUEEZE procedure[216] which found the electron count of $332e^-$ in two similar volumes of voids of 1146 and 1143 $Å^3$ per unit cell. Each set of $332e^-$ was modelled as fifteen acetonitrile molecules ($22e^-$ x15=$330e^-$).

```
# SQUEEZE RESULTS (APPEND TO CIF)
# Note: Data are Listed for all Voids in the P1 Unit Cell
# i.e. Centre of Gravity, Solvent Accessible Volume,
# Recovered number of Electrons in the Void and
# Details about the Squeezed Material
loop_
  _platon_squeeze_void_nr
  _platon_squeeze_void_average_x
  _platon_squeeze_void_average_y
  _platon_squeeze_void_average_z
  _platon_squeeze_void_volume
  _platon_squeeze_void_count_electrons
  _platon_squeeze_void_content
   1 -0.001  0.001 -0.055      1146       332 ' '
   2 -0.150  0.498 -0.009      1143       332 ' '
_platon_squeeze_details
;
15 acetonitrile molecules per unit cell
;
```

Table A6 Crystal data and structure refinement for [Mn(L4)$(NCS)_2$].

Identification code	mk49	
Empirical formula	$C_{15}H_{17}MnN_5O_2S_2$	
Formula weight	418.40	
Temperature	150(2) K	
Wavelength	0.71073 Å	
Crystal system	Triclinic	
Space group	P-1	
Unit cell dimensions	a = 8.198(3) Å	α= 108.652(5)°
	b = 9.154(3) Å	β= 93.757(5)°
	c = 13.183(5) Å	γ = 90.592(5)°
Volume	934.8(6) $Å^3$	
Z	2	
Density (calculated)	1.486 Mg/m^3	
Absorption coefficient	0.948 mm^{-1}	
F(000)	430	
Crystal size	0.41 x 0.31 x 0.04 mm^3	
Crystal description	yellow plate	
Theta range for data collection	1.63 to 26.44°.	
Index ranges	-10<=h<=10, -11<=k<=11, -16<=l<=16	
Reflections collected	10071	
Independent reflections	3802 [R(int) = 0.0497]	
Completeness to theta = 26.44°	98.4 %	
Absorption correction	Semi-empirical from equivalents	
Max. and min. transmission	0.9658 and 0.6990	
Refinement method	Full-matrix least-squares on F^2	
Data / restraints / parameters	3802 / 0 / 226	
Goodness-of-fit on F^2	1.777	
Final R indices [I>2sigma(I)]	R1 = 0.0792, wR2 = 0.2687	
R indices (all data)	R1 = 0.0964, wR2 = 0.2767	
Largest diff. peak and hole	0.800 and -0.739 e.$Å^{-3}$	

Table A7 Crystal data and structure refinement for H_2L4.

Identification code	mk7	
Chemical formula	$C_{11}H_{15}N_3O_2$	
Formula weight	221.26	
Temperature	150(2) K	
Radiation, wavelength	MoKα, 0.71073 Å	
Crystal system, space group	Monoclinic, $P2_1/c$	
Unit cell parameters	a = 9.874(3) Å	α = 90°
	b = 4.5259(12) Å	β = 94.393(4)°
	c = 24.792(7) Å	γ = 90°
Cell volume	1104.7(5) Å^3	
Z	4	
Calculated density	1.330 g/cm^3	
Absorption coefficient μ	0.094 mm^{-1}	
F(000)	472	
Crystal colour and size	colourless, 0.50 × 0.28 × 0.04 mm^3	
Reflections for cell refinement	1048 (θ range 2.54 to 24.48°)	
Data collection method	Bruker APEX-II CCD	
	ϕ and ω scans	
θ range for data collection	1.65 to 26.38°	
Index ranges	h –12 to 12, k –5 to 5, l –30 to 31	
Completeness to θ = 26.38°	99.3 %	
Intensity decay	0%	
Reflections collected	9082	
Independent reflections	2256 (R_{int} = 0.0663)	
Reflections with $F^2>2\sigma$	1442	
Absorption correction	semi-empirical from equivalents	
Min. and max. transmission	0.5819 and 0.7454	
Structure solution	direct methods	
Refinement method	Full-matrix least-squares on F^2	
Weighting parameters a, b	0.0728, 0.0000	
Data / restraints / parameters	2256 / 0 / 147	
Final R indices [$F^2>2\sigma$]	R1 = 0.0515, wR2 = 0.1282	
R indices (all data)	R1 = 0.0953, wR2 = 0.1482	
Goodness-of-fit on F^2	1.060	
Largest and mean shift/su	0.000 and 0.000	
Largest diff. peak and hole	0.307 and –0.275 e Å^{-3}	

Hydrogen atoms bonded to oxygen atoms were inserted at calculated positions using a riding model. *U*iso(H) values were set to be 1.5 times *U*eq of the carrier atoms.

Table A8 Crystal data and structure refinement for $[Mn(H_2L4)Cl_2]$.

Identification code	mk8	
Chemical formula	$C_{11}H_{15}Cl_2MnN_3O_2$	
Formula weight	347.10	
Temperature	150(2) K	
Radiation, wavelength	MoKα, 0.71073 Å	
Crystal system, space group	Triclinic, $P\bar{1}$	
Unit cell parameters	a = 12.9256(18) Å	α = 75.820(2)°
	b = 14.278(2) Å	β = 78.056(2)°
	c = 17.022(2) Å	γ = 73.644(2)°
Cell volume	2890.2(7) $Å^3$	
Z	8	
Calculated density	1.595 g/cm^3	
Absorption coefficient μ	1.283 mm^{-1}	
F(000)	1416	
Crystal colour and size	yellow, 0.44 × 0.39 × 0.16 mm^3	
Reflections for cell refinement	7111 (θ range 2.50 to 29.94°)	
Data collection method	Bruker APEX-II CCD	
	ϕ and ω scans	
θ range for data collection	1.25 to 27.00°	
Index ranges	h −16 to 16, k −18 to 18, l −21 to 21	
Completeness to θ = 27.00°	99.5 %	
Reflections collected	27027	
Independent reflections	12569 (R_{int} = 0.0252)	
Reflections with $F^2>2\sigma$	9555	
Absorption correction	semi-empirical from equivalents	
Min. and max. transmission	0.6021 and 0.8210	
Structure solution	direct methods	
Refinement method	Full-matrix least-squares on F^2	
Weighting parameters a, b	0.0610, 1.0911	
Data / restraints / parameters	12569 / 0 / 686	
Final R indices [$F^2>2\sigma$]	R1 = 0.0420, wR2 = 0.1089	
R indices (all data)	R1 = 0.0587, wR2 = 0.1207	
Goodness-of-fit on F^2	1.047	
Largest and mean shift/su	0.001 and 0.000	
Largest diff. peak and hole	1.152 and −0.805 e $Å^{-3}$	

Hydrogen atoms bonded to oxygen atoms (O1, O2, O3, O4, O5, O6, O7 and O8) were located from difference maps and positions were refined. *U*iso(H) values were set to be 1.5 times *U*eq of the carrier atoms.

Table A9 Crystal data and structure refinement for $[Mn_2(H_2L4)_2(NCS)_2]$.

Identification code	mk9	
Chemical formula	$C_{26}H_{30}Mn_2N_{10}O_4S_4$	
Formula weight	784.72	
Temperature	150(2) K	
Radiation, wavelength	MoKα, 0.71073 Å	
Crystal system, space group	Monoclinic, $P2_1/c$	
Unit cell parameters	a = 7.2639(12) Å	α = 90°
	b = 24.655(4) Å	β = 98.994(2)°
	c = 9.4710(16) Å	γ = 90°
Cell volume	1675.3(5) $Å^3$	
Z	2	
Calculated density	1.556 g/cm^3	
Absorption coefficient μ	1.052 mm^{-1}	
F(000)	804	
Crystal colour and size	orange, 0.36 × 0.27 × 0.10 mm^3	
Reflections for cell refinement	2277 (θ range 2.33 to 23.06°)	
Data collection method	Bruker APEX-II CCD	
	ϕ and ω scans	
θ range for data collection	1.65 to 26.40°	
Index ranges	h –9 to 9, k –30 to 30, l –11 to 11	
Completeness to θ = 26.40°	99.9 %	
Intensity decay	0%	
Reflections collected	14661	
Independent reflections	3422 (R_{int} = 0.0556)	
Reflections with $F^2>2\sigma$	2591	
Absorption correction	semi-empirical from equivalents	
Min. and max. transmission	0.7033 and 0.9021	
Structure solution	direct methods	
Refinement method	Full-matrix least-squares on F^2	
Weighting parameters a, b	0.0397, 0.2800	
Data / restraints / parameters	3422 / 0 / 216	
Final R indices [$F^2>2\sigma$]	R1 = 0.0385, wR2 = 0.0821	
R indices (all data)	R1 = 0.0584, wR2 = 0.0916	
Goodness-of-fit on F^2	1.047	
Largest and mean shift/su	0.000 and 0.000	
Largest diff. peak and hole	0.309 and –0.364 e $Å^{-3}$	

Hydrogen atoms bonded to oxygen atoms (O1 and O2) were located from difference maps and positions were refined. *U*iso(H) values were set to be 1.5 times *U*eq of the carrier atoms.

Table A10 Crystal data and structure refinement for $[Mn(H_2L_4)_2(N_3)_3Cl]$.

Identification code	mk20	
Chemical formula	$C_{22}H_{30}Cl_{0.55}Mn_2N_{16.35}O_4$	
Formula weight	716.90	
Temperature	150(2) K	
Radiation, wavelength	MoKα, 0.71073 Å	
Crystal system, space group	Monoclinic, $P2_1/c$	
Unit cell parameters	a = 10.3011(10) Å	α = 90°
	b = 19.1704(18) Å	β = 106.1565(13)°
	c = 16.1026(15) Å	γ = 90°
Cell volume	3054.3(5) $Å^3$	
Z	4	
Calculated density	1.559 g/cm^3	
Absorption coefficient μ	0.934 mm^{-1}	
F(000)	1471	
Crystal colour and size	orange, 0.38 × 0.26 × 0.19 mm^3	
Reflections for cell refinement	9980 (θ range 2.32 to 25.73°)	
Data collection method	Bruker APEX-II CCD	
	ϕ and ω scans	
θ range for data collection	1.69 to 26.42°	
Index ranges	h –12 to 12, k –23 to 23, l –20 to 20	
Completeness to θ = 26.42°	99.7 %	
Intensity decay	0%	
Reflections collected	26134	
Independent reflections	6257 (R_{int} = 0.0402)	
Reflections with $F^2>2\sigma$	4617	
Absorption correction	semi-empirical from equivalents	
Min. and max. transmission	0.6264 and 0.7454	
Structure solution	direct methods	
Refinement method	Full-matrix least-squares on F^2	
Weighting parameters a, b	0.0450, 1.9555	
Data / restraints / parameters	6257 / 3 / 438	
Final R indices [$F^2>2\sigma$]	R1 = 0.0401, wR2 = 0.0924	
R indices (all data)	R1 = 0.0634, wR2 = 0.1033	
Goodness-of-fit on F^2	1.033	
Largest and mean shift/su	0.000 and 0.000	
Largest diff. peak and hole	0.833 and –0.315 e $Å^{-3}$	

Hydrogen atoms bonded to oxygen atoms were inserted at calculated positions using a riding model. *U*iso(H) values were set to be 1.5 times *U*eq of the carrier atoms.

Table A11 Crystal data and structure refinement for $[Mn(L5)(NCS)_2]$.

Identification code	mk37T→twin4	
Chemical formula	$C_{17}H_{25}MnN_7S_2$	
Formula weight	446.50	
Temperature	150(2) K	
Radiation, wavelength	MoKα, 0.71073 Å	
Crystal system, space group	Triclinic, $P\bar{1}$	
Unit cell parameters	a = 11.769(2) Å	α = 71.834(3)°
	b = 13.132(2) Å	β = 89.950(3)°
	c = 14.756(3) Å	γ = 84.235(3)°
Cell volume	2150.8(9) $Å^3$	
Z	4	
Calculated density	1.379 g/cm^3	
Absorption coefficient μ	0.824 mm^{-1}	
F(000)	932	
Crystal colour and size	Yellow, 0.51 × 0.21 × 0.06 mm^3	
Reflections for cell refinement	9824 (θ range 2.27 to 26.42°)	
θ range for data collection	1.45 to 26.45°	
Index ranges	h −14 to 14, k −15 to 16, l 0 to 18	
Completeness to θ = 26.45°	98.5 %	
Intensity decay	0%	
Reflections collected	8753	
Independent reflections	8753 (R_{int} = 0.0000)	
Reflections with $F^2>2\sigma$	5734	
Absorption correction	semi-empirical from equivalents	
Min. and max. transmission	0.6786 and 0.9522	
Structure solution	direct methods	
Refinement method	Full-matrix least-squares on F^2	
Weighting parameters a, b	0.0778, 0.0000	
Data / restraints / parameters	8753 / 0 / 495	
Final R indices [$F^2>2\sigma$]	R1 = 0.0510, wR2 = 0.1235	
R indices (all data)	R1 = 0.0893, wR2 = 0.1363	
Goodness-of-fit on F^2	0.972	
Largest and mean shift/su	0.001 and 0.000	
Largest diff. peak and hole	0.732 and −0.497 e $Å^{-3}$	

The crystal lattice was found to be non-merohedrally twinned. Cell_now[217] found two domains and the data were re-integrated [Major component ~70%, twin law; 180° rotation about the real axis 1 0 0]. Twinabs[218] was used for absorption correction and refinement was processed using single component (hklf 4). (Multi diffraction data (hklf 5) did not give better refinement)

Table A12 Crystal data and structure refinement for $[Mn(L5)Cl_2]\cdot MeOH$.

Identification code	mk77-sr	
Chemical formula	$C_{15.50}H_{27}MnN_{11}O_{0.50}$	
Formula weight	430.42	
Temperature	150(2) K	
Radiation, wavelength	MoKα, 0.71073 Å	
Crystal system, space group	Triclinic, $P\bar{1}$	
Unit cell parameters	a = 7.8023(6) Å	α = 78.2787(11)°
	b = 8.9306(7) Å	β = 75.7155(11)°
	c = 15.6115(13) Å	γ = 86.5775(11)°
Cell volume	1032.13(14) $Å^3$	
Z	2	
Calculated density	1.385 g/cm^3	
Absorption coefficient μ	0.668 mm^{-1}	
F(000)	452	
Crystal colour and size	orange, 0.47 × 0.36 × 0.16 mm^3	
Reflections for cell refinement	6531 (θ range 2.33 to 28.34°)	
Data collection method	Bruker APEX-II CCD	
	ϕ and ω scans	
θ range for data collection	2.33 to 28.34°	
Index ranges	h –10 to 10, k –11 to 11, l –20 to 20	
Completeness to θ = 28.34°	99.1 %	
Intensity decay	0%	
Reflections collected	10557	
Independent reflections	5108 (R_{int} = 0.0621)	
Reflections with $F^2>2\sigma$	4500	
Absorption correction	semi-empirical from equivalents	
Min. and max. transmission	0.7442 and 0.9007	
Structure solution	direct methods	
Refinement method	Full-matrix least-squares on F^2	
Weighting parameters a, b	0.0341, 0.0678	
Data / restraints / parameters	5108 / 0 / 248	
Final R indices [$F^2>2\sigma$]	R1 = 0.0282, wR2 = 0.0800	
R indices (all data)	R1 = 0.0317, wR2 = 0.0816	
Goodness-of-fit on F^2	1.021	
Largest and mean shift/su	0.001 and 0.000	
Largest diff. peak and hole	0.371 and –0.326 e $Å^{-3}$	

The number of the atoms in the unit cell instruction and atom list did not match, because because the intensity contribution of disordered a methanol solvate were removed from structure by SQUEEZE procedure.[216] SQUEEZE procedure (below) found an electron count of $17e^-$ in each of two voids of 85 $Å^3$. Each set of $17e^-$ was modelled as one methanol molecule ($18e^-$).

```
# SQUEEZE RESULTS (APPEND TO CIF)
# Note: Data are Listed for all Voids in the P1 Unit Cell
# i.e. Centre of Gravity, Solvent Accessible Volume,
# Recovered number of Electrons in the Void and
# Details about the Squeezed Material
loop_
  _platon_squeeze_void_nr
  _platon_squeeze_void_average_x
  _platon_squeeze_void_average_y
  _platon_squeeze_void_average_z
  _platon_squeeze_void_volume
  _platon_squeeze_void_count_electrons
  _platon_squeeze_void_content
   1  0.000  0.000  0.500        85        17 ' '
;
one methanol molecule for per unit cell (18e-)
;
```

Table A13 Crystal data and structure refinement for $[Mn(L5)Cl_2]$.

Identification code	mk48	
Chemical formula	$C_{15}H_{25}Cl_2MnN_5$	
Formula weight	401.24	
Temperature	150(2) K	
Radiation, wavelength	MoKα, 0.71073 Å	
Crystal system, space group	Orthorhombic, Pbca	
Unit cell parameters	a = 7.5951(13) Å	α = 90°
	b = 15.918(3) Å	β = 90°
	c = 30.723(5) Å	γ = 90°
Cell volume	3714.3(11) $Å^3$	
Z	8	
Calculated density	1.435 g/cm^3	
Absorption coefficient μ	1.004 mm^{-1}	
F(000)	1672	
Crystal colour and size	yellow, 0.26 × 0.23 × 0.14 mm^3	
Reflections for cell refinement	7489 (θ range 2.56 to 25.60°)	
Data collection method	Bruker APEX-II CCD	
	ϕ and ω scans	
θ range for data collection	2.56 to 25.79°	
Index ranges	h –9 to 9, k –19 to 18, l –37 to 33	
Completeness to θ = 25.79°	99.8 %	
Intensity decay	0%	
Reflections collected	19412	
Independent reflections	3559 (R_{int} = 0.0365)	
Reflections with $F^2>2\sigma$	2935	
Absorption correction	semi-empirical from equivalents	
Min. and max. transmission	0.6526 and 0.7453	
Structure solution	direct methods	
Refinement method	Full-matrix least-squares on F^2	
Weighting parameters a, b	0.0310, 1.5778	
Data / restraints / parameters	3559 / 0 / 212	
Final R indices [$F^2>2\sigma$]	R1 = 0.0285, wR2 = 0.0650	
R indices (all data)	R1 = 0.0388, wR2 = 0.0694	
Goodness-of-fit on F^2	1.034	
Largest and mean shift/su	0.001 and 0.000	
Largest diff. peak and hole	0.272 and –0.221 e $Å^{-3}$	

Table A14 Crystal data and structure refinement for $[Mn(H_2L6)Cl(H_2O)]Cl \cdot H_2O$

Identification code	mk71r→mk71	
Empirical formula	$C_{13}H_{23}C_{l2}MnN_3O_4$	
Formula weight	411.18	
Temperature	150(2) K	
Wavelength	0.71073 Å	
Crystal system	Monoclinic	
Space group	$P2_1/c$	
Unit cell dimensions	a = 10.9211(8) Å	α= 90°
	b = 12.0382(9) Å	β= 109.8301(11)°
	c = 15.3331(11) Å	γ = 90°
Volume	1896.3(2) $Å^3$	
Z	4	
Density (calculated)	1.440 Mg/m^3	
Absorption coefficient	0.997 mm^{-1}	
F(000)	852	
Crystal size	0.30 x 0.22 x 0.13 mm^3	
Crystal description	orange lath	
Theta range for data collection	1.98 to 28.32°.	
Index ranges	-14<=h<=14, -16<=k<=16, -20<=l<=20	
Reflections collected	18855	
Independent reflections	4723 [R(int) = 0.0284]	
Completeness to theta = 28.32°	99.9 %	
Absorption correction	Semi-empirical from equivalents	
Max. and min. transmission	0.8813 and 0.7540	
Refinement method	Full-matrix least-squares on F^2	
Data / restraints / parameters	4723 / 0 / 210	
Goodness-of-fit on F^2	1.047	
Final R indices [I>2sigma(I)]	R1 = 0.0429, wR2 = 0.1096	
R indices (all data)	R1 = 0.0587, wR2 = 0.1202	
Largest diff. peak and hole	0.792 and -0.502 $e.Å^{-3}$	

Hydrogen atoms bonded to oxygen atoms (O1, O2, O3 and O4) were located from difference maps and positions were refined. *U*iso(H) values were set to be 1.5 times *U*eq of the carrier atoms.

Table A15 Crystal data and structure refinement for $[Mn(H_2L7)(NCS)_2]\cdot dmf$.

Identification code	mk88	
Chemical formula	$C_{20}H_{30}MnN_6O_3S_2$	
Formula weight	521.56	
Temperature	150(2) K	
Radiation, wavelength	MoKα, 0.71073 Å	
Crystal system, space group	Monoclinic, $P2_1/c$	
Unit cell parameters	a = 8.5916(4) Å	α = 90°
	b = 8.2974(4) Å	β = 91.7307(8)°
	c = 35.1501(18) Å	γ = 90°
Cell volume	2504.6(2) Å^3	
Z	4	
Calculated density	1.383 g/cm^3	
Absorption coefficient μ	0.726 mm^{-1}	
F(000)	1092	
Crystal colour and size	yellow, 0.412 × 0.110 × 0.065 mm^3	
Reflections for cell refinement	6505 (θ range 2.37 to 26.34°)	
Data collection method	Bruker APEX-II CCD	
	ϕ and ω scans	
θ range for data collection	1.16 to 26.41°	
Index ranges	h −10 to 10, k −10 to 10, l −43 to 43	
Completeness to θ = 26.41°	100.0 %	
Intensity decay	0%	
Reflections collected	21498	
Independent reflections	5140 (R_{int} = 0.0307)	
Reflections with $F^2>2\sigma$	4270	
Absorption correction	semi-empirical from equivalents	
Min. and max. transmission	0.6339 and 0.7454	
Structure solution	direct methods	
Refinement method	Full-matrix least-squares on F^2	
Weighting parameters a, b	0.0328, 1.0459	
Data / restraints / parameters	5139 / 0 / 295	
Final R indices [$F^2>2\sigma$]	R1 = 0.0296, wR2 = 0.0683	
R indices (all data)	R1 = 0.0393, wR2 = 0.0727	
Goodness-of-fit on F^2	1.032	
Largest and mean shift/su	0.001 and 0.000	
Largest diff. peak and hole	0.417 and −0.384 e Å^{-3}	

Hydrogen atoms bonded to oxygen atoms (O1 and O2) were located from difference maps and positions were refined. *U*iso(H) values were set to be 1.5 times *U*eq of the carrier atom for O1 and O2.

Table A16 Crystal data and structure refinement for $[Mn(H_2L7)(H_2O)Cl_2]\cdot 0.3H_2O$.

Identification code	mk85→sad	
Empirical formula	$C_{15}H_{25.60}Cl_2MnN_3O_{3.30}$	
Formula weight	426.62	
Temperature	296(2) K	
Wavelength	0.71073 Å	
Crystal system	Monoclinic	
Space group	$P2_1/c$	
Unit cell dimensions	a = 14.4544(6) Å	a= 90°
	b = 8.6208(4) Å	b= 112.4257(6)°
	c = 16.9691(7) Å	g = 90°
Volume	1954.58(15) $Å^3$	
Z	4	
Density (calculated)	1.450 Mg/m^3	
Absorption coefficient	0.968 mm^{-1}	
F(000)	888	
Crystal size	0.31 x 0.25 x 0.24 mm^3	
Crystal description	yellow, trigonal prism	
Theta range for data collection	1.52 to 28.93°.	
Index ranges	-19<=h<=19, -11<=k<=11, -23<=l<=23	
Reflections collected	20073	
Independent reflections	5164 [R(int) = 0.0238]	
Completeness to theta = 28.93°	99.9 %	
Absorption correction	None	
Refinement method	Full-matrix least-squares on F^2	
Data / restraints / parameters	5164 / 0 / 258	
Goodness-of-fit on F^2	1.022	
Final R indices [I>2sigma(I)]	R1 = 0.0274, wR2 = 0.0680	
R indices (all data)	R1 = 0.0329, wR2 = 0.0707	
Largest diff. peak and hole	0.450 and -0.275 $e.Å^{-3}$	

Hydrogen atoms bonded to oxygen atoms (O1, O2, O3 and O4) were located from difference maps and positions were refined. *U*iso(H) values were set to be 1.5 times *U*eq of the carrier atoms. One of the alcohol groups is disordered in the structure and this was modelled over two positions in a 0.70:0.30 ration C1O1:C1'O1'. One of the methyl groups (C3) shows some disorder and this has been modelled as a rotation about the C2-C3 bond. Site occupancy factors were set at 0.70 C3 at 0.30 for C3'. In the structure there is uncoordinated partial occupancy (0.30) water molecule found.

Table A17 Crystal data and structure refinement for $[Mn(H_2L8)(NCS)_2(dmf)]\cdot dmf$.

Identification code	mk84	
Chemical formula	$C_{23}H_{37}MnN_7O_4S_2$	
Formula weight	594.66	
Temperature	150(2) K	
Radiation, wavelength	MoKα, 0.71073 Å	
Crystal system, space group	Monoclinic, $P2_1/c$	
Unit cell parameters	a = 14.9551(12) Å	α = 90°
	b = 11.0509(9) Å	β = 100.0429(13)°
	c = 18.4767(14) Å	γ = 90°
Cell volume	3006.8(4) Å^3	
Z	4	
Calculated density	1.314 g/cm^3	
Absorption coefficient μ	0.617 mm^{-1}	
F(000)	1252	
Crystal colour and size	yellow, 0.39 × 0.21 × 0.07 mm^3	
Reflections for cell refinement	6961 (θ range 2.30 to 28.06°)	
Data collection method	Bruker APEX-II CCD	
	ϕ and ω scans	
θ range for data collection	1.38 to 28.33°	
Index ranges	h −19 to 19, k −14 to 14, l −24 to 24	
Completeness to θ = 28.33°	99.8 %	
Intensity decay	0%	
Reflections collected	30036	
Independent reflections	7485 (R_{int} = 0.0353)	
Reflections with $F^2>2\sigma$	5595	
Absorption correction	semi-empirical from equivalents	
Min. and max. transmission	0.7948 and 0.9581	
Structure solution	direct methods	
Refinement method	Full-matrix least-squares on F^2	
Weighting parameters a, b	0.0680, 1.9609	
Data / restraints / parameters	7485 / 0 / 342	
Final R indices [$F^2>2\sigma$]	R1 = 0.0461, wR2 = 0.1207	
R indices (all data)	R1 = 0.0664, wR2 = 0.1392	
Goodness-of-fit on F^2	1.063	
Largest and mean shift/su	0.044 and 0.001	
Largest diff. peak and hole	1.811 and −1.078 e Å^{-3}	

Hydrogen atoms bonded to oxygen atoms were inserted at calculated positions using a riding model. *U*iso(H) values were set to be 1.5 times *U*eq of the carrier atoms.

Table A18 Crystal data and structure refinement for $H_2L10 \cdot H_2O$

Identification code	mk01	
Chemical formula	$C_{42}H_{40}N_6O_5$	
Formula weight	708.80	
Temperature	150(2) K	
Radiation, wavelength	MoKα, 0.71073 Å	
Crystal system, space group	Monoclinic, C2/c	
Unit cell parameters	a = 23.8510(13) Å	α = 90°
	b = 12.9688(7) Å	β = 114.0772(8)°
	c = 12.3835(7) Å	γ = 90°
Cell volume	3497.2(3) $Å^3$	
Z	4	
Calculated density	1.346 g/cm^3	
Absorption coefficient μ	0.090 mm^{-1}	
F(000)	1496	
Crystal colour and size	yellow, 0.60 × 0.28 × 0.11 mm^3	
Reflections for cell refinement	5957 (θ range 2.28 to 29.81°)	
Data collection method	Bruker APEX-II CCD	
	ϕ and ω scans	
θ range for data collection	1.83 to 29.84°	
Index ranges	h –33 to 33, k –17 to 18, l –17 to 17	
Completeness to θ = 29.84°	99.8 %	
Reflections collected	19364	
Independent reflections	5005 (R_{int} = 0.0243)	
Reflections with $F^2>2\sigma$	3919	
Absorption correction	semi-empirical from equivalents	
Min. and max. transmission	0.9473 and 0.9905	
Structure solution	direct methods	
Refinement method	Full-matrix least-squares on F^2	
Weighting parameters a, b	0.0642, 1.5272	
Data / restraints / parameters	5005 / 0 / 251	
Final R indices [$F^2>2\sigma$]	R1 = 0.0422, wR2 = 0.1148	
R indices (all data)	R1 = 0.0550, wR2 = 0.1240	
Goodness-of-fit on F^2	1.058	
Largest and mean shift/su	0.001 and 0.000	
Largest diff. peak and hole	0.362 and –0.232 e $Å^{-3}$	

Hydrogen atoms bonded to phenolic oxygen atoms (O1 and O2) and the water molecule (O3) were located from difference maps and positions were refined. *U*iso(H) values were set to be 1.5 times *U*eq of the carrier atoms.

Table A19 Crystal data and structure refinement for $[Mn(H_2L9)Cl_2]\cdot MeOH$.

Identification code	PG71→sad	
Chemical formula	$C_{20}H_{19}Cl_2MnN_3O_3$	
Formula weight	475.22	
Temperature	150(2) K	
Radiation, wavelength	MoKα, 0.71073 Å	
Crystal system, space group	Monoclinic, $P2_1/c$	
Unit cell parameters	a = 12.4143(15) Å	α = 90°
	b = 17.149(2) Å	β = 105.410(2)°
	c = 9.8600(12) Å	γ = 90°
Cell volume	2023.7(4) $Å^3$	
Z	4	
Calculated density	1.560 g/cm^3	
Absorption coefficient μ	0.944 mm^{-1}	
F(000)	972	
Crystal colour and size	Red, 0.45 × 0.33 × 0.19 mm^3	
Reflections for cell refinement	2790 (θ range 2.45 to 24.65°)	
Data collection method	Bruker APEX-II CCD	
	ϕ and ω scans	
θ range for data collection	1.70 to 28.36°	
Index ranges	h −16 to 16, k −22 to 22, l −13 to 13	
Completeness to θ = 28.36°	99.8 %	
Intensity decay	0%	
Reflections collected	20698	
Independent reflections	5053 (R_{int} = 0.0609)	
Reflections with $F^2>2\sigma$	3731	
Absorption correction	semi-empirical from equivalents	
Min. and max. transmission	0.9584 and 0.9913	
Structure solution	direct methods	
Refinement method	Full-matrix least-squares on F^2	
Weighting parameters a, b	0.0170, 0.6885	
Data / restraints / parameters	5053 / 0 / 272	
Final R indices [$F^2>2\sigma$]	R1 = 0.0390, wR2 = 0.0799	
R indices (all data)	R1 = 0.0630, wR2 = 0.0884	
Goodness-of-fit on F^2	1.047	
Largest and mean shift/su	0.001 and 0.000	
Largest diff. peak and hole	0.334 and −0.304 e $Å^{-3}$	

Hydrogen atoms bonded to oxygen atoms (O1, O2 and O3) were located from difference maps and positions were refined. *U*iso(H) values were set to be 1.5 times *U*eq of the carrier atoms.

Table A20 Crystal data and structure refinement for $[Mn_3(L9)_2(OAc)_2(MeOH)_2]\cdot 2MeOH$.

Identification code	mk151b	
Empirical formula	$C_{46}H_{48}Mn_3N_6O_{12}$	
Formula weight	1041.72	
Temperature	150(2) K	
Wavelength	0.71073 Å	
Crystal system	Monoclinic	
Space group	$P2_1/c$	
Unit cell dimensions	a = 23.000(2) Å	α= 90°
	b = 12.5247(11) Å	β= 109.0662(13)°
	c = 16.6909(14) Å	γ = 90°
Volume	4544.4(7) $Å^3$	
Z	4	
Density (calculated)	1.523 Mg/m^3	
Absorption coefficient	0.891 mm^{-1}	
F(000)	2148	
Crystal size	0.42 x 0.39 x 0.13 mm^3	
Crystal description	red lath	
Theta range for data collection	0.94 to 26.47°.	
Index ranges	-28<=h<=28, -15<=k<=15, -20<=l<=20	
Reflections collected	39189	
Independent reflections	9353 [R(int) = 0.0433]	
Completeness to theta = 26.47°	99.5 %	
Absorption correction	Semi-empirical from equivalents	
Max. and min. transmission	0.8929 and 0.7059	
Refinement method	Full-matrix least-squares on F^2	
Data / restraints / parameters	9353 / 0 / 610	
Goodness-of-fit on F^2	1.026	
Final R indices [I>2sigma(I)]	R1 = 0.0356, wR2 = 0.0945	
R indices (all data)	R1 = 0.0496, wR2 = 0.1040	
Largest diff. peak and hole	0.564 and -0.464 $e.Å^{-3}$	

Hydrogen atoms bonded to oxygen atoms (O9, O10, O11 and O12) were located from difference maps and positions were refined. *U*iso(H) values were set to be 1.5 times *U*eq of the carrier atoms.

Table A21 Crystal data and structure refinement for $[Mn_2Ca(L9)_2(OAc)_2(MeOH)_2]\cdot 2MeOH$.

Identification code	mk151a	
Empirical formula	$C_{46}H_{48}CaMn_2N_6O_{12}$	
Formula weight	1026.86	
Temperature	150(2) K	
Wavelength	0.71073 Å	
Crystal system	Triclinic	
Space group	$P\bar{1}$	
Unit cell dimensions	a = 9.7797(16) Å	α= 105.194(3)°
	b = 10.9467(18) Å	β= 97.922(3)°
	c = 12.067(3) Å	γ = 111.677(2)°
Volume	1118.2(4) $Å^3$	
Z	1	
Density (calculated)	1.525 Mg/m^3	
Absorption coefficient	0.751 mm^{-1}	
F(000)	532	
Crystal size	0.21 x 0.15 x 0.04 mm^3	
Crystal description	Red Block	
Theta range for data collection	1.81 to 26.45°.	
Index ranges	-12<=h<=12, -13<=k<=13, -15<=l<=15	
Reflections collected	12971	
Independent reflections	4591 [R(int) = 0.0926]	
Completeness to theta = 26.45°	99.5 %	
Absorption correction	Semi-empirical from equivalents	
Max. and min. transmission	0.9706 and 0.8570	
Refinement method	Full-matrix least-squares on F^2	
Data / restraints / parameters	4591 / 0 / 307	
Goodness-of-fit on F^2	0.950	
Final R indices [I>2sigma(I)]	R1 = 0.0477, wR2 = 0.0998	
R indices (all data)	R1 = 0.0950, wR2 = 0.1141	
Largest diff. peak and hole	0.456 and -0.702 $e.Å^{-3}$	

Hydrogen atoms bonded to oxygen atoms (O5 and O6) were located from difference maps and positions were refined. *U*iso(H) values were set to be 1.5 times *U*eq of the carrier atoms.

Table A22 Crystal data and structure refinement for H_3L11.

Identification code	222	
Chemical formula	$C_{27}H_{30}N_4O_3$	
Formula weight	458.55	
Temperature	150(2) K	
Radiation, wavelength	MoKα, 0.71073 Å	
Crystal system, space group	monoclinic, $P2_1/c$	
Unit cell parameters	a = 10.1165(13) Å	α = 90°
	b = 11.0952(14) Å	β = 97.8766(18)°
	c = 22.017(2) Å	γ = 90°
Cell volume	2447.9(5) Å^3	
Z	4	
Calculated density	1.244 g/cm^3	
Absorption coefficient μ	0.083 mm^{-1}	
F(000)	976	
Crystal colour and size	yellow, 0.62 × 0.52 × 0.37 mm^3	
Reflections for cell refinement	6763 (θ range 2.57 to 26.30°)	
Data collection method	Bruker APEX-II CCD	
	ϕ and ω scans	
θ range for data collection	1.87 to 26.39°	
Index ranges	h –12 to 12, k –13 to 13, l –27 to 27	
Completeness to θ = 26.39°	99.8 %	
Intensity decay	0%	
Reflections collected	20753	
Independent reflections	5010 (R_{int} = 0.0316)	
Reflections with $F^2>2\sigma$	3831	
Absorption correction	semi-empirical from equivalents	
Min. and max. transmission	0.6117 and 0.7454	
Structure solution	direct methods	
Refinement method	Full-matrix least-squares on F^2	
Weighting parameters a, b	0.0333, 0.6460	
Data / restraints / parameters	5010 / 0 / 310	
Final R indices [$F^2>2\sigma$]	R1 = 0.0345, wR2 = 0.0807	
R indices (all data)	R1 = 0.0526, wR2 = 0.0920	
Goodness-of-fit on F^2	1.030	
Largest and mean shift/su	0.001 and 0.000	
Largest diff. peak and hole	0.166 and –0.175 e Å^{-3}	

Hydrogen atoms bonded to oxygen atoms were inserted at calculated positions using a riding model. *U*iso(H) values were set to be 1.5 times *U*eq of the carrier atoms.

Table A23 Crystal data and structure refinement for [Mn(L11)].

Identification code	222mnso4	
Chemical formula	$C_{27}H_{27}MnN_4O_3$	
Formula weight	510.47	
Temperature	150(2) K	
Radiation, wavelength	MoKα, 0.71073 Å	
Crystal system, space group	Monoclinic, $P2_1/n$	
Unit cell parameters	a = 7.8372(15) Å	α = 90°
	b = 25.541(4) Å	β = 96.737(3)°
	c = 11.609(2) Å	γ = 90°
Cell volume	2307.7(7) $Å^3$	
Z	4	
Calculated density	1.469 g/cm^3	
Absorption coefficient μ	0.611 mm^{-1}	
F(000)	1064	
Crystal colour and size	Green, 0.33 × 0.19 × 0.11 mm^3	
Reflections for cell refinement	1730 (θ range 2.38 to 21.87°)	
Data collection method	Bruker APEX-II CCD	
	ϕ and ω scans	
θ range for data collection	1.59 to 26.44°	
Index ranges	h –9 to 9, k –31 to 31, l –14 to 14	
Completeness to θ = 26.44°	99.7 %	
Intensity decay	0%	
Reflections collected	20149	
Independent reflections	4739 (R_{int} = 0.0873)	
Reflections with $F^2>2\sigma$	3096	
Absorption correction	semi-empirical from equivalents	
Min. and max. transmission	0.5887 and 0.7454	
Structure solution	Patterson method	
Refinement method	Full-matrix least-squares on F^2	
Weighting parameters a, b	0.0621, 0.2363	
Data / restraints / parameters	4739 / 0 / 316	
Final R indices [$F^2>2\sigma$]	R1 = 0.0499, wR2 = 0.1122	
R indices (all data)	R1 = 0.0906, wR2 = 0.1318	
Goodness-of-fit on F^2	1.001	
Largest and mean shift/su	0.001 and 0.000	
Largest diff. peak and hole	0.555 and –0.524 e $Å^{-3}$	

The structure was solved by the Patterson method**.**

Table A24 Crystal data and structure refinement for $[Mn(L16)](ClO_4)_2$.

Identification code	mk92	
Empirical formula	$C_{25}H_{29}Cl_2MnN_7O_8$	
Formula weight	681.39	
Temperature	150(2) K	
Wavelength	0.71073 Å	
Crystal system	Monoclinic	
Space group	$P2_1$	
Unit cell dimensions	a = 9.1381(4) Å	α= 90°
	b = 9.8480(4) Å	β= 90.6516(6)°
	c = 15.9901(7) Å	γ = 90°
Volume	1438.89(11) $Å^3$	
Z	2	
Density (calculated)	1.573 Mg/m^3	
Absorption coefficient	0.706 mm^{-1}	
F(000)	702	
Crystal size	0.30 x 0.22 x 0.13 mm^3	
Crystal description	yellow lath	
Theta range for data collection	2.23 to 26.40°.	
Index ranges	-11<=h<=11, -12<=k<=12, -19<=l<=19	
Reflections collected	12593	
Independent reflections	5772 [R(int) = 0.0172]	
Completeness to theta = 26.40°	99.7 %	
Absorption correction	Semi-empirical from equivalents	
Max. and min. transmission	0.8813 and 0.7540	
Refinement method	Full-matrix least-squares on F^2	
Data / restraints / parameters	5772 / 1 / 433	
Goodness-of-fit on F^2	1.055	
Final R indices [I>2sigma(I)]	R1 = 0.0296, wR2 = 0.0785	
R indices (all data)	R1 = 0.0321, wR2 = 0.0799	
Absolute structure parameter	0.018(13)	
Largest diff. peak and hole	0.698 and -0.331 $e.Å^{-3}$	

One of the perchlorate anions is disordered and this was modelled over two positions in a 60:40 ratio (Cl2O5O6O7O8): (Cl2'O5'O6'O7'O8').

Table A25 Crystal data and structure refinement for $[Mn(L18)](ClO_4)_2$.

Identification code	mk34	
Empirical formula	$C_{27}H_{33}Cl_2MnN_7O_8$	
Formula weight	709.44	
Temperature	150(2) K	
Wavelength	0.71073 Å	
Crystal system	Triclinic	
Space group	P-1	
Unit cell dimensions	a = 10.8583(15) Å	α= 77.534(2)°
	b = 12.0916(16) Å	β= 71.604(2)°
	c = 12.9669(17) Å	γ = 71.206(2)°
Volume	1516.9(4) $Å^3$	
Z	2	
Density (calculated)	1.553 Mg/m^3	
Absorption coefficient	0.673 mm^{-1}	
F(000)	734	
Crystal size	0.36 x 0.22 x 0.18 mm^3	
Crystal description	yellow block	
Theta range for data collection	1.67 to 26.44°.	
Index ranges	-13<=h<=13, -15<=k<=15, -16<=l<=16	
Reflections collected	13604	
Independent reflections	6228 [R(int) = 0.0217]	
Completeness to theta = 26.44°	99.6 %	
Absorption correction	Semi-empirical from equivalents	
Max. and min. transmission	0.7454 and 0.6490	
Refinement method	Full-matrix least-squares on F^2	
Data / restraints / parameters	6228 / 0 / 461	
Goodness-of-fit on F^2	1.044	
Final R indices [I>2sigma(I)]	R1 = 0.0369, wR2 = 0.0858	
R indices (all data)	R1 = 0.0489, wR2 = 0.0925	
Largest diff. peak and hole	0.293 and -0.493 $e.Å^{-3}$	

One of the propyl arms is disordered and this was modelled over two positions. Site occupancy factors were set at 0.60 C11 at 0.40 for C11'. One of the perchlorate anions is disordered and this was modelled over two positions in a 50:50 ratio (Cl1O1O2O3O3): (Cl1'O1'O2'O3'O4').

Table A26 Crystal data and structure refinement for $[Mn(L19)Cl_2]$.

Identification code	mnbenz	
Chemical formula	$C_{27}H_{29}Cl_2MnN_5$	
Formula weight	549.39	
Temperature	150(2) K	
Radiation, wavelength	MoKα, 0.71073 Å	
Crystal system, space group	Triclinic, $P\bar{1}$	
Unit cell parameters	a = 11.457(2) Å	α = 109.256(3)°
	b = 15.849(3) Å	β = 94.894(3)°
	c = 17.696(3) Å	γ = 109.083(3)°
Cell volume	1308.0(5) $Å^3$	
Z	2	
Calculated density	1.395 g/cm^3	
Absorption coefficient μ	0.734 mm^{-1}	
F(000)	570	
Crystal colour and size	yellow, 0.29 × 0.10 × 0.10 mm^3	
Reflections for cell refinement	2155 (θ range 2.26 to 22.63°)	
Data collection method	Bruker APEX-II CCD	
	ϕ and ω scans	
θ range for data collection	1.94 to 26.40°	
Index ranges	h –11 to 11, k –14 to 14, l –16 to 16	
Completeness to θ = 26.40°	99.6 %	
Intensity decay	0%	
Reflections collected	11664	
Independent reflections	5355 (R_{int} = 0.0369)	
Reflections with $F^2>2\sigma$	3617	
Absorption correction	semi-empirical from equivalents	
Min. and max. transmission	0.8152 and 0.9302	
Structure solution	direct methods	
Refinement method	Full-matrix least-squares on F^2	
Weighting parameters a, b	0.0431, 0.0000	
Data / restraints / parameters	5355 / 0 / 346	
Final R indices [$F^2>2\sigma$]	R1 = 0.0407, wR2 = 0.0846	
R indices (all data)	R1 = 0.0742, wR2 = 0.0968	
Goodness-of-fit on F^2	0.987	
Largest and mean shift/su	0.003 and 0.000	
Largest diff. peak and hole	0.318 and –0.238 e $Å^{-3}$	

One of the butyl chains (C1-C4) is disordered and this was modelled over two positions in a 65:35 ratio (C(1)- C(4):C(1)'-C(4)').

Table A27 Crystal data and structure refinement for [Mn(L19)(NCS)$_2$].

Identification code	mnbenz2	
Chemical formula	$C_{29}H_{29}MnN_7S_2$	
Formula weight	594.65	
Temperature	150(2) K	
Radiation, wavelength	MoKα, 0.71073 Å	
Crystal system, space group	Triclinic, P $\bar{1}$	
Unit cell parameters	a = 8.6123(9) Å	α = 73.4928(16)°
	b = 11.6211(12) Å	β = 84.3097(16)°
	c = 15.7406(16) Å	γ = 70.9302(15)°
Cell volume	1427.5(3) Å^3	
Z	2	
Calculated density	1.383 g/cm^3	
Absorption coefficient μ	0.641 mm^{-1}	
F(000)	618	
Crystal colour and size	yellow, 0.40 × 0.15 × 0.07 mm^3	
Reflections for cell refinement	4688 (θ range 2.50 to 28.09°)	
Data collection method	Bruker APEX-II CCD	
	ϕ and ω scans	
θ range for data collection	1.35 to 28.29°	
Index ranges	h −11 to 11, k −15 to 15, l −20 to 20	
Completeness to θ = 28.29°	99.2 %	
Intensity decay	0%	
Reflections collected	14654	
Independent reflections	7035 (R_{int} = 0.0230)	
Reflections with $F^2>2\sigma$	5633	
Absorption correction	semi-empirical from equivalents	
Min. and max. transmission	0.7837 and 0.9565	
Structure solution	direct methods	
Refinement method	Full-matrix least-squares on F^2	
Weighting parameters a, b	0.0570, 0.1200	
Data / restraints / parameters	7035 / 0 / 354	
Final R indices [$F^2>2\sigma$]	R1 = 0.0356, wR2 = 0.0922	
R indices (all data)	R1 = 0.0495, wR2 = 0.1046	
Goodness-of-fit on F^2	1.065	
Largest and mean shift/su	0.002 and 0.000	
Largest diff. peak and hole	0.393 and –0.309 e Å^{-3}	

Table A28 Crystal data and structure refinement for [Mn(L19)(NO_3)$_2$].

Identification code	mnbenz4r→sad	
Chemical formula	$C_{27}H_{29}MnN_7O_6$	
Formula weight	602.51	
Temperature	150(2) K	
Radiation, wavelength	MoKα, 0.71073 Å	
Crystal system, space group	Triclinic, P1	
Unit cell parameters	a = 9.2324(5) Å	α = 105.1521(7)°
	b = 11.5235(7) Å	β = 103.2441(18)°
	c = 15.6572(9) Å	γ = 113.3035(7)°
Cell volume	1387.24(16) Å^3	
Z	2	
Calculated density	1.442 g/cm^3	
Absorption coefficient μ	0.531 mm^{-1}	
F(000)	626	
Crystal colour and size	yellow, 0.29 × 0.25 × 0.20 mm^3	
Reflections for cell refinement	6174 (θ range 2.42 to 26.24°)	
Data collection method	Bruker APEX-II CCD	
	ϕ and ω scans	
θ range for data collection	2.02 to 26.42°	
Index ranges	h −11 to 11, k −14 to 14, l −18 to 18	
Completeness to θ = 26.42°	99.9 %	
Intensity decay	0%	
Reflections collected	16617	
Independent reflections	5716 (R_{int} = 0.0248)	
Reflections with $F^2>2\sigma$	4882	
Absorption correction	semi-empirical from equivalents	
Min. and max. transmission	0.8617 and 0.9031	
Structure solution	direct methods	
Refinement method	Full-matrix least-squares on F^2	
Weighting parameters a, b	0.0339, 0.3890	
Data / restraints / parameters	5716 / 0 / 372	
Final R indices [$F^2>2\sigma$]	R1 = 0.0299, wR2 = 0.0721	
R indices (all data)	R1 = 0.0375, wR2 = 0.0757	
Goodness-of-fit on F^2	1.031	
Largest and mean shift/su	0.001 and 0.000	
Largest diff. peak and hole	0.263 and −0.212 e Å^{-3}	

Table A29 Crystal data and structure refinement for $[Mn(L19)_2](ClO_4)_2 \cdot ½dmf$.

Identification code	mnbenz1	
Empirical formula	$C_{55.50}H_{61.50}Cl_2MnN_{10.50}O_{8.50}$	
Formula weight	1137.49	
Temperature	150(2) K	
Wavelength	0.71073 Å	
Crystal system	Monoclinic	
Space group	P2/c	
Unit cell dimensions	a = 12.7776(18) Å	α= 90°
	b = 14.119(2) Å	β= 92.433(2)°
	c = 15.533(2) Å	γ = 90°
Volume	2799.9(7) $Å^3$	
Z	2	
Density (calculated)	1.349 Mg/m^3	
Absorption coefficient	0.395 mm^{-1}	
F(000)	1190	
Crystal size	0.57 x 0.25 x 0.08 mm^3	
Crystal description	yellow block	
Theta range for data collection	1.60 to 26.40°.	
Index ranges	-15<=h<=15, -17<=k<=17, -19<=l<=19	
Reflections collected	24216	
Independent reflections	5739 [R(int) = 0.0204]	
Completeness to theta = 26.40°	99.7 %	
Absorption correction	None	
Refinement method	Full-matrix least-squares on F^2	
Data / restraints / parameters	5739 / 46 / 378	
Goodness-of-fit on F^2	1.118	
Final R indices [I>2sigma(I)]	R1 = 0.0531, wR2 = 0.1660	
R indices (all data)	R1 = 0.0598, wR2 = 0.1721	
Largest diff. peak and hole	0.844 and -0.372 e.$Å^{-3}$	

One of the butyl chains (C24-C27) is disordered and this was modelled over two positions in a 60:40 ratio (C24- C27:C24'-C27').

The number of the atoms in the unit cell instruction and atom list did not match, because because the intensity contribution of a disordered dmf molecule was removed from structure by SQUEEZE procedure.[216] SQUEEZE procedure (below) found the electron count of $39e^-$ in each of two voids of 136 $Å^3$. Each set of $39e^-$ was modelled as one dmf molecule ($40e^-$).

```
# SQUEEZE RESULTS (APPEND TO CIF)
# Note: Data are Listed for all Voids in the P1 Unit Cell
# i.e. Centre of Gravity, Solvent Accessible Volume,
# Recovered number of Electrons in the Void and
# Details about the Squeezed Material
loop_
  _platon_squeeze_void_nr
  _platon_squeeze_void_average_x
  _platon_squeeze_void_average_y
  _platon_squeeze_void_average_z
  _platon_squeeze_void_volume
  _platon_squeeze_void_count_electrons
  _platon_squeeze_void_content
   1  0.000  0.241  0.750       136        39 ' '
   2  0.000  0.759  0.250       136        39 ' '
_platon_squeeze_details
;
one dmf molecule for per unit cell (40e-)
;
```